Corrosion at the Head - Neck Taper Interface of Artificial Hip Joints

By

Richard Michael Ryan Dyrkacz

A thesis submitted to
the Faculty of Graduate Studies
in partial fulfillment of
the requirements for the degree of
Doctor of Philosophy

Department of Mechanical and Manufacturing Engineering
Faculty of Graduate Studies
University of Manitoba
Winnipeg, Manitoba, Canada

Abstract

The aim of this thesis was to determine if the size of the femoral head can influence corrosion at the head-neck taper interface of total hip arthroplasty (THA) prostheses. A hypothesis was developed that large head sizes could result in a greater toggling torque at the head-neck taper interface by increasing the distance between the centre of the femoral head to the centre of the neck taper. This could result in increased micromotion and deteriorate the passive oxide film along the head-neck taper interface; thus, making the taper interface vulnerable to corrosion.

A retrieval analysis of 74 THA prostheses studied the corrosion damage at the head-neck taper interface. This study revealed that prostheses featuring 36 mm femoral heads had significantly greater head taper corrosion than prostheses with a 28 mm head. Finite element analysis was performed afterwards to identify if the use of large femoral heads can increase the micromotion at the head-neck taper interface due to a greater toggling torque. This experiment demonstrated that with a larger head size the micromotion at the head-neck taper interface increases. An *in vitro* corrosion fatigue study was performed afterwards following ASTM F1875-98. When applying an off-axis fatigue load, prostheses featuring a 36 mm femoral head displayed significantly more corrosion damage at the head-neck taper interface than those with a 28 mm femoral head. Axial fatigue loading was also applied; negligible corrosion damage at the head-neck taper interface was discovered in comparison to the prostheses that received an out of axis load. This verifies that the use of large femoral heads can result in increased head-neck taper corrosion due to a greater toggling torque.

Acknowledgments

I wish to convey my sincere appreciation to my advisor, Dr. Urs Peter Wyss, for his continued enthusiasm, valuable guidance, and ongoing support throughout this project.

I would also like to extend my gratitude to the members of my thesis committee: Jan-M. Brandt, Jason B. Morrison, Olanrewaju A. Ojo, and Thomas R. Turgeon. Also, I would like to thank my external examiner, Dr. Jason Carey, from the University of Alberta.

I would like to put a special acknowledgement to Ian Polyzois and Sean O'Brien. Thank you for helping me with their technical advice for the finite element analysis and their never-ending support.

I want to thank Martin Petrak and the staff at the Concordia Hip and Knee Institute for their support through this project by providing me access to their implant retrieval database, high-performance computing cluster, and the Instron load frame. Additionally, I wish to acknowledge Alexander Vecherya, Matthew Gale, and Lawrence Cruz for their technical support throughout my research and Trevor Gascoyne's assistance with Geomagic Studio.

I wish to acknowledge Michele Berthelette, Darren Hart, Shawn Wiebe, and Tasneem Vahora for helping me score the prostheses for corrosion and fretting damage.

I would also like to acknowledge Stacey Hildebrand who helped create the finite element models, taught me ABAQUS, created some of the AutoCAD drawings, and designed a drop tower.

I would like to also acknowledge Dr. Thorsten Schwenke for the Thelkin load frame and manufacturing the head and neck tapers for the *in vitro* corrosion fatigue tests performed in this thesis. I would also like to recognize Trevor Smith and Mike Boskwick for their technical support with the Thelkin load frame.

Of course, I could have never finished this thesis without the support from my colleagues and friends. In particular, I wish to acknowledge Anastassiya Yudintseva, Jeff Delorme, Solomon Boakye-Yiadom, Omudhohwo (Omus) Oshobe, Brian Stimpson, Craig Milligan, Kris Nabess, Sean Patterson, Nathan Kesler, and Emmanuel Ocran. I would also like to thank all of the students that I have helped as a teaching assistant who inspired me to never give up on my goals.

The financial support provided for this research by The Natural Sciences and Engineering Research Council (NSERC), DePuy-Synthes, the Alexander Gibson Fund, and the University of Manitoba is greatly acknowledged.

Finally, I would also like to thank my parents for their never-ending support.

Dedication

This thesis is dedicated to my parents, my friends, and all of the students that I have had a pleasure to teach throughout the years.

Table of Contents

Front Matter

Table of Contents v

List of Tables ix

List of Figures xii

List of Abbreviations xvi

List of Symbols xx

List of Copyrighted Material xxii

Author's Declaration xxiii

Chapter 1 – Introduction **1**

1.1 General Overview 1

1.2 Objectives, Research Methodology, and the Significance of the Research 2

1.3 Scope of Work 6

Chapter 2 – Literature Review **9**

2.1 Introduction 9

2.2 Anatomy of the Hip Joint 9

2.3 Total Hip Arthroplasty 12

2.3.1 Patient Symptoms 12

2.3.2 The Modern Total Hip Arthroplasty Prosthesis 14

2.3.3 Femoral Head Size 21

2.4 Metallic Materials used in Total Hip Arthroplasty 27

2.4.1 Cobalt – Chromium Alloys 28

2.4.2 Titanium Alloys 31

2.4.3 316L Stainless Steel 32

2.5 Corrosion 33

2.5.1 Introduction to Corrosion 34

2.5.2 The Biological Environment 43

2.5.3 The Passive Oxide Film 44
2.5.4 Forms of Corrosion 47
2.5.5 Inflammatory Cell Induced Corrosion 56
2.5.6 Electrolytes for Corrosion Fatigue Testing 59
2.5.7 Wear Nomenclature 60
2.5.8 The Consequences of Wear Particles and Corrosion Products 65
2.5.9 Adverse Local Tissue Reactions 67
2.6 Fretting 70
2.6.1 Introduction to Fretting 71
2.6.2 Theories and Characterizations of Fretting 74
2.6.3 Friction 78
2.7 Corrosion and Fretting in Total Hip Arthroplasty 82
2.7.1 The Link Between Corrosion and Fretting in Total Hip Arthroplasty Prostheses 83
2.7.2 Multiple Modular Sites: A Focus on the Neck-Stem Taper Interface 93
2.7.3 Corrosion Products 100
2.7.4 Tribology and Tribocorrosion 101
2.8 Preventing Corrosion and Fretting Damage in Total Hip Arthroplasty 105
2.8.1 Assembly Procedure 106
2.8.2 The Debate of Single Alloys versus Mixed Alloys 108
2.8.3 Conical Half Angle 110
2.8.4 Taper Size 112
2.8.5 Ceramic Femoral Heads 113
2.8.6 Metal-on-Metal versus Metal-on-Polyethylene Articulations 115
2.8.7 Ion Implantation and Coating 116
2.8.8 Femoral Head Size and Neck Length 117

Chapter 3 – The Influence of Head Size on Corrosion and Fretting Behaviour at the Head-Neck Taper Interface of Artificial Hip Joints **120**

3.1 Introduction 120

3.2 Methodology 123

3.3 Results 127

3.4 Discussion 133

3.5 Conclusion 137

Chapter 4 – Finite Element Analysis of the Head – Neck Taper Interface of Modular Hip Prostheses **139**

4.1 Introduction 139

4.2 Methodology 141

4.2.1 Finite Element Modeling 141

4.2.2 Femoral Head Size and Material Combinations 144

4.2.3 Assembly Force 144

4.2.4 Taper Size 145

4.2.5 The Distance Between the Centre of the Femoral Head to the Centre of the Neck Taper 145

4.2.6 Axial and Out of Axis Loading 146

4.2.7 Testing for Convergence 146

4.3 Results 147

4.3.1 Assembly Displacement 147

4.3.2 Micromotion at the Head-Neck Taper Interface 150

4.3.3 Stress Analysis at the Head-Neck Taper Interface 154

4.4 Discussion 156

4.5 Conclusion 161

Chapter 5 – In Vitro Corrosion Fatigue Testing of Modular Hip Prostheses 164
5.1 Introduction 164
5.2 Methodology 166
5.3 Results 169
5.4 Discussion 175
5.5 Conclusion 179

Chapter 6 – Discussion 180
6.1 Can Retrieval Analyses Tell Us What Causes Taper Corrosion? 180
6.2 Finite Element Analysis 186
6.3 Discussion of the *in vitro* Corrosion Fatigue Experiment 190
6.4 Corrosion Scoring Techniques 193

Chapter 7 – Conclusion 198
7.1 Summary of Conclusions 198
7.2 Novelty of the Research 203
7.3 Recommendations for Future Work 205

Appendix A 210

Appendix B 223

Bibliography 230

List of Tables

Table 2.1. The advantages and disadvantages of THA prosthesis articulations. (p. 18)

Table 2.2. Common medical device applications of 316L stainless steel, cobalt-chromium alloys, and titanium based alloys. (p. 27)

Table 2.3. Mechanical properties of 316L stainless steel, cast and wrought cobalt-chromium alloy, Ti6Al4V, and human bone. (p. 28)

Table 2.4. Summary of the variation in ΔH, ΔS, and T for the spontaneity of a reaction based on the Gibbs free energy. (p. 38)

Table 2.5. The standard electrochemical / EMF Series. (p. 40)

Table 2.6. The chemical composition of normal human blood plasma. (p. 44)

Table 2.7. The Goldberg technique for scoring corrosion and fretting damage at the head-neck taper interface. (p. 85)

Table 3.1. Patient information and reasons for implant removal. (p. 124)

Table 3.2. Criteria for scoring the severity and area of corrosion and fretting damage. (p. 126)

Table 3.3. Frequency of heads and necks with signs of corrosion and fretting damage. (p. 128)

Table 3.4. The mean and standard deviations of the corrosion and fretting scores for the heads and necks. Significant statistical differences were found in the head corrosion scores between: companies A and B for the 28 mm heads; companies A and B for the 36 mm heads; and the 28 and 36 mm heads. (p. 129)

Table 4.1. Mechanical properties of CoCr and Ti6Al4V. (p. 144)

Table 4.2. The maximum von Mises stress at the head-neck taper interface. (p. 154)

Table 5.1. The average corrosion and fretting scores for the head and neck tapers. (p. 171)

Table 5.2. The average corrosion and fretting scores on the medial and lateral sides of the prostheses that received out of axis fatigue loading. (p. 171)

Table 5.3. The average corrosion and fretting scores on the superior and inferior regions of the head-neck taper interface. (p. 171)

Table 5.4. The volumetric wear damage of the head and neck tapers after receiving out of axis fatigue loading. (p. 173)

Table 6.1. Summary of the literature with respect to if the femoral head influences head-neck taper corrosion. (p. 184 – 185).

Table 6.2. Head-neck taper interface material combinations simulated by Zou et al. (p. 189)

Table 6.3. Summary of the finite element analysis of the head-neck taper interface for the *in vitro* corrosion fatigue testing experiments. (p. 191)

Table 6.4. The corrosion scores of the head-neck taper interface separated by the superior and inferior regions from the *in vitro* corrosion fatigue testing experiment. (p. 194)

Table 6.5. The fretting scores of the head-neck taper interface separated by the superior and inferior regions from the *in vitro* corrosion fatigue testing experiment. (p. 194)

Table 6.6. Corrosion scores of the head and neck tapers from the retrieval analysis separated by the superior and inferior regions. (p. 195)

Table 6.7. Fretting scores of the head and neck tapers from the retrieval analysis separated by the superior and inferior regions. (p. 196)

Table 6.8. Corrosion scores of the head and neck tapers from the retrieval analysis separated by the opposing quadrants. (p. 196)

Table 6.9. Fretting scores of the head and neck tapers from the retrieval analysis separated by the opposing quadrants. (p. 196)

Table B1. Convergence of displacement and maximum von Mises stresses when varying the head size for the single alloy material combination (12/14 mm taper with 4000 N assembly force). (p. 224)

Table B2. Convergence of displacement and maximum von Mises stresses when varying the head size for the mixed materials combination (12/14 mm taper with 4000 N assembly force). (p. 225)

Table B3. Convergence of displacement and maximum von Mises stresses for the different taper sizes (44 mm femoral head with a 4000 N assembly force). (p. 226)

Table B4. Convergence of displacement and maximum von Mises stresses when varying the assembly force (44 mm femoral head with a 4000 N assembly force). (p. 227)

Table B5. Convergence of displacement and maximum von Mises stresses when varying the distance between the centre of the femoral head and the centre of the neck taper (44 mm femoral head with a 4000 N assembly force). (p. 228)

Table B6. Convergence of displacement and maximum von Mises stresses when varying the angle of loading during the compression phase. (p. 229)

List of Figures

Figure 1.1. An assembled THA prosthesis with a metal-on-polyethylene articulation. (p. 3)

Figure 1.2. The disassembled head-neck taper interface of a THA prosthesis. (p. 3)

Figure 2.1. Anatomy of the femur (SAWBONES™ model). (p. 10)

Figure 2.2. Anatomy of the pelvis (SAWBONES™ model). (p. 11)

Figure 2.3. Anatomy of the acetabulum (SAWBONES™ model). (p. 11)

Figure 2.4. The THA prosthesis with a metal-on-polyethylene articulation. (p. 15)

Figure 2.5. The neck length and offset of the neck segment of a THA prosthesis. (p. 20)

Figure 2.6. Migration of chloride anions to the metal cations to form metal chlorides. (p. 49)

Figure 2.7. A scanning electron microscopy image of intergranular corrosion along the neck taper. Grains have been disintegrated from the CoCr alloy. (p. 54)

Figure 2.8. Schematic of pitting corrosion. (p. 55)

Figure 2.9. Pitting corrosion damage along a CoCr neck taper. (p. 56)

Figure 2.10. Summary of the outcomes of THA prostheses due to the onset of corrosion and fretting. (p. 67)

Figure 2.11. The three regimes of fretting. (p. 76)

Figure 2.12. The Stribeck curve. (p. 103)

Figure 2.13. The conical half angle for a taper. (p. 110)

Figure 2.14. The three locking mechanisms for the head-neck taper interface: A) zero-mismatch; B) positive mismatch (bottom-locking); C) negative mismatch (top-locking). (p. 111)

Figure 3.1. Scanning electron microscopy (SEM) images of CoCr alloy heads and necks that were not implanted in comparison to implants with little, moderate, and severe

corrosion damage. A) SEM of a CoCr alloy neck that has not been implanted. B) Arrows pointing to machining grooves for a CoCr alloy head with little corrosion and fretting damage. C) Arrow pointing to etching marks from fretting for a CoCr alloy head with moderate corrosion and fretting damage. D) Neck of a CoCr alloy stem with significant corrosion and fretting damage. (p. 122)

Figure 3.2. The relationship between the head and neck for A) corrosion damage and B) fretting damage. (p. 130)

Figure 3.3. The relationship between corrosion and fretting damage along the heads. (p. 131)

Figure 3.4. The relationship between corrosion and fretting damage along the necks. (p. 132)

Figure 3.5. The toggling torque of the femoral head during out of axis loading. (p. 135)

Figure 4.1. A) The head-neck taper interface subjected to assembly, compression, and tension loading. B) Overhead view of the semi-circular region for the assembly force. C) Axial assembly force being applied to the femoral head. D) Out of axis compression force being applied to the femoral head. (p. 143)

Figure 4.2. The displacement of the femoral head onto the neck taper when modifying: A) the femoral head size and the material combinations of the head-neck taper interface; B) the assembly force; C) the taper size; and D) the distance between the centre of the femoral head to the centre of the neck taper. (p. 148 – 149)

Figure 4.3. The micromotion of the centre of the engaged head taper during the compression phase when modifying: A) the femoral head size and the material combinations of the head-neck taper interface; B) the assembly force; C) the taper size; D) the distance between the centre of the femoral head to the centre of the neck taper; and E) the angle of loading. (p. 151 – 153)

Figure 4.4. The von Mises stresses (MPa) of the femoral head and neck during: A) the assembly phase as the force is applied in the direction of the long axis of the neck taper; B) the recovery phase; C) the compression phase where 3300 N of force is directed towards the femoral head 30° away from the long axis of the neck taper; and D) the tension phase where 100 N of force is applied 30° away from the long axis of the neck taper. (p. 156)

Figure 5.1. A close-up of the apparatus prior to fatigue testing: A) frontal view; B) side view. (p. 168).

Figure 5.2. Corrosion and fretting damage of the head and neck tapers after fatigue testing for a 28 mm femoral head that received out of axis fatigue loading. A) Neck taper on

the medial side. B) Neck taper on the lateral side. C) Femoral head taper on the medial side. D) Femoral head taper on the lateral side. (p. 172)

Figure 5.3. Corrosion and fretting damage of the head and neck tapers after fatigue testing for a 36 mm femoral head that received out of axis fatigue loading. A) Neck taper on the medial side. B) Neck taper on the lateral side. C) Femoral head taper on the medial side. D) Femoral head taper on the lateral side. (p. 172)

Figure 5.4. Corrosion and fretting damage of a neck taper (A) and the corresponding 36 mm femoral head taper (B) after axial fatigue loading. (p. 172)

Figure 5.5. Scanning electron microscopy images of: A) a pristine neck taper that did not receive an assembly force or undergo fatigue testing; B) a neck taper from a 28 mm femoral head subjected to out of axis fatigue loading; C) a neck taper from a 36 mm femoral head that underwent out of axis fatigue loading; D) a neck taper from a 36 mm femoral head subjected to axial fatigue loading. (p. 173)

Figure 5.6. The toggling torque of the femoral head during out of axis loading. (p. 176)

Figure A1. The 28 mm femoral head. (p. 211)

Figure A2. The 36 mm femoral head. (p. 212)

Figure A3. The 44 mm femoral head. (p. 213)

Figure A4. The 10/12 mm neck taper. (p. 214)

Figure A5. The 12/14 mm neck taper. (p. 215)

Figure A6. The 14/16 mm neck taper. (p. 216)

Figure A7. The 44 mm femoral head (the femoral head is 3 mm below the centre of the neck taper). (p. 217)

Figure A8. The 44 mm femoral head (the femoral head is 1 mm below the centre of the neck taper). (p. 218)

Figure A9. The 44 mm femoral head (the centre of the femoral head is aligned with the centre of the neck taper). (p. 219)

Figure A10. The 44 mm femoral head (the femoral head is 1 mm above the centre of the neck taper). (p. 220)

Figure A11. The 44 mm femoral head (the femoral head is 3 mm above the centre of the neck taper). (p. 221)

Figure A12. The 44 mm femoral head (the femoral head is 7 mm above the centre of the neck taper). (p. 222)

List of Abbreviations

$\mu A/cm^2$	Microamps per Centimetre Squared
µg	Micrograms
µg/L	Micrograms per Litre
µm	Micrometres
λ	Heresy Number
AA	Antibiotic/Antimyocyotic
Ag	Silver
Al	Aluminum
Al_2O_3	Aluminum Oxide
ALTR	Adverse Local Tissue Reaction
ALVAL	Aseptic Lymphocyte Dominated Vasculitis Associated Lesions
ASTM	American Society for Testing and Materials
Au	Gold
Ca	Calcium
Cl	Chloride
cm	Centimetre
CMM	Coordinate Measuring Machine
Co	Cobalt
CoCr	Cobalt Chromium
CoCrMo	Cobalt Chromium Molybdenum
Cr	Chromium

CrN	Chromium Nitride
Cr_2O_3	Chromium (III) Oxide
Cu	Copper
D	Displacement
DMEM	Dulbecco's Modified Eagle's Medium
e	Electron
EDS	Energy Dispersive X-ray Spectroscopy
EDTA	Ethylenediaminetetra Acetic Acid
Fe	Iron
FEA	Finite Element Analysis
GPa	Gigapascals
g/cm^3	Grams per Centimetre Cubed
g/L	Grams per Litre
H	Hydrogen
H^+	Proton
HLA	Horizontal Lever Arm
H_2O	Water
H_2O_2	Hydrogen Peroxide
HCO_3^-	Bicarbonate
H_2PO4^-	Dihydrogen Phosphate
Hv	Vickers Hardness Number
Hz	Hertz
ISO	International Organization for Standardization

K	Potassium
kg	Kilogram
kV	Killivolts
Li	Lithium
M	Metal Atom / Molar
M^+	Metal Cation
Mg	Magnesium
Mixed	CoCr Femoral Head Assembled to a Titanium Alloy Stem
mm	Millimetres
mm/s	Millimetres per Second
Mo	Molybdenum
MPa	Megapascals
mV	Millivolts
N	Newtons
n	Number
Na	Sodium
NaCl	Sodium Chloride
Nb	Niobium
Nm	Newton Metres
Nmol/L	Nanomoles per Litre
O	Oxygen
OH^-	Hydroxide
P	Phosphorus

Pb	Lead
PBS	Phosphate Buffered Saline
PE	Polyethylene
pH	Power of Hydrogen
PMMA	Polymethylmethacrylate
P	Phosphorus
Pt	Platinum
PTFE	Polytetrafluoroethylene
Redox	Oxidation-Reduction
Rq_{mat}	Mean Square Surface Roughness
SEM	Scanning Electron Microscopy
SF-12	Short Form 12
T	Tangential Force
THA	Total Hip Arthroplasty
Ti	Titanium
Ti6Al4V	Titanium 6% Aluminum 4% Vanadium Alloy
Ti6Al7Nb	Titanium 6% Aluminum 7% Niobium
TiO_2	Titanium Dioxide
TKA	Total Knee Arthroplasty
TMZF	Titanium Molybdenum Zirconium Iron
UHMWPE	Ultra High Molecular Weight Polyethylene
Zn	Zinc

List of Symbols

α	Statistical Significance Level
μ	Coefficient of Friction
μ_K	Coefficient of Kinetic Friction
μ_S	Coefficient of Static Friction
λ	Lubrication Number
ρ	Spearman Rank Correlation Coefficient
$<$	Less Than
$\leq$	Less Than or Equal to
$>$	Greater Than
$\geq$	Greater Than or Equal to
$=$	Equals
ΔE	Potential Difference
ΔG	Change in Gibbs Free Energy
ΔH	Change in Enthalpy
ΔS	Change in Entropy
º	Degrees
ºC	Degrees Celsius
•	Free Radical
’	Minutes
”	Seconds
+	Positive Offset

-	Negative Offset
±	Standard Deviation
E°	Potential Difference of the Reaction Under Standard State Conditions
F	Faraday's Constant
F_f	Friction Force
F_K	Kinetic Friction Force
F_N	Normal Friction Force
F_S	Static Friction Force
$F_{S, max}$	Maximum Static Friction Force
F_x	Force in the x-direction
F_y	Force in the y-direction
F_z	Force in the z-direction
G	Gibbs Free Energy
g	Acceleration due to Gravity
H	Enthalpy
K_{eq}	Equilibrium Constant
m	Mass
p	p - Value
R	Ideal Gas Constant
S	Entropy
T	Temperature (Kelvin)
W	Gravitational Force
z	Central Film Thickness

List of Copyrighted Material

Chapters three and four were accepted for publication in the Journal of Arthroplasty and Tribology International, respectively:

R. M. R. Dyrkacz, J. M. Brandt, O. A. Ojo, T. R. Turgeon, and U. P. Wyss, "The influence of head size on corrosion and fretting behaviour at the head-neck interface of artificial hip joints," *Journal of Arthroplasty*, vol. 28, pp. 1036-1040, 2013.

R. M. R. Dyrkacz, S. T. O'Brien, J. M. Brandt, J. B. Morrison, O. A. Ojo, T. R. Turgeon, and U. P. Wyss, "Finite element analysis at the head-neck taper interface of modular hip prostheses," *Tribology International*, currently in press, 2015.

Author’s Declaration

I, Richard Michael Ryan Dyrkacz, hereby declare that the entire result presented in this thesis is the sole product of my work under the supervision and approval from my supervisors and examiners.

I am aware that my thesis may be made electronically available to the public.

Chapter 1 – Introduction

1.1 General Overview

Metals are commonly used as materials in modern medicine to repair and replace anatomical structures. A popular application of metals in medicine is bone replacement and repair with some examples including fracture plates, screws, and staples. Metals are also employed in other realms of medicine such as dentistry and are used for designing components of various medical devices such as artificial hearts, pacemakers, and catheters.

One of the most commonly practiced orthopaedic operations worldwide is total hip arthroplasty (THA). THA is a surgical procedure to implant an artificial hip joint into a patient that replaces the femoral head and acetabulum. Metals are commonly used as a material to design artificial hip joints because of their superior mechanical strength.

Recently, the number of THA procedures has substantially increased and current trends indicate that THA procedures will further increase with time. The main reason is due to an aging baby boomer population [1]. Additionally, the incidence of obesity is increasing and it is estimated that 65% of the U.S. population is overweight [1]. If a patient has excessive body weight, this can gradually deteriorate the hip joint over time.

THA operations are relatively expensive. In 2009, there were 284,708 operations performed in the U.S. that resulted in a net cost of $4.48 billion [2]. Kurtz et al. projected

that there were 208,600 primary THA procedures performed in the U.S. during 2005 and that this number would increase to 572,000 by 2030 [3]. On a related topic, a revision surgery is a procedure where the surgeon removes and replaces a problematic prosthesis. In regard to THA revisions performed in the U.S., Kurtz et al. indicated that there were 40,800 revision surgeries in 2005 and predicted that there would be 96,700 by 2030 [3].

Metals are generally susceptible to two types of failure. The first is mechanical failure, which is a bulk issue since the material's mechanical properties are determined by its flaws. However, metals can be subjected to chemical failure, particularly corrosion. Corrosion is a process in which a material degrades, deteriorates, or gets destroyed due to its interaction with the surrounding environment [4]. In regard to THA prostheses, corrosion is a significant issue caused by the harsh physiological environment of the human body. By having a corroded THA prosthesis, the patient may experience pain, hypersensitivity to metals, adverse tissue reactions, and may require the implant to be removed.

1.2 Objectives, Research Methodology, and the Significance of the Research

Although THA is generally considered to be a highly successful operation, corrosion is a significant issue that can affect the longevity of the prosthesis and can have harmful consequences to the patient. Metal ions and particles from a THA prosthesis can

get released into the patient's body by wear or corrosion and may result in pain, hypersensitivity, adverse local tissue reactions, and revision surgery.

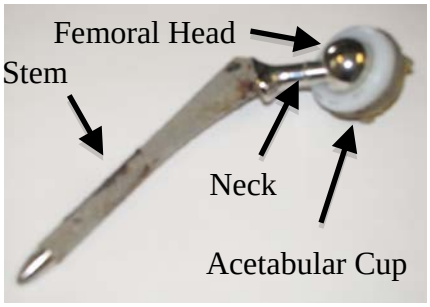

Figure 1.1. An assembled THA prosthesis with a metal-on-polyethylene articulation.

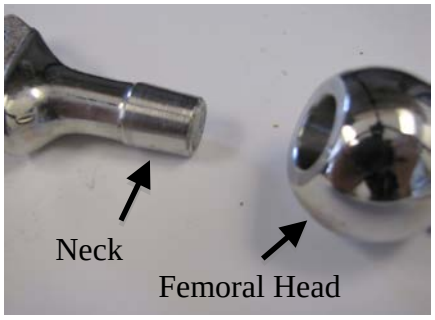

Figure 1.2. The disassembled head-neck taper interface of a THA prosthesis.

In regard to THA prostheses, corrosion primarily occurs at the head-neck taper interface. Corrosion can occur at the neck-stem taper interface if there is modularity at this region. The head and neck interlock with each other and are held together by frictional forces. Through this taper connection, the head and neck are capable of withstanding significant tensile, compressive, and torsional loads [5]. In practice, surgeons commonly use femoral head sizes of 28 mm, 32 mm, or 36 mm. Some surgeons implant large femoral

heads (diameter ranges between 36 mm to 60 mm +) to increase the range of motion, improve stability, and to decrease the risk of dislocation [6]. The main disadvantage of large femoral head sizes is that there is an increase in stress along the articulating cup. In rare circumstances where a large femoral head has a metal-on-polyethylene articulation, this can lead to fracture of the polyethylene liner [7].

In the orthopaedic community, corrosion at the head-neck taper interface has been repeatedly reported [5, 8-16]. This is a growing concern and the orthopaedic community is looking for solutions to minimize head-neck taper corrosion. Researchers are currently trying to develop strategies to prevent head-neck taper corrosion from occurring.

The main objective of the research presented in this thesis was to determine if the size of the femoral head plays a role in head-neck taper corrosion for THA prostheses. To answer this question, the following steps were taken:

1. An extensive literature review was conducted to establish the mechanisms of how head-neck taper corrosion occurs for THA prostheses. Additionally, this literature review addresses how fretting is related to corrosion, how corrosion damage at the head-neck taper interface can be assessed, and some suggestions to prevent head-neck taper corrosion.
2. A retrieval analysis was carried out to determine if THA prostheses featuring 36 mm femoral heads display more corrosion damage at the head-neck taper interface than THA prostheses with a 28 mm femoral head. To achieve this, all of the femoral heads and stems were manufactured from one of two companies, consist-

ed of CoCr alloy, featured a 12/14 mm taper connection, had a metal-on-polyethylene articulation, and were implanted for at least one month.

3. Finite element models of the head-neck taper interface were developed to examine the micromotion between the femoral head and neck due to forces from activities of daily living. Besides measuring the micromotion due to head size, the following variables were also considered: the material combinations of the head-neck taper interface; the assembly force; the taper size; the distance between the centre of the femoral head to the centre of the neck taper; and the angle of loading.
4. Finally, an *in vitro* corrosion fatigue testing experiment was performed to verify if head-neck taper corrosion is influenced by the femoral head size and the angle of loading. The main advantage of this experimental study was to remove a number of variables that can influence head-neck taper corrosion that could not be removed in a retrieval analysis study such as the variations in implantation time, manufacturing brands, and the assembly force.

1.3 Scope of Work

This thesis consists of seven chapters and two appendices:

- Chapter 1 is an introduction to the research described in this thesis as well as the methodology performed to achieve the objectives, a discussion why this research was performed, and summarizes the shape of the work that is presented.
- Chapter 2 summarizes the literature pertaining to head-neck taper corrosion of THA prostheses. There are three goals of this literature review. First, this literature review attempts to provide the reader a sufficient background to further understand the problem this thesis explores. Second, this literature review provides a summary of what is known about corrosion and fretting damage with respect to the head-neck taper interface of THA prostheses. Finally, this literature review attempts to show the gaps of knowledge in regard to head-neck taper corrosion of THA prostheses.
- Chapter 3 describes a retrieval analysis that was performed which consists of 74 THA prostheses. The goal of this retrieval analysis was to determine if THA prostheses with 36 mm femoral heads have significantly more corrosion and fretting damage at the head-neck taper interface than THA prostheses with a 28 mm femoral head. The prostheses that were selected in this study were manufactured from one of two companies, had a 12/14 mm taper, consisted solely of CoCr alloy, featured a metal on polyethylene articulation, and had a minimum implantation time of one month. A novel scoring method was developed such that three researchers

evaluated the THA prostheses for macroscopic corrosion and fretting damage. Additionally, scanning electron microscopy and energy dispersive x-ray spectroscopy were performed to examine the microscopic damage and to characterize the corrosion products, respectively.

- Chapter 4 is an overview of a finite element analysis of the head-neck taper interface of THA prostheses. For this investigation, six variables were examined to determine their influence on the displacement during the assembly procedure, the micromotion at the head-neck taper interface during compression and tension, and the maximum von Mises stress at the head-neck taper interface. The six variables that were explored in this study include: the femoral head size; the material combinations; the assembly force; the taper size; the distance between the centre of the femoral head to the centre of the neck taper; and the angle of loading.
- Chapter 5 is a summary of an *in vitro* corrosion fatigue testing experiment that was performed to determine if 36 mm femoral heads have more head-neck taper corrosion damage than 28 mm femoral heads. For this study, 28 and 36 mm CoCr femoral heads were assembled onto 12/14 mm CoCr neck tapers. An axial assembly force of 2000 N was applied and the head-neck taper interface was subjected to ten million cycles of loading (300 N to 3300 N) at a frequency of 5 Hz in phosphate buffered saline at a maintained temperature of 37°C. Additionally, the angle of loading was modified (out of axis and axial loading) to determine if the toggling torque at the head-neck taper interface plays a role in head-neck taper corrosion.

- Chapter 6 contains a thorough discussion of the retrieval analysis, the finite element analysis, and the *in vitro* corrosion fatigue tests. This chapter emphasizes why the toggling torque is a critical factor that contributes to head-neck taper contribution and how it increases with a larger head size. Additionally, this chapter also discusses the conclusions that were arrived in this thesis and how they compare to the work done by other researchers in the field. This chapter summarizes the limitations of the research presented in this thesis and discusses the advantages of the novel technique that was developed to assess corrosion and fretting damage at the head-neck taper interface.
- Chapter 7 summarizes the results from the retrieval analysis, the finite element analysis, and the *in vitro* corrosion fatigue testing experiment and the novelty of the research discussed in this thesis. Finally, this chapter provides recommendations for future work that should be considered for preventing corrosion damage at the head-neck taper interface.
- Appendix A contains the schematic drawings of the head and neck tapers that were used for the finite element analysis described in Chapter 4.
- Appendix B displays the demonstration of convergence for the finite element analysis presented in Chapter 4.

Chapter 2 – Literature Review

2.1 Introduction

There are three goals of this literature review. The first is to provide the reader a sufficient background to further understand the problem this thesis explores. Second, this chapter summarizes the literature with respect to corrosion at the head-neck taper interface. Finally, this chapter addresses gaps in the literature with respect to what is known about corrosion at the head-neck taper interface.

2.2 Anatomy of the Hip Joint

The hip joint consists of a ball-and-socket configuration with three degrees of freedom and movement of the leg occurs along three planes: flexion-extension (sagittal plane); abduction-adduction (frontal plane); and internal-external rotation (transverse plane) [17]. As shown in Figure 2.1, the superior segment of the femur has a portion of bone that is partially spherical; this is the femoral head. The femoral head is covered by a layer of hyaline cartilage to achieve smooth movement with the acetabulum [18]. The hip

joint is able to achieve movement of the leg at the hip due to the articulation between the femoral head and the acetabulum. Inferior to the head and neck of the femur are the greater and lesser trochanter structures, which are involved in muscle attachment.

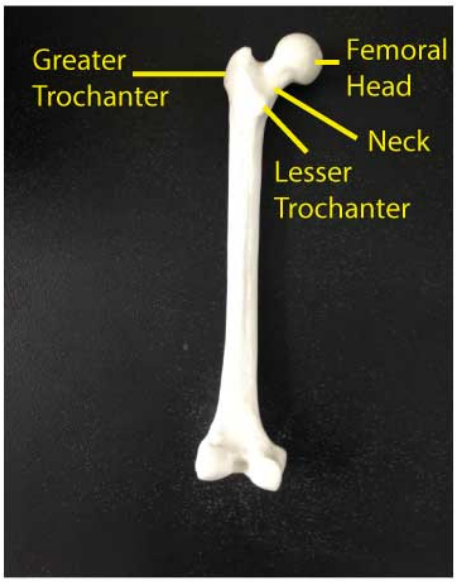

Figure 2.1. Anatomy of the femur (SAWBONES™ model).

The pelvis primarily consists of two mirror-image interconnected large bones (os coxae) where one segment is on the left-hand-side and the other segment is on the right-hand-side. These bones are united at the pubis symphesis, which is located at the anterior of the pelvis, as well as the sacrum, which can be found on the posterior of the pelvis as illustrated in Figure 2.2 [19]. The sacrum is a triangular-shaped bone located in the upper-back portion of the pelvis and supports the spine [19]. The two os coxae bones, the sacrum and the coccyx, make up the pelvic girdle.

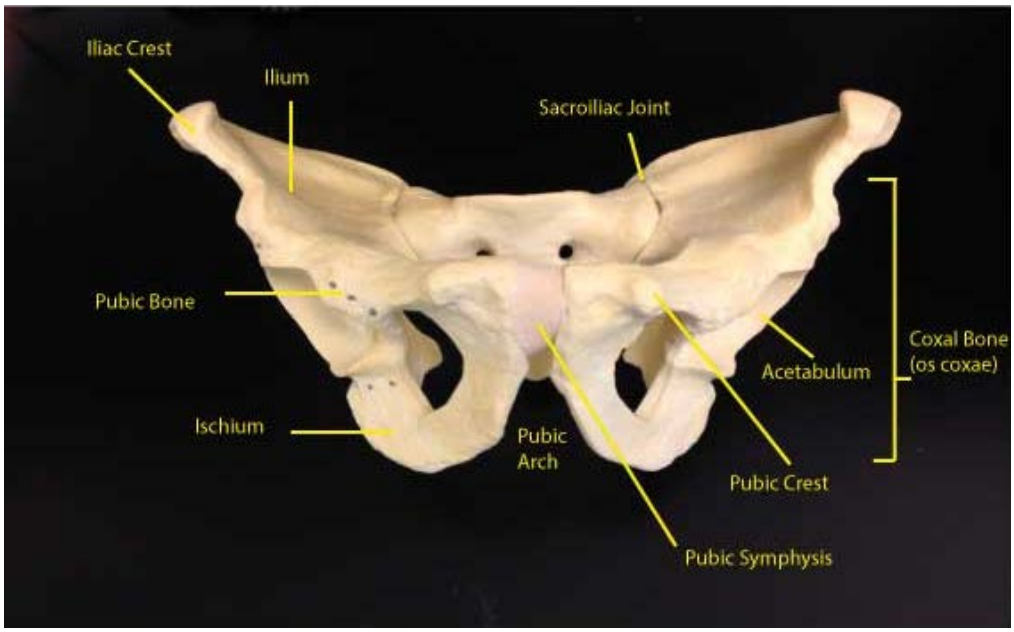

Figure 2.2. Anatomy of the pelvis (SAWBONES™ model) [20].

The acetabulum is a deep-socket structure of the pelvis as shown in Figures 2.2 and 2.3. The acetabulum is formed by the union of three pelvic structures: the ilium; the ischium; and the pubis [21].

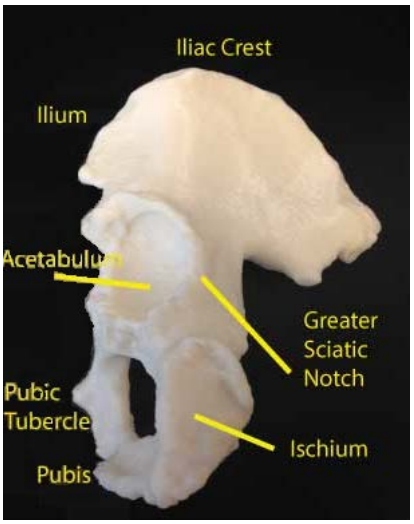

Figure 2.3. Anatomy of the acetabulum (SAWBONES™ model) [21].

2.3 Total Hip Arthroplasty

2.3.1 Patient Symptoms

There are a number of reasons why a patient may require an artificial hip joint. These reasons include: osteolysis; osteoarthritis; osteonecrosis; rheumatoid arthritis; fracture of the femoral neck; inflammatory arthritis; developmental dysplasia; Paget's disease; arthrodesis (fusion) takedown, tumours; road accidents; and injuries from war [22]. The following provides a brief description of some of these disorders.

Osteolysis – Osteolysis is the degeneration and dissolution of bone that may be caused by disease, infection, or ischemia. Osteolysis occurs when the bone matrix undergoes active resorption by osteoclasts during the formation of natural bone tissue. During osteolysis, bone gets deteriorated during the process of bone resorption due to the removal or loss of calcium [22]. Osteolysis may also be influenced by bone tumours, cysts, or chronic inflammation.

Osteoarthritis – Osteoarthritis is a cluster of disorders that can result in the structural and functional failure of joints along with a progressive loss in cartilage that may lead to bone cysts (an abnormal membranous sac containing fluid or semisolid material) [17, 23]. Osteoarthritis is common in the elderly, as well as patients with trauma or a

congenital abnormality of the hip joint [24]. At the hip joint, cartilage acts as a cushion between the femoral head and the acetabulum. When osteoarthritis occurs at the hip joint, the femoral head and/or the acetabulum become deformed, which can result in pain due to increased friction at the articulation site [22].

Osteonecrosis – Osteonecrosis is a disease that involves cellular death in bone tissue that can be caused by an inadequate supply of blood, injury, or disease [22, 25]. With the progression of osteonecrosis, the bone structures forming the hip joint may collapse [22]. Osteonecrosis can be contributed to a number of factors such as alcoholism, drugs, and fracture of the hip [25].

Rheumatoid Arthritis – Patients with rheumatoid arthritis suffer from a chronic systematic condition that may result in joint pain, swelling, and stiffness throughout the synovial joints [26]. Inflammation occurs along the lining of the joint, which produces chemical changes in the synovial fluid so it becomes thicker [22]. By having a change in the synovial fluid's composition, this can deteriorate cartilage and make movement of the hip joint painful [22].

Developmental Dysplasia – Developmental dysplasia is a condition where the femoral head has inappropriate contact with the acetabulum that can result in dislocation (luxation), partial dislocation (subluxation), or hip instability such that the femoral head pops in and out of the socket [22]. For most patients, developmental dysplasia is not pre-

sent at birth and progresses with time; hence, the term developmental is used in comparison to congential [22].

Arthrodesis (Fusion) Takedown – Arthrodesis occurs when there is fusion along the articulation site. This increases bone cell proliferation to achieve stability that is relatively painless [22].

2.3.2 The Modern Total Hip Arthroplasty Prosthesis

The purpose of the artificial hip joint is to minimize the patient's pain at the hip joint and improve the functional outcome while achieving the lowest complication rate [27, 28]. There are currently more than a million artificial hip joint procedures performed worldwide each year [29]. These procedures are becoming more common in younger patients; however, most procedures are performed on patients over the age of 60 [24].

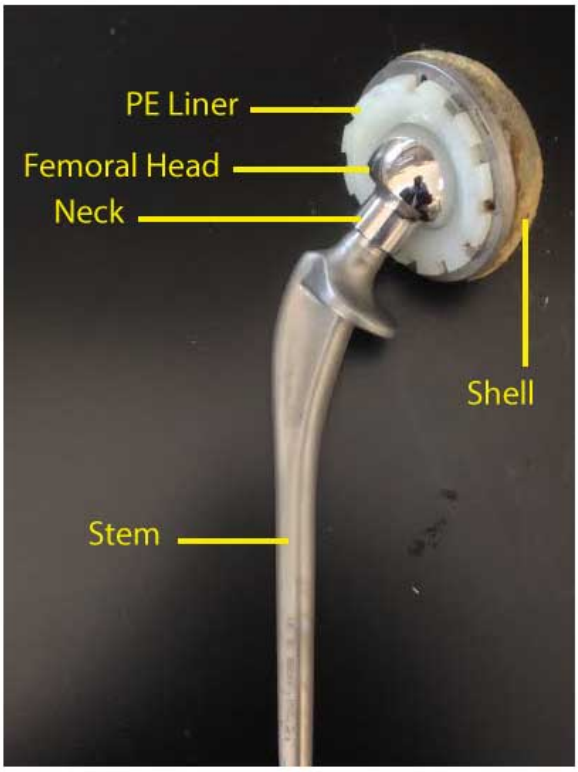

Figure 2.4. The THA prosthesis with a metal-on-polyethylene articulation.

Hip arthroplasty procedures can be classified into two categories: total hip arthroplasty (THA) [30] and hemiarthroplasty [31]. In a THA procedure, the surgeon will replace the femoral bone stock (femoral head and neck) with a metal or ceramic femoral head [24]. This artificial femoral head is attached to the stem component, which is inserted into the femur. The femoral head and stem can be a single component or consist of two separate components, otherwise known as a modular hip prosthesis. Modular hip prostheses are assembled during surgery using impact forces from surgical hammer blows. The stem can be fixed to the femur using a cement compound or through a frictional fit [24]. Additionally, a cup that is made of metal, ceramic, or a plastic is press-

fitted into the acetabulum and articulates with the femoral head [24]. With hemiarthroplasty, the surgeon replaces one-half of the hip joint with a prosthesis and leaves the other aspect in its natural state without alterations (e.g. replace the femoral head and leave the acetabulum or replace the acetabulum and leave the femoral head) [31].

As reported by the Canadian Institute for Health Information, the following is the breakdown of the different types of hip prostheses, sorted by articulation type, for patients within Canada [32]:

- 73% for metal-on-polyethylene
- 9% for metal-on-metal
- 8% ceramic-on-ceramic
- 5% ceramic-on-polyethylene

During 2005 to 2008, approximately 35% of THA procedures performed in the U.S. consist of a metal-on-metal bearing articulation [33]; however, implanting metal-on-metal THA prostheses has sharply declined over the past few years. Metal-on-metal THA bearings were reintroduced in 1997 to reduce the occurrence of osteolysis, have less volumetric wear in comparison to metal-on-polyethylene bearing articulations, and were aimed at younger patients with the notion that these prostheses could last a lifetime [34-36]. However, metal-on-metal THA prostheses have been reported to have three times the failure rate of metal-on-polyethylene THA prostheses, which is attributed to edge wear and an increased bearing torque [37]. By having greater wear and loading at the head-

neck taper interface, metal ions and corrosion products can be released to the patient's body [37]. As a consequence, this can lead to adverse local tissue reactions (ALTRs) [36]. Table 2.1 provides a summary of the advantages and disadvantages of the different articulation types for THA prostheses.

Table 2.1. The advantages and disadvantages of THA prosthesis articulations.

Articulation Type	Advantages	Disadvantages
Metal-on-Polyethylene	• Cost-effective • Design with the most experience • Most common THA prosthesis in Canada [32]	• Can produce polyethylene particles that can result in osteolysis • High wear volume • Aseptic loosening • Recommended for elderly patients • If the femoral head penetrates the PE liner, this can reduce the range of motion • Vulnerable to pitting damage (not corrosion but from third body wear particles)
Metal-on-Metal	• Aimed for younger patients [34-36] • Low volumetric wear rate [34-36] • Improves stability with a large femoral head	• Can generate metal particles that can enter the bloodstream and surrounding tissues • The patient may experience pain, hypersensitivity, and ALTRs [38] • Greater revision rates than hip resurfacing arthroplasty [34] and THA prostheses with a ceramic on polyethylene articulation [39] • Up to three times the failure rate of metal on polyethylene THA prostheses due to edge wear and an increased bearing torque [37]
Ceramic-on-Ceramic	• Corrosion resistant • Low wear rate • Scratch resistant • Low surface roughness • High wettability • Good lubrication	• Vulnerable to fracture • Most expensive articulation for a THA prosthesis • May generate third body wear • Squeaking may occur
Ceramic-on-Polyethylene	• Reduced wear rate in comparison to metal- on-polyethylene • The elasticity of UHMWPE decreases the fracture risk of the ceramic femoral head	• Residual polyethylene wear with late risk of aseptic loosening [40] • Vulnerable to fracture

The Morse taper concept was introduced to hip prostheses in Germany in 1974 [41, 42]. This design allows intimate contact between the neck, or trunnion, of the femoral stem (male component) and the bore of the head (female component) [43]. The 12/14 mm 5° 43’ 30” taper is considered to be the gold standard for THA prostheses [44, 45]. There are currently more than 30 types of head-neck taper interfaces for THA prostheses and there is no form of standardization for designing and manufacturing the head-neck taper interface [46]. The taper interface can vary due to the following parameters: proximal diameter; distal diameter; taper length; angle; manufacturing tolerances; surface finish; and surface treatment [46]. This taper is successful because the head-neck taper interface has excellent resistance to rotator and distractive stresses. Standardization of the head-neck taper connection is critical to the survival of THA prostheses; however, neck tapers are not standardized and vary in terms of length, the base dimension, and the taper angle [43]. By having an angular mismatch, this can result in substantial fretting damage and may lead to revision surgery. Additionally, many necks are threaded. These threaded surfaces may not be uniformly patterned which can result in variations in terms of thread height, pitch, and surface roughness [43]. Consequently, these variations can affect the micromotion at the head-neck taper interface; thus, potentially playing a role in fretting and corrosion damage [47].

Modular hip prostheses are advantageous for many reasons. For instance, the surgeon can adjust the leg length and hip stability of the patient during surgery by modifying the neck length, the inventory size will decrease, and the femoral stem can be implanted prior to the insertion of the acetabular component [5, 13]. Other advantages include increased flexibility during surgery, reduced costs, the use of different materials for the fix-

ation and articulation [5, 13], and the femoral head can be removed to allow exposure of the acetabulum during revision surgery [42]. Some of the potential disadvantages of modular hip prostheses include: wear debris production; periprosthetic bone resorption; and aseptic loosening due to osteolysis [48-50].

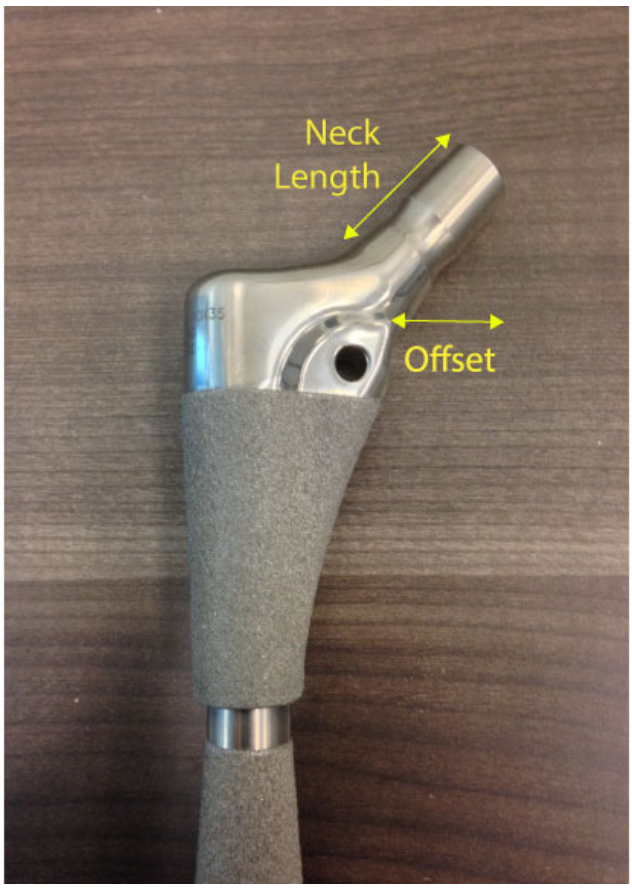

Figure 2.5. The neck length and offset of the neck segment of a THA prosthesis.

The neck offset is the horizontal distance from the centre of the base of the neck to the centre of the tip of the neck [51]. Meanwhile, the neck length is the hypotenuse of the offset and the vertical height from implant shoulder to tip centre [51].

Càles reported that the distance between the top of the neck taper to the ceiling of the head taper can affect the tensile stress distribution [44, 52]. As this distance decreases, the tensile stresses increase at the head-neck taper interface. From this, the recommended distance should be at least 1.5 millimetres or greater.

Recently, manufacturers have introduced dual modular THA prostheses in which there is not only a modular head-neck taper interface, but there is also a modular neck-stem taper interface. By having a modular neck-stem taper interface, this allows the surgeon to adjust the offset, version, and limb length; thus, making the prosthesis more customized to the patient [53]. One of the original double taper stems is the Profemur Z, which has been reported with a large number of failures at the neck-stem taper interface., particularly corrosion and fretting.

2.3.3 Femoral Head Size

John Charnley originally intended that his THA prosthesis design would have a head size of 41.5 mm [54]. Later, Charnley discovered problems when he placed the femoral heads against a liner made of PTFE (polytetrafluoroethylene). Charnley then decided to reduce the size of the femoral head to 22.25 mm [55] because of the limited availability of polymeric materials to orthopaedic surgeons. As a result, femoral head sizes between 22 to 32 mm were universally accepted for over 50 years [54].

The concept of implanting large femoral heads was introduced in 2003 as a solution to treat femoral neck fractures in metal-on-metal hip resurfacing prostheses when the

acetabular component was well-fixed [56]. These prostheses had a 12/14 mm head-neck taper interface and were considered advantageous because of the low incidence of dislocation and had a reduced wear rate [56]. The main advantage of large femoral heads is that they are closer in anatomical size to the femoral head and can provide the patient with an increased range of motion [54].

Many THA prostheses have a limited range-of-motion because of component-to-component impingement [54]. This problem is commonly found in smaller head sizes [57], especially those that feature skirts [58]. Burroughs et al. reported that head sizes of 38 mm to 46 mm provide a greater range-of-motion than head sizes of 32 mm or less [54]. Because the range-of-motion is increased, larger femoral heads reduce the possibility of dislocation. Queen et al. found that 18 months after surgery, patients with a THA prosthesis with a head size greater than 36 mm display abnormal flexion and extension while climbing stairs [59].

Smaller femoral heads are also more susceptible to dislocation because these heads are countersunk into the polyethylene liner to deepen their position. To achieve this, a chamfer is required on the polyethylene liner to prevent the reduction in the range-of-motion from component-to-component impingement. However, the chamfer can increase the chances of dislocation if the femoral head achieves a metastable position. Meanwhile, femoral head sizes with a diameter greater than 32 mm have increased stability without requiring a deepened position into the polyethylene [54].

Burroughs et al. conducted an *in vitro* study to observe how head size and the head-neck length affects the range-of-motion [60]. This experiment was performed using

an anatomical goniometer that tested 28 mm, 32 mm, 38 mm, and 44 mm diameter femoral heads within a 61 mm acetabular shell. For each femoral head size, there were five neck lengths. Burroughs et al. discovered that the 38 mm and 44 mm heads had more range-of-motion than the 28 mm and 32 mm heads for all angles tested. The greatest difference in the range-of-motion prior to impingement occurring was between the 38 mm and 44 mm heads versus the 28 mm and 32 mm heads that had a skirt (+7 mm and +10.5 mm neck lengths). Additionally, increasing the head-neck length resulted in increased flexion as well as internal rotation at 90° of flexion before impingement.

Zijlstra et al. conducted a randomized clinical study to observe if metal-on-metal THA prostheses with an average head diameter of 48 mm improved the patient's range-of-motion one year post-operatively in comparison to THA prostheses with a 28 mm femoral head and a metal-on-polyethylene articulation [61]. Each group consisted of 25 patients. Zijlstra et al. reported that after one year, the large head size cohort had a greater improvement in internal rotation (14°) versus the small head size group (7°); however, the standard error measurement was 4°. Meanwhile, there were no significant differences between the two head size groups when measuring external rotation, flexion, extension, abduction, and adduction. From this study, Zijlstra concluded that larger heads may not necessarily enhance the patient's range-of-motion. Similar to Zijlstra et al., Allen et al. reported that with larger head sizes, there was no significant difference in the patients' functional outcome after a 12 month post-operative period; however, the dislocation rate decreased with head size [62]. Cooper et al. also speculated that there could be a link between dislocation and head-neck taper corrosion [63].

According to the National Joint Registry for England and Wales [56], as well as some independent centers in the United Kingdom [64], the revision rate for large head metal-on-metal THA prostheses was 7.8% at five years. Bolland et al. reported a revision rate of 8.5% at five years and proposed that this high failure rate may be attributed to the mismatch between the head and neck [56].

Unfortunately, metal-on-metal THA implants with large femoral heads yield poor revision rates. For instance, the revision rate at seven years was 13.6% as reported by the National Joint Registry for England and Wales [65] as well as the Australian Orthopaedic Association [66].

The Australian Orthopaedic Association National Joint Replacement Registry reported in 2010 that metal-on-metal THA revision rates substantially increased when the head size was greater than 32 mm [34]. Additionally, the Canadian Institute for Health Information reported that patients with a metal-on-metal THA prosthesis with a large femoral head have a 5.9% chance of undergoing revision surgery within five years whereas 2.7% of patients with a metal-on-polyethylene THA prosthesis would require revision surgery [32]. Similarly, the 2010 England Wales National Joint Registry reported that the revision rate of large head diameter metal-on-metal THA prostheses at five years was 7.8% [67]. One of the main reasons for this is that large femoral heads can generate more volumetric wear regardless of the articulating material [68-70]. In particular, polyethylene cups in particular have been known to be vulnerable to excessive wear and periprosthetic osteolysis [60].

Large femoral heads are not suitable for all patients. Some patients may have a small acetabular bone stock which would not support a femoral head with a diameter greater than 32 mm while achieving a minimum 5 mm thickness for the corresponding polyethylene liner [54]. In terms of selecting the femoral head size, smaller heads are generally chosen for patients who are elderly, have a light frame, and/or are female [62].

Bolland et al. conducted a mid-term clinical study of large head metal-on-metal THA prostheses and attempted to identify potential sites of failure from retrieval analyses and to identify factors that could be linked to revision surgery [56]. This study consisted of 199 hips (185 patients) with a mean follow-up period of 62 months. Bolland et al. observed that patients with a large head diameter metal-on-metal THA prosthesis who had undergone or were awaiting revision surgery had significantly elevated concentrations of cobalt in comparison to the non-revision cohort [56]. Of the 17 patients who had undergone revision surgery, 14 patients had an ALTR. Bolland et al. observed corrosion and wear damage at the head-neck taper interface as well as corrosion damage along the stem surface.

Langton et al. commented that three key factors may contribute to these poor revision rates: the trunnion dimensions; trunnion surfaces; and the femoral head size [71].

1. Trunnion Dimensions: By reducing the length of the trunnion, the trunnion's base rests within the taper, which can lead to edge loading [71]. By reducing the taper size (e.g. 14/16 mm to 12/14 mm), this leads to less surface area to

achieve a sufficient interference fit. This can increase the risk of micromotion, which can lead to the risk of fretting and corrosion.

2. Trunnion Surfaces: Many modern trunnions are rigged to accommodate ceramic and metallic femoral heads [71]. However, the machining grooves can lead to an imprint on the metallic femoral heads. This plastic deformation can contribute to increased contact stresses and wear damage. Consequently, the localized pits may allow corrosion to occur over a larger surface area.

3. Large Head Sizes: The concept of implanting large heads was introduced to achieve less wear damage, reduce the risk of dislocation, and improve the patient's range-of-motion [71]. Currently, there are at least a million large head diameter metal-on-metal THA prostheses implanted worldwide [35]. However, a larger head size increases the horizontal lever arm, which has been known to increase the wear rate [71].

Large diameter femoral heads ranging from 38 mm to 58 mm provide head-to-neck ratios and jumping distances that exceed the physiologic range of motion at the hip joint [72]. The head-to-neck ratio is critical for improving the range-of-motion due to component-to-component impingement. By using larger femoral heads, this is the most direct technique to improve the head-to-neck ratio [54].

When designing a hip prosthesis that features a large femoral head, sleeves may be used so the femoral head contacts the neck. However, micromotion can occur between the neck-sleeve interface, which can lead to wear and corrosion damage [73].

2.4 Metallic Materials used in Total Hip Arthroplasty

For over a century, scientists have implanted a wide variety of metals into the human body to treat several ailments [74]. Metals such as aluminum, copper, magnesium, carbon steels, iron, nickel, silver, and zinc have been implanted inside the human body [74]. Unfortunately, all of these metals are known to be too reactive and/or toxic in the human body when implanted for long-term use [74].

Most metals in modern medicine currently consist of three alloys: cobalt-chromium (CoCr) alloys; titanium alloys (particularly Ti6Al4V); and 316L stainless steel [75]. These three alloys are used in a variety of applications. Table 2.2 lists some common applications of these materials [74] whereas Table 2.3 lists their mechanical properties in comparison to bone [74, 76].

Table 2.2. Common medical device applications of 316L stainless steel, cobalt-chromium alloys, and titanium based alloys [74].

Material	Applications
316L Stainless Steel	Joint replacement prostheses, orthopaedic fracture plates, cranial plates, spinal rods, stents, catheters, dental implants
CoCr Alloys	Joint replacement prostheses, heart valves, dental implants, orthopaedic fracture plates, spinal rods
Titanium Alloys	Joint replacement prostheses, cranial plates, dental implants, dental wires, orthopaedic fracture plates, ablation catheters, stents, maxillofacial reconstruction

Table 2.3. Mechanical properties of 316L stainless steel, cast and wrought cobalt-chromium alloy, Ti6Al4V, and human bone [74, 76].

Material	Tensile Strength (MPa)	Yield Strength (MPa)	Vickers Hardness (H_v)	Young's Modulus (GPa)	Fatigue Limit (GPa)
316L Stainless Steel	650	280	190	211	0.28
Wrought CoCr Alloy	1540	1050	450	541	0.49
Cast CoCr Alloy	690	490	300	241	0.30
Ti6Al4V	1000	970	---	121	---
Cortical Bone	137.3	---	26.3	13.7	---

Many metallic prostheses are susceptible to corrosion when implanted in the body. This may result in adverse effects to the patient and functional failure of the device [74]. To prevent this, many metallic prostheses are pre-passivated before final packaging. This may involve techniques such as acid baths, anodizing processes for titanium alloys [77], or electropolishing for stainless steel and cobalt based alloys [78].

2.4.1 Cobalt – Chromium Alloys

Cobalt-chromium (CoCr) alloys are used extensively in THA prostheses, particularly the femoral head [14]. The reason for this is that CoCr alloy has excellent wear resistance properties, superior hardness, and great strength [14, 74]. As a pure metal, cobalt is vulnerable to corrosion and is not that ductile; however, cobalt has been reported to stimulate erythropoietin production [79].

CoCr alloys are also used in orthopaedic devices and fall under three categories: cast (low carbon); wrought; and wrought (high carbon) alloys [74]. The cast CoCr alloy is implemented when designing complex shapes that cannot be machined such as stem components [74]. In contrast, the femoral head can be designed using the wrought (high carbon) CoCr alloy [74].

Martin et al. reported that for passive oxide films formed along CoCrMo alloys, the film consists of cobalt, chromium, and molybdenum ions that are electrostatically attracted to proteins to form the film [80]. High carbon content (0.15% to 0.25%) CoCrMo alloys display better tribocorrosion resistance, less friction, and reduced wear than low carbon content (0.06%) CoCrMo alloys [81].

When released into soft tissues, cobalt takes the form of its cation, Co^{2+} [82]. A blood serum concentration of 5 µg/L for cobalt is considered to be toxic whereas a concentration of 20 µg/L can lead to major complications [83]. Van der Straeten et al. reported a strong correlation between patients with a high cobalt concentration in the blood and "the prevalence of sleeping disorders, cognitive problems, equilibrium disturbances, neuropathic symptoms, fatigue, somatic disorders and mood changes" [83]. In contrast, trivalent chromium ions cannot pass through the cell membrane and remain in the blood [83]. Trivalent chromium ions unite with phosphate to form to a Cr(III)-phosphate complex whereas no chromium (VI) ions are found in tissues [84].

Coleman et al. conducted a study to analyze the concentration of cobalt in blood after CoCr THA prostheses had been implanted in patients for one year [85]. Coleman et al. observed that after a year of implantation, the patients had a significant increase in the concentration of cobalt ions in their blood [85]. Although it is possible that some of these

cobalt ions may be from corrosion, Coleman et al. speculated that the elevation in cobalt was most likely due to wear from the articulating surfaces [85].

Morapudi et al. examined 53 patients with a unilateral metal-on-metal THA prosthesis and 53 additional patients with bilateral metal-on-metal THA prostheses to determine if the bilateral patients have greater serum cobalt and chromium levels [86]. Morapudi et al. discovered that for the patients with bilateral metal-on-metal THA prostheses, the cobalt and chromium concentrations were 34 nmol/L and 23 nmol/L of cobalt and chromium, respectively, whereas the unilateral group had cobalt and chromium levels of 14 nmol/L and 21 nmol/L, respectively [86]. As a result, there were no significant differences for either cobalt or chromium between the two groups [86]. According to the Medicines and Healthcare Products Regulatory Agency, clinically significant concentrations of cobalt and chromium are 120 nmol/L and 135 nmol/L, respectively [86]. In contrast with Morapudi, Watanabe et al. found a significant difference in cobalt and chromium concentrations between patients with bilateral metal-on-metal THA prostheses and those with a unilateral metal-on-metal THA prosthesis [87]. Additionally, Watanabe et al. reported significant differences of cobalt and chromium concentrations in serum for implants with large femoral heads three and six months post-operatively, as well as high cup inclination and highly active patients [87].

Unlike many metals, molybdenum is readily absorbed from the intestinal tract [79]. Acute molybdenum toxicity can lead to diarrhea, coma, and cardiac failure. High molybdenum levels may result in inhibiting ceruloplasmin, cytochrome oxidase, glutaminase, choline esterase, and sulphite oxidase.

Research has been performed to determine if the content of carbon in CoCr alloys affects corrosion behaviour [88]. Lewis et al. determined that carbide inclusions do not enhance the alloy's resistance to corrosion.

2.4.2 Titanium Alloys

Titanium was first introduced as a biomaterial in the 1960's and has been increasing in popularity ever since [74]. Presently, titanium and its alloys are the preferred metal for biomedical implants with Ti6Al4V (6% aluminum, 4% vanadium, 0.25% maximum iron, 0.2% maximum oxygen, and the remainder being titanium) [89] being one of the more popular alloys. This can be attributed to the passive oxide film that forms along the surface which prevents corrosion and is not reactive; thus, making titanium an attractive metal for biomedical applications [74]. Titanium alloy's modulus of elasticity is also closer to bone than CoCr alloy.

In terms of titanium's disadvantages, this passive oxide film is vulnerable to fretting, a form of surface damage caused by low-amplitude oscillatory sliding between two contacting surfaces [90]. Titanium wear particles have been found in tissues local to the head-neck taper interface of THA prostheses instead of precipitated corrosion products [91, 92]. When titanium and CoCr alloy THA prostheses are subject to corrosion or fretting damage, titanium tends to stain the surrounding periprosthetic tissues to a greater extent than CoCr [93].

Oxygen may diffuse through the passive oxide film during fabrication, which may result in embrittlement [94]. Titanium alloys tend to have a low surface hardness and are more susceptible to scratching, burnishing, and loss of sphericity in comparison to cobalt heads (HS21, ASTM F-75) [46].

Crevice corrosion has been reported to occur along the titanium alloy femoral stem and the cement interface [95]. Ti6Al4V is vulnerable to crevice corrosion due to the presence of dissolved and trapped metals cations. Generally, Ti6Al4V implants are not implanted with cement due to the possibility of corrosion and increased dissolution rates as a result of the crevice formed between the metal and the cement [96].

2.4.3 316L Stainless Steel

When stainless steel was first developed, many scientists originally thought it would be an excellent biomaterial because of its resistance to corrosion. When 18-8 stainless steel was first implanted into the human body, intergranular corrosion was present, which was attributed to its 0.08% carbon content [74]. Additionally, 18-8 stainless steel implants featured pitting due to the minimal presence of molybdenum [74].

The only stainless steel that is presently used in orthopaedic devices is 316L stainless steel, which contains molybdenum [74, 97]. Generally, 316L stainless steel is a popular biomaterial because of its low carbon content (0.03%), which can decrease the onset of intergranular attack [74]. Nonetheless, 316L stainless steel can still corrode in the human body and has been known to release iron, nickel, and chromium, all of which

are carcinogenic and are known to be allergens [98]. In a study conducted by Sivakumar and Rajeswari, more than 90% of the failures of 316L stainless steel implants were attributed to crevice corrosion and pitting [98].

Between CoCr, Ti6Al4V, and 316L stainless steel, 316L stainless steel is the most vulnerable to crevice corrosion [99, 100]. When examining these three materials under fretting corrosion testing, 316L stainless steel displayed the most weight loss from fretting in comparison to CoCrMo regardless of the number of cycles of loading [45].

2.5 Corrosion

The aim of this subsection is to discuss corrosion with respect to THA prostheses. The topics that are to be addressed include: an overview of corrosion; the environment of the human body; the passive oxide film and how it prevents corrosion; the forms of corrosion that affect the head-neck taper interface of THA prostheses; the four tissue responses to biomaterials; inflammatory cell induced corrosion; the consequences of corrosion in the human body; and a summary of the literature concerning adverse local tissue reactions (ALTRs).

2.5.1 Introduction to Corrosion

Corrosion occurs when a material is gradually degraded, deteriorated, or destroyed upon interacting with its surrounding environment [4]. Corrosion consists of a series of electrochemical reactions that involve the transfer of electrons between an electrode and an electrolyte [4]. An electrode is an electronic conductor that allows electrons to be transferred to an electrolyte, which is an ionic conducting solution that allows bidirectional flow of charge carriers [101].

For metallic species to corrode, two fundamental characteristics are required: thermodynamic driving forces and kinetics. Thermodynamic driving forces consist of a series of oxidation and reduction reactions that dictates how much energy is required to drive the reaction as well as the amount of energy released. In contrast, thermodynamic kinetics focuses on the rate of the oxidation and reduction reactions and the kinetic barriers. Factors that may influence the rate of the oxidation and reduction reactions include those that reduce the rate or prevent the reactions from occurring.

The oxidation number, or oxidation state, of each atom in a molecule states how many electrons it is capable of donating or accepting in the overall bonding of the molecule [101]. A chemical reaction in which the oxidation number of any of the reactants changes is called an oxidation-reduction (or redox) reaction [101]. When corrosion occurs, one of the key reactions is the loss of electrons from a metal atom and its oxidation number increases. In other words, the metal atom (M) takes on the form of a cation by releasing n amount of electrons (e) and its oxidation number increases by n as shown in the

following reaction [4]. This metal (M) is referred to as the anode and the chemical reaction at this site is an oxidation reaction. The anode is a reducing agent because by giving up electrons, it reduces another atom that gains the electrons [101].

$$M \rightarrow M^{n+} + ne^-$$

When considering the head-neck taper interface of THA prostheses, the oxidation of cobalt would be as follows:

$$Co \rightarrow Co^{2+} + 2e^-$$

Additionally, chromium is also susceptible to oxidation; however, Cr_2O_3 is produced. Cr_2O_3 which forms a part of bilayer in the passive oxide film that protects the CoCr alloy from head-neck taper corrosion.

$$2Cr + 3H_2O \rightarrow Cr_2O_3 + 6H^+ + 6e^-$$

These free electrons are capable of migrating and may propagate away from the metal atom. The atom that receives the electrons (M) becomes reduced and is known as the cathode. The reduced atom is an oxidizing agent because it oxidizes another atom that loses the electrons [101]. In terms of electron production and consumption, the rate of oxidation equals the rate of reduction during corrosion [4].

$$M^{n+} + ne^- \rightarrow M$$

The following reduction reactions can occur at the head-neck taper interface.

$$O_2 + 2H_2O + 4e^- \rightarrow 4OH^-$$

$$O_2 + 2H_2O + 2e^- \rightarrow H_2O_2 + 2OH^-$$

$$O_2 + H_2O + e^- \rightarrow HO_2^{\bullet} + OH^-$$

$$HO_2^{\bullet} + H_2O \rightarrow H_2O_2 + OH^-$$

$$H_2O_2 + 2e^- \rightarrow 2OH^-$$

The thermodynamic driving force coerces the oxidation of metal atoms to form cations. There are two forms of energy that are present during corrosion: a chemical driving force and an electrostatic force [91]. Gibbs free energy (G) is the energy associated with a chemical reaction that can be used to do work [101]. The magnitude of the change in Gibbs free energy (ΔG) is the energy that is available to do useful work for a chemical reaction [101]. To calculate the Gibbs free energy under standard state conditions (temperature = 298K; pressure = 1 atmosphere; concentration of the aqueous solution at 1M) , Equation 1 is used (R = 8.31J/mol.K; T = temperature of 298 K) [101]:

$$\Delta G^\circ = -2.3RT \log(K_{eq}) \qquad \text{(Equation 1)}$$

If the standard state Gibbs free energy is known and K_{eq} needs to be determined, K_{eq} can be solved using Equation 2:

$$K_{eq} = 10^{-\Delta G°/5700} \quad \text{(Equation 2)}$$

The Gibbs free energy is critical for the chemical driving force and is a thermodynamic state function that measures the process-initiating work obtainable from a thermodynamic system at a constant temperature and pressure. The Gibbs free energy can be calculated with Equation 3 where H represents enthalpy, T is the Kelvin temperature, and S is entropy [101].

$$G = H - TS \quad \text{(Equation 3)}$$

Equation 4 can be applied to calculate the change in Gibbs free energy [101].

$$\Delta G = \Delta H - T\Delta S \quad \text{(Equation 4)}$$

The Gibbs free energy can help determine whether or not a given reaction will occur based on the following criteria [102]:

1. If the Gibbs free energy is greater than zero, the reaction requires energy and will not spontaneously occur.
2. If the Gibbs free energy is less than zero, the reaction will spontaneously occur and does not require additional energy to drive the reaction.
3. If the Gibbs free energy is equal to zero, the system will be in equilibrium in which the rate of the forward reaction is equal to the rate of the reverse reaction.

Table 2.4 summarizes the combinations of ΔH, ΔS, and temperature that can determine the sign of ΔG and the spontaneity of a reaction.

Table 2.4. Summary of the variation in ΔH, ΔS, and T for the spontaneity of a reaction based on the Gibbs free energy [101, 102].

ΔH	ΔS	ΔG	Spontaneous Reaction?
-	+	-	Spontaneous
+	+	- At High Temperature	Spontaneous
+	+	+ At Low Temperature	Not Spontaneous
-	-	+ At High Temperature	Not Spontaneous
-	-	- At Low Temperature	Spontaneous
+	-	+	Not Spontaneous

An electrostatic driving force is present when positively and negatively charged particles (metal cations and electrons) are separated from each other during corrosion [91]. By separating the metal cations from the electrons, an electrical double layer can form that acts as a capacitor. This results in a potential difference (ΔE) between the interface of the metallic specimen and the surrounding solution. The change in the Gibbs free energy for a redox reaction can be determined using Equation 5 (n is the number of electrons; F is Faraday's constant = 96,500 C/mol; and ΔE is the potential difference) [101]:

$$\Delta G = -nF\Delta E \qquad \text{(Equation 5)}$$

The potential difference can be used to determine the reactivity of the driving force that brings about the oxidation reaction [101]. Since a reaction is spontaneous if ΔG is negative, this equation tells us that the reaction in a cell will be spontaneous if the potential difference is positive [101]. By having a negative potential difference, the Gibbs free energy will be positive and the corresponding reaction will not spontaneously occur [101].

The electrochemical series is a scale that ranks the reactivity of a metal from the least reactive (noble) to the most reactive (base) under standard conditions. With respect to corrosion, the electrochemical series can identify if a metal will corrode under standard conditions. Table 2.5 lists the reactivity of various metals where E° represents the potential difference of the reaction under standard state conditions and indicates whether the reaction is shifted to the left or to the right of the hydrogen equilibrium [4]. This scale is assumed under thermodynamic considerations such that there is nothing preventing the oxidation of the metal and the potentials listed is for the boundary between the solution and the metal. The potential difference varies for the atoms and their corresponding ions. By having a potential difference, the amount of electrons that adhere to the metal electrode will differ from that of the hydrogen half-cell reaction (E° = 0V). The more negative the reduction potential, the reactant will be a more powerful reducing agent [101]. Meanwhile, the more positive the reduction potential, the reactant will be a greater oxidizing agent [101]. However, if there are two hydrogen electrodes covered with platinum, both electrodes would ideally contain the same number of electrons and there would be no potential difference [4].

Table 2.5. The standard electrochemical / EMF series [4].

Equilibrium	E^o (Volts)
$Li^+_{(aq)} + e^- \rightleftharpoons Li_{(s)}$	- 3.03
$K^+_{(aq)} + e^- \rightleftharpoons K_{(s)}$	- 2.92
$Ca^{2+}_{(aq)} + 2e^- \rightleftharpoons Ca_{(s)}$	- 2.87
$Mg^{2+}_{(aq)} + 2e^- \rightleftharpoons Mg_{(s)}$	- 2.37
$Al^{3+}_{(aq)} + 3e^- \rightleftharpoons Al_{(s)}$	- 1.66
$Ti^{2+}_{(aq)} + 2e^- \rightleftharpoons Ti_{(s)}$	- 1.60
$TiO_{2\,(aq)} + 4H^+_{(aq)} + 4e^- \rightleftharpoons Ti_{(s)} + 2H_2O_{(g)}$	- 0.86
$2H_2O_{(aq)} + 2e^- \rightleftharpoons 2OH^-_{(s)}$	- 0.83
$Zn^{2+}_{(aq)} + 2e^- \rightleftharpoons Zn_{(s)}$	- 0.76
$Cr^{3+}_{(aq)} + 3e^- \rightleftharpoons Cr_{(s)}$	- 0.74
$Cr^{2+}_{(aq)} + 2e^- \rightleftharpoons Cr_{(s)}$	- 0.56
$Fe^{2+}_{(aq)} + 2e^- \rightleftharpoons Fe_{(s)}$	- 0.44
$Co^{2+}_{(aq)} + 2e^- \rightleftharpoons Co_{(s)}$	- 0.28
$Pb^{2+}_{(aq)} + 2e^- \rightleftharpoons Pb_{(s)}$	- 0.13
$Fe^{3+}_{(aq)} + 3e^- \rightleftharpoons Fe_{(s)}$	- 0.04
$2H^+_{(aq)} + 2e^- \rightleftharpoons H_{2(g)}$	0
$Ti(OH)^{3+}_{(aq)} + H^+ + e^- \rightleftharpoons Ti^{3+}_{(s)} + H_2O_{(g)}$	+ 0.06
$Cu^{2+}_{(aq)} + 2e^- \rightleftharpoons Cu_{(s)}$	+ 0.34
$O_{2(aq)} + 2H_2O_{(aq)} + 4e^- \rightleftharpoons OH^-_{(s)}$	+ 0.40
$Ag^+_{(aq)} + e^- \rightleftharpoons Ag_{(s)}$	+ 0.80
$Pt^{2+}_{(aq)} + 2e^- \rightleftharpoons Pt_{(s)}$	+ 1.20
$Au^{3+}_{(aq)} + 3e^- \rightleftharpoons Au_{(s)}$	+ 1.50

Some metals are resistant to corrosion because their potential difference from the equilibrium is highly positive. This means that the oxidation reaction's chemical driving force is poor [4]. For example, both gold and silver have positive potentials and have a negligible chemical driving force to perform an oxidation reaction under standard state

conditions. Even during nonstandard conditions, biomaterials that are made of gold and silver would most likely stay in the metallic state if implanted in the body. On the other hand, lithium and potassium have negative potential differences, indicating that both of these elements are very reactive. If lithium and potassium were implanted into the body, there would be a vigorous, exothermic oxidation reaction.

As shown in Table 2.5, many metals have negative standard potentials and may corrode when implanted in the body. For example, titanium is commonly used in THA prostheses and has a negative potential difference. Consequently, titanium is likely to undergo oxidation due to the chemical driving force and is susceptible to corrosion. However, titanium can react with other compounds in the body (e.g. water, oxygen, and other oxidizing species) and is capable of returning to its cationic state.

As indicated, the kinetics of the oxidation and reduction reactions dictates whether or not corrosion will occur. Some examples of kinetic barriers that control the rates of the oxidation and reduction reactions include polymeric coatings and passivation. Passivation involves an oxide film formation along the surface of the metal. By having kinetic barriers for a corrosion reaction, there are three outcomes [4]:

1. Cations from the metal specimen will be prevented from migrating towards the solution.
2. Anions from the solution will be unable to propagate towards the metal.
3. There will be a disturbance in allowing the electrons to travel through the boundary layer between the metal and the solution.

Many biomaterials used in orthopaedics are constructed from alloys that are dependent on the technique of passivation to prevent oxidation from occurring. By having an oxide film that spontaneously forms along the metallic surface, metal ions and electrons will be unable to propagate through the film [4]. To act as a kinetic barrier, the oxide film must achieve a certain number of criteria [4]:

1. The oxide film should not be porous.
2. The propagation of electrons and ions across the oxide film can be prevented through the atomic structure. If there are defects in the organization of the oxide film's atomic structure, the oxide film will not be efficient in regard to the propagation of ionic species. Some examples of atomic defects include vacancies (missing atoms in the crystal structure) and impurities with different valence states.
3. When dealing with mechanical factors such as fretting, micromotion, and abrasion, the oxide film needs to remain in contact with the surface of the alloy and not deteriorate. If the oxide film does deteriorate, the metallic surface will be fully exposed to the solution and oxidation could occur.

2.5.2 The Biological Environment

A successful biomaterial is considered to be a device that performs its desired function and is biocompatible when implanted in the body. By being biocompatible, the material is able to perform with an appropriate host response in a specific application [103].

When implanting a biomaterial into a patient, the surgeon faces the challenge of selecting the appropriate material(s) and how it will interact when inside the human body. Not only can corrosion occur, but many materials and their debris are toxic to the body, which may result in ALTRs.

Biological fluid is an aerated solution that consists of 0.9% NaCl, along with many other salts, and has a temperature of 37˚C [4]. The normal pH of body fluid ranges from 7.35 to 7.45 [104]. The human body also contains water and proteins that can interact with the biomaterial. Anions in the body include chloride, bicarbonate, and phosphate [74]. Some reactive cations include sodium, potassium, calcium, hydrogen, and magnesium ions [74]. Table 2.6 presents the chemical composition of normal human blood plasma. Meanwhile, the hip joint contains synovial fluid. To mimic synovial fluid for testing THA prostheses, bovine calf serum is commonly used.

Table 2.6. The chemical composition of normal human blood plasma [105].

Ion	Concentration (mmol l^{-1})
Na^{+}	142.0
K^{+}	5.0
Mg^{2+}	1.5
Ca^{2+}	2.5
Cl^{-}	103.0
HCO_3^{-}	27.0
PO_4^{2-}	1.0
SO_4^{2-}	0.5

2.5.3 The Passive Oxide Film

Most orthopaedic alloys are dependent on the passive oxide film to minimize the transportation of metal ions and electrons through the film and to prevent oxidation from taking place [46]. CoCr and titanium alloys do have protection from corrosion due to the presence of a thin oxide film (Cr_2O_3 for CoCr alloys and TiO_2 for Ti6Al4 alloy) [100]. The oxide film is capable of slowing down the rate of dissolution by altering the rate of ion transfer through the film through a number of factors. These factors include: the oxide film's thickness; the presence of defects; the chemical composition; and the structure. More importantly, the effectiveness of the oxide film is ultimately dictated by the surrounding environmental conditions such as the electrolyte's composition, the redox conditions, the temperature, pH, and the contact time with the electrolyte.

Martin et al. reported that for oxide films formed along CoCrMo alloys, the film consists of cobalt, chromium, and molybdenum ions that are electrostatically attracted to proteins to form the film [80]; however, Ocran arrived at a different conclusion than Martin et al. by indicating that cobalt is not present in the oxide film [40]. Instead, Ocran argued that cobalt is oxidized directly into the solution and does not contribute to the formation of the oxide film. To support this, Ocran conducted an *in vitro* study with CoCr to determine which of the following electrolytic solutions yields the highest corrosion current density: 0.14 M NaCl; phosphate buffered saline; and clinically relevant simulated body fluid. When Ocran performed inductively coupled plasma mass spectroscopy, the concentration of cobalt and molybdenum ions were substantially greater for phosphate buffered saline in comparison to 0.14 M NaCl and the clinically relevant simulated body fluid. Meanwhile, the concentration of chromium for phosphate buffered saline was significantly lower than 0.14 M NaCl and clinically relevant simulated body fluid. Since cobalt does not contribute to the formation of the passive oxide film, this can account for the continuous anodic dissolution of CoCr alloy.

Ocran reported that a potential in the range of -600 mV to 480 mV leads to a consistent current density that can result in the formation of a passive oxide film that protects the CoCr alloy from electrochemical degradation [40]. After this passive domain, Ocran observed the transpassive region for CoCr alloy when the potential exceeded 480 mV. During the transpassive region, the passive oxide film deteriorated due to an exponential increase in the current, which led to the release of Cr^{3+} and Cr^{6+} cations.

The passivation of pure cobalt occurs only in alkaline solutions [100]. Meanwhile, the TiO_2 oxide layer is thermodynamically stable between a pH range of 2 to 12 and is resistant to dissolution unless if hydrofluoric acid or hydrogen peroxide are present [100].

CoCr and titanium alloys are capable of forming an oxide film to combat corrosion [106]. By increasing the stress and applying micromotion at the head-neck taper interface, this can rupture the oxide film and make the alloys vulnerable to crevice corrosion since biological fluid is trapped within the taper interface. Although the oxide film can be repassivated, the oxygen molecules are reduced; thus, making the oxide film have a decreased resistance to corrosion [107]. Consequently, the pH within the crevice of the head-neck taper interface can range from 1 to 3 [108].

In a recent retrieval analysis, Witt et al. proposed a hypothesis to explain the destruction of the oxide film along the head-neck taper interface of THA prostheses that can lead to corrosion damage [109]. Witt et al. argued that there is a direct relationship between wear along the bearing interface and corrosion damage at the head-neck taper interface. Witt et al. noted that wear along the bearing articulation was greater for hard-on-hard articulations during poor lubrication, which can generate large frictional moments. These moments can increase the shear stresses at the head-neck taper interface; thus, deteriorating the oxide film and making the taper interface vulnerable to corrosion. From this, Witt et al. demonstrated that there is a strong relationship between the wear of the bearing surface and head-neck taper corrosion.

Although oxide films are known to form along alloy surfaces, proteins can adhere to the surface to form a biofilm [100, 110]. Although most oxide films are 1 to 4 nanome-

ters thick [111-113], the thickness of the TiO_2 layer can range from 10-30 μm [114]. Additionally, albumin has been known to interact with the repassivation of TiO_2 as a result in the change in its charge due to its zwitterion characteristics [100].

These biofilms can lubricate the surface but also enhance the deterioration of the base alloy due to corrosion [115]. The fretting current tends to increase as the passive oxide film increases [116]. By having an anodic potential, the fretting current tends to increase linearly with the potential [116].

2.5.4 Forms of Corrosion

There are eight forms of corrosion that are known to occur: uniform corrosion; pitting; selective leaching; erosion corrosion; stress corrosion; intergranular corrosion; crevice corrosion; and galvanic corrosion [4]. In regard to the head-neck taper interface of THA prostheses, crevice corrosion, galvanic corrosion, pitting, and intergranular corrosion are the most dominant. This section will provide a brief summary of these four forms of corrosion.

Crevice Corrosion

Crevice corrosion is a form of intense localized corrosion that usually occurs within shielded areas of metallic surfaces or crevices [4]. Crevice corrosion is commonly

associated with small volumes of stagnant solution caused by holes, gasket surfaces, lap joints, surface deposits, and crevices [4]. Crevice corrosion commonly occurs between the head-neck and neck-stem interfaces of THA prostheses, but it has also been reported to occur at the interface between a titanium alloy femoral stem and bone cement [95].

For crevice corrosion to occur in THA prostheses, a small amount of biological fluid enters the crevice even if the crevice is only a few thousandths of an inch thick. The crevice must be wide enough to allow fluid entry but also be narrow enough so that the biological fluid remains stagnant [4].

Crevice corrosion occurs through a couple of chemical reactions. First, the metallic surface becomes oxidized and loses electrons; thus, metal cations are formed. Second, oxygen and water react with the loose electrons that were released from the metal oxidation reaction to form hydroxide anions as shown [4].

$$M \rightarrow M^{+} + e^{-} \qquad \text{(oxidation reaction)}$$

$$O_2 + 2H_2O + 4e^{-} \rightarrow 4OH^{-} \qquad \text{(reduction reaction)}$$

With this reduction reaction, the amount of oxygen inside the crevice of the head-neck taper interface will gradually become depleted [117]. By having the oxidation reaction continuously occurring, the crevice will be filled with metal cations as illustrated in Figure 2.8 [4, 117]. These cations will electrostatically attract chloride anions from the biological fluid to enter the crevice and form metal chlorides [4, 117].

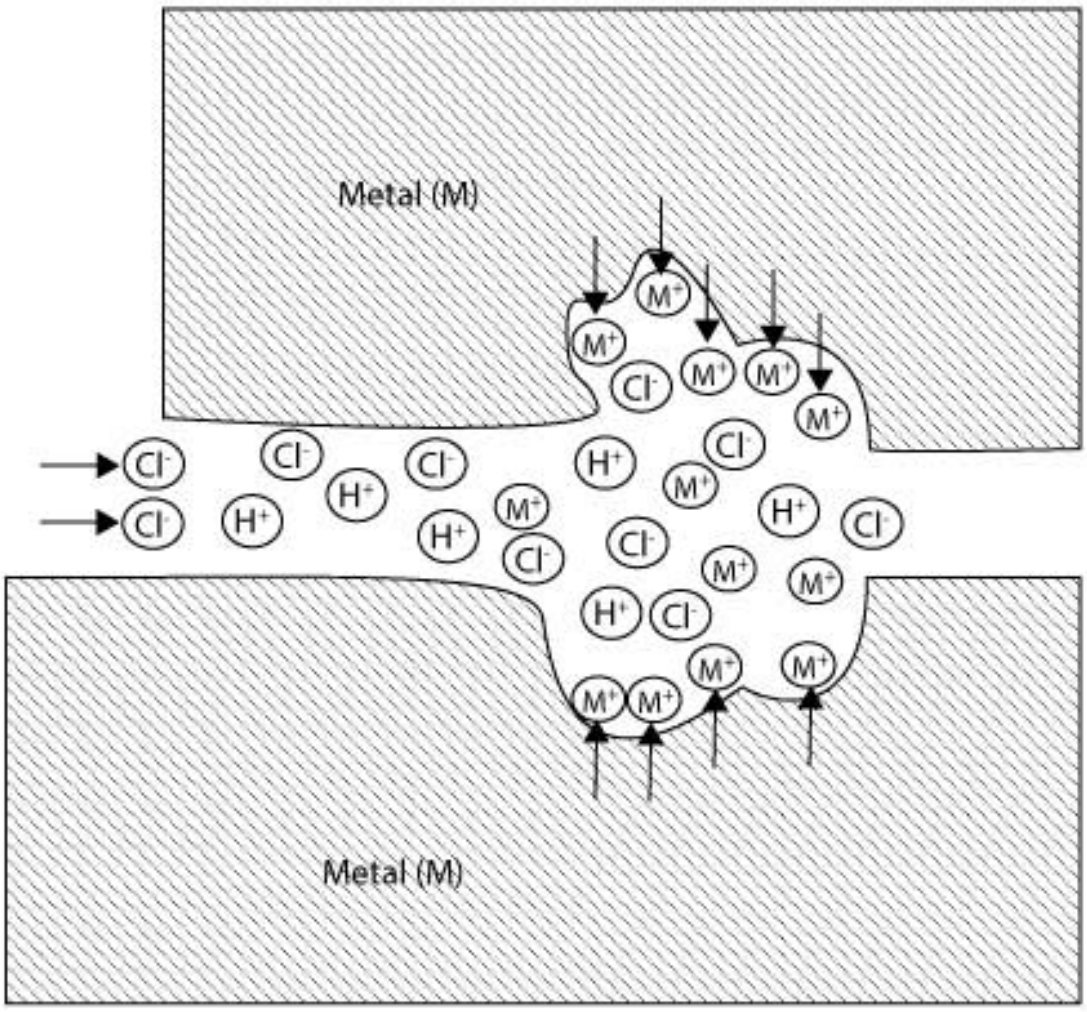

Figure 2.6. Migration of chloride anions to the metal cations to form metal chlorides.

The metal chlorides are capable of hydrolyzing to form hydrochloric acid, which can accelerate crevice corrosion [117]. By having a high concentration of hydrochloric acid, this will dramatically decrease the pH within the head-neck taper interface [117]. The metal components will also lose their passive oxide film not only to fretting action, but also from the hydrochloric acid [117]. Consequently, the oxide film will become

thermodynamically unstable and the head-neck taper interface shall become vulnerable to corrosion [117].

Galvanic Corrosion

A potential difference usually exists between two dissimilar metals when they are immersed in an electrolyte [4]. By placing these metals in contact with each other, the potential difference between the metals will cause the electrons to flow from one metal to another [4]. The least corrosion resistant metal is the anode and the more corrosion resistant metal is the cathode [4]. The cathode generally corrodes very little or not at all in this couple [4]. By having an electric current between two metals in an electrolyte, this form of corrosion is called galvanic, or two-metal, corrosion [4]. The driving force for corrosion is the potential difference between the two metals [4]. For THA prostheses, it is common to assemble a CoCr femoral head onto a Ti6Al4V stem. The main advantage of this is prosthesis design is a combination of the CoCr femoral head's strength and the elasticity of the Ti6Al4V stem is similar to bone [107].

Cook et al. conducted an *in vitro* experiment and examined 108 cementless femoral heads and stems for corrosion damage at the head-neck taper interface [118]. For their study, Cook et al. obtained 29 mixed alloy prostheses (CoCr head and Ti6Al4V stem), 76 prostheses made solely out of CoCr, and three prostheses consisting of Ti6Al4V [118]. All of the prostheses were subject to mechanical testing with a force range of from 225 to 2250 N with a frequency of 10 Hz [118]. The prostheses were subjected to either 1, 5, or

10 million cycles of loading in saline solution [118]. Only five out of 76 (6.6%) prostheses that had a CoCr femoral head and stem had corrosion damage, which was only considered to be mild [118]. Meanwhile, only two out of three (66.7%) prostheses that had a Ti6Al4V head and stem were subjected to mild corrosion [118]. In regard to the mixed alloy prostheses, 19 out of 29 (65.5%) prostheses displayed no signs of corrosion [118]. In contrast, three out of 29 (10.3%) prostheses featuring a CoCr head and a Ti6Al4V stem had moderate corrosion whereas only seven of the 29 (24.1%) had mild corrosion [118].

Collier et al. conducted a retrieval analysis of 139 THA prostheses to determine if different material combinations at the head-neck taper interface influence corrosion and fretting damage [9, 11]. Collier et al. studied 80 prostheses that were all CoCr, 11 prostheses that were all Ti6Al4V, and 48 prostheses that were mixed alloy (CoCr head and Ti6Al4V stem) [9, 11]. None of the single alloy THA prostheses displayed any signs of corrosion [9, 11]. In contrast, 25 of the 48 (52.1%) mixed alloy THA prostheses featured corrosion damage [9, 11]. None of the THA prostheses that were surgically removed before a time period of 9.8 months featured any corrosion or fretting damage [9, 11]. However, all of the THA prostheses removed after a period of 40 months featured corrosion damage [9, 11]. By performing scanning electron microscopy (SEM), pitting was discovered along the Ti6Al4V neck and the CoCr head [9, 11]. Profilometry revealed that corrosion was prevalent along the CoCr head with an average depth of 0.015 millimetres [9, 11].

Similar to Collier et al., Lieberman et al. performed a retrieval analysis of 48 THA prostheses to analyze the presence of corrosion damage due to different material

combinations at the head-neck taper interface [13]. For this investigation, the prostheses were divided into three groups. The first group consisted of 26 THA prostheses with a CoCr head and stem [13]. The second group featured 10 THA prostheses with a CoCr head and a Ti6Al4V stem [13]. In the third group, there were 12 THA prostheses that had a CoCr head with a Ti6Al4V stem that were locked by a shrink-fit [13]. None of the prostheses in the first group featured any corrosion damage at the head-neck taper interface [13]. In contrast, one taper interface in the second group featured some corrosion damage [13]. For this implant, Lieberman et al. believed that crevice corrosion might have taken place [13]. With the third group, there was no corrosion damage reported [13]. With the third group as an example of zero tolerance, this can eliminate crevice corrosion from occurring at the head-neck taper interface [13]. By decreasing the tolerance level, Lieberman et al. noticed that this significantly increases the amount of force required to separate the mating surfaces and may minimize the micromotion and fluid within the taper interface [13].

Gilbert et al. also examined the possibilities of galvanic corrosion by doing a retrieval analysis involving 148 THA prostheses [14]. For this study, there were 111 mixed alloy prostheses (Ti6Al4V stem and CoCr head) and 37 THA prostheses that consisted solely of CoCr [14]. Through observation, 16% of the necks and 35% of the femoral heads for the mixed alloy prostheses featured moderate to severe corrosion damage [14]. Meanwhile, 14% of the necks and 23% of the heads for the single alloy prostheses displayed moderate to severe corrosion [14]. Further analysis revealed that for the single and mixed alloy prostheses, the heads featured more corrosion damage than the necks [14]. Gilbert et al. noted that there was a relationship between corrosion damage and implanta-

tion time for both groups [14]. Using SEM, Gilbert et al. was able to discover etching, pitting, fretting, intergranular attack, and selective leaching of cobalt [14].

From these examples in the literature, galvanic corrosion appears to be a major form of corrosion damage at the head-neck taper interface of THA prostheses. When comparing mixed alloy prostheses to single alloy prostheses, mixed alloy prostheses tend to have a higher frequency and severity of corrosion damage at the head-neck taper interface despite the small difference in the electrical potential between the two alloys [9, 11, 13, 14, 118]. One of the advantages of THA prostheses is that the surgeon can select different head and stem components for assembling the prosthesis; however, this may lead to different material combinations and increase the risk for galvanic corrosion. By assembling a prosthesis with different head and neck designs (e.g. different companies, models), this can create different tolerances that can result in crevice corrosion.

Intergranular Corrosion

When a metal corrodes, uniform attack generally occurs since the grain boundaries are more reactive than the matrix [4]. But in some circumstances, grain interfaces can be reactive and trigger intergranular corrosion [4]. Intergranular corrosion occurs when there is a localized attack along or adjacent to grain boundaries with relatively little corrosion of the grains [4].

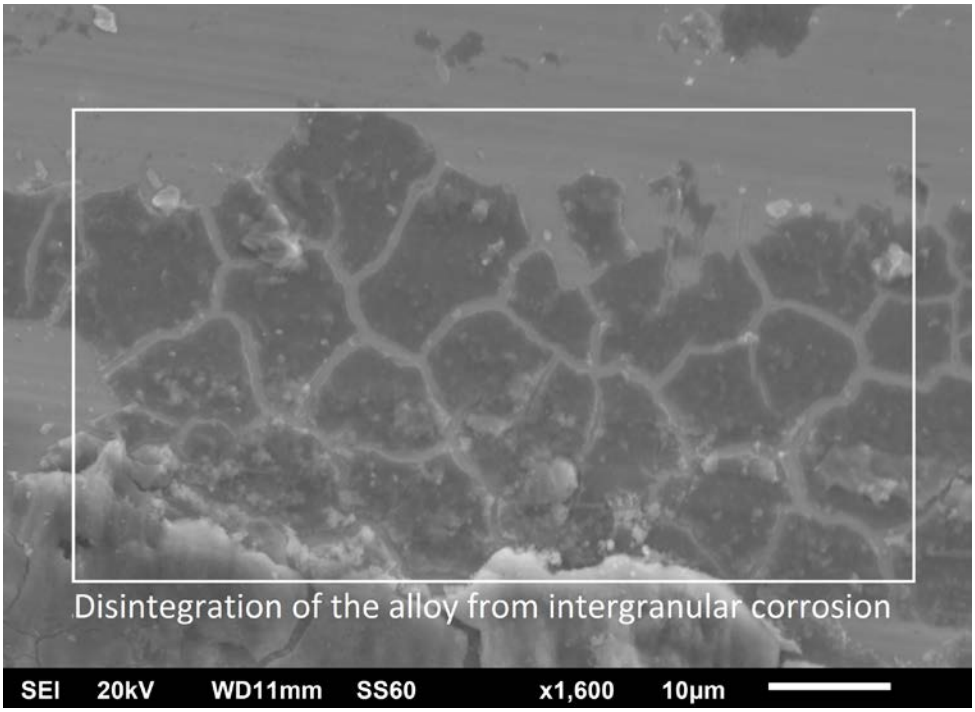

Figure 2.7. A scanning electron microscopy image of intergranular corrosion along the neck taper. Grains have been disintegrated from the CoCr alloy.

When intergranular corrosion occurs, the alloy disintegrates (the grains fall out) and/or loses its strength [4]. Intergranular corrosion can be initiated due to the presence of impurities along the grain boundaries, the enrichment of an alloying element, or the depletion of an alloy element along the grain boundary [4]. For example, stainless steels are subject to intergranular corrosion due to the depletion of chromium along the grain-boundary regions [4]. When 316L stainless steel was first implanted into humans, heterogeneous intergranular distribution of carbon was detected and this triggered intergranular corrosion [4]. By limiting the carbon content of austenitic stainless steels to a maximum of 0.03%, 316L stainless steels are less vulnerable to corrosion [119].

Pitting

Pitting is a form of extremely localized corrosion damage with holes along the metallic surface caused by the dissolution of the passive oxide film and the formation of cavities surrounded by an intact passivated surface [4]. These holes may have a small or large diameter, but are typically small [4]. Pits are usually described as a cavity or hole within the surface diameter having roughly the same length as its depth [4]. Although oxide films do exhibit resistance to corrosion damage, they are susceptible to pitting [74]. With respect to metal implants, the extent of pitting can be further increased due to the presence of proteins in body fluid and serum [120, 121]; however, pitting can be prevented for CoCr alloy prostheses by inserting molybdenum (a weight percentage of 2-3%).

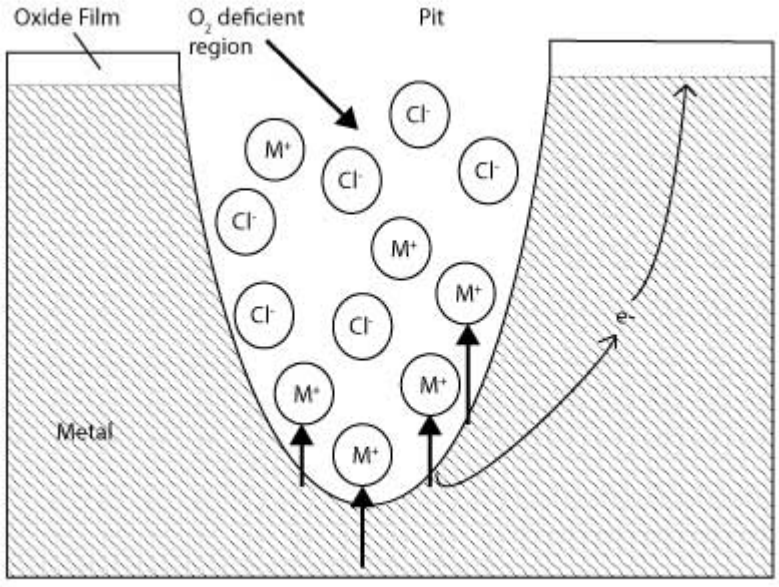

Figure 2.8. Schematic of pitting corrosion.

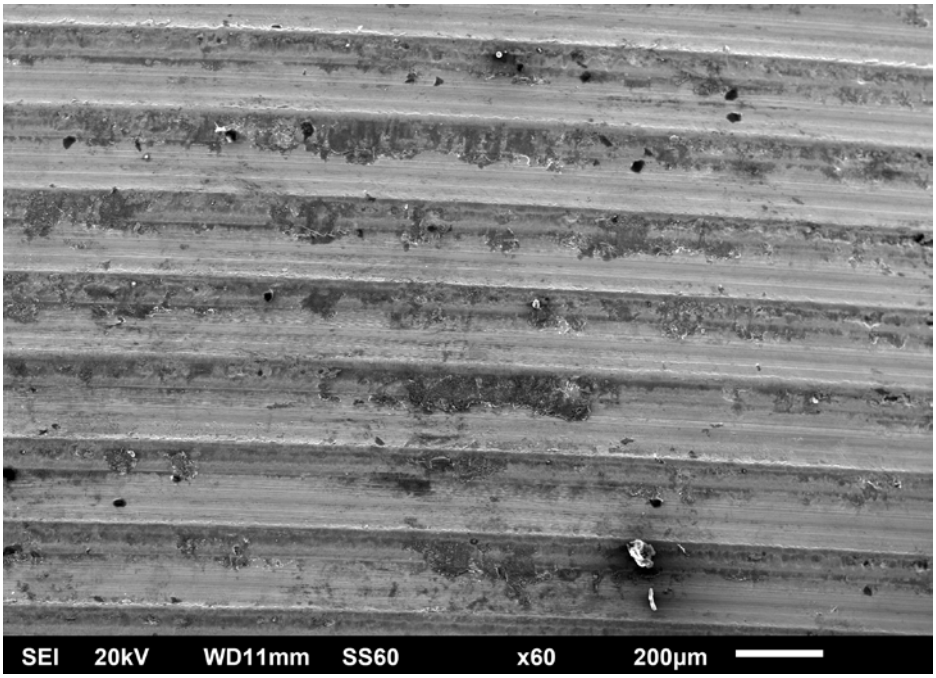

Figure 2.9. Pitting corrosion damage along a CoCr neck taper.

2.5.5 Inflammatory Cell Induced Corrosion

Recently, Gilbert et al. has proposed that there may be an alternative form of corrosion damage where cells attack the metallic surface and this has been demonstrated in two separate retrieval analyses. First, Gilbert et al. examined two metal-on-metal THA prostheses and the CoCrMo acetabular liners displayed corrosion damage along the taper region [122]. Steam sterilization was performed on the acetabular liners and three different SEM techniques were performed (secondary electron imaging from 2 to 4 kV and 13 to 15 kV, backscattered electron imaging at 15 kV). The 2 to 4 kV secondary electron imaging revealed cellular membranes and biological components since the low energy

electrons did not penetrate through the cell. Energy dispersive x-ray spectroscopy (EDS) revealed that these cells had carbon-rich chemistry. Additionally, Gilbert et al. noted that the corrosion damage did not display any indicators of fretting or mechanically-assisted crevice corrosion. Instead, there were fissures and signs of intergranular and pitting corrosion. From this, Gilbert et al. concluded that inflammatory cell induced corrosion may directly attack the surface of CoCrMo implants.

In a second retrieval analysis, Gilbert et al. obtained 69 CoCrMo components from 51 THA and total knee arthroplasty (TKA) implant systems and analyzed them for inflammatory cell induced corrosion [123, 124]. To do this, Gilbert et al. performed digital optical microscopy, SEM, and EDS. From this analysis, Gilbert et al. detected the presence of inflammatory cell induced corrosion in 51 of 69 components (74%), which included bearing and non-bearing surfaces. Gilbert et al. noted that the corrosion damage had a similar characteristic to osteoclasts when remodelling bone. There were individual spots of discoloured regions with a ruffled topography and there were pits with circular and irregular crater-like features. There were also ring-like patterns on the metallic surfaces, which indicates the secretion of acid and reactive oxygen species. Gilbert et al. hypothesized that migration of the activated cells took place within the ruffled membrane. These cells were between 20 to 300 μm in size.

Gilbert et al. speculated that these ruffled membranes belong to migratory phagocytic cells but also noted that larger foreign body giant cells were also present. The ruffled border on these phagocytic cells are known to have secretory vescicles that can re-

lease reaction species capable of attacking the CoCrMo surface. Inflammatory cells can use acid and reactive oxygen species to attack foreign bodies and bacteria.

Gilbert et al. observed that all 51 of the corroded implants featured linear streaks of deposited iron in areas with corrosion damage. Normally, CoCrMo alloy contains very little iron (<0.75% weight percentage); however, iron plays a critical role in the inflammation of joints [125]. Iron can encourage inflammation when reactive oxygen species are nearby and iron is a key component of the mononuclear phagocytic system. Gilbert et al. proposed that these phagocytic cells participate in Fenton reactions to produce reactive oxygen species, which can affect the electrochemical behaviour of CoCrMo. The Fenton reaction is known to occur along the ruffled membrane of phacocytic cells [123]. By releasing cobalt and chromium cations during corrosion, these cations can further enhance the Fenton reactions. Not only has inflammatory cell induced corrosion has been detected on CoCrMo alloy, but Cadosch et al. has discovered mechanism in stainless steel and titanium [126, 127].

$$Fe^{2+} + H_2O_2 \rightarrow Fe^{3+} + OH^{\bullet} + OH^{-} \text{ [128]}$$

Even though researchers have concentrated their efforts on taper corrosion of THA prostheses through the mechanically-assisted crevice corrosion mechanism, new research will have to be done to further understand the inflammatory cell induced corrosion phenomenon.

2.5.6 Electrolytes for Corrosion Fatigue Testing

According to ASTM standard F1875-98, saline solution or a proteinaceous solution should be used for *in vitro* corrosion fatigue testing of THA prostheses [129]. Recently, Ocran performed an *in vitro* experiment using pin-on-disc testing to determine which electrolytic solution is ideal to test THA prostheses for corrosion and fretting damage at the head-neck and neck-stem taper interface [40]. Ocran tested three different types of solutions to examine the corrosion current density of medical grade CoCrMo alloy: 0.14 M NaCl, phosphate buffered saline, and clinically relevant simulated body fluid [130]. Clinically relevant simulated body fluid is a serum based fluid that consists of albumin, α-1, α-2, β-, and γ-globulins, phosphate buffered saline, sodium hyaluronate, ethylenediaminetetra acetic acid (EDTA), and antibiotic/antimyocotic (AA) with an average protein concentration of 30 g/L [40].

Ocran observed that the use of 0.14 M NaCl and clinically relevant simulated body fluid for CoCrMo alloy resulted in corrosion current densities of 4.21 $\mu A/cm^2$ and 4.98 $\mu A/cm^2$, respectively. Meanwhile, phosphate buffered saline was determined to be a more aggressive electrolyte with a corrosion current density of 18.57 $\mu A/cm^2$. To explain for the high corrosion current density of phosphate buffered saline, Ocran hypothesized that the presence of phosphate ions adsorb onto the CoCrMo surface to form $H_2PO_4^-$, which is the conjugate base of the weak acid, phosphoric acid. These ions may have increased the dissolution rate of the CoCrMo surface and had an influence on the high corrosion current densities and catalyzed the reduction reaction for water. In contrast, the

proteins in the clinically relevant simulated body fluid delays the dissolution rate and adsorb onto the oxide film; thus, decreasing the corrosion current density of CoCrMo. By using clinically relevant simulated body fluid, CoCr alloy is easy to passivate since the critical anodic current density is slightly greater than the passive anodic current density. This oxide film is a bilayer with an inner oxide layer and an outer organometallic layer. By using clinically relevant simulated body fluid, the presence of the proteins and organometallic complexes reduce the influence of the phosphate ions by adsorbing onto the alloy before the phosphate ions; therefore, decreasing the corrosion current density of CoCr alloy into more clinically relevant rates. By increasing the immersion time, the difference between these two current densities gradually increases; therefore, a more effective oxide film forms with time. Additionally, Ocran did not recommend using 0.14 M NaCl solution for *in vitro* corrosion fatigue testing because the corrosion products and mechanisms may differ than what occurs in the *in vivo* setting. In summary, Ocran recommended using clinically relevant simulated body fluid since it can mimic the corrosion and fretting damage that is found in an *in vivo* environment.

2.5.7 Wear Nomenclature

In the literature, many wear terms are interchanged. The purpose of this section is to clarify some of these terms. Wear of a THA prosthesis is generally considered to be the removal of material by mechanical action that results in a dimensional change of the surface as well as a reduction in the mass of the implant [131]. Wear modes deals with

the overall conditions that the THA prosthesis functions *in vivo* along with the contact surfaces. There are four types of wear modes [131]:

1. Mode 1 occurs when two bearing surfaces are articulating against each other. For a THA prosthesis, mode 1 damage could occur when the femoral head is articulating against a polyethylene liner.
2. Mode 2 happens when a bearing surface articulates against a non-bearing surface. For example, the femoral head may contact with the rim of a socket.
3. Mode 3 is similar to mode 1 except that there are third body particles between the two bearing surfaces (e.g. PMMA cement).
4. During mode 4, two non-bearing surfaces articulate against each other. Fretting at the head-neck taper interface of THA prostheses is example of mode 4.

With respect to wear mechanisms, this refers to the mechanical-chemical processes that results in wear damage [131]. There are four types of wear mechanisms: adhesive wear; abrasive wear; fatigue wear; and tribochemical wear.

1. **Adhesive Wear** – There may be a local chemical bond between two contacting surfaces. If one surface should get pulled away, this will result in motion and adhesion may occur. Adhesion can result in the formation of pits and scratches (a form of abrasive wear). Additionally, adherent particles may be dragged along the surface or they may break loose and become third-body abrasive particles.

2. **Abrasive Wear** – When an asperity that is attached to one surface is dragged and pressed onto an opposing surface, this results in abrasive wear. Also, a third-body particle can be trapped between the two bearing surfaces and can abrade both surfaces at the same time.

3. **Fatigue Wear** – During the process of fatigue wear, a material is cyclically loaded and this results in surface and/or subsurface cracks. These cracks may unionize and result in the loss of a fragment of the surface. Fatigue wear can occur on the microscopic level and result in damage such as pits.

4. **Tribochemical Wear** – Tribochemical wear occurs when a material is removed due to mechanically activated reactions while interacting with the environment. During the process of tribochemical wear, the kinetic energy that is introduced during contact drives the chemical reactions that normally would not occur.

Corrosion is not a form of wear. Instead, corrosion is an electrochemical process that can result in the removal of material and corrosion does not require wear to occur. However, wear of a metallic surface always involves corrosion except for non-reactive metals such as gold [131].

Wear damage is the change in texture, appearance, and/or the composition of a metallic surface caused by a wear mechanism [131]. There are many forms of wear damage such as: scratching; polishing; gouges; cracks; pitting; etching; embedded third-body

particles; surface discolouration; surface deposits; and tribochemical reaction layers [131].

- **Scratching** – Scratching occurs when one or more wear mechanisms causes an increase in the number or the severity of scratches along the surface. Scratching metallic surfaces tends to increase the surface roughness parameters.
- **Polishing** – Polishing, like scratching, occurs through a number of wear mechanisms although abrasion is quite common. However, polishing occurs when there is a reduction in the number and/or severity of the scratches along the surface. Generally, polishing decreases the surface roughness parameters, which may reduce the wear rate.

- **Gouges** – Gouges are plastically deformed regions or lines that are caused by contact with a sharp corner or edge from another surface (mode 2).

- **Cracks** – A crack may be generated from a single event failure. For example, a hard asperity is dragged and pressed against the surface, which leaves behind tensile cracks that are perpendicular to the sliding direction. However, cracks may be created through the fatigue wear process. In the fatigue wear scenario, the cracks are initiated and grow throughout the loading cycles.

- **Pitting** – Pitting is a form of surface damage characterized by surface indentations in which the dimensions are comparable in any direction unlike a scratch, gouge, or crack where the length can be many magnitudes greater than the width. Pits may be visible by the naked eye or they can be microscopic in size.

- **Etching** – Etching is attributed to fretting and/or corrosion. Etching marks tend to have an area that is much greater than a pit.
- **Embedded Third-Body Particles** – These third-body particles become trapped between the surfaces and can abrade a surface. These particles were originally not present between the surfaces.

- **Surface Discolouration** – Surface discolouration refers to a thin, translucent coating of organic or inorganic material or oxides that may be detected by the eye due to colour diffraction patterns.

- **Surface Deposits** – Surface deposits can consist of proteins that are denatured due to thermal and mechanical processes, precipitated salts, or any other materials that were originally not present on the surface. Surface deposits are generally thicker than surface films and usually increases the surface's roughness.

- **Tribochemical Reaction Layers** – Tribochemical reaction layers are created by chemical interactions with the environment after being mechanically activated.

Tribochemical reaction layers generally consist of a blend of the original surface material and foreign substances.

The last aspect of wear to be addressed is the surface feature. A surface feature is a unique region that has been worn and/or corroded and/or may exhibit a form of damage with a distinct spatial distribution.

2.5.8 The Consequences of Wear Particles and Corrosion Products

Corrosion at the head-neck taper interface can reduce the prosthesis' structural integrity, but the soluble and solid corrosion products may migrate from the taper interface to the surrounding tissue [132]. If these corrosion products reach biological tissues, they may trigger local and distal tissue reactions [132].

Jacobs et al. characterized the locally distributed solid corrosion products found in blood and serum of 15 patients with a unilateral THA prosthesis [132]. Of the 15 prostheses, five did not experience any form of corrosion whereas 10 prostheses had moderate to severe corrosion damage at the head-neck taper interface [132]. By using electron microprobe analysis, Jacobs et al. were able to detect three classes of corrosion products [132]:

Class I: Cr, Mo, and Ti oxides

Class II: Co, Cr, and Mo chlorides

Class III: Chromium orthophosphate hydrate

Classes I and II were primarily found in the same local regions proximal to the head-neck taper interface and were rarely found in tissues that were distal to the prosthesis [132]. In contrast, the chromium orthophosphate hydrate rich deposits were observed along the bore rim and the neck [132]. Of the ten moderately to severely corroded THA prostheses, nine had chromium orthophosphate hydrate rich deposits along the head-neck taper interface [132].

Jacobs et al. noticed that patients who had moderately or severely corroded THA prostheses had significant concentrations of cobalt and chromium in urine and serum in contrast to patients with no or mild corrosion [132]. Also, cobalt and chromium concentrations were much higher for patients with THA prostheses than the control groups (no metal prostheses) [132].

Chromium phosphate is often present in the corrosion residue of retrieved implants [108]. In contrast, cobalt is more soluble and may propagate to surrounding tissues, which can lead to an ALTR [108].

Corrosion and fretting of THA prostheses have various consequences that can lead to complications for the patient such as pain, hypersensitivity, ALTRs, and revision surgery. Figure 2.12 provides a summary of how corrosion and fretting may lead to failure of THA prostheses and require revision surgery.

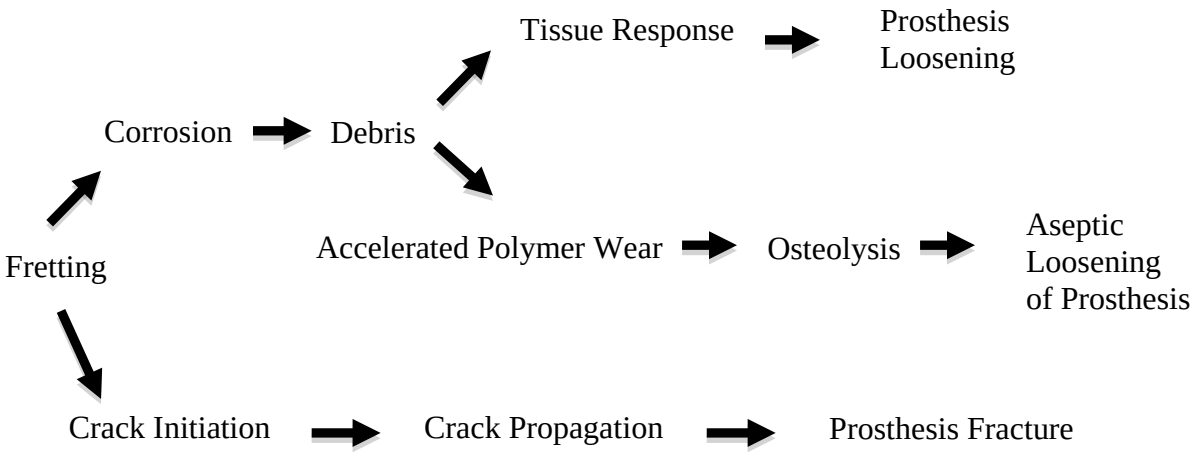

Figure 2.10. Summary of the outcomes of THA prostheses due to the onset of corrosion and fretting.

2.5.9 Adverse Local Tissue Reactions

A pseudotumour is "a granulomatous or destructive cystic or solid lesion, which resembles a true tumour but is neither infectious nor neoplastic in nature and develops adjacent to THA implants" [133]. Pseudotumours were initially discovered in patients with metal-on-metal THA and metal-on-metal hip resurfacing prostheses [134]. Pseudotumours can be identified by the presence of significant "tissue necrosis, chronic inflammatory reaction, and perivascular and diffuse lymphocytic aggregates" [134]. Pseudotumours usually consist of a granulomatous or cystic lesion that resembles a tumour and is commonly found outside the prosthesis [135]. Although some, but not all, patients with pseudotumours experience pain, pseudotumours can cause damage to local bone and soft tissue, and instability of the prosthesis [134, 136].

Metallic prostheses are subject to wear, which is the erosion of material from a solid surface by the action of another solid [137]. By having wear between the articulating surfaces, this may release metal particles into the surrounding tissue. If this should happen, the metal particles may accumulate in histiocytes and synoviocytes, which can be transported to regional lymph nodes; this process is known as metallosis [138]. Metallosis is a condition where metallic debris accumulates in the soft tissues of the body [139]. As a result, extensive fibrosis may occur in the form of a pseudotumour.

The term adverse local tissue reaction (ALTR) refers to any soft tissue reaction that is linked to either metal hypersensitivity, aseptic lymphocyte-dominated vasculitis associated lesions (ALVAL), pseudotumour, and metallosis [140]. There is no clear distinguished boundaries between the terms metallosis, ALVAL and pseudotumour [135]. Instead, the acronym ALTR is used to describe failures of THA prostheses that are linked to pain, a sterile effusion, metallosis, and/or macroscopic necrosis. Pseudotumours can also cause damage to periarticular soft tissues, which may trigger soft-tissue and muscle necrosis, osseous denudation, hip dislocations, and pathological fractures. Metal hypersensitivity is suspected to be linked to pseudotumour formation [135].

Metal-on-metal THA prostheses are well known for releasing chromium and cobalt ions into the patient's bloodstream and joint capsule primarily due to wear [140].The amount of metal ions and particles released into the patient's body is significantly much more than THA prostheses with a metal-on-polyethylene articulation [141].

Wear debris, which can be in soluble and in particulate forms, can be caused by mechanical wear, corrosion, or a combination of both [135]. Metal-on-metal articulations

can generate 6.7 x 10^{12} to 2.5 x 10^{14} particles per year. Some researchers have hypothesized that wear debris is the true culprit of pseudotumour formation [142-144].

Cook et al. reported two cases of pseudotumour formation due to corrosion at the head-neck taper interface. The prostheses consisted of Accolade femoral stems made from TMZF (titanium, molybdenum, zirconium, and iron) that were coupled to CoCrMo femoral heads with diameters of 40 mm and 44 mm [145]. Cook et al. highlighted several factors that may have contributed to the formation of the pseudotumours [145]. These factors include: mechanically-assisted crevice corrosion; angular mismatch; galvanic corrosion; and the use of proximal contacting tapers.

Chana et al. reported a pseudotumour forming with reddish-brown fluid forming near the hip joint capsule for a 50 mm CoCrMo femoral head attached to an Accolade stem (TMZF) with either a C-Taper or a V40 Taper adaptor sleeve (Ti6Al4V) [146]. Chana et al. examined the taper interface and found black debris, which was determined to be chromium orthophosphate, a corrosion product [147]. Chana et al. speculated that the corrosion products within the taper interface migrated to the surrounding tissue to form a pseudotumour [146]. Chana et al. indicated that the corrosion product was formed due to the mismatch of the components. The mismatch at the head-adapter taper interface resulted in increased micromotion, which promoted corrosion and fretting damage.

Scully and Teeny wrote a case report of an 80 year-old male patient who developed a pseudotumour on his right hip after an implantation time of 6 years and 2 months [133]. The patient received a #6 uncemented titanium-tapered stem (TMZF Femoral Hip Stem; Stryker) with a 32 mm CoCr femoral head with a +4 offset and a +10 highly cross-

linked PE liner [133]. Scully and Teeny indicated that there was a soft tissue mass that was 15 cm long and 10 cm wide located anterior to the greater trochanter [133]. Scully and Teeny noted that surface corrosion took place at the head-neck taper interface but there was no substantial wear damage along the polyethylene liner or the exterior of the femoral head [133]

Cooper et al. examined the tissues adjacent to ten patients with THA prostheses that contained taper corrosion at the head-neck taper interface [148]. For all patients, the base of the taper was covered in black, flaky material. Cooper et al. reported that the patients had large soft-tissue masses as well as surrounding tissue damage. Additionally, abnormal fluid that was either milky white or brownish was discovered during surgical entry into the hip joint. Serum cobalt and chromium levels were more elevated than the pre-operative state, with a great difference in cobalt released in comparison to chromium. These conclusions are in agreement with research that has been performed by Garbuz et al. [149] and Langton et al [150].

2.6 Fretting

Fretting is believed to have a major role in head-neck taper corrosion of THA prostheses. This subsection summarizes the subject of fretting and describes the different types, theories, and characterizations. A brief discussion on friction and how it can affect the head-neck taper interface is also presented.

2.6.1 Introduction to Fretting

Fretting is a form of surface damage caused by low-amplitude oscillatory sliding between two contacting surfaces [151]. When two solid materials slide against each other and the amplitude is less than a few millimetres, fretting damage usually occurs [152]. Fretting amplitudes are usually less than a millimetre and normally range between 10 to 50 μm [153]. If this disturbs the formation of the passive oxide layer, this can result in fretting corrosion damage, which usually occurs for non-noble metals. If the fretting amplitude is less than a millimetre, the wear rate is dependent on the load and the amplitude of the motion [152]. Fretting has been detected in orthopaedic devices since the late 1960's [154]. A material's damage to fretting usually increases with the number of cycles; however in some circumstances, the fretting damage can reach a plateau [99]. Fretting has been observed in all quasi-static loaded assemblies including keys, cables, cranes, and orthopaedic implants [155]. When considering the head-neck taper interface of THA prostheses, the micromotion can damage the oxide film and the metal grains closest to the implant surface. Interface wear can also occur, which allows small metal particles to be removed from the surface. This can result in third-body wear or the particles may be oxidized in the local environment [108].

There are two categories of micomotion: recoverable and subsidence. Recoverable micromotion occurs when an implant returns to its initial position after loading. In contrast, subsidence micromotion occurs when the implant does not return to its original position [156].

Micromotion at the head-neck taper interface can cause deterioration of the passive oxide film [108]. Evidence of fretting on materials can be evidenced by fine scars that tend to be unidirectional. Wear along the taper interface may result in the release of metal particles from the surface [108]. These particles may undergo oxidation and trigger third-body wear [108]. When the oxide film is deteriorated or damaged, repassivation occurs and the passive oxide film can be regenerated.

The head-neck taper interface of THA prostheses can experience tiny displacement amplitudes that may endanger the biocompatibility of the device [151]. Fretting is a form of erosion corrosion; erosion occurs under aqueous conditions while fretting occurs under atmospheric conditions [4]. Fretting damage can be discovered by detecting pits and/or grooves along the metallic surface with corrosion products nearby [4]. These pits can act as stress raisers for the metallic surface [4]. Fretting can deteriorate the metallic surfaces while producing oxide debris [4]. By increasing the neck offset and the neck length, this increases the nonsagittal moment, which increases the micromotion at the head-neck taper interface that results in fretting [157, 158]. Also, fatigue fracture may occur due to fretting because components may become loosened and allow excessive strains [4]. For fretting to occur, three conditions must be met [4]:

1. The surfaces that are in contact with each other are subjected to a load.
2. The surfaces that are in contact with each other should vibrate or have relative motion against each other. Even having a micromotion of 10^{-8} cm can initiate fretting damage.

3. Slip or deformation should occur along the surfaces caused by the applied loads and the relative motion of the interface.

In the literature, the terms fretting wear, fretting fatigue, and fretting corrosion are commonly interchanged; however, each of these terms is unique. Fretting wear refers to two components that slide against each other in a controlled manner when a normal load is applied [151]. During fretting wear, debris particles are commonly observed [151]. Fretting wear can be detected by characteristics such as striations, directionality, and fine wear debris [152].

Fretting fatigue refers to the relative displacement caused by cyclic loading of one of the components and is superimposed to the normal load [151]. Fretting fatigue is a combination of cyclic loading and fretting wear [152]. Fretting fatigue characterizes the reduction in fatigue life and is often used when crack initiation is observed in the contact region [151]. During fretting fatigue, fatigue cracks can develop and the action of fretting can further accelerate the formation and propagation of these cracks with the end result being the fracture of the component [152].

Finally, fretting corrosion occurs if oxide formation is present during wearing [152]. With fretting corrosion, surface damage is caused by sliding with corrosion present [151]. Fretting corrosion primarily occurs for non-noble metals [152].

With fretting wear, fretting fatigue, and fretting corrosion occurring, the following processes may occur simultaneously: debris particle generation; crack formation; crack propagation; and corrosion [151]. Even though these phenomena may be observed,

usually one or two of these processes is dominant, which is dependent on the environmental and loading conditions [151].

Fretting can translate from non-abrasive to abrasive wear behaviour [152]. Initially, fretting is usually non-abrasive, which can be attributed to adhesive, repeated-cycle deformation, or chemical wear mechanisms, or a combination of these. For unlubricated metals, the wear rate tends to be inversely related to the frequency when in the range of 10 to 20 Hz since the oxide film has more time for reformation at lower frequencies.

One of the key problems of evaluating the corrosion and fretting damage at the head-neck taper interface is quantifying the amount of material lost at the taper interface [159]. Underwood et al. developed a procedure using a Taylor Hobson Talyrond Roundness instrument to allow the measurement of wear and surface roughness. With this instrument, the following parameters can be measured: taper angle; depth and length of damage; 3D surface maps; and surface topography. In a similar fashion, Vincelli et al. have demonstrated that a coordinate measuring machine can be used to measure the wear damage at the head-neck taper interface [160].

2.6.2 Theories and Characterizations of Fretting

There are two different theories for fretting: the wear-oxidation and the oxidation-wear hypotheses [4]. The wear-oxidation hypothesis was based on the idea that cold welding or fusion occurs along the boundary between the contacting metallic surfaces [4]. These surfaces are subjected to stress and relative motion [4]. As a result, the contact points between the surfaces gets ruptured; therefore, producing metallic debris [4]. The

metallic debris is then instantly oxidized due to heat caused by friction and the size of the particles [4]. The wear-oxidation hypothesis states that friction triggers damage along the metallic surface and that oxidation of the metallic fragments is a secondary effect [4].

The oxidation-wear hypothesis states that the majority of metallic surfaces are shielded from oxidation by a thin oxide film [4]. When these metallic surfaces contact each other and are placed under load and repetitive micromotion, the oxide film will be ruptured [4]. As a result, oxide debris is produced [4]. Current theories suggest that the exposed metal surface reoxidizes and the cycle repeats itself [4]. The oxidation-wear hypothesis indicates that accelerated oxidation is triggered by frictional effects [4]. The mechanism of fretting at the head-neck taper interface appears to occur by this phenomenon since the passive oxide film is deteriorated by fretting and corrosion occurs afterwards.

Even though there are two separate theories for fretting, they have the same conclusion: the metallic interfaces are damaged and oxide debris is generated [4]. Fretting has been discovered on many different types of surfaces and materials such as the noble metals, glass, ruby, and mica [4]. The presence of oxygen has also been known to accelerate fretting damage of many materials, particularly iron alloys [4].

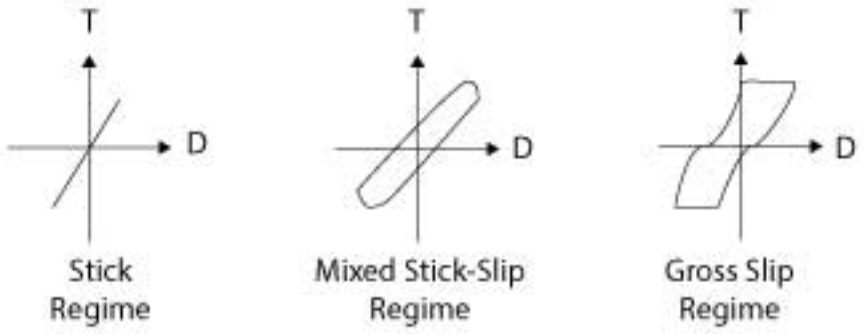

Figure 2.11. The three regimes of fretting [151].

As suggested by Schaaff and Duisabeau et al., there appears to be three regimes of fretting: stick; mixed stick-slip; and the gross slip regime as illustrated in Figure 2.13 [151, 161]. All of these regimes have a direct relationship between the tangential force (T) and the displacement (D) [151, 161]. The area of the tangential force and the displacement loop corresponds to the dissipated energy due to the friction between the contact surfaces [161]. The dissipated energy occurs through processes that include plastic deformation, debris production, and heat dissipation [161].

With the stick regime, the relationship between the tangential force and the displacement is linear and there is minimal particle or debris production [151]. The stick regime is a closed cycle that relates to the elastic regime when there is no observed wear or energy dissipation [161]. The contact surfaces are “stuck” together during the closed cycle mode. One hypothesis to account for the imposed displacement is the elastic deformation of the device and the sample.

In regard to the mixed stick-slip regime, there is an elliptical hysteresis loop to demonstrate the relationship between the tangential force and the displacement [151, 161]. The mixed stick-slip regime represents the partial slip fretting state [161]. During this mode, one aspect of the surface slips while the other aspect sticks [161]. The mixed stick-slip regime best represents fretting fatigue since this regime is known to result in crack initiation, propagation, and is near the stick slip boundary [151, 161]. During the mixed stick slip regime, the elliptic cycles are related to cracking. Even if cracks are not deep enough to decrease the contact rigidity, this can result in micromotion during contact. Extensive debris and particles can be produced during this regime [155].

The gross slip regime has a parallelogram-shaped hysteresis loop to illustrate the relationship between the tangential force and the displacement [151]. During the gross slip regime, the surface slips and results in significant abrasive wear [161]. With the gross slip regime, fretting produces substantial amounts of debris particles [151]. As reported by Duisabeau et al., fretting at the head-neck taper interface is believed to occur through this mechanism [162].

The fretting regimes are dictated by several mechanical parameters such as normal load, amplitude, displacement, rigidity of the device, and contact geometry as well as physicochemical properties (e.g. adhesion) [155]. The fretting regime can trigger a unique material response. With the closed regime, cracking or no degradation may occur. In the gross slip regime, particle detachment may occur. However in partial slip mode, cracking, particle detachment, and no degradation may occur.

By having fretting occurring at the head-neck taper interface, this can initiate a chain of events that can affect the functionality of the THA prosthesis and cause harm to

the patient. Many THA prostheses are designed using CoCr and Ti6Al4V alloys. Both of these alloys are capable of forming a protective passive oxide film to protect the head-neck taper interface from corrosion when in contact with biological fluid [151]. However, the fretting action between the bore of the head and the neck of the stem can lead to destruction and breakdown of the oxide film [151]. This can expose the metallic surfaces to biological fluid, which can result in mechanically-assisted crevice corrosion, pitting, or galling [151]. This may also result in the release of metal particles that can trigger a host-tissue response [151]. The host-tissue response includes inflammation and immunological reactions that can lead to loosening of the prosthesis [151]. The metal particles and corrosion products from the head-neck taper interface are also capable of migrating in the body locally and systematically [151]. By having local migration of these particles, this can accelerate the wear of polyethylene between the femoral head and the acetabular cup [151]. This can initiate osteolysis in the region between the prosthesis and the bone; therefore, leading to aseptic loosening of the implant [151].

2.6.3 Friction

Friction is the reluctance of a body when it moves over another body during direct contact. When two materials are in contact with each other, there is an electrical attraction between the atoms of these two surfaces. This electrical attraction is due to friction. Friction is the parallel component of the contact force exerted by a surface on an object. Friction can be classified into two categories: static friction and kinetic, or sliding, fric-

tion. Static friction (F_s) occurs when there is no relative movement between the two surfaces. In contrast, kinetic friction (F_k) occurs when there is relative motion between the contacting surfaces. The magnitude of the frictional force of an object, static or kinetic, can be influenced by the composition of the material, the objects' surface finish, and if there is lubrication between the two surfaces.

When an object is lying along a surface, there are two forces acting on the object. The first force is the gravitational force (W), which acts downwards on the object. This is the product of the object's mass (m) and the acceleration due to gravity (g).

$$W = mg \qquad \text{(Equation 6)}$$

If the gravitational force was the only force acting on the object, then the object would pass through the surface that is supporting it. A second force acts on the object, the normal force (F_N), which is the perpendicular component of the contact force exerted by a surface on an object.

$$F_N = mg \qquad \text{(Equation 7)}$$

When an object is lying along a horizontal surface with no downward forces besides gravity, the normal force is equal to the weight of the object; however, there are some circumstances such that the normal force is not equal to the object's weight.

The frictional force (F_f) exerted by an object's surface is related to its normal force. The magnitude of the kinetic friction force (F_k) by an object is proportional to the object's normal force based on the coefficient of friction (μ_k). For all pairs of surfaces, the coefficient of friction can range 0 to 1 and depends on what type of surface the object is resting on as well as the material of the object. As the coefficient of friction increases, the corresponding frictional force also increases.

$$F_k = F_N \mu_k \qquad \text{(Equation 8)}$$

The coefficient of friction is independent of the shape and the size of the components, the contact area, and the types of loads and their magnitudes when acting along the object [163]. The coefficient of friction can also be influenced by the mean contact pressure, which can be attributed to the shape of the object. However, this is not a critical issue for the head-neck taper interface for THA prostheses [163].

Determining the static frictional force is similar to the kinetic frictional force; however, there are two key differences. First, there is a coefficient of static friction (μ_s) between the two contacting surfaces. Generally the coefficient of static friction is greater than the corresponding coefficient of kinetic friction. Second, when determining the magnitude of the static frictional force, there's no general formula for solving the force of static friction; however, the formula to solve the maximum force of static friction is pro-

vided below. The direction of the force of static friction is always opposite to the direction of the object's intended velocity and parallel to the surface the object is resting on.

$$F_{s,\,max} = F_N \mu_s \qquad \text{(Equation 9)}$$

The coefficient of friction is critical to the survivorship of THA prostheses when fatigue loading occurs at the head-neck taper interface [164] as well as maintaining fixation between the stem and the surrounding bone and/or cement. By maximizing the value of the coefficient of friction, this can be beneficial as this will decrease the likelihood of fretting [165]. Additionally, static and kinetic frictional forces do exist for THA prostheses. The static frictional force is present at the head-neck taper interface during the assembly procedure when the surgeon strikes the femoral head with a hammer. In regard to kinetic friction, there is micromotion between the femoral head and the neck of the stem when the patient is performing activities of daily living. This micromotion can result in fretting damage. If micromotion occurs between the head and neck, the head must overcome kinetic frictional forces.

Fessler and Fricker conducted a study where they tried to determine the coefficient of static friction for cone tapers featuring a universal head on a stem spigot [163]. To determine the coefficient of static friction, Fessler and Fricker conducted axial push-on and lift-off testing, as well as push-on and twist-off testing, of the heads on the stem spigots at room temperature [163]. From this investigation, Fessler and Fricker reported

that the coefficient of static friction between a CoCrMo head and either a CoCrMo or Ti6Al4V stem spigot was 0.15 [163]. For a stainless steel femoral head on a stainless steel stem spigot, the coefficient of static friction was determined to be 0.13. They also addressed that the coefficient of static friction was independent of the taper geometry, the magnitude of the push-on force, the head taper half-angle, the taper half-angle mismatch, and non-axisymmetric taper contact [163].

When the orthopaedic surgeon is performing the THA assembly procedure, he or she will try to avoid contact with the taper; however, it is possible that blood and other biological fluids may come into contact with the bore of the head and/or the neck of the stem. Even if the surgeon wipes off the taper surfaces, the taper surfaces will still be lubricated. As highlighted in their paper, Fessler and Fricker indicated that the lubrication between the head and the stem spigots generally do not have an influence on the coefficient of friction [163]. Fessler and Fricker also stated that grooved spigot surfaces produced inconsistent and generally less friction than ground spigot surfaces [163].

2.7 Corrosion and Fretting in Total Hip Arthroplasty

This section focuses on corrosion and fretting damage with respect to THA prostheses. Corrosion and fretting damage is explored in the literature at the head-neck and neck-stem taper interfaces, the phenomenon of tribocorrosion, and the corrosion products that can be found at the head-neck taper interface for THA prostheses.

2.7.1 The Link Between Corrosion and Fretting in Total Hip Arthroplasty Prostheses

Cater and Hicks reported the first incidence of corrosion in orthopaedic devices in 1956 for fine-threaded Sherman type stainless steel screws [166]. Cohen and Lindenbaum first reported fretting corrosion in 1968 between implanted plates and screws and identified four contributing factors [154]:

1. Corrosive Wear – Mechanical action deteriorates a surface's protective layer and makes the object vulnerable to corrosion damage.
2. Surface Fatigue – Stress results in surface or subsurface cracks and spalling.
3. Adhesive Wear – Particles are pulled off one surface after microscopic spot welding of asperities on the two surfaces has occurred because of loading.
4. Abrasive Wear – The harder material can create grooves along a softer material's surface.

Cohen and Lindenbaum argued that fretting corrosion is a blend of abrasive, corrosive, and adhesive wear, although surface fatigue may serve a minor role [154]. By having fretting damage occur at the head-neck taper interface, this may trigger a biological reaction around the bone stock [167].

Corrosion at the head-neck taper interface was first reported in the early 1980's [168, 169]. Corrosion at this site can be observed by the presence of a white haziness, discolouration, and/or blackened debris [170]. Pivec et al. speculated that taper corrosion occurs up to one-third of all modular implants [108].

Corrosion at the head-neck taper interface is a critical issue for THA prostheses [171]. Metal particles, whether released due to corrosion or from wear, can lead to metabolic, bacteriologic, immunogenic, and oncogenic reactions [172]. Even when released in the biological environment, wear particles could be vulnerable to corrosion [173]. As reported in the literature, corrosion at the head-neck taper interface can trigger pain or result in ALTRs [174, 175].

When corrosion occurs along the neck portion of the head-neck taper interface, the surgeon has to ask him or herself if the stem should be removed. Currently, there are no guidelines for this issue [176]. If the stem is to remain implanted in the patient, the corrosion products may result in an ALTR and/or increase the likelihood of corrosion damage along the bore of the femoral head. On the other hand by removing the stem, this will solve the issue of the corrosion products on the implant; however, this can result in patient morbidity such as soft tissue damage, femoral fracture, bone loss, and the inability to achieve fixation [176].

Table 2.7. The Goldberg technique for scoring corrosion and fretting damage at the head-neck taper interface.

Severity of Corrosion and Fretting Damage	Score	Criteria
None	1	No visible corrosion observed No visible signs of fretting observed
Mild	2	Less than 30% of the taper surface is discoloured or dull A single band or bands of fretting scars involving three or fewer machine lines on the taper surface
Moderate	3	More than 30% of the taper surface is discoloured or dull or less than 10% of the taper surface contains black debris, pits, or etching marks Several bands of fretting scars or a single band involving more than three machine lines
Severe	4	More than 10% of the taper surface features black debris, pits, or etching marks Several bands of fretting scars with several adjacent machine lines or flattened areas with nearby fretting scars

The most popular technique for analyzing taper corrosion is the Goldberg method [177]. To assess the validity of this technique, two researchers assessed 100 metal-on-metal THA prostheses for corrosion damage [178]. From this study, the agreement between the researchers for the corrosion and fretting scores of the head taper were 95% and 82%, respectively [178]. With respect to the neck taper, the agreement for corrosion and fretting were 90% and 85%, respectively [178]. Hothi et al. noted that the slight disagreement in fretting scores can be attributed to the examiners' ability to distinguish fretting damage from assembly or revision damage [178]. Although the Goldberg technique appears to be reliable between users for assessing corrosion damage, its main weakness lies in the fact that it concentrates on the severity of the taper damage and does not put

much emphasis on the area of damage. When examining the severity of corrosion damage for a moderate score, it is debatable as to whether a discoloured or dull taper surface with more than 30% of the area affected is comparable to a taper surface with black debris, pitting, or etch marks with a taper area of less 10% affected.

To examine the corrosion and fretting damage at the head-neck taper interface of THA prostheses, visual scoring is often performed by many researchers because it is a quick and easy way to assess the damage. The downfall of this technique is that no quantitative information is provided in terms of how much material is lost from the surface [179]. Underwood et al. conducted a study of 91 metal-on-metal THA prostheses and used the Goldberg scoring system to assess for corrosion and fretting damage [177] while measuring the wear damage [179]. Underwood et al. found that when they compared the visual corrosion and fretting scores to the measurement of the wear along the taper surface, they found that Goldberg's scoring technique "did not accurately predict the magnitude of the depth or volume of material loss from the retrieved heads" [179].

Higgs et al. analyzed the corrosion and fretting damage of 106 THA prostheses with a metal-on-metal articulation featuring 76 heads, 31 stems (22 modular necks), ten modular CoCr acetabular liners, and five corresponding acetabular shells [170]. Fretting and corrosion damage were discovered in 68 of 76 (89%) head tapers, 21 of 31 (68%) stem tapers, 20 of 22 (91%) male neck tapers, 10 of 10 (100%) modular liners, and 5 of 5 (100%) modular shells.

Higgs et al. identified a relationship between implantation time and corrosion damage with respect to head tapers, stem tapers of modular stems, and the male neck ta-

pers of modular stems [170]. At the head-neck taper interface, the head tapers displayed greater corrosion and fretting scores than the neck tapers, but they were positively related to each other. Also, there was less corrosion and fretting damage on similar alloys in comparison to mixed alloy prostheses. Higgs et al. also reported that corrosion and fretting damage occurred along the shell-liner interface. Damage consisted of scratching and discolouration along the backside of the rims of the liners as well as circular fretting patterns on the acetabular shells.

Langton et al. noted that as the head offset and head diameter increased, so did the taper damage [71]. In particular, Langton et al. reported that as the horizontal lever arm (HLA) becomes larger, the taper wear increases. The HLA can become larger by increasing these three factors: head offset; bearing diameter; and the varus neck shaft angle. Additionally, an extended neck length [156] or contamination of the taper interface with debris [180] may trigger corrosion occurring at the head-neck taper interface.

Collier et al. conducted a retrieval analysis to examine the presence of corrosion damage at the head-neck taper interface for three different head and neck combinations for THA prostheses: CoCr heads and stems; Ti6Al4V heads and stems; and CoCr heads matched with a Ti6Al4V stem [181]. None of the single alloy implants displayed any signs of corrosion; however, 17 of the 30 mixed alloy implants (CoCr head with a Ti6Al4V stem) displayed signs of corrosion. For this mixed alloy group, the 32 mm heads had a greater frequency of corrosion damage (10/14) than the 28 mm heads (7/15). Additionally, the 32 mm heads had more area of corrosion damage (average of 27% for

those affected by corrosion) in comparison to the 28 mm heads (average of 17% for those affected by corrosion) [181].

Panagiotidou et al. performed an *in vitro* corrosion fatigue testing experiment following the ASTM F1875-98 standard to identify if the surface finish and the contact area can influence corrosion and fretting damage at the head-neck taper interface of THA prostheses [182]. For this investigation, 28 mm CoCr femoral heads were matched with full length or reduced length 12/14 mm Ti6Al4V stems [182] and were loaded for ten million cycles with a force range from 100 N to 3100 N at a frequency of 4 Hz [182]. Panagiotidou et al. identified that small tapers, especially those with a roughened surface, were more susceptible to corrosion and fretting [182]. This can be attributed to a reduced surface area at the taper interface and the bending forces are concentrated at these regions [182].

Panagiotidou et al. also investigated how the surface finish and the contact area at the head-neck taper interface influence corrosion and wear damage [183]. The tapers in this study consisted of a 12/14 mm neck with a cone angle ranging from 5°37’ to 5°42’ [183]. The neck components were separated into two main categories. The first cohort had a full length taper contact while the second set had a region that was reduced to two flats that consequently reduced the surface area along the head-neck taper interface [183]. Two types of tests were performed. The first test consisted of rough “mini-neck” length tapers that were compared to rough standard length neck tapers [183]. For the second test, rough mini-neck tapers were compared to smooth mini-neck tapers [183]. All of the femoral heads were 28 mm in diameter, consisted of CoCrMo alloy, had a cone angle of

5°43’30’’, and a +8 offset [183]. *In vitro* corrosion fatigue testing was performed for ten million cycles with a force range from 100 to 3100 N at 4 Hz in phosphate buffered saline [183].

After conducting testing, Panagiotidou et al. observed that the surface roughness along the head taper was more prominent when the head-neck contact area was reduced [183]. Additionally, the taper of the femoral head had an increase in surface roughness once it was assembled onto a rough neck taper [183]. Also, there was some deterioration of the passive oxide film on the rough, but not the smooth, neck tapers [183]. From this study, Panagiotidou et al. concluded that the surface area and surface finish influences corrosion and wear damage at the head-neck taper interface [183].

Meyer et al. conducted a retrieval analysis of 114 large diameter metal-on-metal THA prostheses from 110 patients to determine if there was a link between head-neck taper corrosion and instability [184]. Additionally, Meyer et al. also examined the periprosthetic tissues for metal and if the concentration of the metal particles was correlated to head size [184]. The mean head diameter was 46 mm (range between 48 to 58 mm) [184]. Of these tapers, 107 (94%) contained black corrosion products at the head-neck taper interface and all 107 femoral heads showed signs of instability on the neck taper as discovered during revision surgery [184]. Also, 106 (93%) of the hips displayed joint effusions and tissues with a grayish necrotic appearance and 90 hips (79%) contained an extended bursa formation that resembled pseudotumours [184]. Meyer et al. also found no link between head size and the amount of metal released at the head-neck taper interface [184].

Schramm et al. quantified the wear of the head-neck taper interface of THA prostheses and examined the changes in metallurgy for three modular stems through *in vitro* fatigue testing and also analyzed a single prosthesis that was implanted in a patient for 66 months [167]. Fatigue testing was performed following and exceeding the guidelines highlighted in ISO 7206. Testing was performed for 10 to 12 million cycles at 2 Hz, axial loads up to 4000 N, and 0.9% NaCl saline solution was used. Schramm et al. discovered that greater wear damage, including minor plastic deformation, was found along the medial side that was attributed to fretting mechanisms.

Schramm et al. also examined the *in vitro* fretting and corrosion behaviour of three THA prostheses [167]. The goal was to explore the mechanical stability and changes at the head-neck taper interface after loading. The prostheses were MRP-Titan made and consisted of Ti6Al7Nb for the stem components and Al_2O_3 for the femoral heads. Cyclic loading was performed according to ISO 7206. However, Schramm et al. modified this standard by increasing the axial load up to 4000 N and increased the duration of the loading up to 12 million cycles. The inferior 100 mm of the prostheses were embedded in PMMA. In contrast, the superior 200 mm was surrounded by 0.9% NaCl solution at a temperature of 37°C. Additionally, the surfaces of the female components were coated with bone debris and blood. To examine the corrosion and fretting damage, Schramm et al. used optical microscopy, SEM, and visual inspection. Schramm et al. discovered for the three prostheses that wear occurred along the taper interface of the sleeves. This was evident by the presence of two wear rings along the medial and lateral areas of the extension sleeves. SEM revealed a 0.5 mm crack for a prosthesis that was subjected to 12 mil-

lion cycles of loading as well as tiny secondary cracks that were parallel to the primary crack. Schramm et al. discovered that the wear damage was greater in area and more severe in the medial region in comparison to the lateral region. Also, Schramm et al. found signs of fretting (plastic oscillation proofs that were parallel to the sliding direction) as well as TiO_2 particles that were generated by fretting. Due to the action of fretting, Schramm et al. stated by generating debris particles, this may trigger a biological reaction between the bone stock and the implants. When comparing the surface roughness of the prostheses' stems, the mean surface roughness decreased by 5% in comparison to the preloaded state. Despite the presence of fretting and corrosion, Schramm et al. insisted that the advantages of modularity outweigh the potential risks of mechanical failure.

Even modular connections for monopolar hemiarthroplasty implants are susceptible to corrosion damage [185, 186]. Whitehouse et al. conducted a case report of a 72 year-old man with an Accolade TMZF Plus stem (Howmedica/Osteonics) (vitallium alloy, CoCrMo) and a unipolar Unitrax 54 mm outer diameter endoprosthetic head (vitallium alloy, CoCrMo) [186]. For this prosthesis, the only modular junctions were the stem-sleeve and the head-sleeve interfaces [186]. Whitehouse et al. discovered corrosion damage along the neck of the stem as well as the inner sleeve surface [186]. Additionally, metallosis occurred with black corrosion products along the neck and there was a pseudotumour adjacent to the prosthesis with visible metal particles [186]. Even though there was a material difference between the stem, the sleeve, and the femoral head, this could have contributed to galvanic corrosion despite a small difference in the electrical potential. Whitehouse et al. speculated that the small contact area with the V40 taper, a narrow

neck design, and the low rigidity of the neck contributed to corrosion damage [186]. This report by Whitehouse et al. is the first case where a pseudotumour formed for a hip prosthesis that did not feature a bearing surface and the source of damage occurred at a taper interface.

Chandrasekaran et al. conducted a fatigue testing experiment on ten Richards Modular Hip System prostheses in deionized water and the components were manufactured from Ti6Al4V alloy [187]. The loading conditions consisted of a cyclic load of 2000 N with a range of 100 N and each test was carried out for five million cycles at 6 Hz. Six of these prostheses had negligible titanium release; three had moderate release of titanium, and one prosthesis had substantial release of titanium. Chandrasekaran et al. discovered that by releasing more titanium, there appeared to be more fretting damage along the test specimens and less pull-off force was required to separate the modular connection. Chandrasekaran et al. emphasized that “manufacturing induced discontinuities in the matching tapers might result in more fretting motion between modular components resulting in the possibility of increased release of debris and ions”. Some potential adverse effects of fretting at the modular connection include loosening of this connection, osteolysis, and accelerated articular wear due to debris particles.

2.7.2 Multiple Modular Sites: A Focus on the Neck-Stem Taper Interface

Orthopaedic manufacturers are currently developing THA prostheses with more sites of modularity [165]. By having a modular neck-stem interface, this gives the surgeon greater flexibility in implant position and to replicate the patient's natural femoral offset, length, and version [188]. By having more modular sites, the possibility of fretting rises [165]. To demonstrate this point, Weinstein et al. examined 100 patients with CoCr or stainless steel orthopaedic prosthetics or internal fixation devices and wanted to determine the causes of failure and/or revision [189]. Thirty implants consisted of only one component whereas 70 implants featured multiple components. For these 30 single component implants, there were no signs of corrosion. When examining 28 stainless steel screw and plate type prostheses, 27 of these featured crevice corrosion and fretting damage along the contact surfaces. In particular, this was primarily prevalent along the countersink portion of the screw hole and the screw's chamfer surface. There was no link between implantation time and the severity of corrosion from a six month implantation time and onwards. Weinstein et al. also reported that there were no cases of corrosion resulting in fatigue failure. From this study, Weinstein et al. concluded that implants manufactured from two or more components are more vulnerable to corrosion than components with no modular sites.

One of the key disadvantages of modular orthopaedic devices is that each additional modular interface becomes a potential site for corrosion, fretting, and wear [190-

194]. Multiple studies have reported that corrosion and fretting damage does not solely occur at the head-neck taper interface, but at other modular sites such as the stem-neck interface of THA prostheses [180, 195, 196].

Corrosion along the neck-stem taper interface is a relatively new problem that can lead to ALTRs and has been found for necks that consist of CoCr and Ti6Al4V [134, 197-199]. Currently, two modular neck-stem THA prostheses have been recalled: the ABG II Modular and the Rejuvenate Modular, both from Stryker Orthopaedics [108, 200]. In particular, the Rejuvenate Modular prostheses have been reported to have a high rate of corrosion damage that can lead to the formation of ALTRs [108, 200].

Molloy et al. performed a study of 15 patients who received the ABG II dual modular hip system [107]. For all of these patients, Molloy et al. observed higher than normal cobalt ion levels in the blood serum but chromium levels were within normal range. Molloy et al. performed revision surgery for seven of these 15 patients. For these prostheses, the head-neck taper interface (CoCr femoral head on CoCr neck) displayed no or very little corrosion damage. Meanwhile, the neck-stem taper interface (CoCr neck on Ti6Al4V stem) displayed either moderate to severe corrosion damage in all cases. In particular, Molloy et al. reported that the corrosion damage was concentrated on the superior portion of the taper interface and there was no fretting damage on any of the neck-stem taper interfaces. Molloy et al. also noted that pseudotumours were found for all patients that had undergone revision surgery.

Similar to Molloy et al., Meftah et al. conducted an investigation involving 123 Rejuvenate THA prostheses (97 were modular and 26 were non-modular) to determine

the failure rate due to corrosion [201]. When Meftah et al. measured the blood serum concentrations of cobalt and chromium ions, there were substantial differences between the modular and non-modular groups. The mean concentration of cobalt in the modular and non-modular groups were 5.4 ± 5.7 µg/L and 1.6 ± 1.5 µg/L, respectively ($p = 0.04$). For the chromium ions, the blood serum concentrations were 2.1 ± 1.5 µg/L and 0.9 ± 0.5 µg/L for the modular and non-modular groups, respectively ($p = 0.01$). Meftah et al. also noted that the high cobalt and chromium levels were strongly correlated to patients who were younger, had bilateral THA prostheses, and had a high femoral head-neck offset. By having a high femoral head-neck offset, this can result in greater lever-arm forces at the neck-stem taper interface. None of the non-modular prostheses were revised but 23 (28%) of the modular prostheses were revised. For all of these revised modular prostheses, Meftah et al. reported that the head-neck taper interface did not display any signs of corrosion damage; however, moderate and severe corrosion damage was detected at the neck-stem taper interface. Additionally, only two (9%) of these revised cases had a pseudotumour present whereas eight cases (35%) had an ALTR. Meftah et al. speculated that one of the reasons for the failure rate was attributed to the material difference between the CoCr neck and the TMZF stem body along with an inadequate taper fit. By having a difference in the materials at the neck-stem taper interface, this could have resulted in substantial micromotion that deteriorated the oxide film and make the region vulnerable to crevice corrosion.

Kretzer et al. reported that despite the additional modular interface, modular neck THA prostheses do not result in elevated systemic titanium ion levels in comparison to

stems without a modular neck interface [202]. However, Kretzer did observe elevated levels of titanium in patients in comparison to controls without an implant [203]. If failure should occur along the neck-stem taper interface, the surgeon can treat the patient by performing a revision surgery with a ceramic femoral head [134]. In rare cases, corrosion can result in fracture of the modular neck [197].

In one retrieval analysis, Gill et al. attempted to account for why there was no taper corrosion at the head-neck taper interface but corrosion occurred along the neck-stem taper interface for the ESKA dual-modular short stem prosthesis with a metal-on-polyethylene articulation [196]. Gill et al. hypothesized that the neck-stem taper interface experiences more micromotion due to the HLA [196]. Additionally, these two taper interfaces experience different loading conditions. The stresses along the head-neck taper interface are low since the forces are directed through the center of the head [196]. Meanwhile, the neck-stem taper interface is loaded eccentrically, which can lead to higher stresses [196].

Higgs et al. conducted a retrieval study consisting of 134 femoral heads and 60 stems (41 had a modular neck-stem taper interface) to determine if there is a relationship between corrosion and fretting damage at the head-neck taper interface in comparison to the neck-stem taper interface [204]. Additionally, Higgs et al. examined the components to determine which design parameters contributed towards corrosion and fretting damage using the Goldberg corrosion scoring system. Higgs et al. found that as the implantation time increased, the corrosion damage of the heads and stem tapers was more prominent, but not the tapers of the modular necks [204]. The head tapers also displayed more corro-

sion damage than the neck tapers [204]. Additionally, Higgs et al. noted a correlation between head size and head taper corrosion and that there may be a link between head-neck and neck-stem taper corrosion [204].

Even though corrosion and fretting are more likely to appear for THA prostheses with a head-neck and a neck-stem interface, corrosion and fretting behaviour is a combination of a multitude of factors. In one case study by Ellman and Levine, they reported a 59 year old male who had a double-tapered THA prosthesis that fractured [106]. The fracture was believed to be influenced by a multitude of factors such as crevice corrosion, fretting, patient obesity, large head size (52 mm), a metal-on-metal articulation, a large neck, and the patient's activity level [106].

Cooper et al. examined the tissues adjacent to ten patients with modular hip prostheses that featured corrosion damage at the head-neck taper interface [148]. For all patients, the base of the taper was covered in black, flaky material. Cooper et al. reported that the patients had large soft tissue masses as well as surrounding tissue damage. In addition, serum cobalt and chromium levels were more elevated than the pre-operative state, with a great difference in cobalt released in comparison to chromium. This finding is in agreement with studies performed by Garbuz et al. [149] and Langton et al [150]. Also, abnormal fluid that was either milky white or brownish was discovered during surgical entry into the hip joint.

Using ANSYS finite element software, Abdullah created a 3D model replica of the neck-stem taper interface of the PCA No. 5 (Howmedica) hip prosthesis [165]. Only half of the stem was modelled using symmetry constraints along the plane that divides the

neck into two halves to reduce the computation time [165]. The model was meshed using hexahedral (brick) elements (SOLID45) [165]. For the neck-stem taper interface, 3D node-to-node contact elements were implemented (CONTAC52) [165]. These elements were selected such that the two surfaces could maintain or break physical contact so they could slide against each other [165]. Abdullah also applied a boundary condition along the bottom surface of the neck such that there were no degrees of freedom at that site [165]. To measure the effect of angular mismatch, three conditions were chosen: zero, negative, and positive [165]. Five loading schemes were applied with an assembly force (0 N, 3114 N, and 5500 N) followed by two loading cycles (2000 N, 3114 N, and 5500 N) [165]. Abdullah did not specify how the assembly forces were chosen, but selected the loading cycles ranging from three to seven times the body weight of a 75 kg person to simulate walking at a normal to a fast pace [205]. In normal and fast walking, the load on the THA prostheses ranges from three to four times the patient's body weight [205].

Abdullah found that by increasing the assembly load, this helped secure the lock between the stem and the neck components and this reduced the fretting, stress, and micromotion at the neck-stem taper interface during loading [165]. By having an increased assembly load, this could extend the lifetime of the prosthesis due to the decrease in fretting damage [165]. Additionally, increasing the coefficient of friction reduced the micromotion caused by fretting [165]. Abdullah also observed that the zero angular mismatch yields the most micromotion at the neck-stem taper interface [165]. Abdullah recommended a positive mismatch for the neck-stem taper interface (cone angle of the neck is two minutes above the female taper of the stem) [165].

Vundelinckx et al. measured the serum cobalt and chromium levels in 19 asymptomatic patients with an ABG II Modular THA prosthesis featuring a modular neck-stem taper interface that had either a ceramic-on-ceramic (n = 6) or a ceramic-on-polyethylene (n = 13) articulation [140]. Fifteen patients had a cobalt concentration of more than the reference value of 1 µg/L [140]. However for chromium, only two patients had a greater concentration than the reference value of 1 µg/L [140]. Generally, the concentrations of cobalt were greater than chromium [140]. Research by Gill et al. [196] and Merritt et al. [206] has demonstrated that cobalt can quickly propagate away from the joint and be excreted in urine whereas chromium remains stored within the tissue and requires more time to diffuse away. Additionally, Vundelinckx et al. reported that a separate patient not linked to the 19 asymptomatic patients developed a large ALTR approximately two years post-operatively [140]. Vundelinckx et al. reported that there was severe corrosion damage at the neck-stem taper interface and the measured concentrations of cobalt and chromium were 2.1 µg/L and 7.4 µg/L, respectively [140]. From this study, Vundelinckx et al. demonstrated that neck-stem taper corrosion can occur and elevate the cobalt and chromium serum concentrations and ALTRs can be triggered even with low metal ion serum levels [140].

On a related topic, taper corrosion has also been found for TKA prostheses [207]. Arnoldt et al. conducted a retrieval study of 198 TKA implants and examined the prevalence of taper corrosion [208] using the Goldberg corrosion scoring system [15]. Arnoldt et al. obtained 101 femoral components and 97 tibial components. For these implants, 90 had a threaded taper interface whereas 10 had a conical taper interface. Arnholdt et al. re-

ported mild to severe corrosion damage for 94 of the 101 (93%) femoral components and for 90 of the 97 (93%) tibial components. Additionally, the conical tapers displayed significantly more corrosion damage than the threaded tapers. Arnholdt et al. hypothesized that the threaded taper connection delivers less micromotion than the conical tapers. Similar to the head-neck taper interface of THA prostheses, galvanic corrosion was detected along the male conical tapers and they displayed more severe corrosion damage than the single alloy prostheses. Arnholdt et al. also indicated that anatomical location and the weight of the patients were positively related to the corrosion scores.

2.7.3 Corrosion Products

McMaster and Patel presented a case report of a corroded CoCrMo taper for a TKA revision that triggered an ALTR [207]. EDS was performed to analyze the chemical composition of the taper [207]. EDS revealed that the taper contained oxygen, molybdenum, and chromium [207]. This suggests that the black encrustations along the taper are chromium and molybdenum oxides, which they suggest is a corrosion product for a CoCrMo alloy [207].

Additionally, increased levels of molybdenum may be detected along the corroded region. This was reported by Cook et al. in a study that investigated corrosion damage along the countersink portion of a screw and plate apparatus [99].

Langton et al. examined the material loss along the ASR XL and DePuy's Articuleze (Pinnacle) to determine risk factors for taper failure [71]. When EDS was performed, the pits contained chromium as well as chlorides and oxides; thus, indicating that corrosion took place.

Cooper et al. examined 12 Rejuvenate (Stryker) prostheses from 11 patients featuring a dual-taper stem [168]. This prosthesis consists of a femoral component consisting of TMZF with a CoCr alloy neck component. Cooper et al. reported corrosion damage at the neck-stem taper interface and ALTRs were present for all prostheses. Serum metal ion levels consisted of a greater concentration of cobalt than chromium and titanium. Cooper et al. detected substantial corrosion and fretting damage at the neck-stem taper interface. When performing EDS, cobalt was substantially depleted; thus, suggesting that selective leaching took place. In particular, a chromium phosphate corrosion product had formed. When analyzing the head-neck taper interface, pitting corrosion was found and classified in six of ten cases.

2.7.4 Tribology and Tribocorrosion

Tribology is a branch of mechanical engineering and materials science that deals with the friction, wear, and lubrication of interacting surfaces that are in relative motion to each other [209]. When surfaces are in contact and have relative motion to each other, wear can occur through different forms such as abrasion, adhesion, and erosion. Wear

damage can be prevented by applying a lubricant between the two contacting surfaces or by modifying the surface properties with a surface finish.

A tribological system can be broken down into three main branches: the physical properties of the materials; the mechanics of the tribological contact; and the environment [40]. The wear resistance of a material is dependent on its material properties such as its hardness, modulus of elasticity, ductility, yield strength, and rigidity. Additionally, the material's microstructure can have an influence on the damage through variables as the grain size, the presence of defects, inclusions, segregations, or the dislocation density. In regard to tribological contact mechanics, the amount of damage that occurs depends on the applied force, the type of contact (e.g. sliding, rolling, fretting, etc.), the motion, and the size and shape of the contacting bodies [40].

The Stribeck curve is a graph that can be used to analyze the lubrication contact between the surfaces. The Stribeck curve plots the coefficient in friction as a function of viscosity, speed, and load, which is the dimensionless Hersey number [210, 211]. Figure 2.12 provides an illustration of the Stribeck curve.

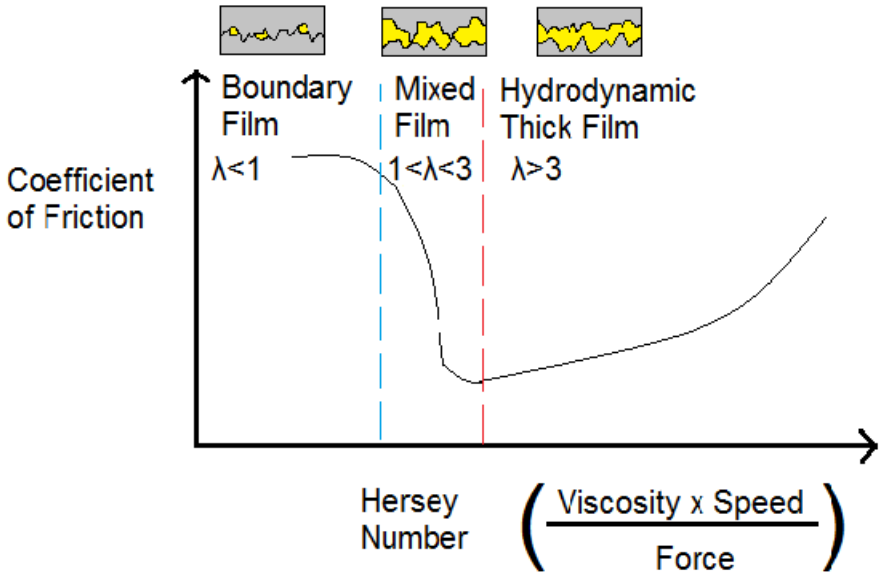

Figure 2.12. The Stribeck curve.

There are three regimes for the Stribeck curve that are based on the λ value obtained in Equation 10: hydrodynamic; mixed, and boundary lubrication. During the hydrodynamic regime (λ > 3), the two material surfaces are separated from each other by the lubricant and the lubricant supports the load [212]. For the mixed film regime (1 > λ > 3), the surfaces are not completely separated from each other and some of the load is transmitted to other materials through surface asperities while rest of the load is supported by the lubricant [212]. During the boundary lubrication regime (λ < 1), there is substantial contact between the surfaces [212]. For the engaged head-neck taper interface, it is believed that boundary lubrication takes place.

$$\lambda = \frac{z}{(Rq_{mat1}^2 + Rq_{mat2}^2)^{1/2}} \quad \text{(Equation 10)}$$

λ = Lubrication number

Rq_{mat1} = Root mean square of surface roughness (m)

z = Central film thickness (m)

Tribocorrosion is a subfield of tribology and it is a material degradation process that results from simultaneous mechanical, chemical, or electrochemical (corrosion) material removal mechanisms [213]. Tribocorrosion, or often referred to as mechanically-assisted crevice corrosion in the literature, is a synergy of corrosion and wear and not a summation of the two processes. Approximately 20% to 50% of material loss in a tribocorrosion system is attributed to corrosion related effects [214]. Total material loss from tribocorrosion can be determined as a combination of the material loss in the absence of corrosion, the material loss due to electrochemical processes in the absence of wear (i.e. corrosion), and the synergy of the effect of wear on corrosion and the effect of corrosion on wear.

By applying a compression force at the femoral head, the head-neck taper interface's corrosion potential will change from a passive to an active region due to the deterioration of the oxide film. Meanwhile, the environment can influence tribocorrosion through a number of variables such as the temperature, pH, viscosity, and electrical conductivity or insulation [40].

For THA prostheses, the head-neck taper interface is vulnerable to tribocorrosion when body fluid enters the taper interface. With a larger head size and an optimized clearance, iso-viscoelastic elasto-hydrodynamic lubrication can be achieved, which decreases the amount of wear damage [40]. Ocran reported that clinically relevant simulated body fluid favors the formation of a hydrodynamic lubrication film at the head-bearing interface for metal-on-metal articulations [40]. When conducting *in vitro* corrosion fatigue testing, Ocran also indicated that the electrolytic solution can modify the passive oxide film's properties, which can have an influence on the tribocorrosion behaviour of CoCr alloy [40].

2.8 Preventing Corrosion and Fretting Damage in Total Hip Arthroplasty

Corrosion and fretting is a significant problem that can occur at the head-neck and neck-stem taper interfaces of THA prostheses. This section addresses some potential solutions to combat corrosion and fretting damage with a focus on the head-neck taper interface. Some of the potential solutions that are discussed in this section include: the assembly procedure; material combinations; the conical half angle; the design of the taper; the use of ceramic femoral heads; the bearing materials; ion implantation and coating techniques; the neck length; and the femoral head size.

2.8.1 Assembly Procedure

Even though there is currently no standardized procedure of designing the head-neck taper interface, standardization is strongly recommended to make THA prostheses safer for patients. For example, many neck tapers vary in terms of length, the base dimension, and the taper angle [43]. Additionally, there is currently no standardized method of assembling the femoral head onto the stem [46]; however to pull the femoral head off of a stem in a laboratory setting, ISO 7206-10 is to be performed [215].

Some common assembly forces that are applied to assemble the head-neck taper interface are 1000 N, 2200 N, 2500 N, and 4000 N [216-219]. In contrast, poor assembly forces are considered to be within the range of 200 N to 500 N [218, 219]. Although most surgeons use a hammer to secure the femoral head onto the neck, some surgeons have indicated that they push the head onto the neck with their hand, which only produces an axial force of approximately 200 N [219]. Meanwhile, some assembly forces are quite excessive and have been reported up to 12000 N. This can result in damage to the femoral head or the bone around the stem [219]. Schlegel et al. reported a hip resurfacing implant that was subjected to a 11000 N assembly force, which resulted in a significant decrease in the strength of the femoral neck [220].

Bitter et al. used finite element analysis (FEA) to determine how the impaction force during the assembly procedure can contribute to micromotion at the head-neck taper interface of THA prostheses [221]. Bitter et al. modeled BIOMET'S Type-1 taper with an adapter and all materials consisted of titanium alloy ($\mu = 0.5$) [221]. A 2300 N

force was applied to assemble the taper onto the neck of the stem [221]. Afterwards, assembly forces of 2000 N, 4000 N, and 15000 N were applied to assemble the femoral head onto the adapter [221]. To verify the results of the FEA, an experimental study was simultaneously conducted that consisted of assembly forces of 4000 N and 15000 N [221]. Bitter et al. found that the greatest contact stresses were along the distal part of the taper [221]. Bitter et al. reported that the least amount of micromotion (1.5 µm) occurred when the femoral head was assembled with a 15000 N assembly load [221]. Meanwhile, the greatest amount of micromotion occurred with an assembly load of 2000 N (7.5 µm) [221].

Rehmer et al. attempted to determine the ideal force for assembling the head-neck taper interface for 32 mm femoral heads that consisted of either CoCr or Al_2O_3 onto CoCr or Ti6Al4V neck adapters [219]. Rehmer et al. also examined the influence of the assembly force and the tool for the assembly procedure [219]. To assemble the head-neck taper interface with a secure connection, Rehmer et al. recommended an impaction force of 4000 N [219]. Additionally, Rehmer et al. reported that multiple strikes with the same hammer featuring either a metal or rubber tip did not enhance the assembly force for any material combination [219].

2.8.2 The Debate of Single Alloys versus Mixed Alloys

In practice, it is common for CoCr femoral heads to be implanted with Ti6Al4V stems. CoCr has sufficient mechanical strength and is an excellent articulation material but its modulus of elasticity is much greater than bone. In contrast, Ti6Al4V is biocompatible, offers resistance to corrosion, and its modulus of elasticity is similar to bone. Cook et al. reported that by having CoCr femoral heads assembled onto Ti6Al4V stems, this can result in a higher frequency and greater corrosion damage at the head-neck taper interface in comparison to stems and femoral heads that consist of CoCr alloy [191].

Higgs et al. and Collier et al. reported increased corrosion damage when coupling mixed alloys together in contrast to single alloy systems with one hypothesis being the difference in the electrical potential between CoCr and Ti6Al4V [181, 204]. In an alternative hypothesis, this may be linked to the difference in the hardness of CoCr (450 Hv) and Ti6Al4V (330 Hv), which can result in more galling and mechanical damage [115, 177, 204, 222].

Kummer et al. conducted an *in vitro* study to see which couple could accelerate crevice corrosion the most: CoCr alloy with pure titanium, Ti6Al4V, or 316L stainless steel [223]. Kummer et al. conducted an electrochemical open-circuit potential measurement test as well as a potentiostatic passive film corrosion measurement test over a ten hour period [223]. Kummer et al. discovered that when CoCr was paired with stainless steel 316L, the couple was unstable and could lead to significantly more corrosion dam-

age over a longer period of time [223]. In contrast, CoCr paired with titanium and Ti6Al4V was stable [223].

McKellop et al. (1992) reported a modular THA prosthesis (Zimmer, Harris – Galante) with a CoCr head and a Ti6Al4V stem that displayed substantial corrosion damage after being implanted in a patient for 35 months [224]. The taper surfaces were discoloured and featured pitting [224]. Selective leaching of titanium was detected as the weight percentage changed from 90% to 58% [224]. Selective leaching also occurred along the taper of the head as the weight percentage of cobalt decreased from 60% to 13% [224]. Chromium remained relatively unchanged along the head taper; however, molybdenum significantly increased from 5% to 29% [224]. This finding suggests that a chromium molybdenum corrosion product formed along the CoCr head taper [224]. Similar to McKellop, Cook et al. also reported a significant increase in the content of molybdenum in a fretting corrosion experiment to further support that chromium molybdenum can be a corrosion product [99].

Even though many researchers have argued that mixed alloy combinations can trigger galvanic corrosion, Cuckler et al. argued that THA prostheses with a CoCr and Ti6Al4V interface can be implanted without any corrosion damage. Cuckler et al. believed that this could be achieved with the proper selection of taper angles, surface finish, and the quality control of the manufacturing process [225].

2.8.3 Conical Half Angle

The conical half angle is a common method to measure the angle (θ) of a taper. Equation 10 can be used to calculate the conical half angle using Figure 2.13 as a reference where R1 and R2 are the radii of the taper and L is the length of the taper.

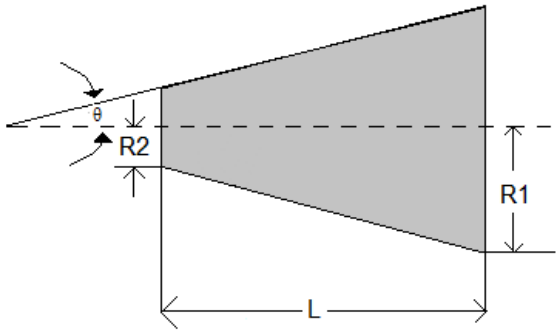

Figure 2.13. The half conical angle for a taper.

$$\theta = \arctan\left(\frac{R1 - R2}{L}\right) \qquad \text{(Equation 10)}$$

When fitting the neck taper into the head taper, there are three types of angular taper matches that can occur based on the difference between the angle of the neck taper (α_N) and the head taper (α_H) that can be determined using Equation 11.

$$\alpha = \alpha_N - \alpha_H \qquad \text{(Equation 11)}$$

Depending on the value for α, there are three types of matches that can occur: a zero-match where α equals 0° (Figure 2.14 A); a positive match (bottom-locking) where α is positive (Figure 2.14 B); and a negative mismatch (top-locking) where α is negative (Figure 2.14C).

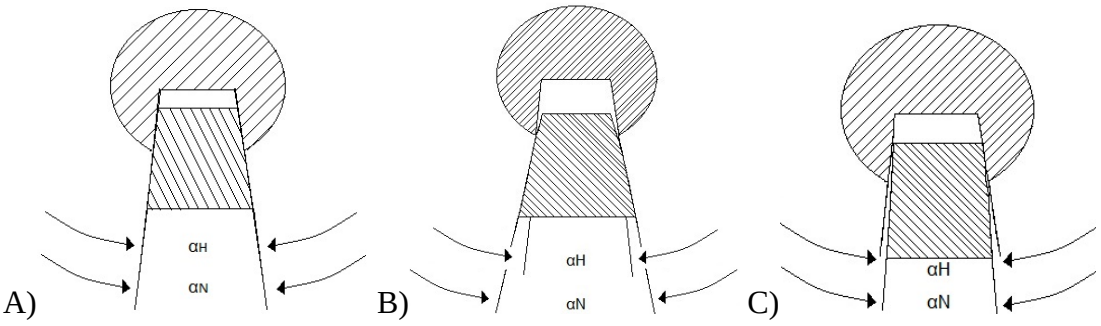

Figure 2.13. The three locking mechanisms for the head-neck taper interface: A) zero-mismatch; B) positive mismatch (bottom-locking); and C) negative mismatch (top-locking).

In industry, the accepted threshold tolerance of the head-neck taper interface is 0.0167° [226]. Parekh et al. created finite element models of the head-neck taper interface to examine how an increase in the conical half-angle of the femoral head taper interface influences micromotion [226]. To do this, nine different mismatches (0.005°, 0.01°, 0.015°, 0.03°, 0.05°, 0.075°, 0.1°, 0.2°, and 0.3°) were created and compared to a perfect angular match (0.0°) [226]. From this investigation, angular mismatches up to 0.075° did not substantially contribute to micromotion along the head-neck taper interface when compared to the case with an angular match [226]. When the angular mismatch increased, the micromotion between the head and neck increased for higher tolerances and there was also an increase in the contact pressure, the maximum von Mises stress, and the shear stress along the proximal-medial aspect of the taper [226]. From this study, an angular mismatch up to 0.075° does not seem to contribute to enhanced micromotion in comparison to the current industry standard of 0.0167° [226]. Nonetheless, an increase in angular mismatch can result in undesired micromotion, which can result in corrosion and fretting damage at the head-neck taper interface.

One of the reasons why the head-neck taper interface is vulnerable to fretting damage is due to the angular mismatch between the head and neck tapers [171]. An angular mismatch can result in poor mechanical stability of the connection and can increase the wear generated along the taper interface [171], [191]. During a typical gait cycle, loading on the hip joint can dislodge the interference fit between the head and neck [171]. Shareef and Levine conducted a FEA study using ANSYS 5.0 to determine how the manufacturing tolerances affect micromotion for a Morse taper [227]. The tolerances were modified on the male component to determine the difference in the magnitude of the micromotion along the Morse taper. Two conclusions were revealed from this study. First, by simulating off-axis loading, the female component tips from its initial placement. As a result, one side of the female component has approximately double the amount of micromotion versus the opposite side. Second, Shareef and Levine confirmed that by increasing the tolerance of the male component, the magnitude of micromotion increased. By increasing the angle tolerance from zero to one minute along the male component, the micromotion increases from 4% to 16%.

2.8.4 Taper Size

Padgett et al. conducted a retrieval study consisting of 54 metal-on-metal THA primary revision prostheses with a diameter greater than 36 mm to determine if taper size influences corrosion or fretting damage at the head-neck taper interface [228]. For this investigation, three different taper geometries were examined: 11/13 mm; 12/14 mm; and Type 1 (taper angle: 4.0°) taper designs [228]. Padgett et al. reported that there were no

significant differences in the volumetric wear rate or corrosion damage; however, there were significant differences in fretting damage. In particular, the Type 1 taper had less fretting damage than 12/14 mm and 11/13 mm tapers [228]. This could be attributed to a smaller contact area at the head-neck taper interface [228].

2.8.5 Ceramic Femoral Heads

One way to potentially reduce the problem of head-neck taper corrosion is to assemble ceramic heads on metallic femoral stems since ceramics do not corrode [229]. Hallab et al. compared the fretting corrosion damage of CoCr stems when paired with zirconia and CoCr femoral heads [230]. Hallab et al. hypothesized that prostheses featuring ceramic femoral heads would generate more debris than prostheses featuring a metallic femoral head [230]. In contrast, the opposite was true: the CoCr femoral head group generated three times more chromium and 11 times more cobalt than the zirconia femoral head group [230]. MacDonald et al. conducted a similar retrieval analysis that consisted of 50 CoCr heads assembled onto a CoCr stem and 50 ceramic heads assembled onto a CoCr stem and the corrosion damage was assessed by using the Goldberg corrosion scoring system [177] to observe if there was a difference in the head-neck taper corrosion between the two groups [231]. MacDonald et al. reported corrosion damage in 42 cases with a ceramic-metal taper combination and in 42 cases for the metal-metal taper combination; however, the corrosion damage was not nearly as substantial for the prostheses

with a ceramic femoral head [204]. MacDonald et al. indicated that although taper corrosion can be minimized with the use of ceramic femoral heads, this technique alone cannot eliminate corrosion damage at the head-neck taper interface

Munir et al. conducted a retrieval analysis of 52 S-ROM components to examine the rate of corrosion damage at the head-neck taper interface as well as the stem-sleeve to see if there were differences due to head size, head materials, bearing surfaces, and regions [47]. The different bearing surfaces included 17 ceramic-on-ceramic, seven ceramic-on-polyethylene, 16 metal-on-metal, and 12 metal-on-polyethylene articulations. Munir et al. discovered that the head-neck tapers and stem-sleeve tapers from metal-on-metal THA prostheses had a significantly greater rate of corrosion damage in comparison to the tapers with a ceramic head [47]. Munir et al. also divided the bearing surfaces into two groups: hard-on hard (includes metal-on-metal and ceramic-on-ceramic) and hard-on-soft (includes metal-on-polyethylene and ceramic-on-polyethylene) [47]. Additionally, Munir et al. reported that the inferior region of the head-neck taper and the medial region of the stem-sleeve taper exhibited the greatest presence of corrosion damage. When looking at the factor of head size, there was a trend that with a larger head size, the corrosion damage became greater at the head-neck taper interface; however, there was no general trend for the stem-sleeve taper [47]. Munir et al. concluded that hard-on-hard bearing surfaces experience greater frictional forces, which can result in a large torque due to the moment arm acting along the stem-sleeve taper [47].

Flohr et al. assembled 48 mm ceramic femoral heads onto Ti6Al4V sleeves that were fitted onto necks consisting of CoCrMo, Ti6Al4V, and 316L stainless steel to exam-

ine the corrosion damage at the stem-sleeve interface [232]. Flohr et al. discovered no corrosion damage despite implanting a large ceramic femoral head [232]. Similarly, Preuss et al. conducted an experimental study to determine if the use of ceramic heads (range 40 mm to 60 mm) can result in significant corrosion and fretting damage at the head-neck taper interface [233]. Like Flohr et al., no major corrosion or fretting damage was detected [233].

2.8.6 Metal-on-Metal versus Metal-on-Polyethylene Articulations

Fricka et al. conducted a retrieval analysis to observe differences in the head-neck taper corrosion behaviour between 19 metal-on-metal THA prostheses and 14 metal-on-polyethylene THA prostheses manufactured from DePuy [234]. Fricka et al. modified the Goldberg corrosion scoring system [177] such that the scoring for corrosion was performed on a 5-point scale. All THA prostheses featured a 12/14 mm taper and consisted of CoCr alloy except for one metal-on-metal prosthesis, which featured a Ti6Al4V stem. In this study, 18 of the 19 metal-on-metal THA prostheses displayed corrosion damage whereas only eight of 14 metal-on-polyethylene THA prostheses featured corrosion damage. The mean corrosion score for the metal-on-metal group was 3.53 ± 1.35 and for the metal-on-polyethylene group, the mean corrosion score was 1.86 ± 0.95. Additionally, the corrosion scores had a moderate correlation with the implantation time. To account for the difference in the corrosion damage between the metal-on-metal and metal-on-polyethylene prostheses, Fricka et al. believed that the fluid interface at the bearing surface played a key role [235, 236]. If there is improper or little fluid-fluid lubrication be-

tween the metallic liner and the femoral head, this could elevate the roughness and friction between the liner and the femoral head. This would increase the friction, and ultimately, the torque at the head-neck taper interface [234].

2.8.7 Ion Implantation and Coating

Dorn et al. conducted an *in vitro* study to identify if necks consisting of CoCr alloy coated with tantalum have more corrosion resistance than necks made from Ti6Al4V alloy [237]. These tests were performed in a dry assembly condition (container with just air) and two wet assembly conditions: one with calf serum and the other being calf serum with bone chips [237]. The Ti6Al4V neck did not experience corrosion in the dry assembly test, but was subjected to corrosion damage for both wet assembly tests [237]. In contrast, none of the CoCr-tantalum coated necks displayed any corrosion damage [237]. This study suggests that CoCr coated with tantalum can prevent taper corrosion [237].

Maurer et al. attempted to determine the most effective way to improve the fretting corrosion resistance of Ti6Al4V by using three different techniques: ion implantation; physical vapour deposition nitriding; and plasma ion nitriding [238]. From these techniques, Maurer et al. found that plasma nitriding of Ti6Al4V was the most effective way to reduce fretting corrosion damage [238]. In a separate study, Traynor et al. found that by coating the taper interface with chromium nitride (CrN), this significantly reduces the corrosion damage along the taper interface [239].

2.8.8 Femoral Head Size and Neck Length

Langton et al. conducted a retrieval analysis to examine the material loss at the head-neck taper interface for the ASR XL and DePuy's Articuleze (Pinnacle) and to identify risk factors for taper failure [71]. Langton et al. noted that as the head offset and head diameter increased, so did the taper damage. In particular, as the HLA increased, the taper wear also became greater. The HLA can become larger by increasing these three factors: head offset; bearing diameter; and the varus neck shaft angle. Like Langton et al., Moga et al. reported that with larger head sizes, significant corrosion damage was found at the head-neck taper interface for prostheses with a metal-on-polyethylene articulation [37].

Noble et al. attempted to determine why large femoral heads lead to more corrosion and fretting damage by conducting a retrieval analysis consisting of 13 metal-on-metal implants ranging from 42 to 54 mm in diameter [240]. Noble et al. believed that designs featuring low bearing clearances and high flexibility are vulnerable to greater micromotion and torque at the head-neck taper interface [240]. If small micromotion occurs the head-neck taper interface, this can indicate elastic deformation; however, large movement could be attributed to slippage [240]. Noble et al. applied a radial compression force along two opposite points on the rim of the acetabular components. The cups were compressed in intervals of 200 N up to a maximum of 2000 N [240]. Noble et al. measured the torque acting at the neck axis as the head articulated through an angular arc of 60 degrees [240]. The torque ranged from 1.17 Nm to 2.23 Nm and the micromotion of the

neck ranged from 7.46 μm to 8.38 μm [240]. Noble et al. noted that as the torque was increased due to compression, this resulted in greater micromotion at the head-neck taper interface [240]. Noble et al. emphasized that the cup compression loads alone did not necessarily guarantee a greater torque along the head-neck taper interface [240]. By increasing the torsional load, this can make the taper interface more susceptible to corrosion damage [241].

Panagiotidou et al. conducted an experimental study consisting of 36 mm CoCr femoral heads paired with CoCr and Ti6Al4V stems with a 12/14 mm taper to determine how torque affects the corrosion and fretting damage at the head-neck taper interface [242]. To examine how torque plays a role in the corrosion and fretting damage, three different offset increments were applied: 0 mm, 5.4 mm, and 7.5 mm [242]. These three offsets produced torques equivalent to 9 Nm, 12 Nm, and 17 Nm, respectively [242]. Panagiotidou et al. observed that by having a greater torque, regardless of the combination of materials for the femoral head and stem, this made the head-neck taper interface more vulnerable to corrosion and fretting damage based on the overall mean current, overall mean fretting current, and overall current change data [242]. Even though one femoral head size was used, Panagiotidou et al. hypothesized that a larger head size could make the head-neck taper interface more vulnerable to corrosion and fretting damage [242].

In a study by Doehring et al., the micromotion of an anatomically placed femoral component was observed by modifying the superolateral relocation and the neck length [156]. Doehring et al. demonstrated that a 25 mm superolateral relocation of the hip cen-

tre increases the micromotion of the femoral component by 13%. When the neck length was extended by 12.5 mm, the micromotion increases by 38%. By extending the neck length, this increases the sagittal and nonsagittal moments acting on the implant, which would increase the femoral component's micromotion.

Chapter 3 – The Influence of Head Size on Corrosion and Fretting Behaviour at the Head-Neck Taper Interface of Artificial Hip Joints

Note: This chapter was published in the Journal of Arthoplasty in 2013 [243].

Abstract: The primary goal of this study was to determine if head size affects corrosion and fretting behavior at the head-neck taper interface of modular hip prostheses. Seventy-four implants were retrieved that featured either a 28 mm or a 36 mm head with a metal-on-polyethylene articulation. The bore of the heads and the neck of the stems were divided into eight regions each and graded by three observers for corrosion and fretting damage separately using modified criteria reported in the literature. The 36 mm head size featured a significant difference in the corrosion head scores ($p = 0.022$) in comparison to the 28 mm heads. This may be attributed to a greater torque acting along the taper interface due to activities of daily living.

3.1 Introduction

Modular hip prostheses are well-known for improving the quality of life for patients who have degenerative hip disorders. Modular hip prostheses have many ad-

vantages in comparison to single component hip prostheses. These advantages include the adjustment of the patient's leg length during surgery, a decreased inventory size, reduced costs, simplified revision procedures, and the femoral stem can be implanted prior to the insertion of the acetabular component [5, 13, 48-50].

One significant problem of modular hip prostheses is that metal ions and particles are not only being generated from wear at the articulation site, but they may also be produced at the head-neck taper interface due to corrosion [5, 6, 244-249]. Excessive concentrations of cobalt and chromium in the body are known to be harmful as they have been linked to lymphatic reactivity, hypersensitivity, local tissue toxicity, chromosomal damage, impaired renal function, and malignant cellular transformations [249, 250]. Additionally, recent reports indicate the possibility of pseudotumours forming in patients due to the presence of increased levels of metal ions from wear and corrosion in hip resurfacing and modular hip prostheses [64, 251-254].

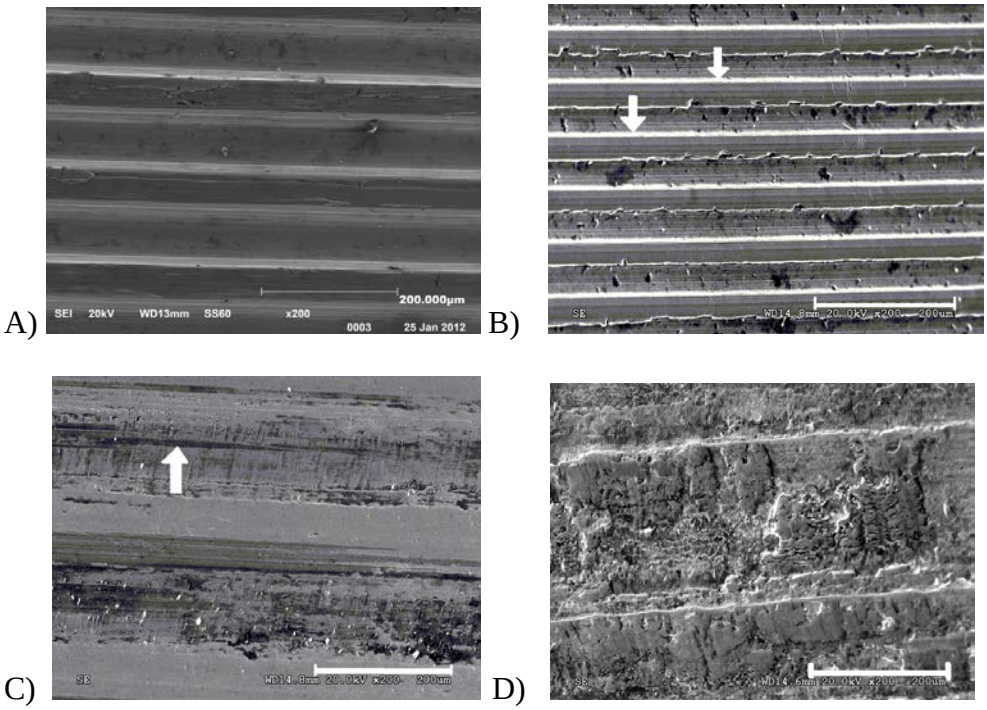

Figure 3.1. Scanning electron microscopy (SEM) images of CoCr alloy heads and necks that were not implanted in comparison to implants with little, moderate, and severe corrosion damage. A) SEM of a CoCr alloy neck that has not been implanted. B) Arrows pointing to machining grooves for a CoCr alloy head with little corrosion and fretting damage. C) Arrow pointing to etching marks from fretting for a CoCr alloy head with moderate corrosion and fretting damage. D) Neck of a CoCr alloy stem with significant corrosion and fretting damage.

Corrosion of taper surfaces in modular hip prostheses is a critical issue that can get worse over time. Figure 3.1 illustrates the progression of a CoCr taper surface that has not been implanted (Figure 3.1 A) to taper surfaces with mild, moderate, and severe corrosion and fretting damage. Figure 3.1 B illustrates a taper surface that contains minimal corrosion and fretting damage. The machining grooves along the head are still detectable as indicated with the two arrows; however, there appears to be pitting between the grooves. The taper surface in Figure 3.1 C contains moderate corrosion and fretting damage. The taper surface displays etching marks as shown by the arrow and the

machining grooves are no longer visible. Finally, the taper surface displayed in Figure 1D features severe corrosion and fretting damage. This image may indicate that not only are the grooves no longer present, but the entire CoCr surface was possibly attacked by the biological fluid within the taper connection.

A retrieval analysis was performed to answer the following questions with respect to corrosion behaviour at the head-neck taper interface of modular hip prostheses. First, does head size influence corrosion or fretting behaviour along the head-neck taper junction? Second, does the head taper display similar corrosion and fretting damage in comparison to the neck taper? Third, does a relationship exist between corrosion and fretting damage? Finally, is there a difference in the corrosion and fretting damage between prostheses manufactured from two different companies?

3.2 Methodology

Modular hip prostheses were retrieved in this study that were implanted for at least one month, featured a 12/14 mm taper, heads and stems consisting of CoCr alloy, and a metal-on-polyethylene articulation. The prostheses were separated into two groups based on comparing the extremes of two popular head sizes. The first group consisted of modular hip prostheses with 28 mm heads whereas the second group had 36 mm heads. The 28 mm and 36 mm head sizes were chosen to represent the extremes of two popular head sizes. The prostheses were examined for corrosion and fretting damage along the bore taper of the head and the neck taper of the stem.

Table 3.1. Patient information and reasons for implant removal.

Patient Information		Reasons For Removal of Implant		
Number of Patients	74	Reason	28 mm Head Group (n)	36 mm Head Group (n)
Number of Males	38	Aseptic Loosening	29	4
Number of Females	36	Instability	7	5
Average Age	65.5 ± 12.3 years	2nd Stage Infection	8	2
Average Implantation Time: Overall	57.7 ± 42.5 months	1st Stage Infection	4	2
Average Implantation Time: 28 mm Head Implants	69.3 ± 39.5 months	Polyethylene Wear	4	0
Average Implantation Time: 36 mm Head Implants	11.6 ± 10.2 months	Osteolysis	2	0
Number of 28 mm Heads Manufactured by Company A	44	Implant Fracture	1	0
Number of 28 mm Heads Manufactured by Company B	15	Malposition	1	0
Number of 36 mm Heads Manufactured by Company A	7	Intrapelvic Cup Migration	0	1
Number of 36 mm Heads Manufactured by Company B	8	Pain Only	0	1
Number of Stems From the 28 mm Head Group Manufactured by Company A	29	Unknown	3	0
Number of Stems From the 28 mm Head Group Manufactured by Company B	6	Total	59	15
Number of Stems From the 36 mm Head Group Manufactured by Company A	0			
Number of Stems From the 36 mm Head Group Manufactured by Company B	5			

To assess for corrosion and fretting damage of all of the prostheses, a modified technique was developed to examine the taper interfaces macroscopically by eye. The neck of the stem and the bore of the head were separated into four quadrants and each quadrant was divided into a superior and inferior region. This technique produced eight regions for the neck and eight regions for the head. To examine the severity of corrosion and fretting damage, each region was scored from zero to three using similar criteria as Goldberg et al. [15] and Kop et al. [12] as shown in Table 3.2. Each region was also given a score ranging from zero to three to represent the amount of area damaged (Table 3.2). After assigning severity and area scores for a region, the two scores were multiplied with each other to form a regional score for corrosion or fretting (maximum score of nine). The eight regional scores were summated to reveal separate corrosion and fretting scores for the head and neck. All modular hip prostheses were evaluated independently by three researchers (two undergraduate students and one graduate student) who had experience working in an orthopaedic laboratory cleaning and inspecting implants for damage. Energy dispersive x-ray spectroscopy was also performed to determine if there was a difference in the chemical composition of the CoCr taper surface when attacked by corrosion and fretting in comparison to a taper surface that has not been implanted.

Table 3.2. Criteria for scoring the severity and area of corrosion and fretting damage [12, 15].

Damage	Severity	Score	Criteria
Corrosion	None	0	No visible corrosion observed
	Mild	1	Surface is discoloured or dull
	Moderate	2	Surface is discoloured or dull; features black debris and pitting
	Severe	3	Black debris, pits, or etching marks
Fretting	None	0	No visible signs of fretting observed
	Mild	1	A single band fretting scar involving three or fewer machine lines along the surface
	Moderate	2	Up to three bands of fretting scars involving three or fewer machine lines or a single band fretting scar involving more than three machine lines
	Severe	3	More than three bands of fretting scars that contain several adjacent machine lines or flattened areas with nearby fretting scars
Area	None	0	No corrosion or fretting observed along the regional area
	Mild	1	Corrosion and / or fretting occupies 1-33% of the regional area
	Moderate	2	Corrosion and / or fretting occupies 34-66% of the regional area
	Severe	3	Corrosion and / or fretting occupies 67-100% of the regional area

To determine the statistical intraclass correlation between the researchers for scoring the implants, the statistical software program SPSS version 19.0 (SPSS Inc., Chicago, Illinois, USA) was used. The Shapiro-Wilk test was performed to determine if the corrosion and fretting scores were normally distributed. In all cases, except for the head corrosion scores for the 36 mm head size group, the corrosion and fretting scores did not display normal distribution. Consequently, the Mann Whitney U test was performed, which is a nonparametric statistical hypothesis test that can be used to determine whether one of two independent sample groups contains significantly larger values. Fisher's Exact test

was also conducted, which is a statistical significance test that is used for categorical data when classifying objects in two different ways. Fisher's Exact test and the Mann Whitney U test were performed with an alpha value of 0.05 to determine if there were significant statistical differences ($p < 0.05$) between the 28 mm and 36 mm head size groups. When examining for correlations, the Spearman rank correlation coefficient was applied.

3.3 Results

This retrieval analysis consisted of 74 modular hip prostheses featuring 59 prostheses with a 28 mm head size and 15 prostheses with a 36 mm head size. The modular hip prostheses were manufactured from two companies (A and B). Of the 74 patients that the prostheses were received from, only 40 stems were retrieved. The rest of the stems were not removed during revision surgery. Details regarding the patients, the prostheses, and the reasons for revision are provided in Table 3.1.

The intraclass correlation coefficient between the three reviewers for scoring corrosion and fretting were 0.70 and 0.48, respectively. According to Fleiss, this is considered to be a fair correlation between the three reviewers for assessing the corrosion and fretting damage [255].

Table 3.3. Frequency of heads and necks with signs of corrosion and fretting damage. Note: For the X/Y notation, X indicates the number of components subjected to corrosion or fretting by the total number of components (Y) manufactured by that company.

Head Size	Corrosion Company A		Fretting Company A		Corrosion Company B		Fretting Company B	
	Neck (X/Y)	Head (X/Y)	Neck (X/Y)	Head (X/Y)	Neck (X/Y)	Head (X/Y)	Neck (X/Y)	Head (X/Y)
28 mm	21/29	32/44	22/29	27/44	4/6	12/15	4/6	10/15
36 mm	N/A	6/7	N/A	2/7	4/5	7/8	3/5	4/8

Fisher's Exact test was conducted to determine if there were significant differences in the ratios for the appearance of corrosion and fretting damage between the two head size groups (Table 3.3). There were no significant differences in frequency of observed corrosion and fretting between the two head size groups. Additionally, there were no significant differences in the ratios of the appearance of corrosion and fretting damage between the two companies.

Table 3.4 provides an overview of the mean corrosion and fretting scores for the heads and necks for the two head size groups. For the 28 mm head size, the average corrosion score for the bore taper was 6.5 ± 9.9 whereas the 36 mm head size had an average score of 13.1 ± 14.4; thus, resulting in a significant difference ($p = 0.022$). Differences in fretting scores between the two head size groups for the bore of the head and the neck of the stem were negligible. When comparing the two head size groups, the 36 mm head size group exhibits greater corrosion scores than the 28 mm head group for the bore of the head and the neck of the stem. The heads and necks manufactured by company B yielded higher corrosion and fretting scores than company A in all instances. The only significant statistical difference between the two companies was found in the head corro-

sion scores ($p = 0.011$). It is also interesting to note that the average implantation times between the 28 mm head group (65.6 ± 34.0 months) and the 36 mm head group (11.6 ± 10.2 months) was substantially different. Additionally, there was not a major discrepancy in the implantation times between company A (60.6 ± 41.1 months) and company B (51.2 ± 45.7 months).

Table 3.4. The mean and standard deviations of the corrosion and fretting scores for the heads and necks. Significant statistical differences were found in the head corrosion scores between: companies A and B for the 28 mm heads [1]; companies A and B for the 36 mm heads [2]; and the 28 and 36 mm heads [3].

Head Size and Company	Average Implantation Time (months)	Neck Corrosion Score	Head Corrosion Score	Neck Fretting Score	Head Fretting Score
28 mm Company A	68.9 ± 30.0	4.0 ± 4.8	5.4 ± 8.3[1]	2.8 ± 3.3	1.4 ± 1.5
28 mm Company B	70.8 ± 45.1	7.1 ± 12.7	10.0 ± 13.4 [1]	3.2 ± 5.4	7.2 ± 12.2
28 mm Overall	69.3 ± 39.5	4.5 ± 6.6	6.5 ± 9.9[3]	2.9 ± 3.6	2.8 ± 6.6
36 mm Company A	8.4 ± 9.0	N/A	6.0 ± 5.1[2]	N/A	0.7 ± 1.3
36 mm Company B	14.4 ± 10.9	5.1 ± 6.4	19.4 ± 17.2 [2]	3.1 ± 4.9	7.6 ± 11.6
36 mm Overall	11.6 ± 10.2	5.1 ± 6.4	13.1 ± 14.4 [3]	3.1 ± 4.9	4.4 ± 9.0

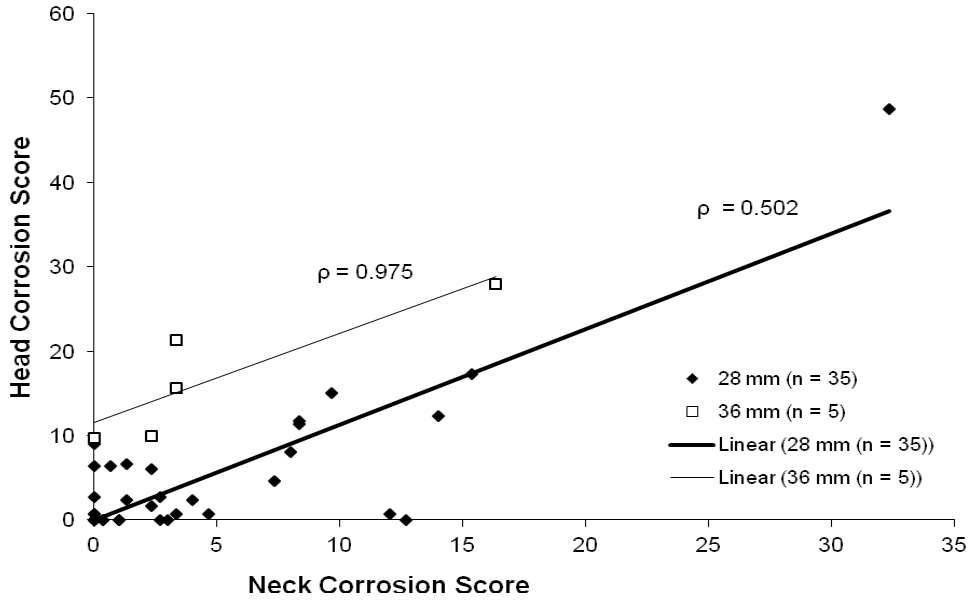

A)

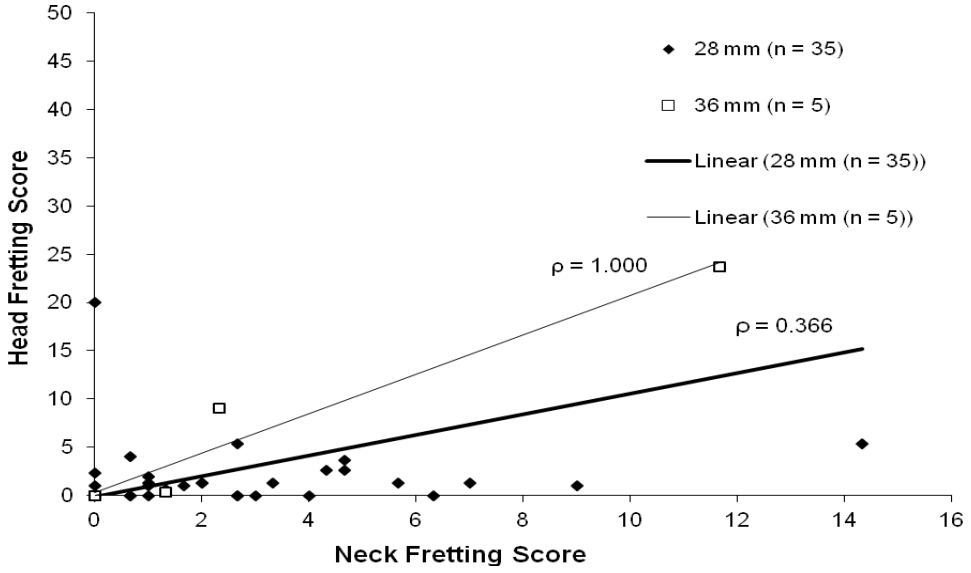

B)

Figure 3.2. The relationship between the head and neck for A) corrosion damage and B) fretting damage.

When examining the relationship between the heads and necks for corrosion damage (Figure 3.2 A), the 28 mm head size group had a Spearman rank correlation coefficient of 0.502 whereas the 36 mm head size group had a Spearman rank correlation coefficient of 0.975. Figure 3.2 A suggests that the relationship between head and neck corrosion is positive and increases with head size. Figure 3.2 B illustrates the relationship between head and neck fretting damage. The Spearman rank correlation coefficient for the 28 mm head size group was 0.366. In contrast, the 36 mm head size group had a Spearman rank correlation coefficient of 1.0. From this data, corrosion and fretting damage between the heads and necks may be correlated with increasing head size.

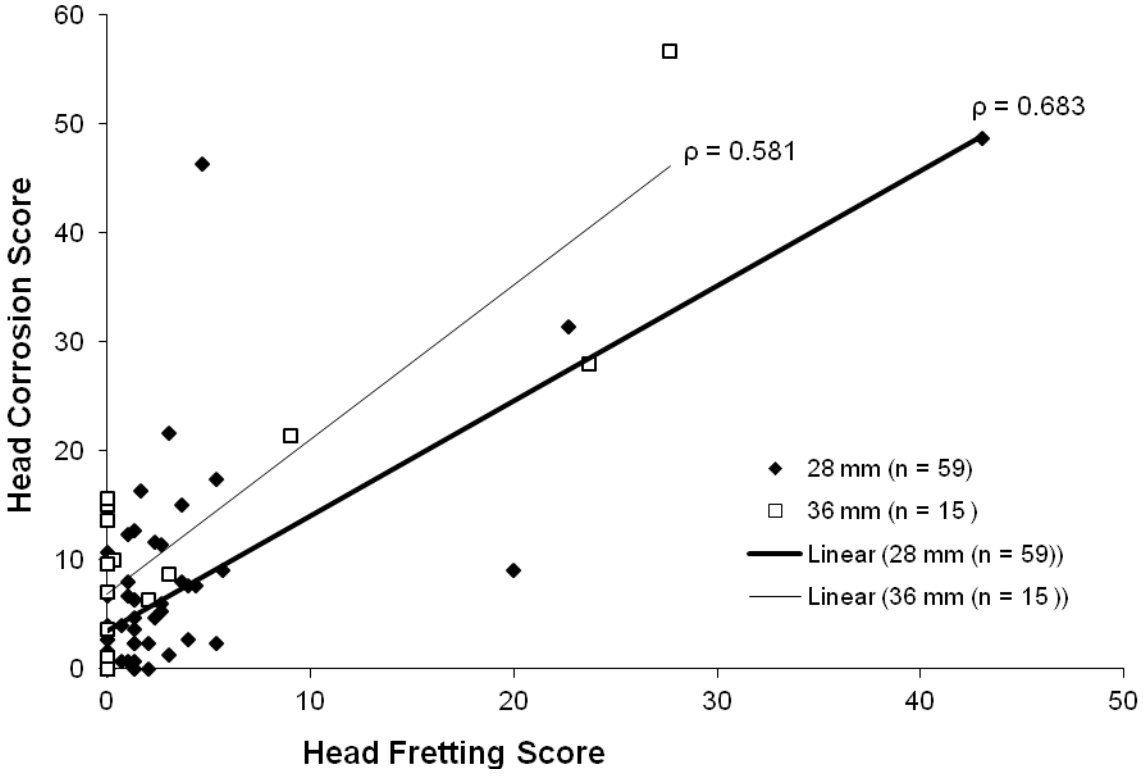

Figure 3.3. The relationship between corrosion and fretting damage along the heads.

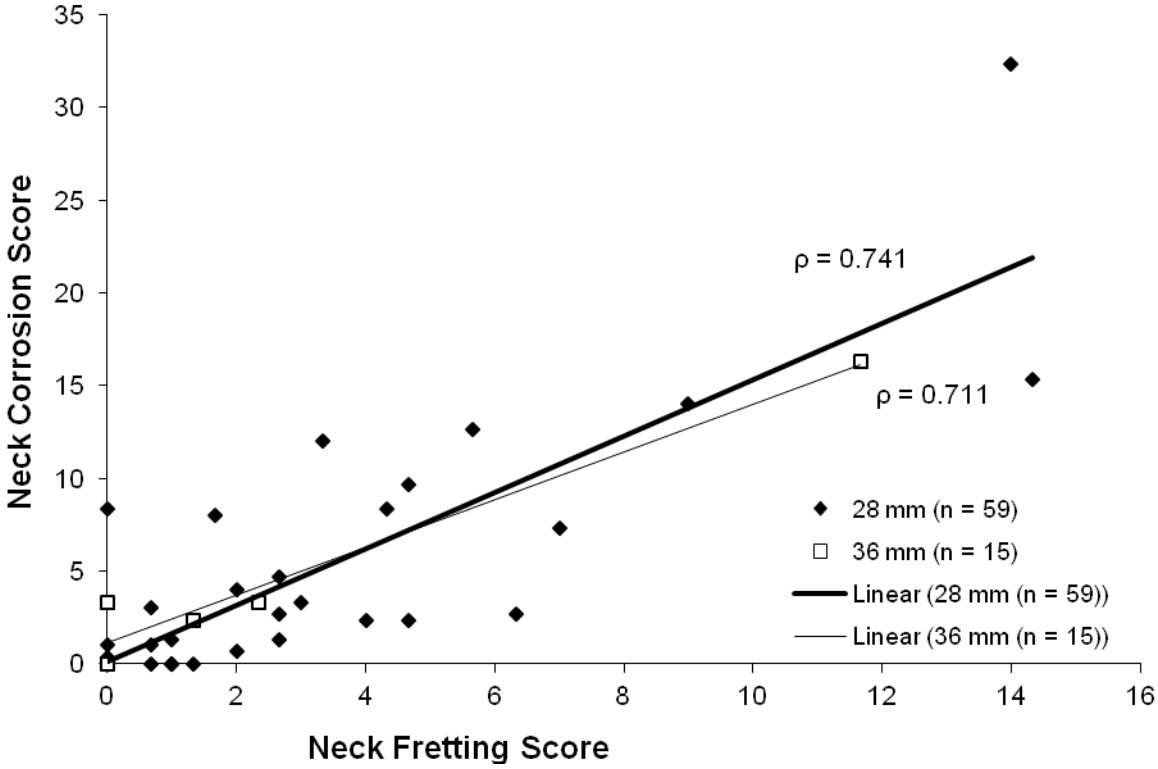

Figure 3.4. The relationship between corrosion and fretting damage along the necks.

The relationship between the corrosion and fretting scores of the heads is illustrated in Figure 3.3. The Spearman rank correlation coefficient was 0.683 for the 28 mm head group and 0.581 for the 36 mm head group. Figure 3.4 illustrates the correlation between the corrosion and fretting scores of the necks. The Pearson rank correlation coefficient for the 28 mm and the 36 mm head size groups were 0.741 and 0.711 for the neck tapers, respectively. From Figures 3.3 and 3.4, there is a positive correlation between corrosion and fretting damage.

Energy dispersive x-ray spectroscopy was performed to identify the molecular weight chemical composition along the bore of the head and the neck of the stem. For the

heads and necks which appeared to be unaffected by corrosion, the molecular weight percentages of cobalt, chromium, and molybdenum ranged from 59-64%, 29-35%, and 4-7.6% respectively. Upon examination of the regions that were severely affected by corrosion and fretting, the molecular weight percentages of cobalt substantially decreased to levels of 3-12%; however, the molecular weight percentage of chromium ranged from 31-34%, indicating that chromium was unaffected. When analyzing the molecular weight percentage of molybdenum, the content was elevated to levels between 20-35%. Chromium and molybdenum are known to form oxide corrosion products [132]. From this analysis, it is believed that chromium and molybdenum form a corrosion product film along the surface.

3.4 Discussion

In practice, surgeons commonly perform total hip replacement procedures using femoral head sizes of 28 mm, 32 mm, 36 mm, or larger. Larger head sizes can increase the range of motion while reducing the risk of dislocation [245]. Disadvantages of large femoral head sizes include increased volumetric wear, thinner polyethylene liners, and an increase in stress along the articulating cup that may lead to fracture of the liner.

This retrieval analysis contains some limitations. First, there were a limited number of 36 mm heads available. Second, only seven stems were retrieved that were manufactured from company A and none were obtained from company B for implants

featuring a 36 mm head. Third, several femoral stem components were not retrieved in this study because the surgeon decided not to remove the stem during revision surgery. These limitations have resulted in a discrepancy between the number of heads and stems for the 28 mm and 36 mm head size groups.

This study found that 36 mm heads of modular hip prostheses had significantly more corrosion damage than 28 mm heads when implanted into the patient. This investigation also revealed that the presence of corrosion for the 36 mm heads and their corresponding necks were more frequent than the 28 mm heads and their necks, but there were no significant differences. To account for these phenomena, the following theory is suggested. Larger head sizes create a greater toggling torque acting along the taper junction during activities of daily living (Figure 3.5). This toggling torque could lead to more micromotion between the head and the neck. This increased micromotion may contribute to the deterioration of the oxide film along the taper junction, which protects the metallic surface from corrosion. Since the metal is unable to repassivate the oxide film quickly enough, the metal would then be more vulnerable to corrosion and fretting attack. Therefore, the use of large head sizes may result in more corrosion and fretting damage along the head-neck taper interface due to a greater toggling torque.

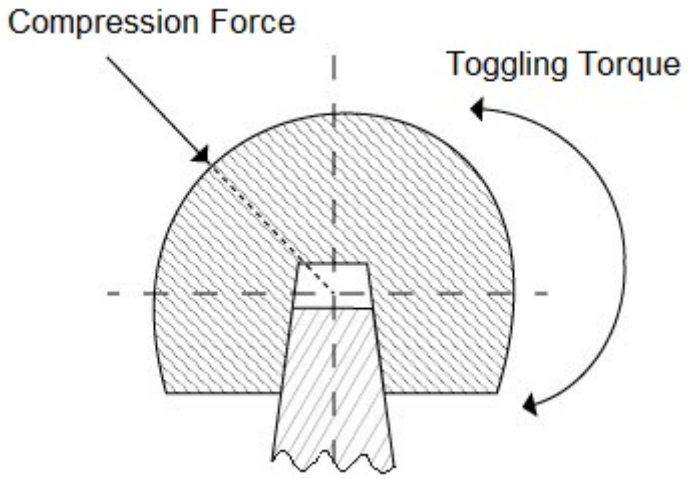

Figure 3.5. The toggling torque of the femoral head during out of axis loading.

In this study, company B yielded higher corrosion and fretting scores than company A. In particular, the difference was significantly greater for head corrosion. There are a number of reasons why there could be a difference in the corrosion and fretting behaviour between the two companies. Such possibilities include differences in fabrication, passivation, tolerance designs, and surface finish.

There was a weak relationship between the corrosion and fretting scores with respect to the implantation time period. Some components do not display any signs of corrosion while other components corrode early and get worse over time. Ideally, modular hip prostheses should have a lifetime of 15 years or more. The implants retrieved from this study were removed much earlier than their expected lifetime for reasons that were not due to corrosion. Some researchers have reported that there is a link between corrosion damage and implantation time [9] while others have reported that there is no correlation [118]. There are a number of explanations that could account for why there was no correlation between corrosion and fretting damage with implantation

time for the retrieved implants. These include differences in loading conditions, assembly techniques, variation in prosthesis designs, tolerances, and passivation.

This investigation attempted to address if corrosion and fretting damage were related to each other. When examining the heads from the two head size groups, there was a correlation between corrosion and fretting damage. By wearing down the protective oxide film along the metallic surface, this could expose the metal to biological fluid that may result in mechanically-assisted crevice corrosion. By having more fretting damage, this would wear down the oxide film even more; thus, exposing more metal to corrosive attack. There were some anomalies in Figures 3.2, 3.3, and 3.4. These anomalies can be attributed to other factors such as implantation time and the assembly procedure.

Additionally, there was a relatively low intraclass correlation coefficient for corrosion and fretting and there are a few reasons for this. All three scorers found that there was some subjectivity in assessing the area of damage for corrosion and fretting. With fretting, the researchers found it difficult at times to distinguish how many machine lines were affected.

3.5 Conclusion

The main goal of this study was to determine if the size of the femoral head in modular hip prostheses affects corrosion and fretting behavior at the taper junction. A retrieval analysis was designed to minimize the number of variables that could potentially influence corrosion and fretting behaviour. The conclusions made from this study are as follows:

- Modular hip prostheses featuring a head component with a 36 mm diameter has greater corrosion damage in comparison to 28 mm heads.
- Modular hip prostheses manufactured by two separate companies exhibit different corrosion and fretting damage, particularly along the bore of the head.
- There is a relationship between the heads and necks for fretting damage which may be attributed to the micromotion between the two surfaces.
- There is a relationship between corrosion and fretting damage.

This study demonstrates that there is a difference in corrosion and fretting behaviour between two different head sizes. By having a larger head size, increased corrosion could potentially generate more metallic ions and propagate to surrounding

tissues. Consequently, this may lead to similar adverse tissue reactions that are being discovered with some metal-on-metal articulations.

Chapter 4 – Finite Element Analysis of the Head – Neck Taper Interface of Modular Hip Prostheses

Note: This chapter has been accepted for publication and is currently in press for Tribology International [256].

Abstract: This study identifies which parameters influence the micromotion at the head-neck taper interface of modular hip prostheses. Finite element analysis was performed where 3D models of the head-neck taper interface were subjected to an assembly force, 3300 N of compression, and 100 N of tension. The micromotion increased as the head size, assembly force, and taper size increased. The micromotion also increased when a mixed alloy material combination was used instead of an all CoCr alloy prosthesis and when the centre of the femoral head was in a more superior position relative to the centre of the neck taper.

4.1 Introduction

Corrosion of modular hip prostheses is a reoccurring problem in the orthopaedic community that has been reported at the head-neck [140, 190, 191, 257-259] and neck-stem taper interfaces [134, 196-200, 260]. Corrosion can generate metallic ions and cor-

rosion products that can enter the patient's body and may result in pain, hypersensitivity, adverse tissue reactions, and revision surgery.

There is currently a debate regarding which factors increase the likelihood of corrosion damage at the head-neck taper interface. Recently, large femoral heads have been reported to increase head-neck taper corrosion damage [37, 71, 195, 242, 243, 261] whereas other researchers have arrived at different conclusions [262-264]. According to the supporters of this argument, the following hypothesis was developed. Large femoral heads could generate a greater toggling torque at the head-neck taper interface due to an increased diameter allowing for larger distances between the centre of the head and the centre of the engaged neck taper. By having an increased toggling torque, this can produce more micromotion at the head-neck taper interface. Micromotion in the range of 10-50 μm can result in fretting, which is a form of surface damage caused by low-amplitude oscillatory sliding between two surfaces [90, 153]. Fretting can deteriorate the passive oxide layer and make the head-neck taper interface more vulnerable to mechanically-assisted crevice corrosion [177].

Many researchers that have focused on taper corrosion have relied on retrieval analyses to support their arguments; however, retrieval analyses have their limitations. By having different loading conditions, implantation times, manufacturing processes, tolerance levels, neck lengths, assembly conditions, and the availability of implants, relying on retrieval analyses alone can be difficult to isolate which factors influence corrosion damage at the head-neck taper interface. Although some *in vitro* corrosion fatigue tests have been performed [167, 182, 187, 240, 242, 265], we are presently unaware of any *in*

vitro studies that have performed to determine if the size of the femoral head influences head-neck taper corrosion.

The objective of this study was to identify which factors influence the micromotion at the head-neck taper interface of modular hip prostheses using finite element analysis. By analyzing the micromotion, this can predict the fretting damage at the head-neck taper interface that is believed to be responsible for corrosion. This paper addresses the factors of head size, material combinations, assembly force, taper size, the distance between the centre of the femoral head to the centre of the engaged neck taper, and a comparison between axial and out-of-axis loading.

4.2 Methodology

4.2.1 Finite Element Modeling

For this study, 3D finite element models were created using Abaqus 6.10 software (3DS Dassault Systèmes, Waltham, MA, USA). To simulate accurate micromotion at the head-neck taper interface, it was critical to replicate the dimensions of the femoral head and neck as well as to apply the mechanical properties of the alloys to the models. To model the head-neck taper interface, a 12/14 mm neck taper was designed with an angle of 5°40’ and a length of 13 mm. Femoral head sizes of 28 mm, 36 mm, and 44 mm with a 0’ tolerance were modeled. The centre of the femoral head was aligned with the centre of

the neck taper. The coefficient of friction at the head-neck taper interface was 0.15 to simulate a ground surface finish [163, 266]. A master-slave technique was applied to the femoral head (master) and neck taper (slave). Additionally, penalty contact was applied with finite sliding at the taper interface along with hard contact.

To reduce the computation time, the femoral heads and necks were modeled in half and z-symmetric boundary conditions were applied along the surfaces [165]. Additionally, a boundary condition was applied at the base of the neck to prevent displacement and rotation from occurring during loading. The models were meshed using hex-dominated elements (mostly hexagonal elements along the body of the femoral head and neck taper with wedges being automatically applied along the surfaces).

For each simulation, there were four phases: the assembly procedure; a recovery phase; compression loading; and tension loading. During the assembly procedure, an axial force was applied to the femoral head as a pressure over a semi-circular contact area that had a diameter equal to 25% of the diameter of the femoral head. The recovery phase proceeded afterwards so that the femoral head would reposition itself along the neck; no forces were applied during this phase. During the third phase, a compression force of 3300 N was applied as a pressure in accordance to ASTM F1875-98 [129]. The 3300 N of compression was directed at an angle of 30° away from the long axis of the neck [267] over a semi-circular contact area equal to 25% of the diameter of the femoral head. Over this same contact area, 100 N of tension was applied as a pressure afterwards to simulate the suction effect during the swing phase caused by a small clearance for implants with a

hard-on-hard articulation [268]. Figure 4.1 illustrates these forces acting on the femoral head.

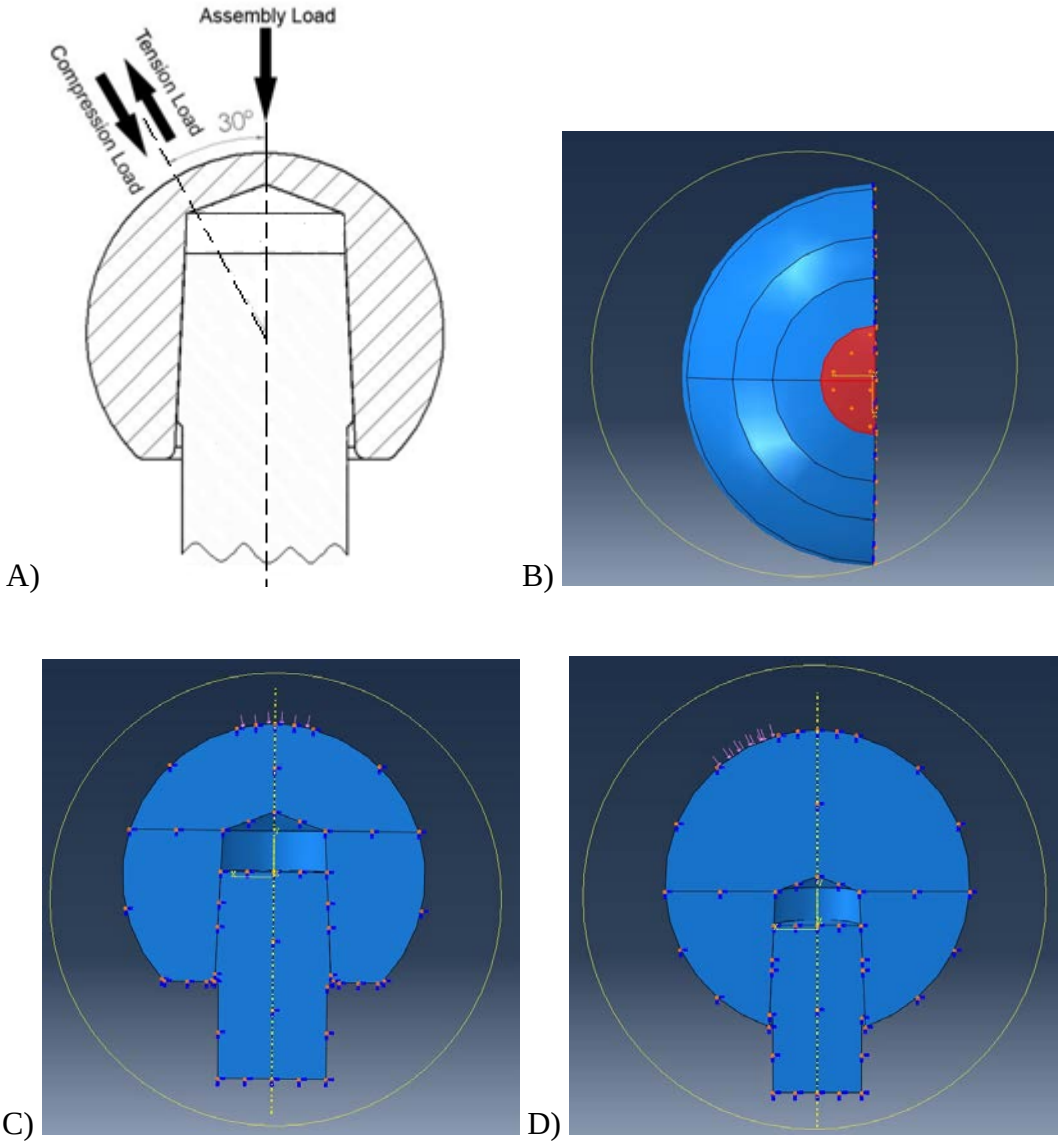

Figure 4.1. A) The head-neck taper interface subjected to assembly, compression, and tension loading. B) Overhead view of the semi-circular region for the assembly force. C) Axial assembly force being applied to the femoral head. D) Out of axis compression force being applied to the femoral head.

4.2.2 Femoral Head Size and Material Combinations

To examine the effect of material combinations on the micromotion, single alloy and mixed alloy combinations were created and tested on 28, 36, and 44 mm femoral heads with a 12/14 mm taper size. The single alloy combination consisted of CoCr alloy for the femoral head and neck whereas the mixed alloy combination consisted of a Ti6Al4V neck paired with a CoCr femoral head. For the single alloy combination, the femoral head and neck had the same modulus of elasticity, density, and Poisson's ratio. The mechanical properties of these alloys can be found in Table 4.1. To secure the femoral head onto the neck, a 4000 N force was applied to the femoral head during the assembly procedure to observe how different head sizes and material combinations affects the micromotion at the head-neck taper interface. Appendix A contains the schematic drawings of the 28 mm, 36 mm, and 44 mm femoral heads.

Table 4.1. Mechanical properties of CoCr and Ti6Al4V [269-271].

Material	Modulus of Elasticity	Density	Poisson's Ratio
CoCr	210 GPa	8.3 g/cm^3	0.3
Ti6Al4V	114 GPa	4.43 g/cm^3	0.342

4.2.3 Assembly Force

When considering the influence of the assembly force on the micromotion at the head-neck taper interface, a 36 mm CoCr femoral head with a 12/14 mm taper and a single alloy material combination was selected. The assembly loads for this part of the study

were 500 N, 1000 N, 2000 N, 3000 N, 4000 N, 5000 N, and 6000 N [216-219, 221]. All of these forces have been known to be used to assemble the head-neck taper interface.

4.2.4 Taper Size

To observe the effect of taper size on the micromotion between the femoral head and neck, a 44 mm CoCr femoral head was assembled onto a CoCr neck with a 4000 N assembly force. Three taper sizes were selected: 10/12 mm; 12/14 mm; and 14/16 mm. Similar to the 12/14 mm neck tapers that were modeled, the 10/12 mm and 14/16 mm tapers had a length of 13 mm. The 44 mm femoral head size was chosen as this was hypothesized to result in more micromotion than a 28 mm and a 36 mm femoral head. Appendix A provides the schematic diagrams of the neck taper sizes.

4.2.5 The Distance Between the Centre of the Femoral Head to the Centre of the Neck Taper

This study also examined how the distance between the centre of the femoral head to the centre of the neck taper affects the micromotion at the head-neck taper interface. For this aspect of the study, a 4000 N axial force was applied to a 44 mm femoral head during the assembly procedure. A taper size of 12/14 mm was chosen and the femoral head and neck were modeled with CoCr alloy. There were three cases where the centre of

the femoral head was above the centre of the neck taper (1 mm, 3 mm, and 7 mm), one case where the centres of the femoral head and neck taper were aligned, and two cases where the centre of the femoral head was below the centre of the neck taper (-1 mm and -3 mm). The 44 mm femoral head size was chosen since the distance between the centre of the femoral head and the centre of the neck taper has a greater variation than a 28 mm and a 36 mm femoral head. The schematic diagrams of the femoral head sizes with the different offsets can be found in Appendix A.

4.2.6 Axial and Out of Axis Loading

This study observed if there was a difference in the micromotion between axial and out of axis loading during compression and tension. To test this parameter, a 44 mm femoral head with a CoCr head and a 12/14 mm neck taper was modeled with their centres aligned. Upon receiving a 4000 N axial assembly force and a recovery period, the out of axis loading model was subjected to compression and tension loading at an angle of 30° away from the long axis of the neck taper. In contrast, the axial loading model had the compression and tension forces being applied in the direction of the long axis of the neck taper.

4.2.7 Testing for Convergence

The maximum von Mises stress was recorded at the head-neck taper interface for each phase. The micromotion between the femoral head and neck was measured at the centre of the engaged head taper. To test for convergence, the default mesh size was originally selected and the element size was reduced by 10% for each iteration. Testing for convergence ended when the assembly displacement and the maximum von Mises stresses for the four phases were less than 10% in comparison to the previous iteration. The proof of convergence can be found in Appendix B.

4.3 Results

4.3.1 Assembly Displacement

Figure 4.2 illustrates the assembly displacement of the femoral head onto the neck taper, which was recorded at the inferior edge of the femoral head. When increasing the head size for the single alloy material combination (Figure 4.2 A), the head size decreased from 61.7 μm for the 28 mm femoral head to 54.5 μm for the 44 mm femoral head. Meanwhile, the assembly displacement of the femoral head for the mixed alloy material combination was approximately 71 μm for all head sizes (Figure 4.2 A). However, the mixed alloy material combination's assembly displacement was greater than the single alloy material combination for all head sizes. As the assembly force was increased (Figure 4.2 B), there was a linear increase in the assembly displacement of the femoral head onto the neck taper. When modifying the taper size (Figure 4.2 C) and the distance

between the centre of the femoral head to the centre of the neck taper (Figure 4.2 D), there was a negligible difference in the assembly displacement.

A)

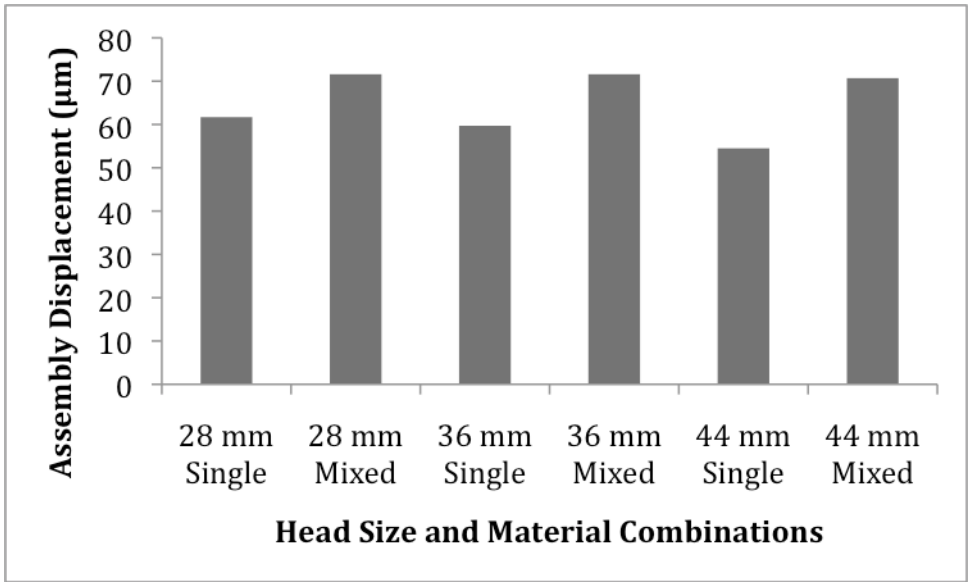

B)

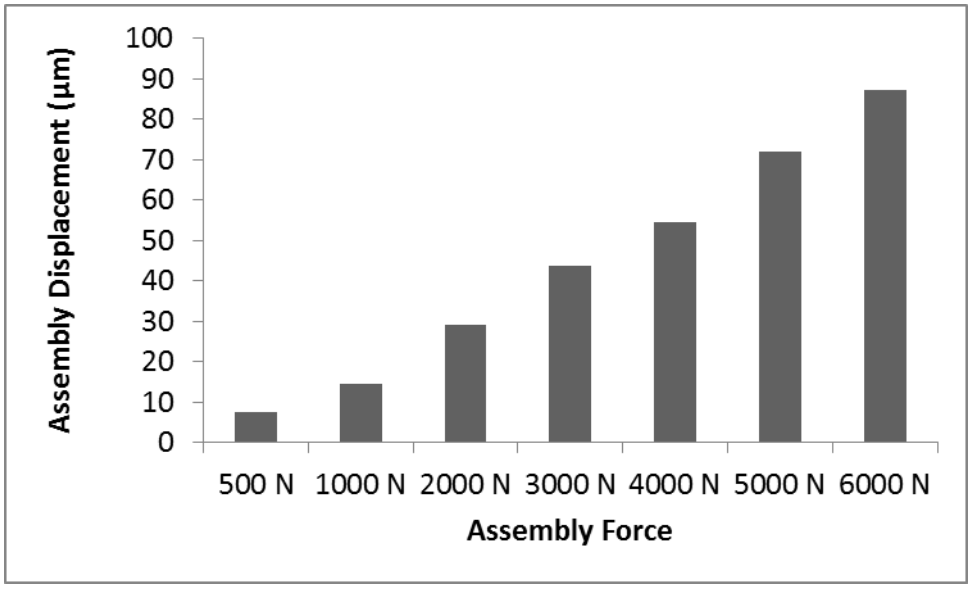

C)

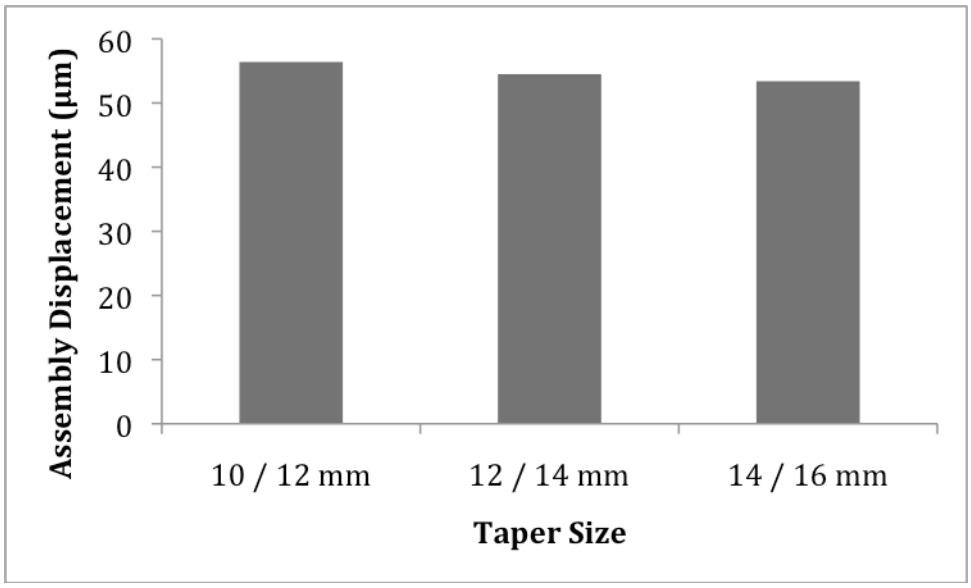

D)

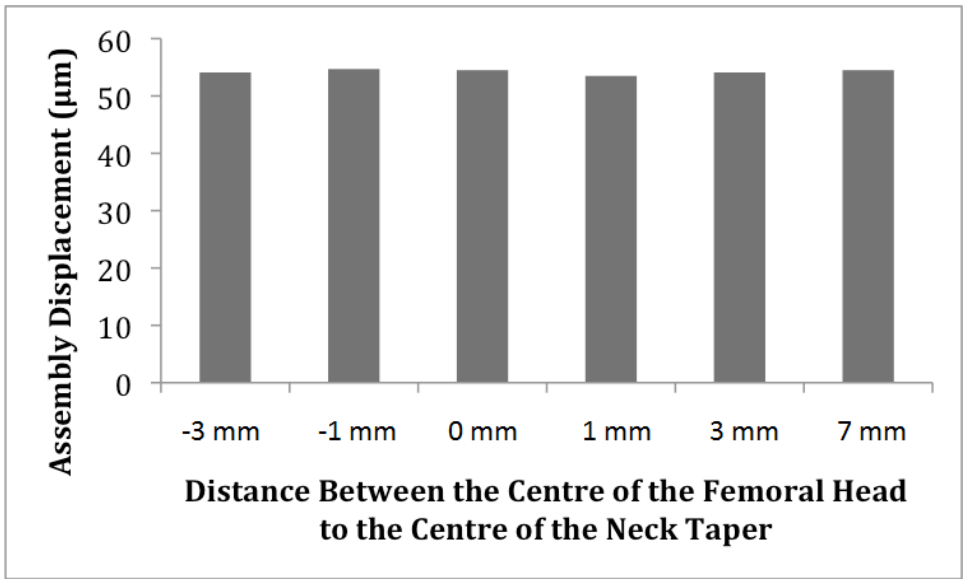

Figure 4.2. The displacement of the femoral head onto the neck taper when modifying: A) the femoral head size and the material combinations of the head-neck taper interface; B) the assembly force; C) the taper size; and D) the distance between the centre of the femoral head to the centre of the neck taper. Note: For Figure 4.2 D, the negative distances indicate that the centre of the femoral head was below the centre of the neck taper whereas the positive distances indicate the centre of the femoral head was above the centre of the neck taper.

4.3.2 Micromotion at the Head-Neck Taper Interface

Figure 4.3 illustrates the micromotion at the head-neck taper interface when modifying the different parameters. When the head size was increased for the single alloy material combination (Figure 4.3 A), the micromotion during the compression phase significantly increased from 3.7 µm for the 28 mm femoral head to 16.4 µm for the 44 mm femoral head. Similarly, this trend also occurred for the mixed alloy material combination (Figure 4.3 A) in which the micromotion during the compression phase was 6.3 µm for the 28 mm femoral head and 27.9 µm for the 44 mm femoral head. When modifying the assembly force for a 36 mm femoral head (Figure 4.3 B), the micromotion decreased substantially from 49.0 µm for a 500 N assembly force to 7.2 µm for the 6000 N assembly force. By increasing the taper size for a 44 mm femoral head (Figure 4.3 C), the micromotion during the compression phase decreased from 24.0 µm for the 10/12 mm taper to 7.9 µm for the 14/16 mm taper. When modifying the distance between the centre of the femoral head to the centre of the neck taper (Figure 4.3 D), the micromotion steadily decreased from 24.5 µm when the distance was 7 mm to 16.4 µm when the centres were aligned. Meanwhile, the micromotion further decreased to 14.4 µm as the centre of the femoral head was positioned 3 mm below the centre of the neck taper. Finally, the compression micromotion was analyzed for out of axis loading with an angle of 30° to axial loading (Figure 4.3 E). For out of axis loading, the micromotion during the compression phase was 16.4 µm; however, the micromotion was 1.7 µm for the axial loaded model.

For all of the models, the tension phase resulted in a micromotion of less than 1 µm except for the 44 mm mixed alloy model (1.5 µm).

A)

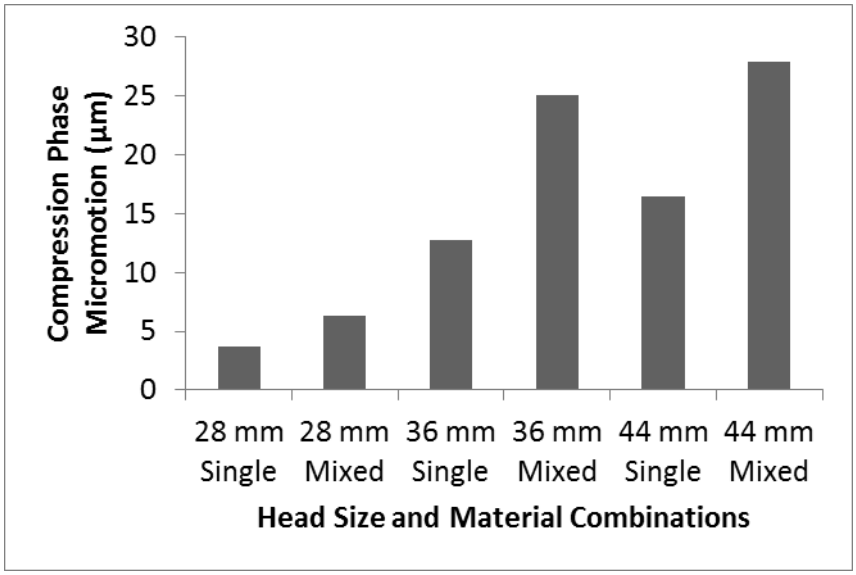

B)

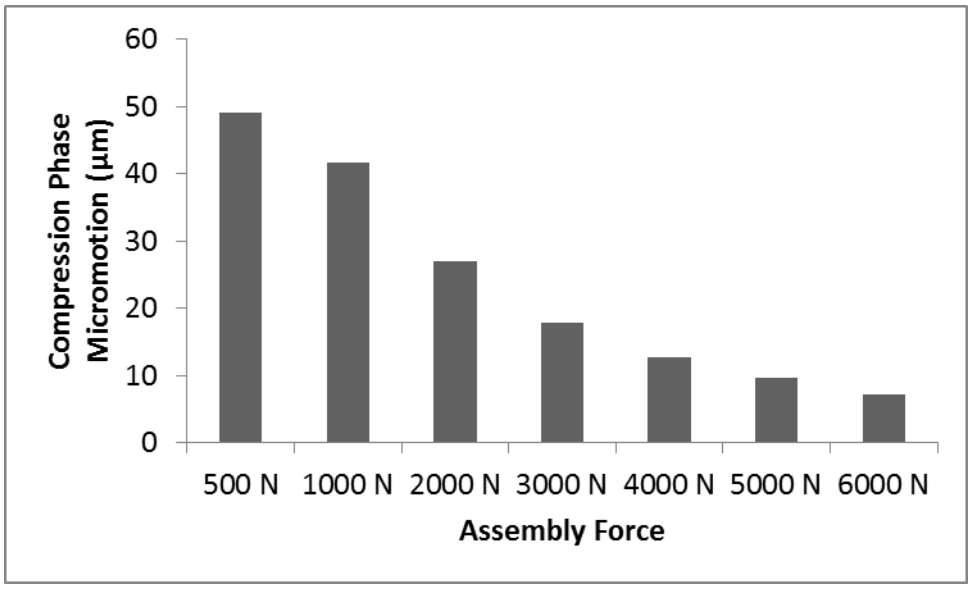

C)

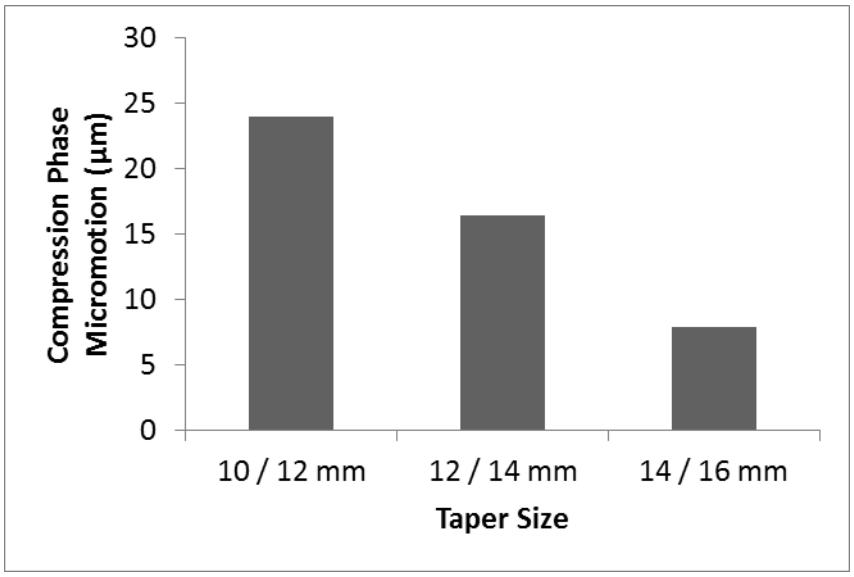
30
25
20
15
10
5
0
Compression Phase Micromotion (µm)
10 / 12 mm
12 / 14 mm
14 / 16 mm
Taper Size

D)

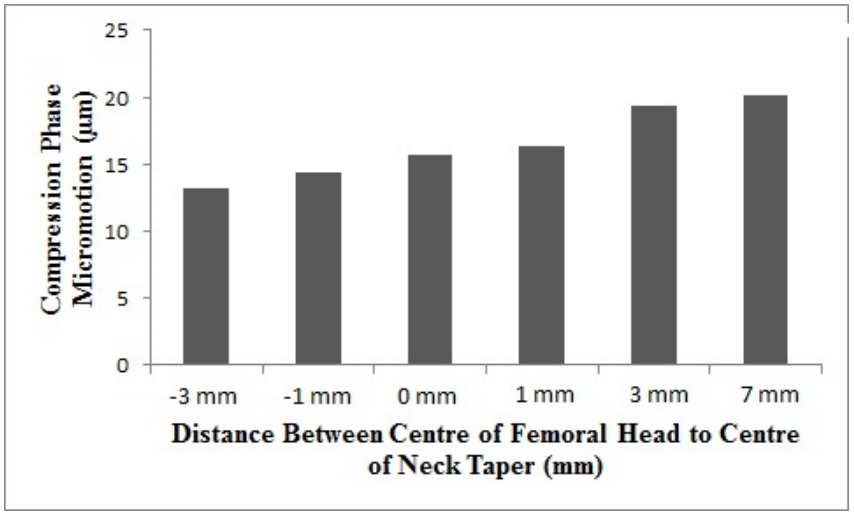
25
20
15
10
5
0
Compression Phase Micromotion (µm)
-3 mm
-1 mm
0 mm
1 mm
3 mm
7 mm
Distance Between Centre of Femoral Head to Centre of Neck Taper (mm)

E)

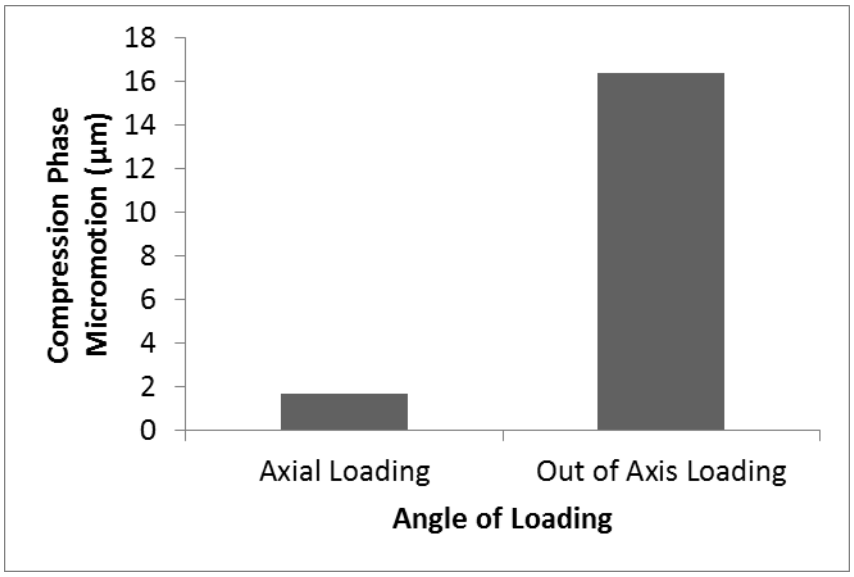

Figure 4.3. The micromotion of the centre of the engaged head taper during the compression phase when modifying: A) the femoral head size and the material combinations of the head-neck taper interface; B) the assembly force; C) the taper size; D) the distance between the centre of the femoral head to the centre of the neck taper; and E) the angle of loading.

4.3.3 Stress Analysis at the Head-Neck Taper Interface

Table 4.2. The maximum von Mises stress at the head-neck taper interface.

A) CoCr head sizes with a 4000 N assembly force and a 12/14 mm CoCr taper.				
Femoral Head Size	Assembly	Recovery	Compression	Tension
28 mm Femoral Head	94.4 MPa	77.7 MPa	81.2 MPa	92.6 MPa
36 mm Femoral Head	72.1 MPa	61.1 MPa	80.0 MPa	51.5 MPa
44 mm Femoral Head	47.2 MPa	43.8 MPa	79.9 MPa	43.6 MPa
B) CoCr head sizes with a 4000 N assembly force and a 12/14 mm Ti6Al4V taper.				
Femoral Head Size	Assembly	Recovery	Compression	Tension
28 mm Femoral Head	80.0 MPa	62.3 MPa	73.2 MPa	62.4 MPa
36 mm Femoral Head	69.1 MPa	57.7 MPa	68.1 MPa	54.7 MPa
44 mm Femoral Head	58.3 MPa	47.4 MPa	61.9 MPa	41.1 MPa
C) 36 mm femoral head with a 12/14 mm taper with a range of assembly forces.				
Assembly Force	Assembly	Recovery	Compression	Tension
500 N	8.8 MPa	7.6 MPa	79.6 MPa	30.0 MPa
1000 N	17.8 MPa	15.4 MPa	79.6 MPa	30.0 MPa
2000 N	35.7 MPa	30.9 MPa	79.6 MPa	30.0 MPa
3000 N	53.5 MPa	46.3 MPa	79.8 MPa	40.7 MPa
4000 N	72.1 MPa	61.1 MPa	80.0 MPa	51.5 MPa
5000 N	75.6 MPa	63.5 MPa	78.1 MPa	63.8 MPa
6000 N	83.2 MPa	71.0 MPa	77.4 MPa	75.2 MPa
D) 44 mm femoral head with different taper sizes with a 4000 N assembly force.				
Taper Size	Assembly	Recovery	Compression	Tension
10/12 mm	43.5 MPa	43.0 MPa	67.0 MPa	43.9 MPa
12/14 mm	47.2 MPa	43.8 MPa	79.9 MPa	43.6 MPa
14/16 mm	53.4 MPa	52.1 MPa	89.4 MPa	51.3 MPa
E) 44 mm CoCr head with a 12/14 mm CoCr neck with different distances between the centre of the head taper to the centre of the neck taper after a 4000 N assembly force.				
Distance between the head and neck taper centres	Assembly	Recovery	Compression	Tension
7 mm (above the neck taper)	58.9 MPa	52.6 MPa	102.2 MPa	46.8 MPa
3 mm (above the neck taper)	51.8 MPa	46.7 MPa	104.8 MPa	45.7 MPa
1 mm (above the neck taper)	49.6 MPa	46.2 MPa	94.6 MPa	44.9 MPa
0 mm (taper centres are aligned)	47.2 MPa	43.8 MPa	79.9 MPa	43.6 MPa
-1 mm (below the neck taper)	49.7 MPa	46.9 MPa	72.2 MPa	46.4 MPa
-3 mm (below the neck taper	48.0 MPa	45.9 MPa	71.0 MPa	46.2 MPa
F) 44 mm CoCr femoral head with a 12/14 mm CoCr neck subjected to a 4000 N assembly force with axis and out of axis loading during compression and tension.				
Angle of Loading	Assembly	Recovery	Compression	Tension
Out of Axis Loading (30º)	47.2 MPa	43.8 MPa	79.9 MPa	43.6 MPa
Axial Loading (0º)	47.2 MPa	43.8 MPa	46.4 MPa	43.9 MPa

Table 4.2 lists the maximum von Mises stress at the head-neck taper interface throughout the four phases. In all of the simulations, the maximum von Mises stress was higher in the assembly phase in comparison to the recovery phase. When the tension phase was applied, the maximum von Mises stress was reduced in comparison to the compression phase. Additionally, the maximum von Mises stress during the compression phase (Figure 4.4 C) and tension phase (Figure 4.4 D) occurred at the bottom quarter of the engaged taper.

As the head size increased, the maximum von mises stress during the assembly and recovery phase substantially decreased for the single alloy (Table 4.2 A) and mixed alloy material combinations (Table 4.2 B). When the assembly force was increased from 500 N to 6000 N (Table 4.2 C), the maximum von Mises stress linearly increased during the assembly and recovery phases. But during the compression phase, the maximum von Mises stress hovered around 80 MPa. When increasing the taper size (Table 4.2 D), the maximum von Mises stress tended to increase for the assembly, recovery, and compression phases. When adjusting the distance between the centre of the femoral head to the centre of the neck taper (Table 4.2 E), the maximum von Mises stress gradually decreased in the compression phase as the centre of the femoral head was positioned more distally. When comparing the axial and out of axis models, the out of axis loading model displayed a maximum von Mises stress of 79.9 MPa whereas the axial loaded model had a maximum von Mises stress of 46.4 MPa.

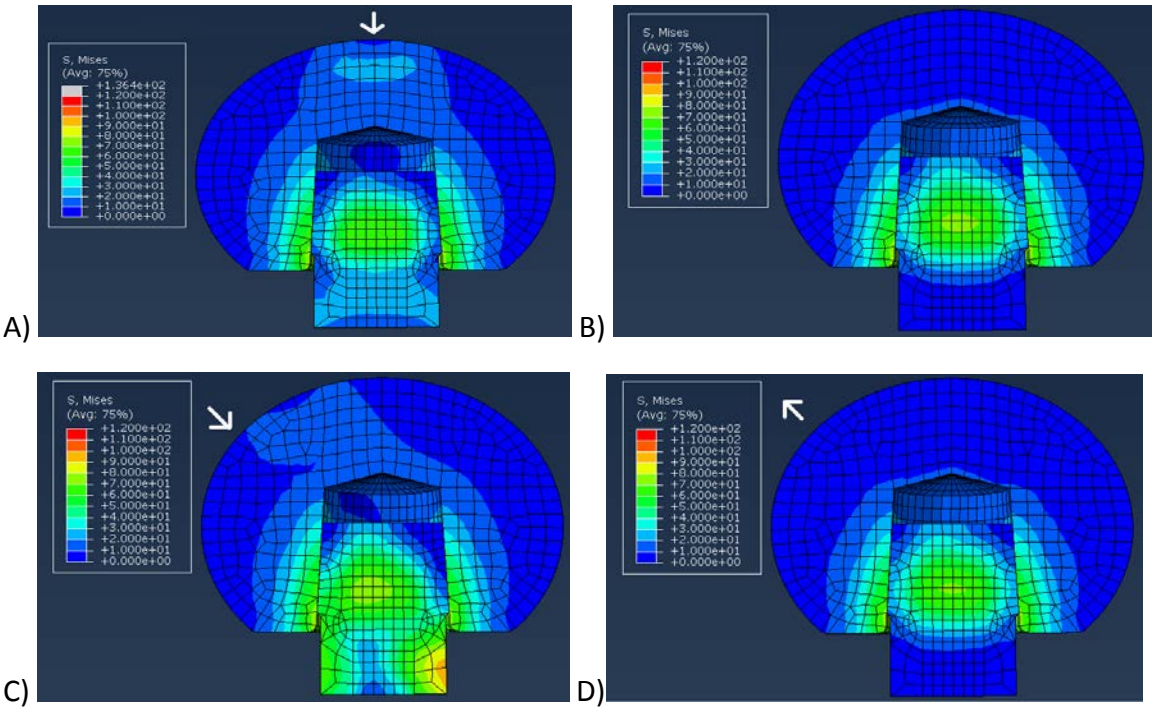

Figure 4.4. The von Mises stresses (MPa) of the femoral head and neck during: A) the assembly phase as the force is applied in the direction of the long axis of the neck taper; B) the recovery phase; C) the compression phase where 3300 N of force is directed towards the femoral head 30° away from the long axis of the neck taper; and D) the tension phase where 100 N of force is applied 30° away from the long axis of the neck taper.

4.4 Discussion

When considering the assembly procedures that were simulated, large diameter femoral heads reduced the maximum von Mises stress at the head-neck taper interface and decreased the overall assembly displacement. To account for this, the stiffness of the femoral head increases with head size. Additionally, the mixed alloy models displayed a greater assembly displacement and reduced the maximum von Mises stress in comparison

to the single alloy models. By having a smaller modulus of elasticity, the Ti6Al4V neck deformed more during the assembly procedure.

When the material of the neck was changed from CoCr to Ti6Al4V, there was a significant difference in the micromotion that was generated during the compression phase. CoCr has a greater modulus of elasticity and is not as vulnerable to galling in comparison to Ti6Al4V [177]. We hypothesize that the difference in the modulus of elasticity between these two alloys was responsible for the increased micromotion at the head-neck taper interface. Many studies have reported that mixed alloy modular hip prostheses are more susceptible to corrosion due to galvanic effects despite the small difference in the electrical potential [177, 257]. Even though galvanic corrosion may take place at the head-neck taper interface, increased micromotion is another consideration that surgeons should be aware of when assembling mixed alloy modular hip prostheses.

In recent retrieval studies, there have been reports that an increase in head size leads to corrosion damage [243, 261] while other researchers have arrived at different conclusions [262]. In this finite element analysis, there was more micromotion at the head-neck taper interface with a larger head size during compression (Figure 4.3 A). When considering the 28 mm head size models that were simulated, the micromotion during the compression phase was 3.7 μm for the single alloy model and 6.3 μm for the mixed alloy model, which is very close to the values reported by Jauch et al. for the taper interface between a stem and a neck adapter (4.3 μm for a CoCr neck adapter on a CoCr stem and 7.8 μm for a Ti6Al4V neck adapter on a CoCr stem) [180]. However, the mi-

cromotion for the 36 mm and 44 mm femoral heads during the compression phase was larger than what Jauch et al. reported.

Researchers have been recently indicating that the assembly force is a contributing factor for corrosion damage at the head-neck taper interface [219]. When an assembly force of 500 N was applied, 49.0 μm of micromotion occurred at the head-neck taper interface during the compression phase. When the assembly force was increased to 2000 N, 27.0 μm of micromotion occurred during the compression phase. This study further supports Rehmer's argument that an assembly force of 4000 N is required to secure the head-neck taper interface and to minimize the micromotion [219], which was reported to be 12.7 μm for this study. Although a minority of orthopaedic surgeons hand-press the femoral head onto the neck, this practice is strongly discouraged since this can generate significant micromotion at the head-neck taper interface, which could lead to extensive corrosion and fretting damage. This study also revealed that an assembly force of 6000 N can reduce the micromotion; however, the assembly force that is delivered must ultimately be safe enough for the patient. Further research needs to be explored on an optimal assembly technique.

This study observed the influence of taper size on the micromotion at the head-neck taper interface. As the taper size increased from 10/12 mm to 14/16 mm, the micromotion decreased from 24.0 μm to 7.9 μm (Figure 4.3 C). By having a larger taper size, this increases the amount of frictional force that the head-neck taper interface must overcome for micromotion to occur. Even though the 14/16 mm taper can reduce micro-

motion, this taper has been known to result in dislocations and may not be the best solution to minimizing corrosion damage at the head-neck taper interface.

Another parameter that was examined was the distance between the centre of the head to the centre of the neck. By having a larger head size, the centre of the femoral head has a wider range of possibilities of where it can be positioned due to different designs. By placing the centre of the femoral head in a more superior position, the micromotion between the head and neck increases due to a larger toggling torque. Surgeons and designers should be aware of the possible consequences of selecting large femoral head sizes and the corresponding neck length in terms of how this can result in head-neck taper corrosion.

This study also demonstrates that with out of axis loading, a 44 mm femoral head with a femoral head and neck designed with CoCr alloy can generate 16.4 μm of micromotion during the compression phase, which is considerably much larger than the axial loaded model (1.7 μm). Some researchers have hypothesized that an increase in head size can lead to greater corrosion and fretting damage due to a greater toggling torque. This simulation further supports the hypothesis that the toggling torque affects the micromotion at the head-neck taper interface, which can become greater with an increased head size and positioning the centre of the femoral head in a more superior position relative to the neck taper.

In all of the models, the maximum von Mises stress at the head-neck taper interface during the compression phase occurred at the bottom quarter of the head taper. We hypothesize that the greatest extent of corrosion and fretting damage at the head-neck ta-

per interface occurs at this site due to the destruction of the passive oxide film on the alloy surface. Upon examining implants in a recent retrieval analysis, we observed that the most corroded regions occurred at the bottom quarter of the engaged head taper [243] and this has also been confirmed by Munir et al. [47].

There are some limitations to this investigation. This study analyzed the micromotion at the head-neck taper interface, which can lead to fretting damage. One of the disadvantages of finite element analysis is that it cannot simulate corrosion damage since corrosion is an electrochemical phenomenon. However, this study was able to predict the micromotion at the head-neck taper interface, which can deteriorate the passive oxide film due to fretting and can make the region vulnerable to corrosion.

Fatigue testing was not simulated and a stabilization study was not conducted. This could potentially affect the results of the simulations with smaller loads. Additionally, none of the simulations featured rotational moments, which can take place at the head-neck taper interface.

The finite element models had a coefficient of friction of 0.15 to simulate the ground surface finish but there are a few limitations with this value. The surface condition of the head-neck taper interface after precision grinding usually differs from the as-received condition. Additionally, the grinding is not perfect as indicated by markings along the bore, which could lead to some local stress concentrations. Even though the coefficient of friction could have been modified with other surface finishes [163], the trends discussed in this paper would most likely remain the same.

During the compression phase, a 3300 N force was applied 30° away from the long axis of the neck based on ASTM F1875-98 [129]. This force represents multiple body weights of the patient and would correspond to the stance phase although this force could change throughout the gait cycle and if the patient had a varus or valgus stance. Upon examining badly worn femoral heads in retrieval analyses, the wear damage is typically found at an angle of about 30° away from the long axis of the neck.

Finally, a 100 N tension force was applied to represent the suction effect during the swing phase for modular hip prostheses with a hard-on-hard articulation and a small clearance. This force could change throughout the swing phase by the actions of the muscles, tendons, and ligaments. During dislocation, patients may have a “clicking” sound due to this tension force.

4.5 Conclusion

The purpose of this study was to identify which factors influence the micromotion at the head-neck taper interface of modular hip prostheses. Micromotion at this interface can lead to fretting damage that deteriorates the passive oxide film on the alloy surface. As a consequence, the taper interface is more vulnerable to crevice corrosion, which can trigger adverse tissue reactions. The following conclusions were revealed in this study:

- By increasing the diameter of the femoral head, the assembly displacement and the maximum von Mises stresses at the head-neck taper connection are reduced. Both of these observations can be attributed to a greater stiffness due to a larger head size. Additionally, large diameter femoral heads result in more micromotion at the head-neck taper interface in comparison to small femoral head sizes, which is attributed to an increased toggling torque.

- The micromotion between the head and neck will increase if the centre of the femoral head is in a more superior position relative to the centre of the neck taper. By placing the centre of the femoral head near or below the centre of the neck taper, micromotion at the head-neck taper interface can be reduced.

- CoCr femoral heads assembled onto Ti6Al4V necks have a greater assembly displacement and more micromotion at the head-neck taper interface than femoral heads and necks consisting solely of CoCr alloy.

- By increasing the assembly force, this will increase the assembly displacement of the femoral head and reduce the micromotion during the compression phase. Although a large assembly force is theoretically recommended, in practice surgeons should deliver an assembly force that is safe for the patient.

- As the taper size increases, this reduces the micromotion at the head-neck taper interface. By having a greater surface area, the head-neck taper interface must overcome greater frictional forces for micromotion to occur. However, the disadvantage of a 14/16 mm taper size is that it can increase the risk of dislocation.

- By applying out of axis loading, this can trigger significantly more micromotion at the head-neck taper interface than axial loading. This supports the argument that the toggling torque is a major factor for corrosion and fretting damage at the head-neck taper interface.

Micromotion at the head-neck taper interface is a catalyst for corrosion damage that can result in pain and revision surgery for the patient. To minimize the micromotion at the head-neck taper interface during cyclic loading, the use of small head sizes, using similar material combinations, placing the centre of the femoral head near or below the centre of the neck taper, and delivering a safe and an appropriate assembly force are recommended.

Chapter 5 – In Vitro Corrosion Fatigue Testing of Modular Hip Prostheses

Abstract: The purpose of this study was to determine if the femoral head size of modular hip prostheses influences head-neck taper corrosion through *in vitro* testing. Femoral heads were assembled onto neck tapers with a 2000 N axial force and subjected to ten million cycles of out of axis loading (300 N to 3300 N) in PBS maintained at 37°C. The femoral heads were pulled off afterwards and examined for corrosion and fretting damage. The prostheses with a 36 mm femoral head had significantly greater neck corrosion ($p = 0.046$), head corrosion ($p = 0.050$), neck fretting ($p = 0.050$), and head fretting scores ($p = 0.050$) in comparison to prostheses assembled with 28 mm femoral heads.

5.1 Introduction

Corrosion damage of modular hip prostheses continues to be a challenge in orthopaedics. By having corrosion damage at the head-neck [170, 171, 181, 182, 184, 258] or neck-stem [108, 134, 140, 180, 195-200, 204] taper interface, the patient may experience

pain, hypersensitivity, adverse tissue reactions [133-135, 174, 272], and may undergo premature revision surgery to remove the prosthesis.

Researchers have been trying to determine which factors can influence head-neck taper corrosion damage. In particular, there has been some discussion if the use of large femoral heads can lead to more corrosion damage. To answer this question, many retrieval analyses have been performed where some researchers have observed that a larger head size can lead to more corrosion damage [243, 261] whereas other researchers have arrived at different conclusions [262]. One of the key weaknesses of a retrieval analysis is that it is challenging to isolate a single variable that can influence head-neck taper corrosion. Many researchers who have studied head-neck taper corrosion using a retrieval analysis design have mixed up different material combinations, taper sizes, offsets, manufacturing brands, manufacturing techniques, and manufacturing tolerances. Additionally, there are variations in the assembly force, the loading conditions, and the implantation time.

Recently, finite element analysis was performed to determine if a larger head size leads to more micromotion at the head-neck taper interface due to a greater toggling torque. By having more micromotion, this can deteriorate the passive oxide film that protects the head-neck taper interface from fretting and corrosion damage. By increasing the head size, the simulations revealed that the micromotion at the head-neck taper interface increases due to a toggling torque. By increasing the distance between the centre of the femoral head to the centre of the neck taper with a larger head size, this produces a greater toggling torque that results in more micromotion at the head-neck taper interface. Ad-

ditionally, finite element analysis was performed on models where axial loading was applied in the direction of the long axis of the neck. These simulations resulted in minimal micromotion at the head-neck taper interface. This suggests that the toggling torque could be a major factor that influences micromotion at the head-neck taper interface that is responsible for corrosion and fretting damage.

The purpose of this investigation was to perform *in vitro* corrosion fatigue testing to determine if a larger head size leads to greater head-neck taper corrosion damage. Additionally, axial loading was performed to determine if the toggling torque is a contributing factor with respect to corrosion and fretting damage.

5.2 Methodology

For this study, femoral heads manufactured from CoCr alloy were assembled onto CoCr alloy neck tapers featuring a 12/14 mm taper with a taper angle of 5°40’. To determine if head size has an influence on head-neck taper corrosion, there were three 28 mm and three 36 mm femoral heads that were assembled onto separate 12/14 mm neck tapers. For the axial loading tests, three additional 28 mm and three 36 mm femoral heads were assembled onto separate neck tapers.

In vitro corrosion fatigue testing was performed with an Instron ElectroPuls™ E10000 Linear-Torsion load frame in accordance to ASTM F1875-98. To assemble the femoral head onto a neck component, a 2000 N axial load was applied. In regard to fa-

tigue testing, a force range of 300 N to 3300 N was applied at a frequency of 5 Hz for ten million cycles. For out of axis testing, fatigue loading was performed at an angle of 30° from the long axis of the neck whereas for the axial loaded prostheses, the fatigue load was applied in the direction of the long axis of the neck. After fatigue testing, the femoral head was pulled off in accordance to ISO 7206-10.

Phosphate buffered saline was used as an electrolyte and maintained at a temperature of 37°C. Recently, Ocran conducted an *in vitro* pin-on-disc experiment [40] to determine which of the following electrolytes should be used for *in vitro* corrosion fatigue testing: 0.14 M NaCl; phosphate buffered saline; or clinically relevant simulated body fluid [130]. Ocran discovered that the use of either 0.14 M NaCl and clinically relevant simulated body fluid leads to low corrosion current densities for CoCr alloy (4.21 $\mu A/cm^2$ and 4.98 $\mu A/cm^2$, respectively). In contrast, phosphate buffered saline is a more aggressive electrolyte for CoCr alloy with a corrosion current density of 18.57 $\mu A/cm^2$. This high corrosion current density for CoCr alloy may be attributed to the presence of phosphate ions that adsorb onto the CoCr alloy surface to form $H_2PO_4^-$. These ions are the conjugate base of phosphoric acid, which is a weak acid that may increase the dissolution rate of CoCr alloy. Meanwhile, the proteins in clinically relevant simulated body fluid can delay the dissolution rate since they can adsorb onto the oxide film; thus, decreasing the corrosion current density of CoCr alloy into a more clinically relevant rate. Ocran discouraged the use of 0.14 M NaCl for testing because the corrosion products and mechanisms may differ than what occurs in an *in vivo* setting. In clinically relevant simulated body fluid, CoCr alloy is easy to passivate since the critical anodic current density

was just slightly greater than the passive anodic current density. As the immersion time increases, the difference between the critical anodic current density and the passive anodic current density gradually increases; thus, forming a more effective passive oxide film with time.

A) 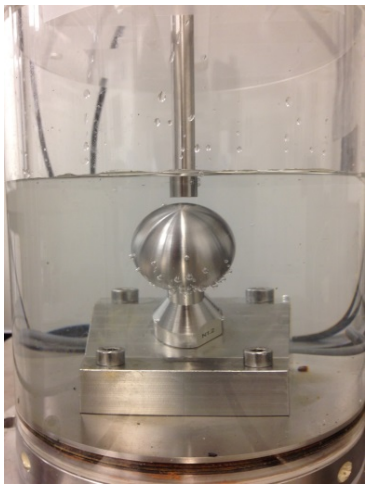 B) 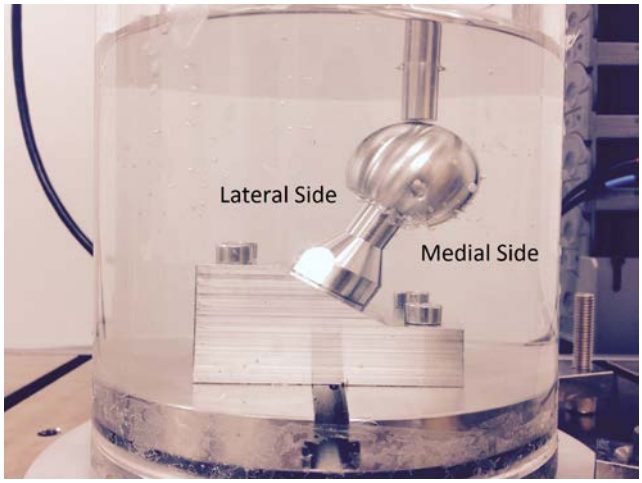

Figure 5.1. A close-up of the apparatus prior to fatigue testing: A) frontal view; B) side view.

To examine for corrosion and fretting damage of the femoral heads and necks, three researchers (two graduate students, one undergraduate student) independently scored the components using criteria that has been previously established [243]. Additionally, scanning electron microscopy and energy dispersive x-ray spectroscopy were performed to further analyze the corrosion and fretting damage as well as to identify the corrosion products that formed along the surface.

The volumetric wear damage was calculated for the head and neck tapers that were subjected to out of axis loading. To do this, a coordinate measuring machine (Zeiss

Prismo Navigator 795) was used to create a 3D surface profile of the head and neck tapers. To create the profiles of the tapers, scanning was achieved by performing concentric circle passes with 0.1 mm point spacing from the bottom to the top of the taper surface at a linear speed of 1 mm/s. The measurement uncertainty of the coordinate measuring machine was 0.0011 mm. After obtaining 3D profiles of the head and neck tapers, these profiles were imported into Geomagic Studio to calculate the volumetric wear.

To determine the agreeability of the corrosion and fretting scores between the three researchers, the intraclass correlation coefficient was determined. Additionally, the Shapiro-Wilk test was performed to test for normality of the corrosion and fretting scores. Depending on the normality of the data, an independent t-test was performed for the normally distributed data sets whereas the Mann-Whitney U test was conducted to identify significant differences for the nonparametric data sets ($\alpha = 0.05$).

5.3 Results

The intraclass correlation coefficient for the corrosion and fretting scores were calculated to determine if there was an agreement in the scoring between the three researchers. The intraclass correlation coefficients for the corrosion and fretting scores were 0.948 and 0.886, respectively. This indicates that there was an excellent agreement between the three researchers for assessing the corrosion and fretting scores.

Table 5.1 presents the average corrosion and fretting scores of the femoral heads and necks. When examining the corrosion and fretting scores between the 28 mm and 36 mm head size groups that were subjected to out of axis loading, the Mann-Whitney U test was performed. Significant differences were found for neck corrosion ($p = 0.046$), head corrosion ($p = 0.050$), neck fretting ($p = 0.050$), and head fretting (0.050). When comparing the prostheses with 36 mm femoral heads that underwent out of axis and axial loading, the axial loaded prostheses had a significant reduction in neck corrosion ($p = 0.046$), head corrosion ($p = 0.046$), neck fretting ($p = 0.050$), and head fretting ($p = 0.050$) due to the absence of a toggling torque. Unlike the two 36 mm femoral head groups, the 28 mm femoral head groups that underwent out of axis and axial loading had no significant differences in the corrosion or fretting scores for the head and neck tapers. Table 2 provides the corrosion and fretting scores for the lateral and medial sides. The medial side of the head and neck tapers tended to have greater corrosion and fretting scores but there were no significant differences. Table 3 presents the corrosion and fretting scores separated by the superior and inferior regions and a t-test was performed since the data was normally distributed. When comparing all of the samples, the inferior region of the head-neck taper interface had significantly more neck corrosion ($p = 0.020$), head corrosion ($p < 0.001$), neck fretting ($p = 0.001$), and head fretting ($p < 0.001$) damage.

Table 5.1. The average corrosion and fretting scores for the head and neck tapers.

Head Size	Neck Corrosion Score	Head Corrosion Score	Neck Fretting Score	Head Fretting Score
28 mm	7.56 ± 3.86	8.44 ± 4.79	2.44 ± 3.15	4.22 ± 2.87
36 mm	24.89 ± 8.85	28.33 ± 8.09	9.11 ± 1.39	10.50 ± 2.50
28 mm Axial Loading	4.56 ± 3.10	12.44 ± 2.36	1.67 ± 1.67	10.22 ± 3.83
36 mm Axial Loading	5.22 ± 3.00	6.22 ± 2.69	5.78 ± 1.26	3.33 ± 0.88

Table 5.2. The average corrosion and fretting scores on the medial and lateral sides of the prostheses that received out of axis fatigue loading.

	Neck Corrosion Medial	Neck Corrosion Lateral	Head Corrosion Medial	Head Corrosion Lateral	Neck Fretting Medial	Neck Fretting Lateral	Head Fretting Medial	Head Fretting Lateral
28 mm Head	1.33 ± 0.34	1.00 ± 0.67	2.22 ± 2.01	1.56± 0.84	1.00 ± 0.88	0.67 ± 0.58	1.33 ± 0.58	1.33 ± 0.67
36 mm Head	9.67 ± 2.03	2.44 ± 1.83	9.22 ± 1.84	5.22 ± 3.42	2.67 ± 0.67	0.89 ± 0.96	4.11 ± 1.17	2.00 ± 1.73

Table 5.3. The average corrosion and fretting scores on the superior and inferior regions of the head-neck taper interface.

	Neck Corrosion Superior	Neck Corrosion Inferior	Head Corrosion Superior	Head Corrosion Inferior	Neck Fretting Superior	Neck Fretting Inferior	Head Fretting Superior	Head Fretting Inferior
28 mm Out of Axis Loading	3.00 ± 1.87	1.67 ± 2.00	5.67 ± 2.69	2.78 ± 2.86	1.33 ± 1.22	2.22 ± 3.42	2.78 ± 1.79	2.44 ± 2.13
36 mm Out of Axis Loading	6.67 ± 3.77	16.44 ± 6.77	5.44 ± 3.47	21.22 ± 9.91	2.33 ± 2.60	6.22 ± 1.30	2.00 ± 2.00	9.67 ± 3.04
28 mm Axial Loading	2.22 ± 2.33	2.33 ± 1.73	6.67 ± 0.87	5.78 ± 1.99	0.44 ± 1.33	1.22 ± 0.97	5.22 ± 2.64	5.56 ± 2.19
36 mm Axial Loading	0.78 ± 0.84	4.89 ± 2.27	1.67 ± 0.67	7.33 ± 1.64	0.33 ± 0.33	5.00 ± 1.00	0.11 ± 0.19	2.78 ± 0.51

A)  B)  C) 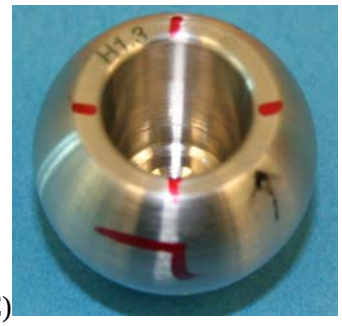 D) 

Figure 5.2. Corrosion and fretting damage of the head and neck tapers after fatigue testing for a 28 mm femoral head that received out of axis fatigue loading. A) Neck taper on the medial side. B) Neck taper on the lateral side. C) Femoral head taper on the medial side. D) Femoral head taper on the lateral side.

A)  B)  C) 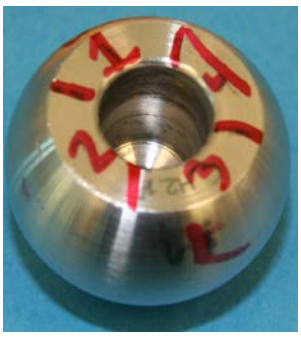 D) 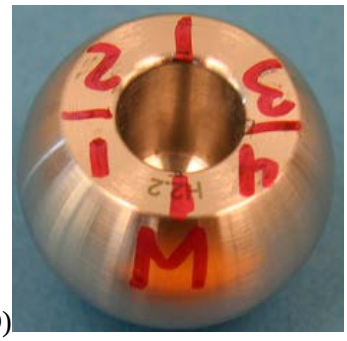

Figure 5.3. Corrosion and fretting damage of the head and neck tapers after fatigue testing for a 36 mm femoral head that received out of axis fatigue loading. A) Neck taper on the medial side. B) Neck taper on the lateral side. C) Femoral head taper on the medial side. D) Femoral head taper on the lateral side.

A)  B) 

Figure 5.4. Corrosion and fretting damage of a neck component (A) and the corresponding 36 mm femoral head (B) after axial fatigue loading.

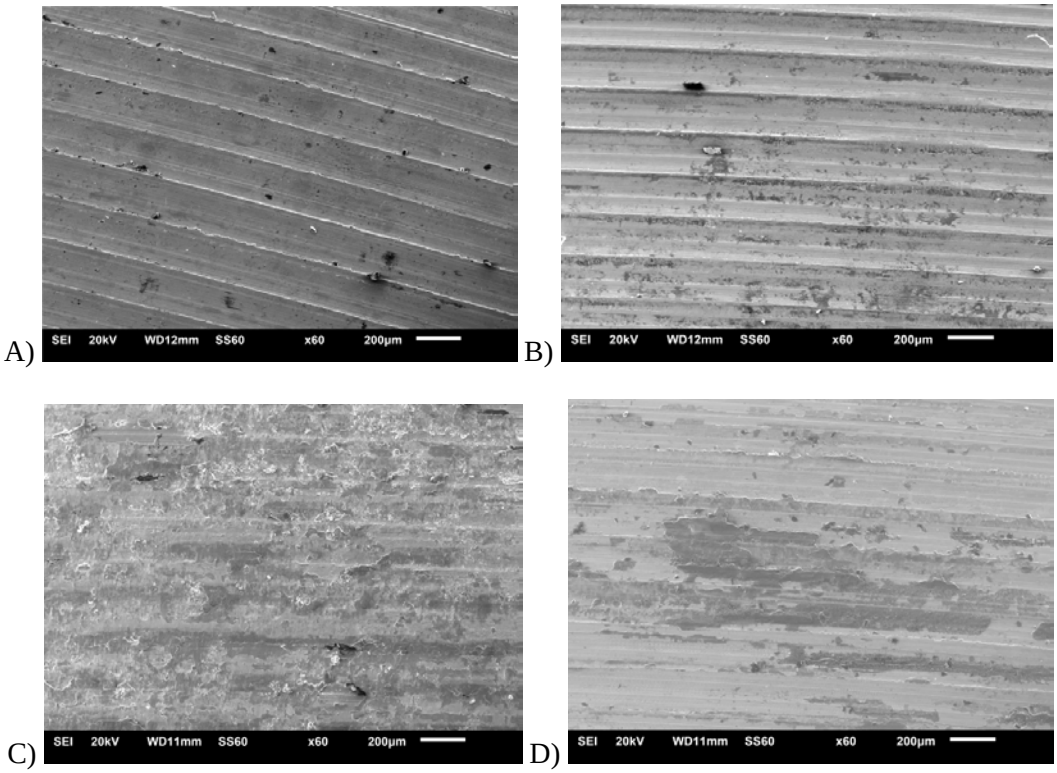

Figure 5.5. Scanning electron microscopy images of: A) a pristine neck taper that did not receive an assembly force or undergo fatigue testing; B) a neck taper from a 28 mm femoral head subjected to out of axis fatigue loading; C) a neck taper from a 36 mm femoral head that underwent out of axis fatigue loading; D) a neck taper from a 36 mm femoral head subjected to axial fatigue loading.

Table 5.4. The volumetric wear damage of the head and neck tapers after receiving out of axis fatigue loading.

Head Size	Neck Taper Volumetric Wear	Head Taper Volumetric Wear
28 mm	0.37 ± 0.05 mm^3	0.44 ± 0.10 mm^3
36 mm	0.94 ± 0.13 mm^3	0.92 ± 0.17 mm^3

Table 5.4 presents the volumetric wear damage of the head and neck tapers that received ten million cycles of out of axis loading. When comparing the 28 mm and 36 mm head size groups, there was significantly more volumetric wear damage for the neck

tapers ($p = 0.002$) and the head tapers ($p = 0.013$) for the 36 mm head size group. When comparing the volumetric wear damage between the head and neck tapers, there were no significant differences for the 28 mm head size group ($p = 0.343$) nor the 36 mm head size group ($p = 0.861$).

Scanning electron microscopy images of the neck taper are presented in Figure 5.5. Figure 5.5A shows a neck taper in the pre-assembled state and its machine lines are intact. Figure 5.5 B is an illustration of a neck taper that was assembled to a 28 mm femoral head and subjected to out of axis fatigue loading. In comparison to Figure 5.5 A, this neck taper features some etching. In contrast, Figure 5.5 C is an image of a neck taper that was assembled to a 36 mm femoral head that received out of axis fatigue loading. The machine lines along this taper are deteriorated and the surface has undergone significant corrosion damage in comparison to the neck taper with a 28 mm femoral head (Figure 5.5 B). Meanwhile, a neck taper that was assembled to a 36 mm femoral head that underwent axial fatigue loading (Figure 5.5 D) still had its machine lines intact; however, there was some etching and corrosion damage along the surface.

When looking at the chemical composition of the neck taper surfaces, there were some variations between the different tests. The pristine neck taper featured weight percentages of the following elements: 26.3% chromium; 57.1% cobalt; 5.5% molybdenum; and the remainder being carbon. For the neck tapers featuring a 28 mm femoral head with an out of axis fatigue load, there was slight selective leaching of cobalt (47.5-51.4%); however, selective leaching was more prominent for the neck tapers featuring a 36 mm femoral head with out of axis fatigue loading (29.7-33.0%). The weight percentages of carbon and chromium remained relatively unchanged for all of the neck tapers. For all of

the prostheses that underwent fatigue loading, oxygen was present along the neck taper. For the neck tapers with a 28 mm femoral head, the weight percentage of oxygen was 7 to 11% but increased for the neck tapers featuring a 36 mm femoral head with a range from 23.0 to 28.6%. Energy dispersive x-ray spectroscopy revealed that chromium phosphate, chromium oxide, molybdenum chloride, and molybdenum oxide corrosion products formed along the surface.

5.4 Discussion

When performing the Shapiro-Wilk test, all of the corrosion and fretting scores displayed a normal distribution except for the 36 mm neck corrosion scores ($p < 0.001$) and the 36 mm axial head corrosion scores ($p < 0.001$). Even though the rest of the scores displayed a normal distribution, these data sets had weak statistical power because of the limited sample size for each group. For this reason, the Mann-Whitney U test was applied to identify significant differences for the corrosion and fretting scores. Even with the use of t-tests, significant differences were still discovered ($p \leq 0.05$) for corrosion and fretting damage between the different head size groups and the angle of fatigue loading.

By applying an out of axis fatigue load, the head-neck taper interface featuring a 36 mm femoral head displayed significantly more corrosion and fretting damage than the prostheses with a 28 mm femoral head. This was confirmed by the corrosion and fretting scores, the assessment of the volumetric wear, the scanning electron microscopy images,

and the energy dispersive x-ray spectroscopy data [168, 259]. Additionally, the presence of chromium phosphate, chromium oxide, molybdenum oxide, and molybdenum chloride confirmed that corrosion had taken place [71, 108, 207]. By having a larger head size, there are more possibilities of where the centre of the femoral head can be positioned as this depends on the offset. By increasing the distance between the centre of the femoral head to the centre of the neck taper, this can increase the lever arm. As a consequence, this can lead to a greater toggling torque that can result in more micromotion at the head-neck taper interface. With this increased micromotion, the passive oxide film can become deteriorated and make the head-neck taper interface more susceptible to crevice corrosion.

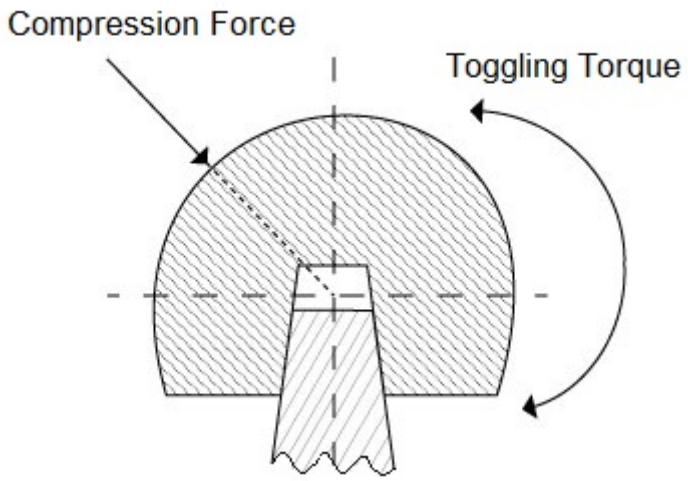

Figure 5.6. The toggling torque of the femoral head during out of axis loading.

To further support the argument that the toggling torque is a contributing factor for head-neck taper corrosion, axial loaded fatigue tests were performed on prostheses featuring 28 mm and 36 mm femoral heads. For the prostheses that had a 36 mm femoral head and were subjected to axial loading, minor head-neck taper corrosion took place in

comparison to the prostheses that received out of axis fatigue loading. Since there was a negligible toggling torque for these tests, minimal micromotion took place at the head-neck taper interface; thus, leaving the passive oxide film intact to prevent head-neck taper corrosion. When examining the prostheses that underwent axial loading, the prostheses with a 28 mm femoral head displayed more head-neck taper corrosion than the prostheses with a 36 mm femoral head. The prostheses with a 28 mm femoral head have a decreased stiffness at the head-neck taper interface in comparison to the prostheses with a 36 mm femoral head. This will result in a greater von Mises stress at the head-neck taper interface. We hypothesize that this increased stress can deteriorate the passive oxide film.

For the prostheses that received out of axis fatigue loading, most of the corrosion and fretting damage occurred on the medial side; however, the only significant difference was discovered for the neck corrosion scores for the 36 mm femoral heads. This may be due to the limited sample size for this experiment. This investigation also revealed that the inferior region of the head-neck taper interface is most vulnerable to corrosion and fretting damage. From a recent finite element analysis [273], this region exhibited the maximum von Mises stress, which corresponds to where the passive oxide film would most likely get deteriorated. This observation is also in agreement with research performed by Munir et al. [47].

The major limitation of this study was the number of samples that were used. Even though there were three prostheses used for the 28 mm and 36 mm femoral heads with out of axis fatigue loading, significant differences were found in the corrosion and fretting scores and the volumetric wear at the head-neck taper interface. By having more

samples, this would have most likely further supported the conclusions that were arrived in this study.

There are several future directions that researchers should consider to prevent head-neck taper corrosion. First, we recommend using clinically relevant simulated body fluid [130] because it can produce similar corrosion damage that can be found in the *in vivo* environment. Additionally, an assembly force of 2000 N was used to follow ASTM F1875-98. Recent research has recommended that a 4000 N assembly force should be applied to prevent micromotion at the head-neck taper interface [219, 273]. Researchers should vary the assembly force through *in vitro* corrosion fatigue testing to determine how this can affect head-neck taper corrosion and what the optimum assembly force should be.

Ceramic femoral heads are one potential solution to prevent corrosion at the head-neck taper interface because ceramics do not corrode; however, the neck taper can still corrode. To redeem the advantages of large head sizes, surgeons can implant large ceramic femoral heads into patients. Presently, it is unknown if the neck tapers will display more corrosion damage when assembled to a large ceramic femoral head. To answer this question, *in vitro* corrosion fatigue testing is recommended.

Finite element analysis has recently revealed that the offset, taper size, and the neck length can influence head-neck taper corrosion due to increased micromotion [266, 273]. To further validate these conclusions, *in vitro* corrosion fatigue testing should be performed to verify these conclusions.

5.5 Conclusion

The purpose of this study was to determine if the size of the femoral head can influence corrosion and fretting damage at the head-neck taper interface of modular hip prostheses through *in vitro* corrosion fatigue testing. Additionally, this paper investigated if the toggling torque is responsible for head-neck taper corrosion by performing out-of-axis and axial fatigue loading. By using a 36 mm femoral head instead of a 28 mm femoral head for out of axis testing, significantly more corrosion and fretting damage and volumetric wear was discovered at the head-neck taper interface. The main argument for this conclusion is that with a larger head size, the distance between the centre of the femoral head to the centre of the neck taper can increase. This can make the toggling torque greater and result in more micromotion at the head-neck taper interface. To further support this hypothesis, modular hip prostheses with assembled 28 mm and 36 mm femoral heads were subjected to axial fatigue loading. A significant reduction in the corrosion and fretting damage was detected at the head-neck taper interface for the prostheses with a 36 mm femoral head. In contrast, the axial loaded prostheses with 28 mm femoral heads displayed more corrosion damage than those with 36 mm femoral heads. For these samples, we hypothesize that the reduction in head size leads to a greater von Mises stress at the head-neck taper interface that can deteriorate the passive oxide film.

Chapter 6 – Discussion

6.1 Can Retrieval Analyses Tell Us What Causes Taper Corrosion?

Retrieval analyses can be helpful to researchers to identify the cause(s) of failure of an implant. For instance, researchers can determine if failure was primarily attributed to poor surgical positioning, excessive wear due to the manufacturing or metallurgy, corrosion, fretting, or a combination of factors [131]. However, retrieval analyses may not be the key to identifying the causes of corrosion and fretting damage at the head-neck taper interface because there are several factors that can be contributing towards these phenomena. These factors include the head size, assembly force, femoral offset, taper size, and the material combinations.

Researchers commonly mix and match different types of THA prostheses to create retrieval analyses; thus, the implants as a collective whole are heterogeneous. By using this strategy, researchers will find it challenging to isolate which variables are responsible for causing head-neck taper corrosion.

To support this argument, let's consider the recent Nassif et al. study, "Taper design affects failure of large-head metal-on-metal total hip replacements" [263]. One of the main problems of retrieval analyses is obtaining implants in sufficient quantities. In Nassif et al.'s study, only 40 femoral heads were obtained along with 6 corresponding stems (15%). By having a very low number of stems available, it is very difficult for Nassif et al. to provide a full picture of the corrosion behaviour occurring at the head-neck taper interface. Despite this, Nassif et al.'s samples were designed by four different manufacturers (DePuy, Zimmer, Biomet, and Wright Medical). As a result, there would most likely be differences in the manufacturing techniques, the tolerances, and the taper angles. When considering the samples themselves, there is no indication of the size of the femoral heads, there are four different material combinations (CoCr head on CoCr neck, CoCr head on Ti6Al4V neck, Ti6Al4V head on CoCr neck, and Ti6Al4V head on Ti6Al4V neck), three different taper sizes (11/13 mm, 12/14 mm, and Type 1), and the femoral offset range of the implants is not mentioned. In this study, Nassif et al. tried to determine if head size was correlated to head-neck taper corrosion but found that there was no relationship. Due to the heterogeneity of the samples along with a variation in the assembly force, a number of factors were most likely contributing to corrosion damage at the head-neck taper interface.

Similarly, Triantafyllopoulos et al. also attempted to determine if head size influences head-neck taper corrosion by conducting a retrieval study of 154 THA prostheses with a metal-on-polyethylene articulation [264]. In Triantafyllopoulos et al.'s study, there were at least five different taper sizes, 74 prostheses had the same material combination for the head-neck taper interface whereas 80 had a mixed material combination,

and there was variation in the treatment of the alloys [264]. From their analysis, Triantafyllopoulos et al. concluded that head size does not influence head-neck taper corrosion. By having heterogeneous samples, it is difficult for Nassif et al., Triantayllopoulos et al., or even Kurtz et al.'s study despite a large sample size (Table 6.1), to determine if head size is responsible for head-neck taper corrosion even though several different variables could be causing this.

There are some limitations in the retrieval analysis that is presented in Chapter 3. In particular, there was a discrepancy in the number of 28 mm (n = 59) and 36 mm femoral heads (n = 15), which could have distorted the results. Additionally, there were variations in the femoral offset, the manufacturing tolerances, and the implantation times. Similar to Nassif et al. and Triantayllopoulos et al., no information was provided with respect to the assembly force.

Although retrieval analyses do have their advantages such as identifying new problems or trends that can lead to solutions, retrieval analyses as an experimental form cannot be used to confirm which factors are truly responsible for head-neck taper corrosion of THA prostheses. Even when trying to design a retrieval analysis to minimize the number of potential variables that can influence head-neck taper corrosion, there are some factors that are unknown. In particular, retrieval analyses do not reveal any information regarding the assembly force unless if the femoral head is still attached to the stem and a pull-off test is performed in accordance to ISO 7206-10 [215].

Recently, a retrieval analysis was performed that examined the corrosion damage at the head-neck taper interface between two sets of implants: 40 mm femoral heads that articulated with polyethylene and monopolar hemiarthroplasty heads that articulated with

cartilage [274]. Additionally, the hemiarthroplasty heads were also split into two groups: heads with a diameter less than 50 mm and heads with a diameter greater than or equal to 50 mm [274]. When comparing the corrosion damage between the 40 mm heads and the hemiarthroplasty heads, there was a significant difference between the two groups ($p = 0.049$) such that the monopolar hemiarthroplasty heads displayed more corrosion damage [274]. When comparing the two head size groups of the monopolar hemiarthoplasty heads, there was a significant difference between the groups since the heads with a diameter greater than or equal to 50 mm displayed significantly more corrosion damage than the heads with a diameter less than 50 mm [274].

Table 6.1 presents an overview of the retrieval analyses that have been performed in the literature to determine whether or not head size influences head-neck taper corrosion.

Table 6.1. Summary of the literature with respect to if the femoral head size influences head-neck taper corrosion.

Author and Year	Does head size affect corrosion?	Sample Size	Sample Inclusion Criteria	Scoring Method
Dyrkacz et al. 2013 [243]	Yes	- Heads (n = 74) - 28 mm (n = 59) - 36 mm (n = 15) - Stems (n = 40) - From 28 mm heads (n = 35) - From 36 mm heads (n = 5)	- 28 and 36 mm head sizes - 12/14 mm taper - Metal on polyethylene articulation - 2 manufacturing brands - Heads and stems are all CoCr alloy - Minimum 1 month implantation time	- Dyrkacz et al. method [80] -3 scorers Note: Corrosion and fretting scores separated by manufacturing brands
Hexter et al. 2012 [261]	Yes	- Head and neck components (n = 111) Note: Did not specify how components of each	- 3 manufacturing brands - DePuy (ASR XL) - Smith & Nephew (BHR) - Zimmer (Durom)	- A five-point Goldberg modified system -1 scorer
Kurtz et al. 2013 [262]	No	- Heads (n = 144) - ≤ 28 mm (n = 56) - 32 mm (n = 43) - 36 mm (n = 36) - ≥ 38 mm (n = 9) - Stems (n = 73)	- 5 manufacturing brands - 1 year minimum implantation time	- Goldberg system [210] - 2 scorers
Langton et al. 2013 [71]	Yes	- THA prostheses (n = 111) - ASR XL (n = 63) - Articuleze (n = 48)	- 1 manufacturer - DePuy	- Coordinate measuring machine used to calculate volumetric wear
Triantafyllopoulos et al. 2014 [264]	No	- Heads (n = 154) - ≤ 26 mm (n = 26) - 28 mm (n = 46) - 32 mm (n = 52) - ≥36 mm (n = 30) - Stems (n = 154) - CoCr (n = 74) - Ti6Al4V (n = 75) - TMZF (n = 5)	- 5 taper sizes - 12/14 mm - C-Taper - V40 - Type 1 - Other - CoCr heads paired with CoCr, TigAl4V, and TMZF stems - No minimal implantation time period (implants from 0 months)	- Goldberg system [210] Note: Number of scorers not specified

Nassif et al. 2014 [263]	No	- Manufacturing brands - DePuy (n = 26) - Wright (n = 5) - Biomet (n = 8) - Zimmer (n = 1) - Taper sizes - 12/14 mm (n = 26) - Type 1 (n = 8) - 11/13 mm (n = 6) -4 head-neck taper interfaces - CoCr Head / CoCr Neck (n = 10) - CoCr Head / Ti6al4V Neck (n = 23) - Ti6Al4V Head / CoCr Neck (n = 1) - Ti6Al4V Head/ Ti6Al4V Neck (n = 6)	- 28 and 36 mm head sizes - 4 manufacturing brands - DePuy - Wright - Biomet - Zimmer - 3 taper sizes - 12/14 mm - Type 1 - 11/13 mm -4 head-neck taper interfaces - CoCr Head / CoCr Neck - CoCr Head / Ti6al4V Neck - Ti6Al4V Head / CoCr Neck - Ti6Al4V Head/ Ti6Al4V Neck	- An eight-point Goldberg modified system Note: Evaluated distal and proximal regional scores
Higgs et al. 2013 [195]	Yes	- Heads (n = 134) - Stems (n = 60) - Modular necks (n = 41) - Modular acetabular liners (n = 18) - Acetabular shells (n = 11) - Manufacturing brands - Zimmer (n = 84) - Biomet (n = 28) - DePuy (n = 20) - Wright (n = 4) - Smith & Nephew (n = 1)	- Metal on metal articulation - Implantation time: 2.9 ± 2.0 years - Range: 0 to 11.0 years - 5 manufacturing brands - Zimmer - Biomet - DePuy - Wright - Smith & Nephew	- Higgs Method [203] - 3 scorers
Panagiotidou et al. 2013 [242] Note: *In vitro* test that studied the link between torque and corrosion	Yes	- Not specified	- 12/14 mm taper - CoCr femoral heads - Ti6Al4V stems - 3 offsets to create torque - 0 mm → 9 Nm - 5.4 mm → 12 Nm - 7.5 mm → 17 Nm	- Overall current - Overall mean fretting current - Overall current change data
Noble et al. 2013 [240]	Yes	- THA prostheses (n = 13)	- 42 to 54 mm head size - Metal on metal articulation - 2 torques: 1.17 Nm and 2.23 Nm	- Measured micromotion - 1.17 Nm = 7.46 µm - 2.23 Nm = 8.38 µm
Dyrkacz et al. 2013 [274]	Yes	- Heads with metal on poly-ethylene articulation - 40 mm (n = 13) - Monopolar heads - < 50 mm monopolar heads (n = 17) - ≥ 50 mm monopolar heads (n = 6)	- 40 mm + head size - Monopolar hemiarthroplasty heads and metal-on-polyethyelene articulation - 12/14 mm taper size - 4 manufacturing brands - CoCr heads	- Dyrkacz et al. method [80] - 1 scorer

6.2 Finite Element Analysis

In the retrieval analysis that is presented in chapter 3, the use of 36 mm femoral heads instead of 28 mm femoral heads resulted in significantly more corrosion damage at the head-neck taper interface. To explain this, a hypothesis was developed such that the distance between the centre of the femoral head to the centre of the neck taper can increase with a larger head size. This increases the lever arm, which can result in a greater toggling torque at the head-neck taper interface. This toggling torque can create more micromotion at the head-neck taper interface. This increased micromotion can deteriorate the passive oxide film and make the region vulnerable to corrosion.

To test this hypothesis, finite element analysis was performed where models of the head-neck taper interface where created with a 28 mm, 36 mm, and a 44 mm femoral head. By increasing the femoral head size, more micromotion occurred at the head-neck taper interface during out of axis loading. This supports the hypothesis that a larger head size can result in a greater toggling torque at the head-neck taper interface. Additionally, the distance between the centre of the femoral head to the centre of the neck taper was increased with larger offsets. This increased the lever arm and resulted in more micromotion at the head-neck taper interface. Additionally, the head-neck taper interface was subjected to axial loading after the assembly procedure and this resulted in negligible micromotion. These findings further support the hypothesis that by increasing the distance between the centre of the femoral head to the centre of the neck taper with a larger head

size, this can result in more corrosion damage at the head-neck taper interface due to a greater toggling torque.

When examining the magnitude of the von Mises stress, the maximum stress occurred at the inferior-medial region of the head-neck taper interface. This region corresponds with the most amount of corrosion damage that was detected for the prostheses in the retrieval analysis as well as the samples from the *in vitro* corrosion fatigue test.

One of the limitations of the finite element study presented in Chapter 4 was that the bearing surface was not considered. Recently, Witt et al. discovered a relationship between wear damage along the bearing surface and the head-neck taper interface [109]. By having a frictional torque at the bearing surface, this can result in rotational micromotion at the head-neck taper interface, which can deteriorate the oxide film along the surface [275]. Presently, it is unknown how much of an effect the micromotion at the head-neck taper interface is influenced by the frictional torque at the bearing surface.

Kluess et al. recently also conducted a finite element analysis to determine if head size, neck length, and taper length affects the mechanical load and the stress at head-neck taper interface of THA prostheses using ABAQUS V. 6.11-2 [266]. Three different head sizes were modeled (32 mm, 44 mm, and 53 mm) and the taper length ranged from 11 mm to 16 mm. Kluess et al. defined the neck length as the distance between the proximal surface of the taper to the centre of rotation of the femoral head and the distances were 0 mm, 4 mm, and 8 mm. CoCr alloy was simulated for the acetabular cup and the femoral head and titanium alloy was assigned to the stem component. The models were loaded with the following forces: Fx = -400.25 N; Fy = -1,844.28 N, and Fz = -235.44 N. Meshing was performed with hexahedral elements with a global size of 1.5 mm.

As Kluess et al. increased the head size, the torque against abduction increased from 2.1 Nm for the 32 mm femoral head and up to 4.1 Nm for the 53 mm femoral head [266]. When Kluess et al. modified the neck length, the micromotion increased as the distance between the centre of the femoral head to the proximal taper surface became greater.

This study by Kluess et al. further supports the argument that by increasing the femoral head size, there is a greater torque that acts at the head-neck taper interface. By having more torque, this can result in more micromotion that can deteriorate the passive oxide film at the head-neck taper interface; thus, making the region vulnerable to corrosion. Additionally, Kluess et al. discovered that as the distance between the centre of the femoral head to the proximal taper increases, this results in more micromotion at the head-neck taper interface [266]. This is similar to the findings in the finite element analysis reported in Chapter 4. By increasing the femoral head size and/or the offset, this increases the distance between the centre of the femoral head to the centre of the neck taper. When this distance increases, this can result in more micromotion at the head-neck taper interface.

In a separate finite element analysis, Zou et al. modeled models of the head-neck taper interface with ANSYS 8.0 to determine how head diameter, taper angle, and materials affects the stress at the head-neck taper interface [276]. Zou et al. created four different head sizes (26 mm, 28 mm, 30 mm, and 32 mm), three different taper angles (5.42º, 6.03º, and 11.42º), and four different material combinations as shown in Table 6.2.

Table 6.2 Head-neck taper interface material combinations simulated by Zou et al. [276].

Combination	Head	Neck
1	CoCr	Ti6Al4V
2	Zirconia	Ti6Al4V
3	Zirconia	CoCr
4	Alumina	Ti6Al4V

When applying the forces, Zou et al. simulated a person with a mass of 75 kg when walking and there were three forces [276]:

- F1 = 907 N (applied 12º above the sagittal plane)
- F2 = 743 N (applied 12º to the frontal plane)
- F3 = 1994 N (applied 40º between the sagittal and transverse planes)

Similar to the finite element analysis that is described in Chapter 4, Zou et al. noticed that as the head diameter increased, the contact stress along the taper interface decreased due to a greater stiffness with a larger head size [276]. Zou et al. reported that when increasing the taper angle between the bore of the head and neck taper, there was a negligible difference between the 5.42º and the 6.02º tapers; however, the contact stress increased with an 11.42º taper. When examining the contact stress at the head-neck taper interface for the different material combinations, Zou et al. reported that the contact stress was greatest for a zirconia femoral head paired with a CoCr neck taper. In contrast, an alumina femoral head paired with a Ti6Al4V neck displayed the least contact stress.

6.3 Discussion of the *in vitro* Corrosion Fatigue Experiment

The purpose of the experimental work was to validate the findings from the retrieval analysis and the finite element analysis under controlled conditions. Additionally, the experimental work tested the hypothesis that the toggling torque is a key factor for head-neck taper corrosion.

During out of axis loading, the prostheses with 36 mm femoral heads displayed significantly more corrosion damage at the head-neck taper interface than the prostheses with 28 mm femoral heads. To test the hypothesis that the toggling torque was a key factor for head-neck taper corrosion, three prostheses with a 36 mm femoral head were subjected to axial fatigue loading for ten million cycles. Upon examining these samples, negligible corrosion damage took place because there was a negligible toggling torque acting at the head-neck taper interface.

To support the conclusion that the toggling torque contributes to head-neck taper corrosion, an additional set of prostheses featuring a 28 mm femoral head were tested with axial fatigue loading under the same conditions. Prior to testing, negligible corrosion damage was hypothesized due to the absence of a toggling torque. When examining the head-neck taper interface for these samples, slightly more corrosion damage was detected along the bore of the head.

When examining the finite element models, there was a substantial difference in the micromotion and maximum von Mises stress along the head-neck taper interface between the 28 mm and 36 mm head size groups when a 4000 N assembly force was applied. For all of the *in vitro* corrosion fatigue tests, a 2000 N assembly force was applied in accordance to the ASTM standard F1875-98 [129]. For a 36 mm femoral head, the micromotion during the compression phase after a 4000 N assembly force was 12.7 µm. In contrast, the micromotion during the compression phase after a 2,000 N assembly force was 27.0 µm. Finite element analysis was also performed on the conditions that were simulated for the *in vitro* corrosion fatigue tests with the 2000 N assembly force. Table 6.3 summarizes the assembly displacement, maximum von Mises stress at the head-neck taper interface, and the micromotion during the compression phase for these tests.

Table 6.3. Summary of the finite element analysis of the head-neck taper interface for the *in vitro* corrosion fatigue testing samples.

Head Size and Angle of Loading	Assembly Displacement (µm)	Max Stress Assembly Phase (MPa)	Max Stress Recovery Phase (MPa)	Max Stress Compression Phase (MPa)	Micromotion Compression Phase: Overall (µm)	Micromotion Compression Phase: Y-direction (µm)
28 mm 30° Out of Axis	30.8	47.0	31.8	56.4	15.4	13.3
28 mm Axial	30.8	47.0	31.8	68.5	27.4	27.3
36 mm 30° Out of Axis	29.1	35.7	30.9	79.6	26.2	21.6
36 mm Axial	29.1	35.7	30.9	58.9	24.2	24.2

For all of the *in vitro* corrosion fatigue tests, a 2000 N assembly force was applied to the femoral head. From what was determined in the finite element analysis and by Rehmer et al. [219], this is an insufficient force and a 4000 N assembly force is recommended. By having a 2000 N assembly force, the femoral head is not positioned properly along the neck taper and is capable of more micromotion during the compression phase. If the femoral head receives a sufficient assembly force, minimal micromotion should take place during axial loading.

In the finite element analysis that was performed in Chapter 4, a 44 mm femoral head displayed 1.8 μm of micromotion during the compression phase. According to Table 6.3, substantial micromotion (overall) occurred for the 28 mm (27.4 μm) and 36 mm femoral heads (24.2 μm) during the compression phase for the axial loaded models. When examining the micromotion for these axial loaded models in the y-direction, a clue is presented. The micromotion in the y-direction of the axial loaded 28 mm and 36 mm femoral heads is 27.3 μm and 24.2 μm. In contrast, negligible micromotion was detected along x and z-axes. This reveals that the femoral head was not properly assembled with the 2000 N assembly force.

To address the question why the 28 mm axial loaded samples yielded more corrosion damage than the out of axis loaded samples, the following hypothesis was developed. For the axial loaded samples, there was an additional 12.1 MPa of stress acting along the head-neck taper interface. This stress may have made it more challenging for the head-neck taper interface to repassivate the oxide film in comparison to the out of axis loaded samples; thus, more corrosion took place.

One of the limitations of the finite element analysis is that a single phase of compression loading was applied. In contrast, the samples during the *in vitro* corrosion fatigue testing underwent ten million cycles of loading with a force ranging from 300 to 3300 N. During axial loading, the samples would have eventually become secured onto the neck taper. It is hypothesized that decreased micromotion for each cycle of loading would have taken place at the head-neck taper interface over time for the axial loaded samples. Additionally, there would have been a greater reduction in the micromotion for the 36 mm femoral heads that underwent axial loading in comparison to the 28 mm femoral heads. By having a substantial reduction in micromotion during axial loading for the 36 mm head samples, this resulted in significantly less corrosion damage at the head-neck taper interface in comparison to the samples that were subjected to an out of axis load.

6.4 Corrosion Scoring Techniques

There are presently a few different techniques for scoring corrosion and fretting damage. In the literature, the most commonly accepted method is the Goldberg scoring system [177] and there are different variations of this in the literature [234, 261, 263]. In this thesis, a novel scoring method was created [243] such that the head and neck tapers were separated into four quadrants and each quadrant was separated by a superior and inferior region; thus, producing eight regions for each taper. Most corrosion and fretting scores, following the Goldberg scoring system, put an emphasis on the severity of the

corrosion and fretting damage and assign a single score for the entire taper. Let's consider the following question: is it beneficial to separate each taper into eight regions to analyze corrosion and fretting damage? In the *in vitro* corrosion fatigue tests, the corrosion and fretting scores were separated by the superior (proximal) and inferior (distal) regions. Table 6.4 provides the corrosion scores based on the superior and inferior regions whereas Table 6.5 contains the fretting scores of the superior and inferior regions.

Table 6.4. The corrosion scores of the head-neck taper interface separated by the superior and inferior regions from the *in vitro* corrosion fatigue testing experiment.

Head Size and Angle of Loading	Neck Corrosion Superior	Neck Corrosion Inferior	Head Corrosion Superior	Head Corrosion Inferior
28 mm Out of Axis	3.00 ± 1.87	1.67 ± 2.00	5.67 ± 2.69	2.78 ± 2.86
36 mm Out of Axis	6.67 ± 3.77	16.44 ± 6.77	5.44 ± 3.47	21.22 ± 9.91
28 mm Axial	2.22 ± 2.33	2.33 ± 1.73	6.67 ± 0.87	5.78 ± 1.99
36 mm Axial	0.78 ± 0.84	4.89 ± 2.87	1.67 ± 0.67	7.33 ± 1.64

Table 6.5. The fretting scores of the head-neck taper interface separated by the superior and inferior regions from the *in vitro* corrosion fatigue testing experiment.

Head Size and Angle of Loading	Neck Fretting Superior	Neck Fretting Inferior	Head Fretting Superior	Head Fretting Inferior
28 mm Out of Axis	1.33 ± 1.22	2.22 ± 3.42	2.78 ± 1.79	2.44 ± 2.13
36 mm Out of Axis	2.33 ± 2.60	6.22 ± 1.30	2.00 ± 2.00	9.67 ± 3.04
28 mm Axial	0.44 ± 1.33	1.22 ± 0.97	5.22 ± 2.64	5.56 ± 2.19
36 mm Axial	0.33 ± 0.33	5.00 ± 1.00	0.11 ± 0.19	2.78 ± 0.51

When analyzing the 36 mm samples that were subjected to out of axis loading, corrosion and fretting damage primarily took place along the inferior portion of the head and neck tapers. Significantly more corrosion damage was detected on the inferior regions of the neck tapers ($p = 0.020$) and the head tapers ($p < 0.001$). Similarly, there was a significant difference in the fretting damage between the superior and inferior regions for the neck tapers ($p = 0.001$) and the head tapers ($p < 0.001$). Although there were no significant differences, the medial side of the head-neck taper interface displayed more corrosion and fretting damage than the lateral side. The most likely reason why significant differences for corrosion and fretting were not detected between the medial and lateral sides is attributed to the low sample size. By having a greater sample size, there most likely would have been significant differences confirming that the medial side has statistically more corrosion and fretting damage than the lateral side.

Additionally, the prostheses from the retrieval analysis were examined to determine if more corrosion or fretting damage occurs along the superior or inferior regions. The scores for corrosion and fretting damage based on the superior and inferior regions can be found on Tables 6.6 and 6.7, respectively.

Table 6.6. Corrosion scores of the head and neck tapers from the retrieval analysis separated by the superior and inferior regions.

Head Size	Neck Corrosion Superior Region	Neck Corrosion Inferior Region	Head Corrosion Superior Region	Head Corrosion Inferior Region
28 mm	1.94 ± 3.16	2.41 ± 2.75	3.14 ± 5.24	3.60 ± 5.54
36 mm	2.20 ± 3.15	2.88 ± 3.14	5.73 ± 7.52	7.40 ± 7.32

Table 6.7. Fretting scores of the head and neck tapers from the retrieval analysis separated by the superior and inferior regions.

Head Size	Neck Fretting Superior Region	Neck Fretting Inferior Region	Head Fretting Superior Region	Head Fretting Inferior Region
28 mm	0.93 ± 1.93	1.99 ± 2.09	1.19 ± 2.42	1.57 ± 4.37
36 mm	0.53 ± 1.02	2.53 ± 3.92	1.67 ± 3.94	2.71 ± 5.35

When observing the data from Tables 6.6 and 6.7, the inferior region of the head and neck components displays more corrosion and fretting damage; however, the only significant difference was found for neck fretting damage for the 28 mm head group ($p < 0.001$).

Table 6.8. Corrosion scores of the head and neck tapers from the retrieval analysis separated by the opposing quadrants.

Head Size	Neck Corrosion Quadrant 1	Neck Corrosion Quadrant 2	Head Corrosion Quadrant 1	Head Corrosion Quadrant 2
28 mm	1.65 ± 2.44	0.77 ± 1.24	1.90 ± 2.16	1.35 ± 2.14
36 mm	2.27 ± 1.79	0.80 ± 1.45	1.67 ± 2.33	1.33 ± 1.67

Table 6.9. Fretting scores of the head and neck tapers from the retrieval analysis separated by the opposing quadrants.

Head Size	Neck Fretting Quadrant 1	Neck Fretting Quadrant 2	Head Fretting Quadrant 1	Head Fretting Quadrant 2
28 mm	1.15 ± 1.58	0.44 ± 0.72	0.83 ± 1.66	0.63 ± 1.50
36 mm	1.00 ± 0.82	0.73 ± 1.16	1.33 ± 2.49	1.04 ± 2.02

Tables 6.8 and 6.9 attempt to answer the question if there is a difference in the corrosion and fretting scores between the medial and lateral sides for the retrieved im-

plants. Due to the unknown orientation for some of the implants, the lateral and medial regions could not be identified. Instead, the corrosion and fretting scores were compared in the opposing quadrants. When considering the implants as a whole, the Mann-Whitney U test was performed since all of the corrosion and fretting scores for the head and neck tapers were not normally distributed. Consequently, significant differences were found for neck corrosion ($p = 0.002$), head corrosion ($p = 0.007$), neck fretting ($p = 0.001$), and head fretting ($p = 0.044$). This data demonstrates that corrosion and fretting damage is not uniform along the head and neck tapers; however, it is speculated that the medial region was the most vulnerable region for corrosion and fretting damage based on the findings from the finite element analysis and the *in vitro* corrosion fatigue tests.

Upon examining the head and neck tapers from the *in vitro* corrosion fatigue experiment and the retrieval analysis, the inferior-medial region of the head-neck taper interface is most vulnerable to corrosion and fretting damage. This further supports the research by Munir et al. [47] and the finite element analysis performed in Chapter 4 such that the maximum von Mises stress takes place along the bottom quarter of the head-neck taper interface. By separating the head and neck tapers into eight regions, this strategy helped identify that the inferior-medial region of head-neck taper interface is most susceptible to corrosion and fretting damage. The Dyrkacz technique has an advantage in comparison to the Goldberg scoring system since the observers can quantitatively identify which regions show corrosion and fretting damage and statistically determine if one region displays significantly more corrosion or fretting damage.

Chapter 7 – Conclusion

7.1 Summary of Conclusions

The aim of this thesis was to determine if the size of the femoral head can influence corrosion and fretting damage at the head-neck taper interface of THA prostheses. To answer this question, a retrieval analysis, a finite element analysis, and an *in vitro* corrosion fatigue experiment were performed. The following is a summary of the findings from each of these investigations.

Retrieval Analysis

The objective of the retrieval analysis was to determine if there was a relationship between head size and corrosion damage at the head-neck taper interface. The following conclusions were revealed in the retrieval analysis:

- THA prostheses with a 36 mm femoral head display more corrosion damage at the head-neck taper interface in comparison to THA prostheses with a 28 mm femoral head. The hypothesis was that large femoral heads can have a greater

toggling torque at the head-neck taper interface because the distance between the centre of the femoral head to the centre of the neck taper can increase with a larger head size. As this distance becomes greater, this increases the lever arm and can result in a greater toggling torque at the head-neck taper interface. This toggling torque can result in more micromotion that can deteriorate the passive oxide film along the head-neck taper interface; thus, making the taper interface vulnerable to corrosion.

- The retrieval analysis compared the corrosion and fretting scores at the head-neck taper interface of the implants from two different companies. There was a considerable difference in the corrosion and fretting scores between these two companies, particularly corrosion damage along the bore of the femoral head. This can be attributed to differences in fabrication, passivation, tolerance designs, and the surface finish.
- There was a relationship between the heads and necks for fretting damage that could have been caused by the micromotion between the two surfaces.
- A relationship between corrosion and fretting damage was discovered for the head and neck tapers.

Finite Element Analysis

The purpose of the finite element analysis was to determine which factors influence the micromotion at the head-neck taper interface of THA prostheses. Micromotion at this interface can deteriorate the passive oxide film and make the taper region susceptible to corrosion. The following conclusions were arrived from the finite element analysis:

- By increasing the diameter of the femoral head, the micromotion at the head-neck taper interface becomes greater. This can increase the distance between the centre of the femoral head to the centre of the neck taper, which can increase the toggling torque.
- As the diameter of the femoral head became larger, the assembly displacement and the maximum von Mises stress at the head-neck taper interface were both reduced. To account for this, the femoral head's stiffness increases with a larger head size.
- By placing the centre of the femoral head in a more superior position relative to the centre of the neck taper, this will result in more micromotion at the head-neck taper interface. In contrast, the micromotion can be reduced if the centre of the femoral head is positioned near or below the centre of the neck taper.
- CoCr femoral heads that are assembled onto Ti6Al4V neck tapers have a greater assembly displacement and more micromotion at the head-neck taper interface in

comparison to a femoral head and neck taper consisting of CoCr. This can be attributed to the difference in the modulus of elasticity between CoCr and Ti6Al4V.

- By increasing the axial assembly force, this will increase the assembly displacement of the femoral head and reduce the micromotion during compression loading. Although large assembly forces are theoretically recommended, in practice surgeons should apply an assembly force that is safe for the patient.
- By increasing the taper size, this can reduce the micromotion at the head-neck taper interface that is attributed to an increased contact area. With a greater contact area, this increases the frictional forces and will minimize the amount of micromotion occurring. Although a 14/16 mm taper is theoretically recommended in comparison to a 10/12 mm or a 12/14 mm taper, the 14/16 mm taper can increase the risk of dislocation.
- By applying out of axis loading, this can result in more micromotion at the head-neck taper interface in comparison to axial loading. This finding supports the hypothesis that was developed in the retrieval analysis study that the toggling torque is a key factor for corrosion and fretting damage at the head-neck taper interface.

In vitro Corrosion Fatigue Experiment

The goal of the *in vitro* corrosion fatigue experiment was to verify that the use of 36 mm femoral heads can lead to more corrosion and fretting damage at the head-neck

taper interface than 28 mm femoral heads in a controlled environment. The following conclusions were revealed:

- THA prostheses with a 36 mm femoral head have significantly more head corrosion, neck corrosion, head fretting, and neck fretting damage than 28 mm femoral heads during out of axis loading. This is supported by the corrosion and fretting scores using the Dyrkacz technique, analyzing the volumetric wear, scanning electron microscopy, and electron dispersive x-ray spectroscopy. This conclusion verifies the findings from the retrieval analysis and the finite element analysis.
- When comparing the axial and out of axis loaded 36 mm femoral head groups, there was significantly less head corrosion, neck corrosion, head fretting, and neck fretting damage for the axial loaded samples. Due to the absence of a toggling torque, very little micromotion took place at the head-neck taper interface; thus, leaving the passive oxide film intact. This finding verifies the hypothesis that the toggling torque is largely responsible for head-neck taper corrosion of THA prostheses.
- When examining the samples featuring a 28 mm femoral head, the axial loaded samples displayed slightly more corrosion damage at the head-neck taper interface in comparison to the out of axis loaded samples. This may have been partially attributed to the 2000 N assembly force since the femoral head was not properly assembled onto the neck taper. Additionally, it is hypothesized that there was a

greater reduction in the micromotion for the 36 mm heads in comparison to the 28 mm heads during axial loading.

In summary, this thesis has arrived at the conclusion that head size influences corrosion and fretting damage at the head-neck taper interface. By increasing the head size, this can increase the distance between the centre of the femoral head to the centre of the neck taper. This results in a larger lever arm which can result in more micromotion at the head-neck taper interface due to a greater toggling torque. This increased micromotion can deteriorate the passive oxide film and make the head-neck taper interface more vulnerable to corrosion damage at the head-neck taper interface, particularly at the inferior-medial region.

7.2 Novelty of the Research

The novelty of this thesis is to demonstrate that the use of large femoral heads (36 mm+) for THA prostheses can result in significantly more corrosion damage at the head-neck taper interface. This was first demonstrated in a retrieval analysis that compared THA prostheses with 28 mm and 36 mm femoral heads. From this investigation, the prostheses with a 36 mm femoral head displayed significantly more corrosion damage. A hypothesis was created such that the use of a large femoral head size can increase the distance between the centre of the femoral head to the centre of the neck taper. This can lead

to an increase in the micromotion at the head-neck taper interface due to a greater toggling torque. Micromotion at the head-neck taper interface can deteriorate the passive oxide film and make the region more vulnerable to corrosion. For the prostheses in the retrieval analysis, significant corrosion and fretting damage was detected on the inferior portion of the head-neck taper interface.

Afterwards, a finite element analysis study was conducted. This investigated further supported the argument that by increasing the distance between the centre of the femoral head to the centre of the neck taper with a larger head size, this can increase the micromotion at the head-neck taper interface due to a greater toggling torque. During the out of axis loading simulations, the maximum von Mises stress at the head-neck taper interface was detected along the inferior-medial region of the taper connection. This study also demonstrated that negligible micromotion took place at the head-neck taper interface during axial loading due to the absence of a toggling torque. Additionally, the finite element analysis revealed that the micromotion at the head-neck taper interface can be reduced by implementing the following strategies:

- Assembling a femoral head and neck consisting solely of CoCr instead of assembling a CoCr femoral head to a Ti6Al4V neck.
- Increasing the axial assembly force.
- Using a larger taper size.
- Modifying the femoral offset such that the centre of the femoral head is near or below the centre of the neck taper.

Finally, the *in vitro* corrosion fatigue experiment verified that the use of 36 mm femoral heads can result in significantly more corrosion and fretting damage at the head-neck taper interface, particularly along the inferior-medial region, in comparison to the prostheses featuring a 28 mm femoral head. Additionally, the axial loaded samples with a 36 mm femoral head displayed minimal corrosion and fretting damage. This validates the hypothesis that the toggling torque is a key factor for corrosion and fretting damage at the head-neck taper interface of THA prostheses.

7.3 Recommendations for Future Work

This thesis addresses that the size of the femoral head can have an influence on the corrosion damage at the head-neck taper interface. Although head size is a single factor that can influence head-neck taper corrosion, many other factors can come into play. The purpose of this section is to recommend some additional research that can be performed to minimize head-neck taper corrosion of THA prostheses.

This thesis demonstrates that when a CoCr femoral head is assembled onto a CoCr neck, there will be more corrosion damage at the head-neck taper interface with a larger head size. One potential solution to head-neck taper corrosion is using ceramic femoral heads since ceramics do not corrode; however, it is unknown if the use of large ceramic femoral heads can result in increased neck taper corrosion. To answer this ques-

tion, *in vitro* corrosion fatigue testing following ASTM F1875-98 [129] could be performed.

In practice, it is common to implant a THA prosthesis with a CoCr femoral head and a titanium alloy stem. Many researchers have reported that galvanic corrosion primarily takes place despite the small potential difference between the two alloys. In the finite element analysis of this thesis, a CoCr femoral head assembled onto a titanium alloy neck displayed significantly more micromotion at the head-neck taper interface regardless of the head size. From this research, it was hypothesized that this increased micromotion was due to the difference in the modulus of elasticity between the two alloys. This could result in more corrosion damage at the head-neck taper interface. To test this hypothesis, *in vitro* corrosion fatigue testing of CoCr femoral heads onto Ti6Al4V necks should be performed while following using the ASTM F1875-98 standard. To determine if the micromotion is responsible for the head-neck taper corrosion for the mixed alloys, it is recommended to assemble CoCr femoral heads onto Ti6Al4V necks and to place them inside beakers with phosphate buffered saline. One set of these prostheses would undergo fatigue testing according to ASTM F1875-98 while another set would remain stationary in the phosphate buffered saline. By doing this experiment, this will determine if the micromotion or a combination of the potential difference and the micromotion between the two alloys is responsible for head-neck taper corrosion.

One method of preventing head-neck taper corrosion is the implementation of surface coatings and ion implantation techniques. Recently, Dorn et al. demonstrated that by coating CoCr with tantalum, this can prevent head-neck taper corrosion damage [237]. Similarly, Traynor et al. coated the taper interface with chromium nitride, which signifi-

cantly reduced corrosion damage [239]. Additionally, Maurer et al. demonstrated that plasma ion nitriding Ti6Al4V can reduce corrosion and fretting damage [238]. Further experimental research should be carried out with these techniques while following the ASTM F1875-98 guidelines [129] to determine if these techniques can effectively prevent head-neck taper corrosion damage. Additionally, corrosion damage is a problem when a CoCr femoral head is assembled onto a Ti6Al4V neck. One potential research project is to perform experimental testing with a CoCr femoral head with a tantalum or a chromium nitride coating at the taper interface and assemble it with a Ti6Al4V stem that underwent plasma ion nitriding. By performing *in vitro* corrosion fatigue testing following ASTM F1875-98 [129], this can demonstrate if the coatings and plasma ion nitriding techniques can effectively prevent head-neck taper corrosion.

As described in Chapter 4, large taper sizes and small femoral offsets can reduce the micromotion at the head-neck taper interface; thus, potentially minimizing the corrosion damage. To verify these conclusions, experimental testing following the ASTM F1875-98 protocol [129] is recommended.

This thesis did not explore if tolerances, as well as bottom-locking or top-locking taper connections, can influence micromotion, fretting, or corrosion at the head-neck taper interface. For future investigations, finite element analysis should be performed to determine if the tolerances and the different locking mechanisms can have an influence on the micromotion at the head-neck taper interface. Afterwards, *in vitro* corrosion fatigue testing could be performed to verify if the tolerances and the different locking mechanisms influence head-neck taper corrosion.

In the finite element analysis that was performed in Chapter 4, there was a trend that by increasing the axial assembly force, this can reduce the micromotion at the head-neck taper interface. By increasing the axial assembly force, this could theoretically reduce corrosion at the head-neck taper interface. To verify this conclusion, it is recommended that experimental testing is performed following the ASTM F1875-98 guidelines [129]. By assembling femoral heads onto neck tapers with a range of forces, the optimal assembly force to prevent head-neck taper corrosion can be determined. By determining this optimal assembly force, this knowledge will be helpful to surgeons and for scientists who wish to perform *in vitro* corrosion fatigue testing.

In practice, the assembly force can vary from surgeon to surgeon. One potential design that could be created is a device that the surgeon can use to deliver the appropriate force to the femoral head that is programmable and accurate. For instance, if a surgeon wants to strike the femoral head with a force of 4000 N, he or she could enter this value into the device and it would strike the femoral head with 4000 N of force. With this invention, the surgeon can safely apply the appropriate assembly load to minimize fracturing the patient's bone as well as securing the femoral head onto the neck taper.

One current problem with THA prostheses is that there are currently no standards for the head-neck taper interface even though the "gold standard" is the 5°43'30" taper [44, 45]. Currently, there are over 30 different designs for the head-neck taper interface as there are variations in the proximal and distal diameters, taper lengths, angles, manufacturing tolerances, surfaces finishes, and the surface treatments [46]. Research should be performed to standardize the head-neck taper interface to effectively reduce wear and corrosion damage.

Recently, Goyal et al. published an article regarding whether or not to remove an implanted femoral stem if the neck segment has taper corrosion [176]. If the stem were to remain implanted, the corrosion products on the neck may lead to ALTR and/or increase the likelihood of corrosion damage on the new femoral head [176]. But if the stem were to be removed, this can lead to patient morbidity such as soft tissue damage, femoral fracture, and the inability to achieve fixation [176]. Presently, there are no standard operating procedures regarding whether or not to remove the implanted stem if the neck segment has severe corrosion damage [176]. Researchers and surgeons should collaborate together to create a set of standards regarding when the stem should be removed based on the severity and area of fretting and corrosion damage along the neck taper.

Appendix A

Appendix A contains all of the schematic computer-aided-design drawings of the femoral heads and neck tapers used for the finite element analysis that is described in Chapter 4.

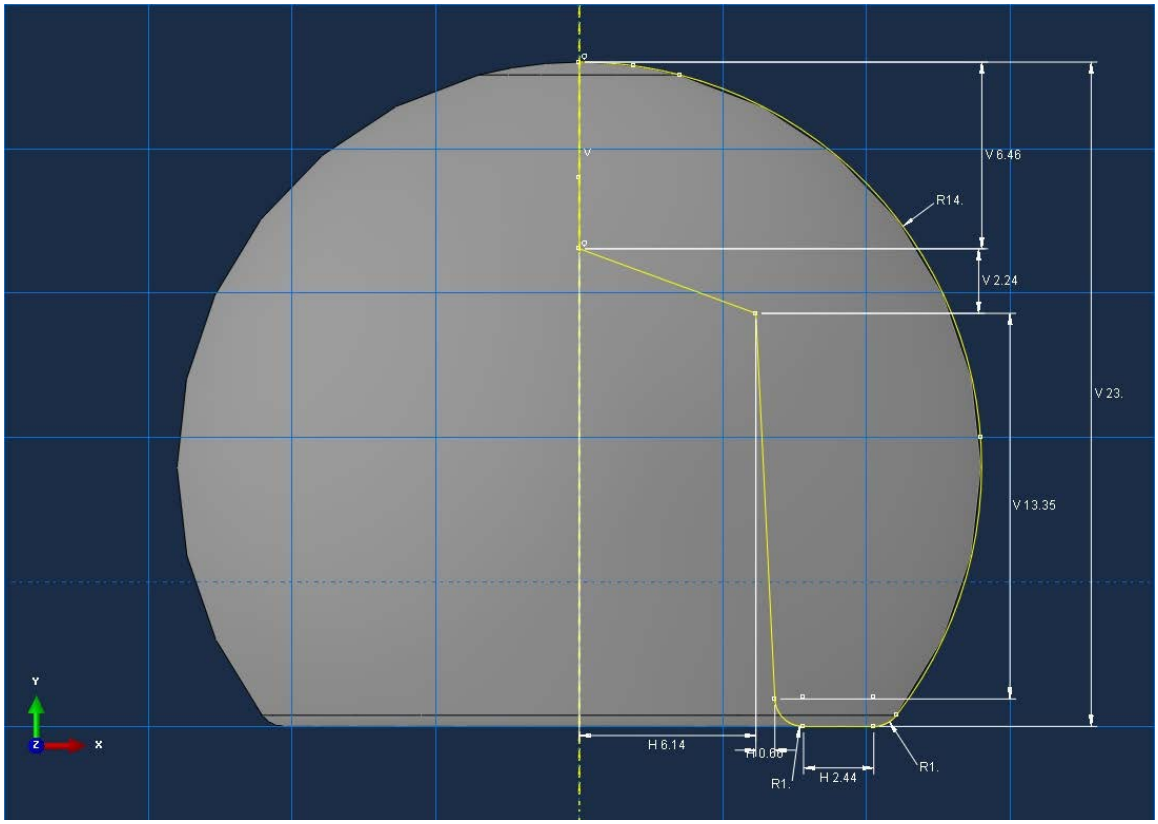

Figure A1. The 28 mm femoral head.

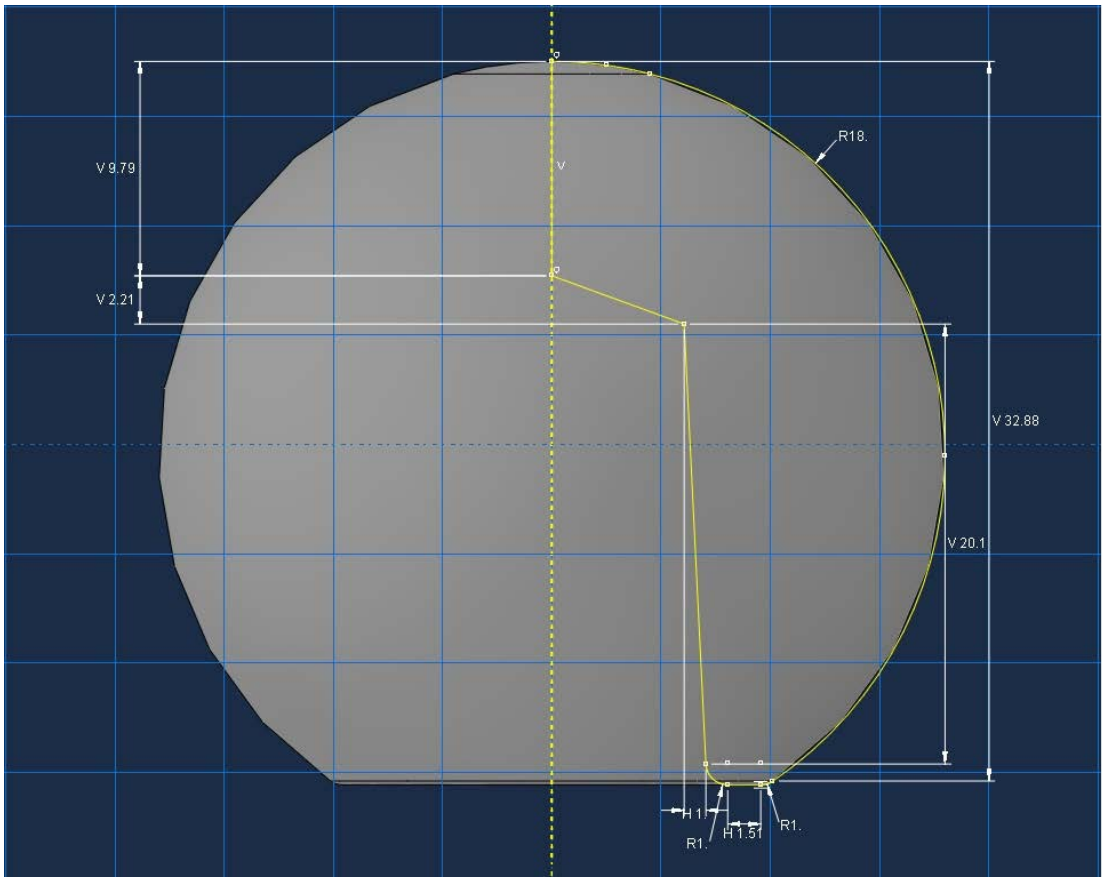

Figure A2. The 36 mm femoral head.

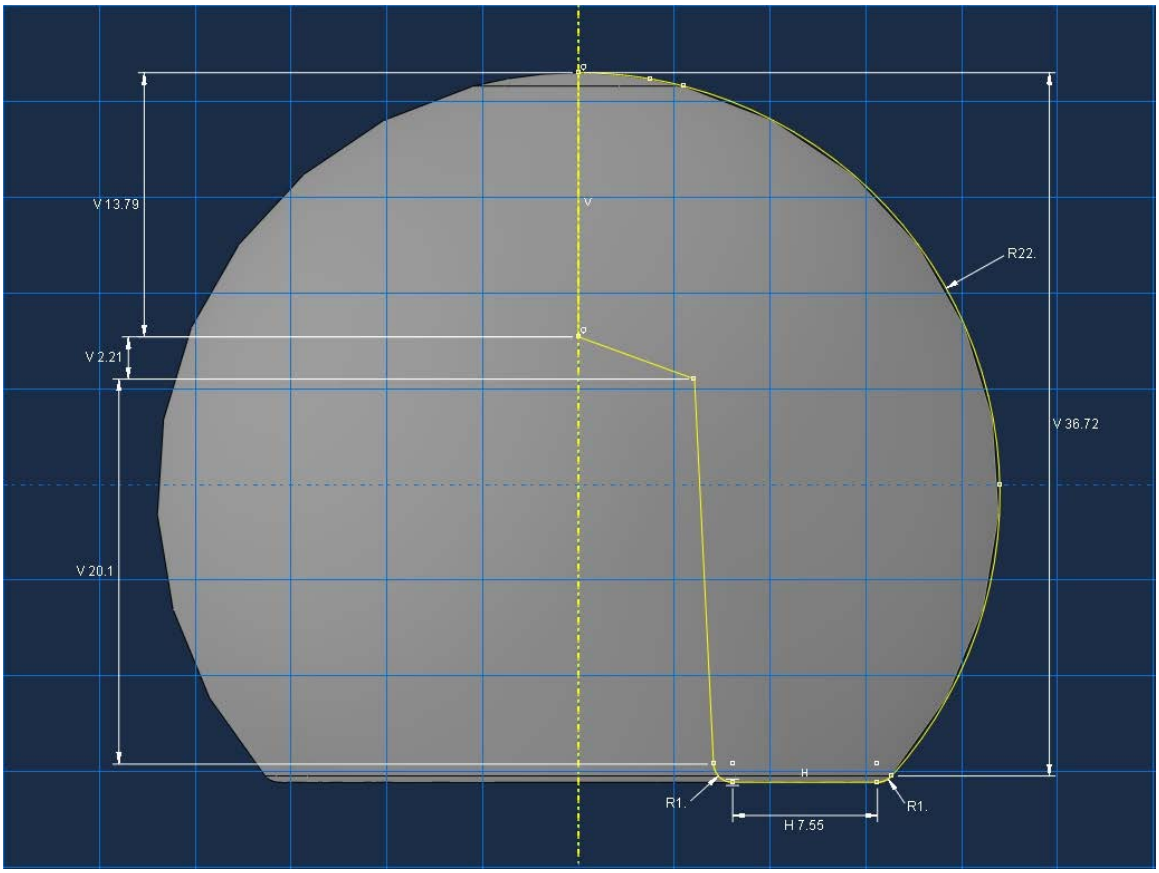

Figure A3. The 44 mm femoral head.

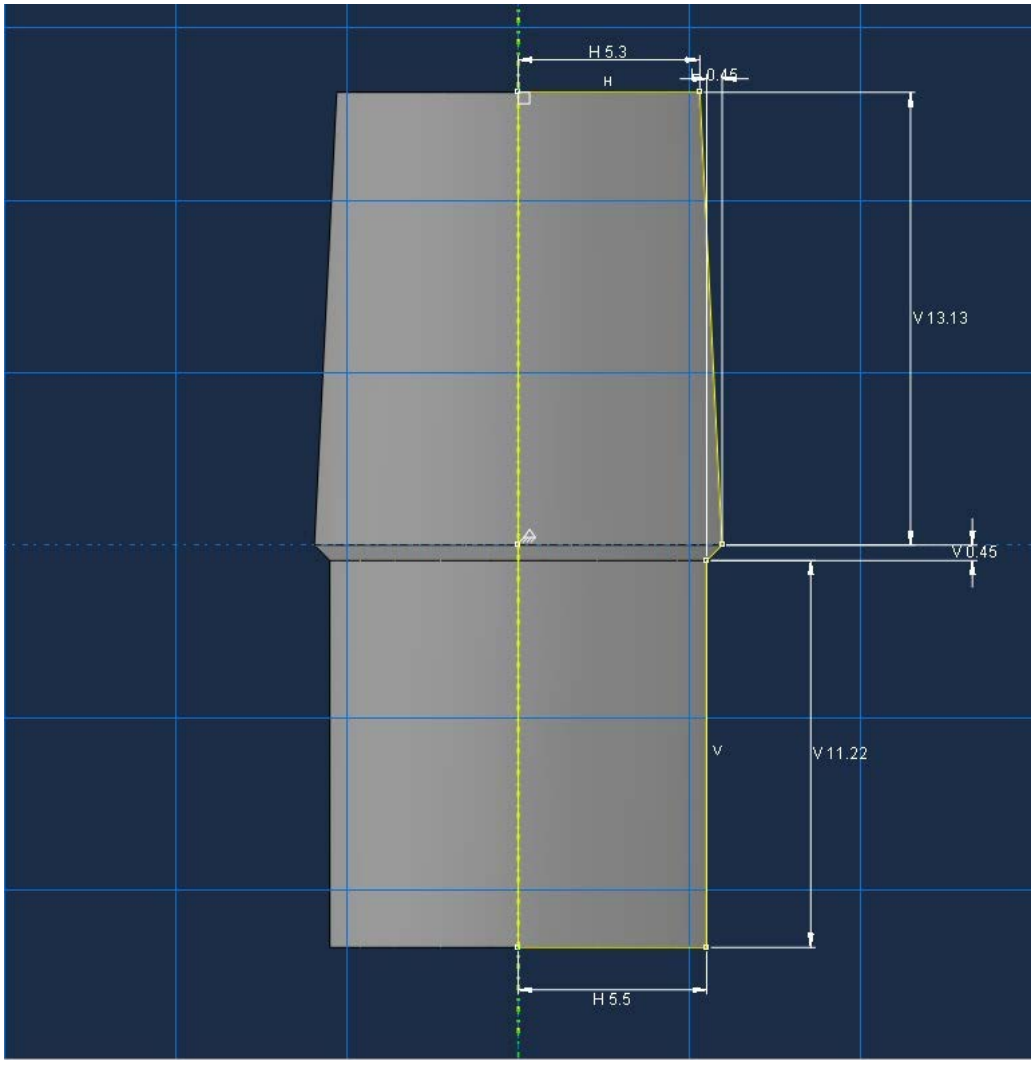

Figure A4. The 10/12 mm neck taper.

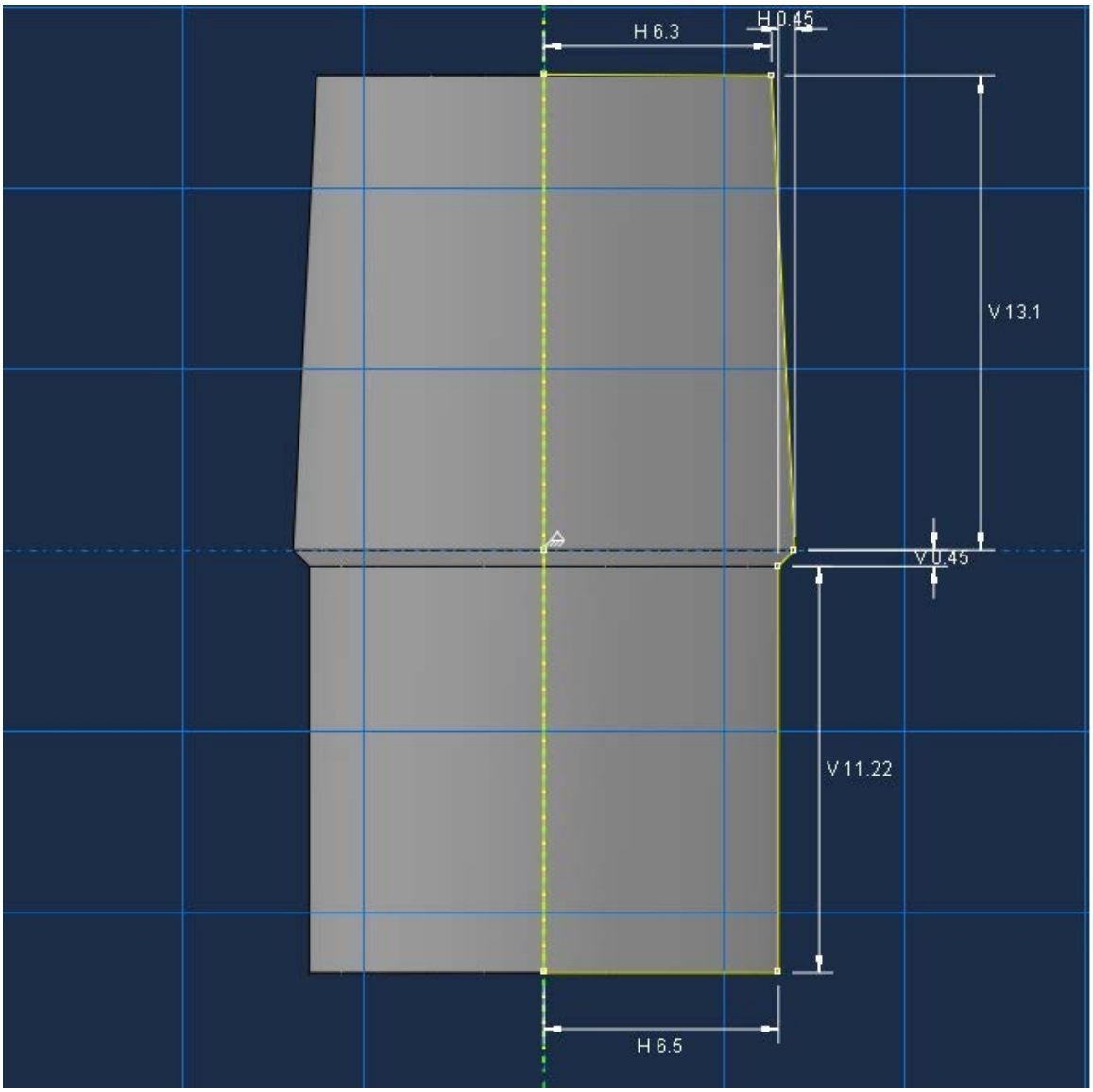

Figure A5. The 12/14 mm neck taper.

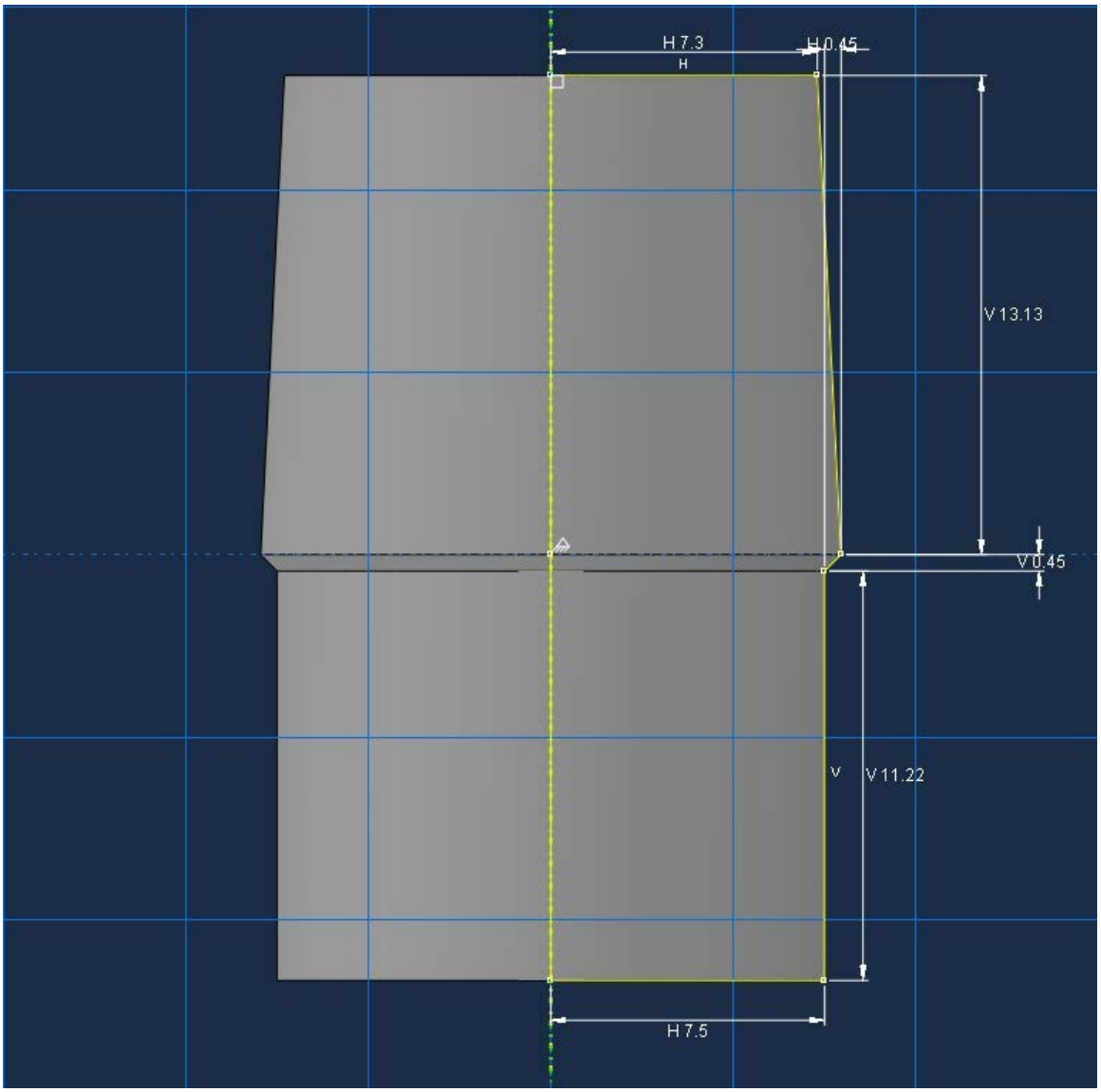

Figure A6. The 14/16 mm neck taper.

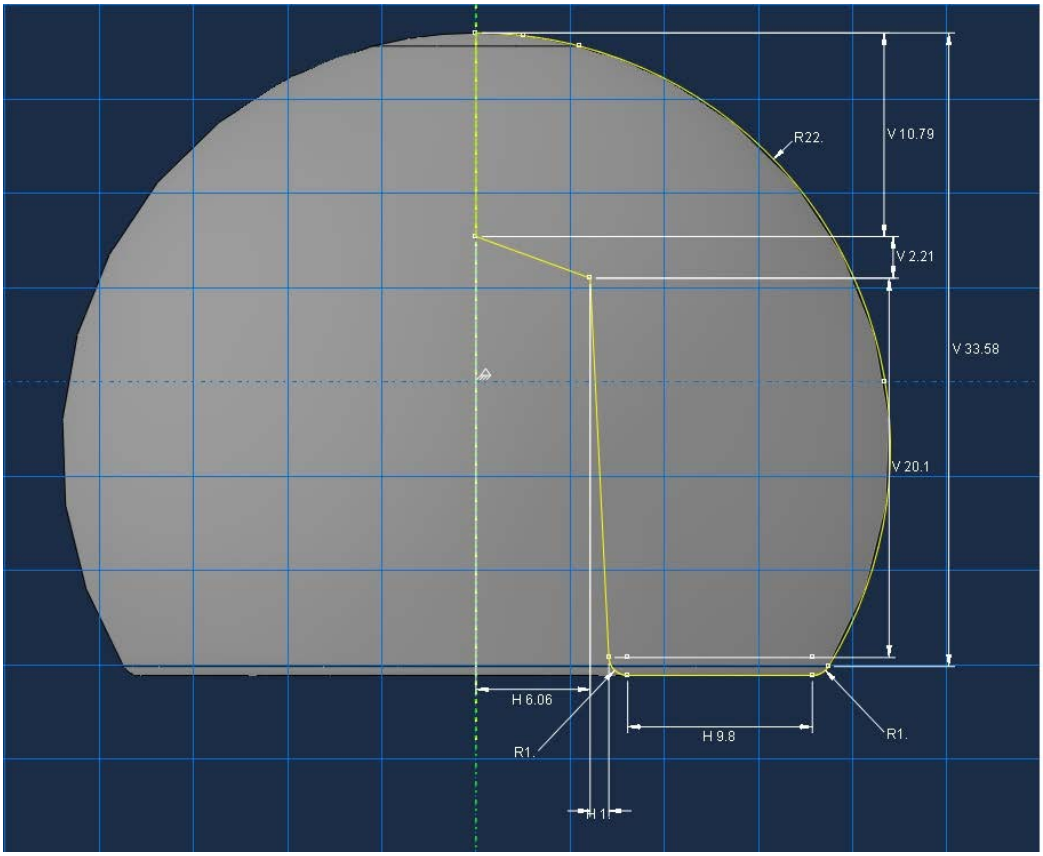

Figure A7. The 44 mm femoral head (the femoral head is 3 mm below the centre of the neck taper).

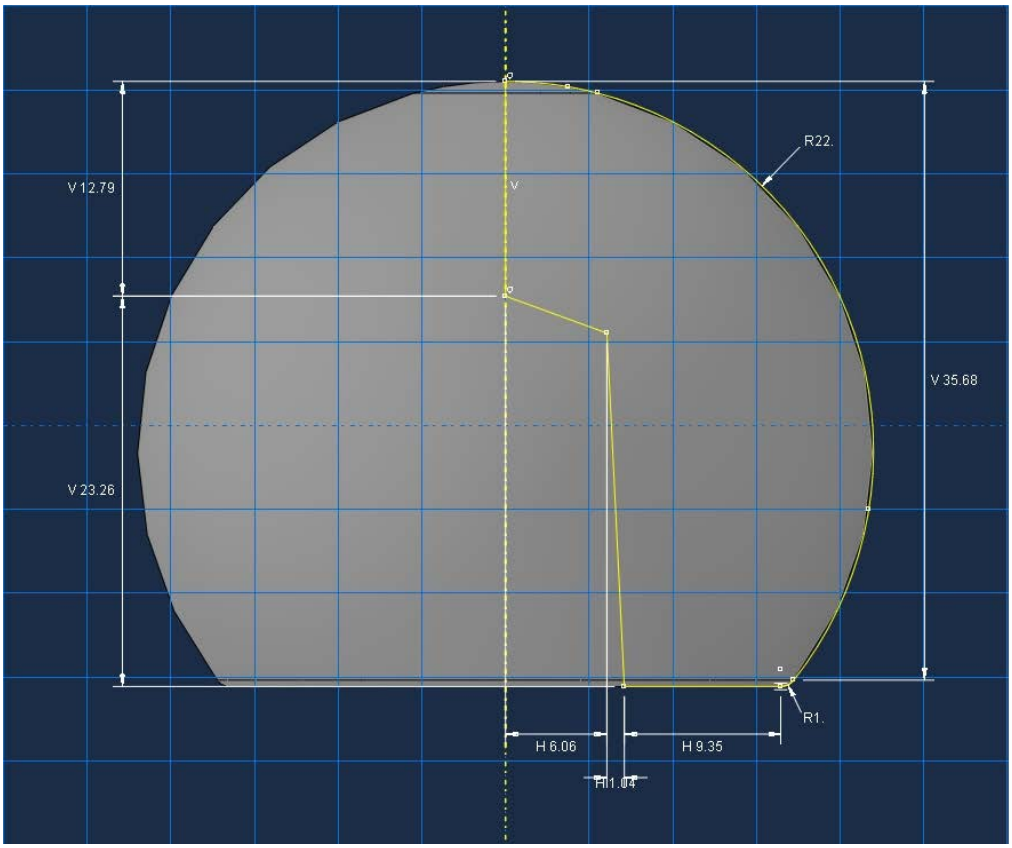

Figure A8. The 44 mm femoral head (the femoral head is 1 mm below the centre of the neck taper).

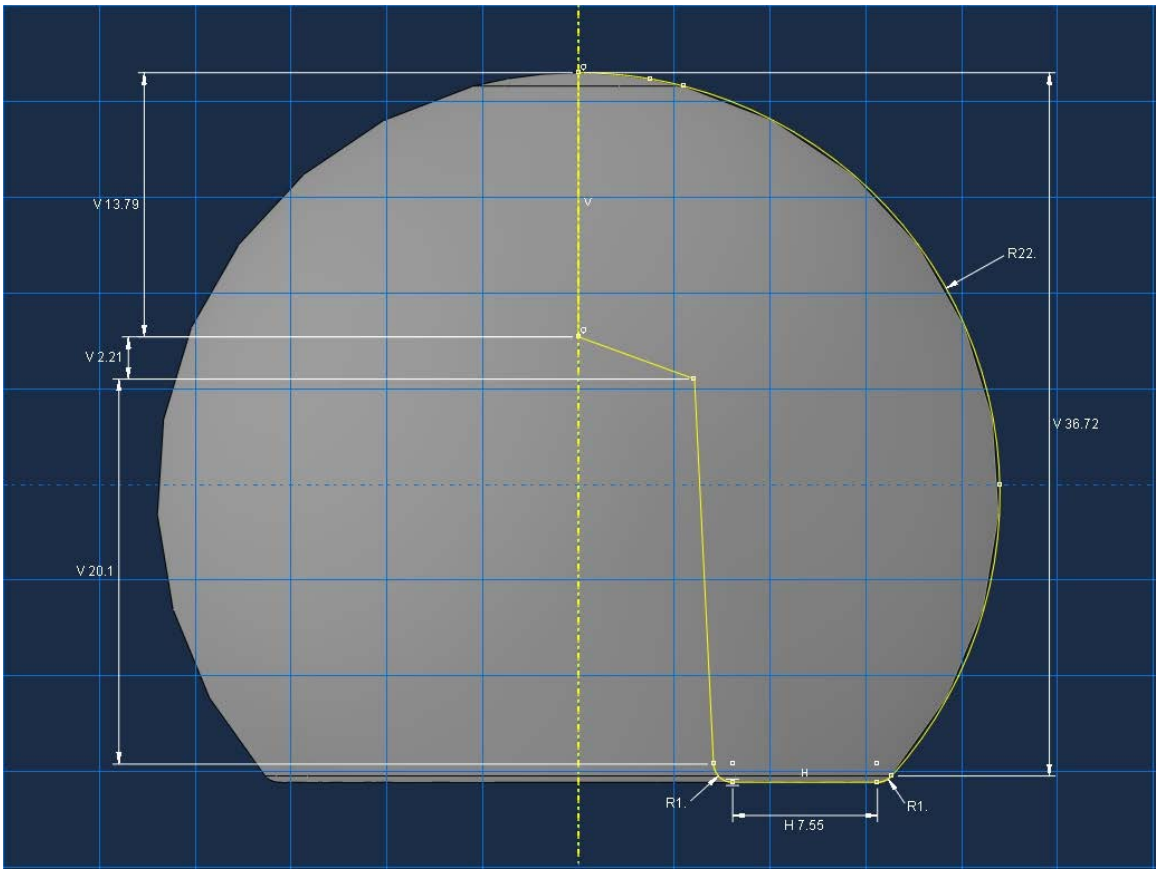

Figure A9. The 44 mm femoral head (the centre of the femoral head is aligned with the centre of the neck taper).

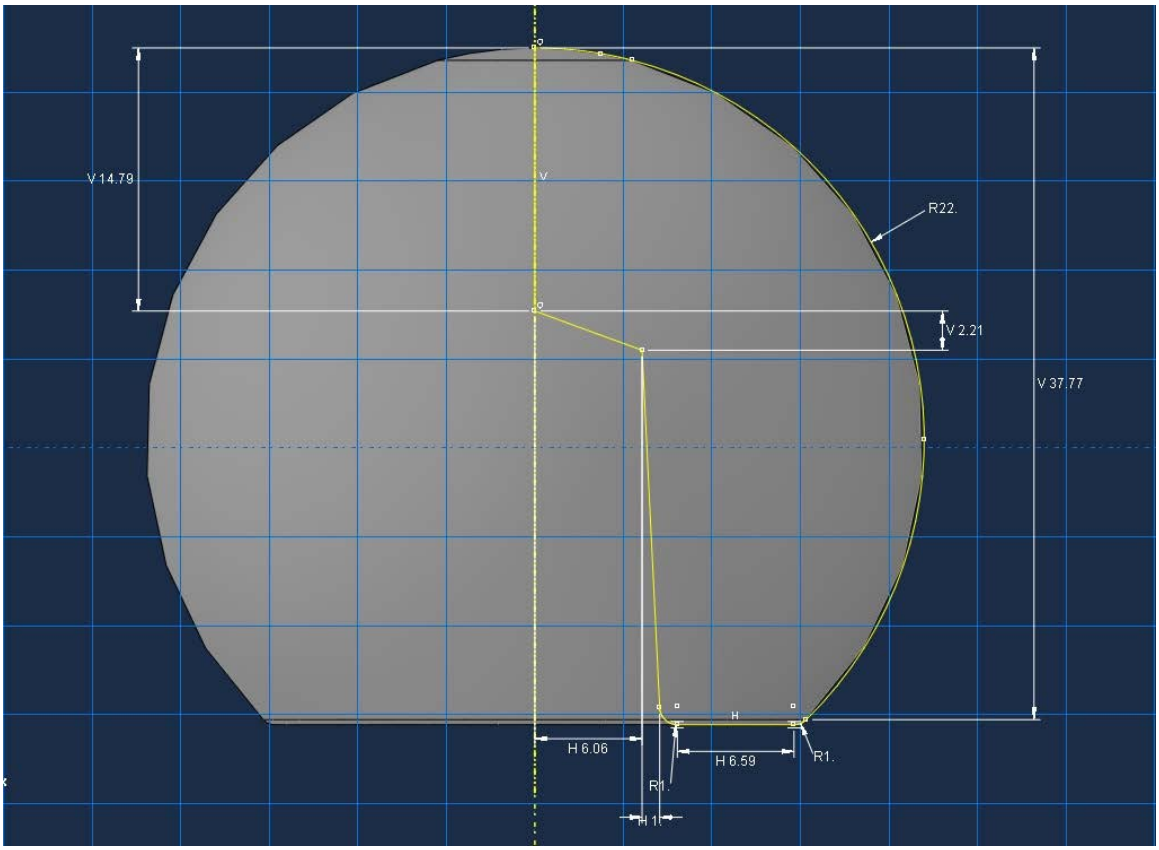

Figure A10. The 44 mm femoral head (the femoral head is 1 mm above the centre of the neck taper).

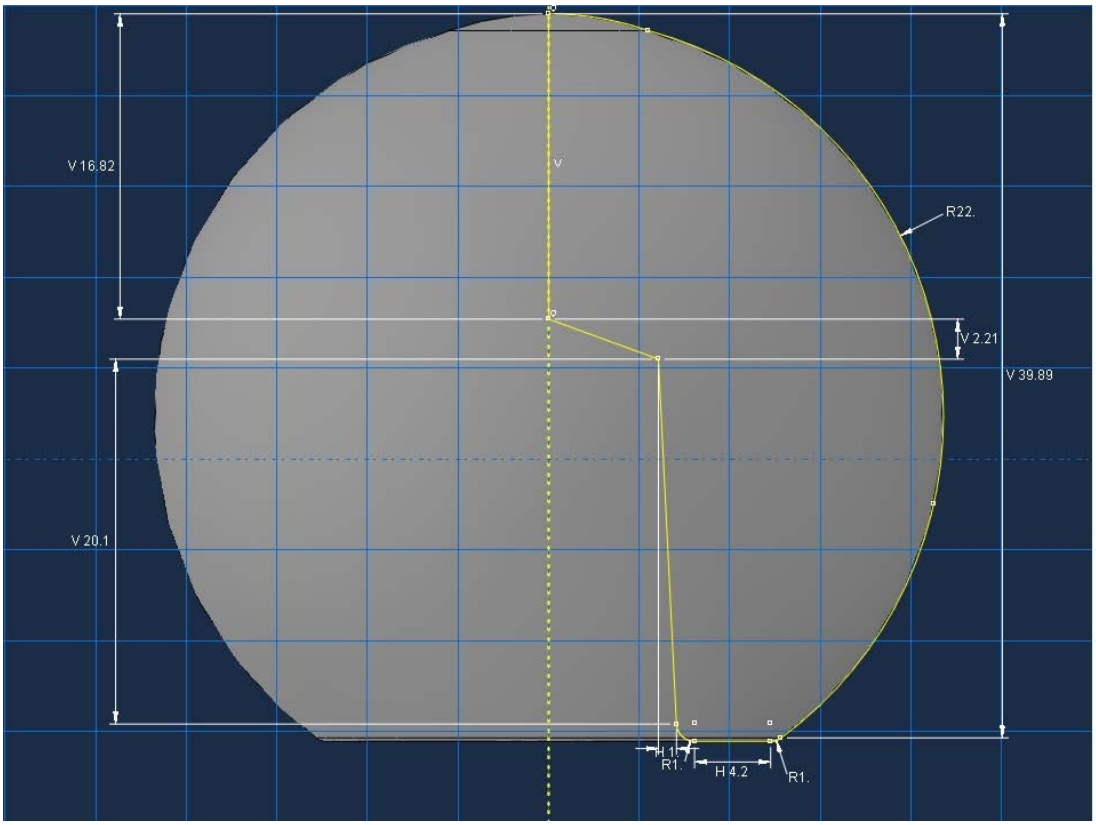

Figure A11. The 44 mm femoral head (the femoral head is 3 mm above the centre of the neck taper).

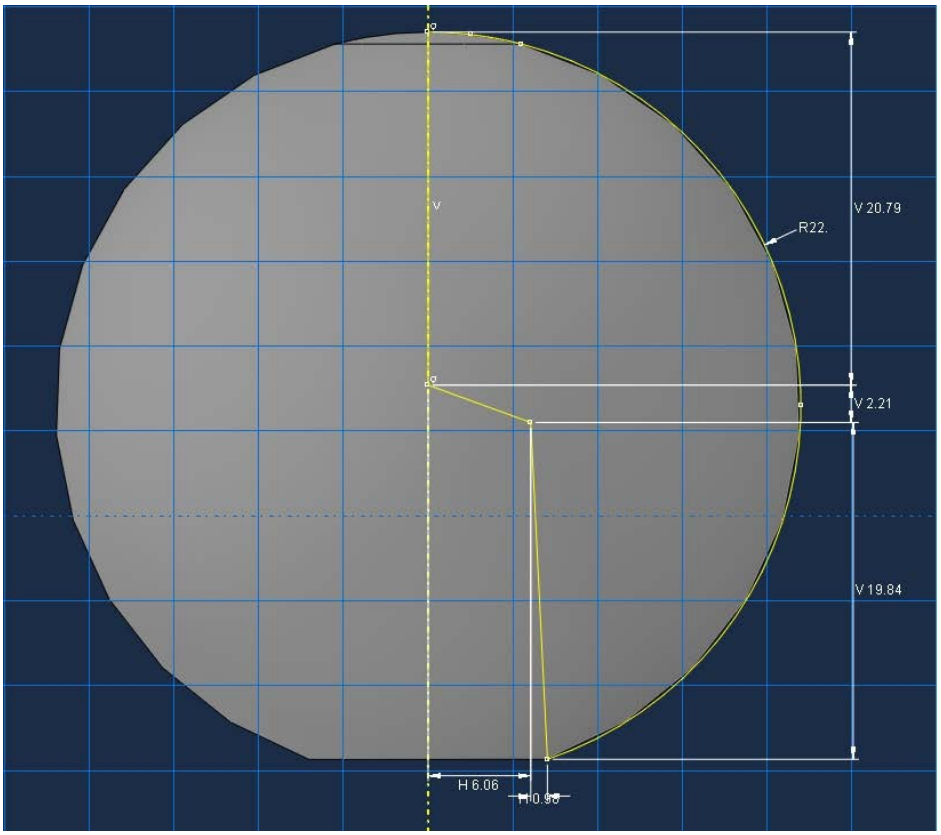

Figure A12. The 44 mm femoral head (the femoral head is 7 mm above the centre of the neck taper).

Appendix B

The purpose of this section is to present the convergence of the data collected in the finite element analysis described in Chapter 4. For each iteration, the element size for the head and neck components were decreased by 10%. For convergence to be achieved, the change in the assembly displacement and the maximum von Mises stress for the assembly, recovery, compression, and tension phases all had to be less than 10%.

Table B1. Convergence of displacement and maximum von Mises stresses when varying the head size for the single alloy material combination (12/14 mm taper with 4000 N assembly force).

Head Size (mm)	Iteration	Head Element Size (mm)	Number of Head Elements	Neck Element Size (mm)	Number of Neck Elements	Displace-ment (μm)	Assembly Maximum Stress (MPa)	Recovery Maximum Stress (MPa)	Compression Maximum Stress (MPa)	Tension Maximum Stress (MPa)
28	1	1.2	2698	1.2	1547	63.6	93.6	83.8	89.6	101.2
28	2	1.08	4232	1.08	1957	61.9	96.9	87.9	82.3	95.3
28	3	0.972	5961	0.972	2625	61.7	94.4	77.7	81.2	92.6
36	1	1.6	3160	1.2	1547	61.1	80.5	70.1	89.6	59.3
36	2	1.44	4400	1.08	1957	59.9	74.3	61.8	83.2	53.4
36	3	1.296	5928	0.972	2625	59.7	72.1	61.1	80.0	51.5
44	1	2	2730	1.2	1547	57.8	54.4	49.8	88.6	50.1
44	2	1.8	3400	1.08	1957	55.5	49.2	45.4	85.5	45.0
44	3	1.62	4551	0.972	2625	54.0	47.2	43.8	79.9	43.6

Table B2. Convergence of displacement and maximum von Mises stresses when varying the head size for the mixed materials combination (12/14 mm taper with 4000 N assembly force).

Head Size (mm)	Iteration	Head Element Size (mm)	Number of Head Elements	Neck Element Size (mm)	Number of Neck Elements	Displace-ment (µm)	Assembly Maximum Stress (MPa)	Recovery Maximum Stress (MPa)	Compression Maximum Stress (MPa)	Tension Maximum Stress (MPa)
28	1	1.2	2698	1.2	1547	70.0	89.4	69.8	82.1	70.3
28	2	1.08	4232	1.08	1957	72.3	82.3	63.3	72.1	63.2
28	3	0.972	5961	0.972	2625	71.6	80.0	62.3	73.2	62.4
36	1	1.6	3160	1.2	1547	79.3	73.5	68.6	77.4	63.1
36	2	1.44	4400	1.08	1957	72.4	76.2	61.2	73.4	57.2
36	3	1.296	5928	0.972	2625	71.6	80.0	62.3	73.2	62.4
44	1	2	2730	1.2	1547	65.9	47.4	39.6	89.6	43.8
44	2	1.8	3400	1.08	1957	72.1	58.2	47.1	86.8	42.2
44	3	1.62	4551	0.972	2625	70.7	58.3	47.4	85.0	41.1

Table B3. Convergence of displacement and maximum von Mises stresses for the different taper sizes (44 mm femoral head with a 4000 N assembly force).

Taper Size (mm)	Iteration	Head Element Size (mm)	Number of Head Elements	Neck Element Size (mm)	Number of Neck Elements	Displace-ment (μm)	Assembly Maximum Stress (MPa)	Recovery Maximum Stress (MPa)	Compression Maximum Stress (MPa)	Tension Maximum Stress (MPa)
10/12	1	2	3230	1.2	1064	58.5	47.5	46.0	71.2	47.1
10/12	2	1.8	4032	1.08	1328	56.4	46.9	44.1	68.8	45.5
10/12	3	1.62	5164	0.972	1932	56.4	43.5	43.0	67.0	43.9
12/14	1	2	2730	1.2	1547	57.8	54.4	49.8	88.6	50.1
12/14	2	1.8	3400	1.08	1957	55.5	49.2	45.4	85.5	45.0
12/14	3	1.62	4551	0.972	2831	54.0	47.2	43.8	79.9	43.6
14/16	1	2	2926	1.2	2040	63.2	58.0	56.0	78.1	57.2
14/16	2	1.8	3906	1.08	2574	56.1	54.0	53.2	87.4	55.9
14/16	3	1.62	5727	0.972	3000	53.1	53.4	52.1	89.4	51.3

Table B4. Convergence of displacement and maximum von Mises stresses when varying the assembly force (44 mm femoral head with a 4000 N assembly force).

Assembly Force (N)	Iteration	Head Element Size (mm)	Number of Head Elements	Neck Element Size (mm)	Number of Neck Elements	Displace-ment (μm)	Assembly Maximum Stress (MPa)	Recovery Maximum Stress (MPa)	Compression Maximum Stress (MPa)	Tension Maximum Stress (MPa)
500	1	1.6	3160	1.2	1853	7.8	8.2	7.4	79.1	35.1
500	2	1.44	4400	1.08	2413	7.3	8.5	7.6	79.4	30.6
500	3	1.296	5928	0.972	3045	7.5	8.8	7.6	79.6	30.0
1000	1	1.6	3160	1.2	1853	15.5	16.1	15.2	85.2	26.6
1000	2	1.44	4400	1.08	2413	14.9	17.0	14.8	82.1	27.5
1000	3	1.296	5928	0.972	3045	14.6	17.8	15.4	79.6	30.0
2000	1	1.6	3160	1.2	1853	28.3	35.2	31.3	78.9	30.2
2000	2	1.44	4400	1.08	2413	29.8	34.1	29.8	79.2	26.7
2000	3	1.296	5928	0.972	3045	29.1	35.7	30.9	79.6	30.0
3000	1	1.6	3160	1.2	1853	45.1	52.6	45.1	81.1	46.2
3000	2	1.44	4400	1.08	2413	44.6	51.3	44.8	79.2	42.9
3000	3	1.296	5928	0.972	3045	43.7	53.5	46.3	79.8	40.7
4000	1	1.6	3160	1.2	1853	57.8	54.4	49.8	88.6	50.1
4000	2	1.44	4400	1.08	2413	55.5	49.2	45.4	85.6	45.0
4000	3	1.296	5928	0.972	3045	54.0	47.2	43.8	79.9	46.3
5000	1	1.6	3160	1.2	1853	72.6	89.1	72.1	79.4	75.2
5000	2	1.44	4400	1.08	2413	72.3	83.2	67.5	80.0	67.7
5000	3	1.296	5928	0.972	3045	72.1	75.6	63.5	78.1	63.8
6000	1	1.6	3160	1.2	1853	89.4	86.2	74.2	80.5	77.3
6000	2	1.44	4400	1.08	2413	86.5	83.9	72.1	78.1	75.8
6000	3	1.296	5928	0.972	3045	87.1	83.2	71.0	77.4	75.2

Table B5. Convergence of displacement and maximum von Mises stresses when varying the distance between the centre of the femoral head and the centre of the neck taper (44 mm femoral head with a 4000 N assembly force). Note: A positive distance refers to the centre of the femoral head being above the centre of the neck taper whereas a negative distance corresponds to the centre of the femoral head being below the centre of the neck taper.

Offset Distance (mm)	Iteration	Head Element Size (mm)	Number of Head Elements	Neck Element Size (mm)	Number of Neck Elements	Displace-ment (μm)	Assembly Maximum Stress (MPa)	Recovery Maximum Stress (MPa)	Compression Maximum Stress (MPa)	Tension Maximum Stress (MPa)
-3	1	2.1	2235	1.2	1547	58.3	53.3	50.5	74.1	51.1
-3	2	1.89	3111	1.08	1957	52.6	50.8	49.1	73.2	49.6
-3	3	1.701	4232	0.972	2831	54.1	48.0	45.9	71.0	46.2
-1	1	1.9	3058	1.2	1547	55.5	47.7	44.0	93.0	42.8
-1	2	1.71	4182	1.08	1957	53.5	49.3	45.9	79.9	45.4
-1	3	1.539	5314	0.972	2831	53.5	49.7	46.9	72.2	46.4
0	1	2	2730	1.2	1547	57.8	54.4	49.8	88.6	50.1
0	2	1.8	4232	1.08	1957	55.5	49.2	45.4	85.5	45.0
0	3	1.62	4551	0.972	2831	54.0	47.2	43.8	79.9	43.6
1	1	2	2338	1.2	1547	59.3	51.2	49.8	92.1	51.3
1	2	1.8	3264	1.08	1957	57.4	49.2	45.2	90.9	46.1
1	3	1.62	4361	0.972	2831	54.7	49.6	46.2	94.6	44.9
3	1	2.1	2100	1.2	1547	59.2	54.4	49.0	117.5	48.3
3	2	1.89	2716	1.08	1957	59.2	48.2	47.2	112.2	45.5
3	3	1.701	3920	0.972	2831	54.2	51.8	46.7	104.8	45.7
7	1	2.1	1.2	1.2	1547	60.1	58.0	53.1	109.0	42.7
7	2	1.89	1.08	1.08	1957	58.4	56.9	52.3	105.3	48.1
7	3	1.701	0.972	0.972	2831	58.4	58.9	52.6	102.2	46.8

Table B6. Convergence of displacement and maximum von Mises stresses when varying the angle of loading during the compression phase.

Angle of Compression Loading	Iteration	Head Element Size (mm)	Number of Head Elements	Neck Element Size (mm)	Number of Neck Elements	Displacement (µm)	Assembly Maximum Stress (MPa)	Recovery Maximum Stress (MPa)	Compression Maximum Stress (MPa)	Tension Maximum Stress (MPa)
0° Axial	1	2	2730	1.2	1547	57.8	54.4	49.8	52.1	47.1
0° Axial	2	1.8	4232	1.08	1957	55.5	49.2	45.4	50.5	45.8
0° Axial	3	1.62	4551	0.972	2831	54.0	47.2	43.8	46.4	43.9
30° Out of Axis	1	2	2730	1.2	1547	57.8	54.4	49.8	88.6	50.1
30° Out of Axis	2	1.8	4232	1.08	1957	55.5	49.2	45.4	85.5	45.0
30° Out of Axis	3	1.62	4551	0.972	2831	54.0	47.2	43.8	79.9	43.6

Bibliography

[1] R. Sorci. (2012, March 20). Increasing incidence of joint replacements burdens healthcare system [Online]. Available: http://www.nerac.com/nerac_insights.php?category=articles&id=150

[2] S. M. Kurtz, "Current trends and projected utilization of total joint replacements," in Orthopaedic Research Society, San Francisco, CA, USA, 2012, p. 182.

[3] S. M. Kurtz, K. Ong, E. Lau, F. Mowat, and M. Halpern, "Projections of primary and revision hip and knee arthroplasty in the United States from 2005 to 2030," J. Bone Joint Surg [Am], vol. 89A, pp. 780-785, 2007.

[4] M. G. Fontana, Corrosion Engineering, 3rd ed. United States of America: McGraw-Hill Custom Publishing, 1986.

[5] N. J. Hallab, C. Messina, A. Skipor, and J. J. Jacobs, "Differences in the fretting corrosion of metal-metal and ceramic-metal modular junctions of total hip replacements," J. Orthop. Res., vol. 22, pp. 250-259, 2004.

[6] W. Brodner, P. Bitzan, V. Meisinger, A. Kaider, F. Gottsauner-Wolf, and R. Kotz, "Serum cobalt levels after metal-on-metal total hip arthroplasty," J Bone Joint Surg [Am], vol. 85, pp. 2168-2173, 2003.

[7] R. D. Crowninshield, W. J. Maloney, D. H. Wentz, S. M. Humphrey, and C. R. Blanchard, "Biomechanics of large femoral heads," Clin. Orthop. Relat. Res., vol. 429, pp. 102-107, 2004.

[8] J. R. Goldberg and J. L. Gilbert, "In vitro corrosion testing of modular hip tapers," J. Biomed. Mater. Res. Part B: Appl. Biomater., vol. 64B, pp. 78-93, 2002.

[9] J. P. Collier, M. B. Mayor, R. E. Jensen, V. A. Surprenant, H. P. Surprenant, J. L. McNamare, et al., "Mechanisms of failure of modular prostheses," Clin. Orthop. Relat. Res., vol. 285, pp. 129-139, 1992.

[10] J. P. Collier, M. B. Mayor, I. R. Williams, V. A. Surprenant, H. P. Surprenant, and B. H. Currier, "The tradeoffs associated with modular hip prostheses," Clin. Orthop. Relat. Res., vol. 311, pp. 91-101, 1995.

[11] J. P. Collier, V. A. Surprenant, R. E. Jensen, M. B. Mayor, and H. P. Surprenant, "Corrosion between the components of modular femoral hip prostheses," J Bone Joint Surg [Br], vol. 74B, pp. 511-517, 1992.

[12] A. M. Kop and E. Swarts, "Corrosion of a hip stem with a modular neck taper junction," J. Arthroplasty, vol. 24, pp. 1019-1023, 2009.

[13] J. R. Lieberman, C. M. Rimnac, K. L. Garvin, R. W. Klein, and E. A. Salvati, "An analysis of the head-neck taper interface in retrieved hip prostheses," Clin. Orthop. Relat. Res., vol. 300, pp. 162-167, 1994.

[14] J. L. Gilbert, C. A. Buckley, and J. J. Jacobs, "In vivo corrosion of modular hip prosthesis components in mixed and similar metal combinations. The effect of crevice, stress, motion, and alloy coupling," Journal of Biomedical Materials Research, vol. 27, pp. 1533-1544, 1993.

[15] J. R. Goldberg, J. L. Gilbert, J. J. Jacobs, T. W. Bauer, W. Paprosky, and S. Leurgans, "A multicenter retrieval study of the taper interfaces of modular hip prostheses," Clin. Orthop. Relat. Res., vol. 401, pp. 149-161, 2002.

[16] J. L. Gilbert, M. Mehta, and B. Pinder, "Fretting crevice corrosion of stainless steel stem-CoCr femoral head connections: comparisons of materials, initial moisture, and offset length," J. Biomed. Mater. Res. Part B: Appl. Biomater., vol. 88B, pp. 162-173, 2009.

[17] W. C. Whiting and R. F. Zernicke, Biomechanics of Musculoskeletal Injury, 2nd ed. Champaign, Illinois, USA: Human Kinetics, 2008.

[18] S. I. Clinic. (2012, April 15). Hip Anatomy [Online]. Available: http://www.sportsinjuryclinic.net/anatomy/hip-anatomy

[19] Wikipedia. (2010, October 6). Sacrum [Online]. Available: http://en.wikipedia.org/wiki/Sacrum

[20] Wordpress. (2012, April 23). Bones of the Body Quiz [Online]. Available: http://bones-of-the-body-quiz.anatomyandphysiologyss.com/pelvic-anatomy-bone/

[21] D. Darling. (2010, October 7). Acetabulum [Online]. Available: http://www.daviddarling.info/encyclopedia/A/acetabulum.html

[22] S. Pramanik, A. K. Agarwal, and K. N. Rai, "Chronology of total hip joint replacement and materials development," Trends in Biomaterials & Artificial Organs, vol. 19, pp. 15-26, 2005.

[23] Farlex. (2009, May 7). Cyst [Online]. Available: http://www.thefreedictionary.com/cyst

[24] W. C. Shiel. (2012, April 23). Total Hip Replacement [Online]. Available: http://www.medicinenet.com/total_hip_replacement/article.htm

[25] Wikipedia. (2012, April 23). Osteonecrosis [Online]. Available: http://en.wikipedia.org/wiki/Osteonecrosis

[26] Wikipedia. (2012, April 23). Rheumatoid Arthritis [Online]. Available: http://en.wikipedia.org/wiki/Rheumatoid_arthritis

[27] A. Judge, N. K. Arden, and A. Price, "Assessing patients for joint replacement: can preoperative Oxford hip and knee scores be used to predict patient satisfaction following joint replacement surgery and to guide patient selection?," Journal of Bone and Joint Surgery [British], vol. 93B, pp. 1660-1664, 2011.

[28] J. M. Quintana, A. Escobar, and I. Arostegui, "Health-related quality of life and appropriateness of knee or hip joint replacement," Archives of Internal Medicine, vol. 166, pp. 220-226, 2006.

[29] J. Gallo, Y. T. Konttinen, S. B. Goodman, J. P. Thyssen, E. Gibon, J. Pajarinen, et al. (2012, June 2). Aseptic loosening of total hip arthroplasty as a result of local failure of tissue homeostasis. Available: http://cdn.intechopen.com/pdfs-wm/26869.pdf

[30] Australian Orthopaedic Institute. (2008, April 23). Hip replacement [Online]. Available: http://www.misinstitute.com/hip.htm

[31] Wikipedia. (2012, April 23). Total hip replacement [Online]. Available: http://en.wikipedia.org/wiki/Total_hip_replacement

[32] Canadian Broadcasting Corporation. (2013, September 30). Metal-on-metal hip implants more likely to need replacement [Online]. Available: http://www.cbc.ca/news/health/metal-on-metal-hip-implants-more-likely-to-need-replacement-1.1330007

[33] K. J. Bozic, S. M. Kurtz, E. Lau, K. Ong, V. Chiu, T. P. Vail, et al., "The epidemiology of total hip arthroplasty bearing usage in the United States," Journal of Arthroplasty, vol. 24, p. e44, 2009.

[34] C. M. Jack, W. L. Walter, A. J. Shimmin, K. Cashman, and R. N. de Steiger, "Large diameter metal on metal articulations. Comparison of total hip arthroplasty and hip resurfacing arthroplasty," Journal of Arthroplasty, vol. 28, pp. 650-653, 2013.

[35] D. Cohen, "How safe are metal-on-metal hip implants?," BMJ, vol. 28, pp. 344-350, 2012.

[36] J. J. Jacobs, "Local metal reactions after metal-metal hip arthroplasty: How frequent? What forms do they take? What causes them? Can we test for them?," presented at the The Hip Society and the American Association of Hip and Knee Surgeons, Las Vegas, Nevada, USA, 2009.

[37] I. Moga, M. A. Harrington, S. Ismaily, and P. C. Noble, "Trunnion surface damage in THR: MPE vs MOM articulations," presented at the International Society for Technology in Arthroplasty, Palm Beach, Florida, USA, 2013.

[38] M. K. D. Benson, P. G. Goodwin, and J. Brostoff, "Metal sensitivity in patients with joint replacement arthroplasties," British Medical Journal, vol. 4, pp. 374-375, 1975.

[39] A. Lübbeke, A. Gonzalez, G. Garavaglia, C. Roussos, A. Bonvin, R. Stern, et al., "A comparative assessment of small-head metal-on-metal and ceramic-on-polyethylene total hip replacement," The Bone and & Joint Journal, vol. 96B, pp. 868-875, 2014.

[40] E. K. Ocran, "Corrosion and fretting corrosion studies of medical grade CoCrMo implant material in a more clinically relevant simulated body environment," Master of Science, Mechanical and Manufacturing Engineering, University of Manitoba, Winnipeg, Manitoba, Canada, 2014.

[41] L. Sedel, "Evolution of alumina-on-alumina implants," Clinical Orthopaedics and Related Research, vol. 379, pp. 48-54, 2000.

[42] C. J. Lavernia, L. Baerga, R. L. Barrack, E. Tozakoglou, S. D. Cook, L. Lata, et al., "The effects of blood and fat on Morse taper disassembly force," American Journal of Orthopedics, vol. 38, pp. 187-190, 2009.

[43] S. Munir, A. Imbuldeniya, W. K. Walter, and W. Walsh, "Variations in the trunnion surface topography between different commercially available hip replacement stems," presented at the International Society for Technology in Arthroplasty, Palm Beach, Florida, USA, 2013.

[44] B. Cales and Y. Stefani, "Risks and advantages in standardization of bores and cones for heads in modular hip prostheses," Journal of Biomedical Materials Research Part A, vol. 43, pp. 62-68, 1998.

[45] I. Clarke, J. Y. Lazennec, A. Brusson, M. Burgett, and T. Donaldson, "Topography of modular junctions in 28 mm MOM - gold-standard European threaded taper (12/14)," presented at the International Society for Technology in Arthroplasty, Palm Beach, Florida, USA, 2013.

[46] A. J. Wassef and T. P. Schmalzried, "Femoral taperosis: An accident waiting to happen?," Bone & Joint Research, vol. 95B, pp. 3-6, 2013.

[47] S. Munir, M. B. Cross, R. Jenabzadeh, A. Sokolova, C. Esposito, D. Molloy, et al., "The effect of bearing surface on corrosion at the modular junctions in total hip arthroplasty," presented at the 25th Congress of the International Society for Technology in Arthroplasty, Sydney, Australia, 2012.

[48] C. B. Rieker, R. Schon, R. Konrad, G. Liebentritt, P. Gnepf, M. Shen, et al., "Influence of the clearance on in-vitro tribology of large diameter metal-on-metal articulations pertaining to resurfacing hip implants," Orthop. Clin. N. Am., vol. 36, pp. 135-142, 2005.

[49] W. C. Witzleb, J. Ziegler, F. Krummenauer, V. Neumeister, and K. P. Guenther, "Exposure to chromium, cobalt and molybdenum from metal-on-metal total hip replacement and hip resurfacing arthroplasty," Acta Orthop., vol. 77, pp. 697-705, 2006.

[50] I. S. Paleochorlidis, L. S. Badras, E. F. Skpetas, V. A. Georgaklis, T. S. Karachalios, and K. N. Malizos, "Clinical outcome study and radiological findings of Zweymuller metal on metal total hip arthroplasty. A follow-up of 6 to 15 years," Hip Intl., vol. 19, pp. 301-308, 2009.

[51] S. Hariri, S. Chun, J. B. Cowan, C. R. Bragdon, H. Malchau, and H. E. Rubash, "Range of motion in a modular femoral stem system with a variety of neck options," Journal of Arthroplasty, vol. 28(9), pp. 1625-1633, 2013.

[52] J. M. Drouin and B. Cales, "Yttria-stabilized zirconia ceramic for improved hip-joint head," Bioceramics, vol. 7, pp. 389-394, 1994.

[53] P. J. Duwelius, B. Burkhart, C. Carnahan, G. Branam, L. M. Ko, Y. X. Wu, et al., "Modular versus nonmodular neck femoral implants in primary total hip arthroplasty: Which is better?," Clinical Orthopaedics and Related Research, vol. 472, pp. 1240-1245, 2014.

[54] B. R. Burroughs, H. E. Rubash, and W. H. Harris, "Femoral head sizes larger than 32 mm against highly cross-linked polyethylene," Clinical Orthopaedics and Related Research, vol. 450, pp. 150-157, 2002.

[55] J. Charnley, Post-operative dislocation. Low friction arthroplasty of the hip. London, U.K.: Springer-Verlag, 1979.

[56] B. J. Bolland, D. Culliford, D. J. Langton, J. P. S. Millington, N. K. Arden, and J. M. Latham, "High failure rates with a large-diameter hybrid metal-on-metal total hip replacement," Journal of Bone and Joint Surgery [British], vol. 93B, pp. 608-615, 2011.

[57] R. M. Hall, P. Sidney, A. Unsworth, and B. M. Wroblewski, "Prevalence of impingement in explanted Charnley acetabular components," Journal of Orthopaedic Science, vol. 3, pp. 204-208, 1998.

[58] M. Yamaguchi, T. Akisue, T. W. Bauer, and Y. Hashimoto, "The spatial location of impingement in total hip arthroplasty," Journal of Arthroplasty, vol. 15, pp. 305-313, 2000.

[59] R. M. Queen, E. T. Newman, A. N. Abbey, T. P. Vail, and M. P. Bolognesi, "Stair ascending and descending in hip resurfacing and large head total hip arthroplasty patients," Journal of Arthroplasty, vol. 28, pp. 684-689, 2013.

[60] B. R. Burroughs, B. Hallstrom, G. J. Golladay, D. Hoeffel, and W. H. Harris, "Range of motion with stability in total hip arthroplasty with 28-, 32-, 38-, and 44 mm femoral head sizes," Journal of Arthroplasty, vol. 20, pp. 11-19, 2005.

[61] W. P. Zijlstra, I. van den Akker-Scheek, M. J. M. Zee, and J. J. A. M. Van Raay, "No clinical difference between large metal-on-metal total hip arthroplasty and 28-mm-head total hip arthroplasty?," International Orthopaedics, vol. 35, pp. 1771-1776, 2011.

[62] C. L. Allen, G. J. Hooper, and C. M. A. Frampton, "Do larger femoral heads improve the functional outcome in total hip arthroplasty?," Journal of Arthroplasty, vol. 29, pp. 401-404, 2014.

[63] J. Cooper, R. M. Urban, C. Deirmengian, W. G. Paprosky, and J. J. Jacobs, "Late dislocation as the presenting symptom of taper corrosion following metal-on-polyethylene total hip arthroplasty," presented at the International Society for Technology in Arthroplasty, Palm Beach, FL, USA, 2013.

[64] H. Pandit, S. Glyn-Jones, P. McLardy-Smith, R. Gundle, D. Whitwell, C. L. M. Gibbons, et al., "Pseudotumors associated with metal-on-metal hip resurfacings," J Bone Joint Surg [Br], vol. 90B, pp. 847-851, 2008.

[65] National Joint Registry for England and Wales. (2011, March 28). National Joint Registry for England and Wales: Eighth annual report [Online]. Available: http://www.njrcentre.org.uk

[66] Australian Orthopaedic Association. (2011, March 28). National Joint Replacement Registry: Annual report [Online]. Available: http://www.dmac.adelaide.edu.au/aoanjrr/documents/AnnualReports2011

[67] National Joint Registry for Englland and Wales. (2010, June 20). 7th Annual Report [Online]. Available: http://www.njrcentre.org.uk

[68] P. F. Lachiewicz, D. S. Heckman, E. S. Soileau, J. Mangla, and J. M. Martell, "Femoral head size and wear of highly cross-linked polyethylene at 5 to 8 years," Clinical Orthopaedics and Related Research, vol. 467, pp. 3290-3296, 2009.

[69] I. Leslie, S. Williams, C. Brown, G. Isaac, Z. Jin, E. Ingham, et al., "Effect of bearing size on the long-term wear, wear debris, and ion levels of large diameter metal-on-metal hip replacements - An in vitro study," Journal of Biomedical Materials Research Part B: Applied Biomaterials, vol. 87B, pp. 163-172, 2008.

[70] M. B. Cross, D. Nam, and D. J. Mayman, "Ideal femoral head size in total hip arthroplasty balances stability and volumetric wear," HSS Journal, vol. 8, pp. 270-274, 2012.

[71] D. J. Langton, R. Sidaganamale, J. K. Lord, A. V. F. Nargol, and T. J. Joyce, "Taper junction failure in large-diameter metal-on-metal bearings," Bone & Joint Research, vol. 1, pp. 56-63, 2012.

[72] S. A. Stuchin, "Anatomic diameter femoral heads in total arthroplasty: A preliminary report," Journal of Bone and Joint Surgery [American], vol. 90A, pp. 52-56, 2008.

[73] B. J. Bolland, E. Gardner, A. Roques, C. Maul, D. Culliford, N. Zeineh, et al., "High taper sleeve ear and failure associated with synergy / BHR large diameter metal on metal total hip replacement," presented at the International Society for Technology in Arthroplasty, Palm Beach, Florida, USA, 2013.

[74] D. Hansen, "Metal corrosion in the human body: the ultimate bio-corrosion scenario," The Electrochemical Society Interface, vol. 17, pp. 31-34, 2008.

[75] J. Black, "Does corrosion matter?," J Bone Joint Surg [Br], vol. 70B, pp. 517-520, 1988.

[76] ASTM International, "Annual book of ASTM standards," in Medical devices; Emergency medical standards vol. vol. 13.01, ed. USA: ASTM International, 1997.

[77] ASTM International, "Standard practice for surface preparation and marking of metallic surgical implants," vol. ASTM F-86 04, ed. USA: ASTM International, 2004.

[78] ASTM International, "Standard specification for chemical passivation treatments for stainless steel parts," vol. ASTM A967-01, ed. USA: ASTM International, 2001.

[79] D. F. Williams, Biocompatibility of Clinical Materials: The properties and clinical uses of cobalt-chromium alloys vol. 1. Boca Raton, Florida, United States of America: CRC Press, 1981.

[80] E. Martin, R. Pourzal, S. Vajpayee, M. Matthew, M. A. Wimmer, and K. Shull, "Mechanisms of tribofilm formation in metal-on-metal hip joint bearings and other metal junctions," presented at the Orthopaedic Research Society, San Antonio, Texas, USA, 2013.

[81] Y. Yan, A. Neville, and D. Dowson, "Tribo-corrosion properties of cobalt-based medical implant alloys in simulated biological environments," Wear, vol. 263, pp. 1105-1111, 2007.

[82] A. J. Hart, P. D. Quinn, B. Sampson, A. Sandison, K. D. Atkinson, J. A. Skinner, et al., "The chemical form of metallic debris in tissues surrounding metal-on-metal hips with unexplained failure," Acta Biomaterialia, vol. 6, pp. 4439-4446, 2010.

[83] C. van der Straeten, D. van Quickenborne, S. Pennynck, K. De Smet, and J. Victor, "Systemic toxicity of metal ions in a metal-on-metal hip arthroplasty population," presented

at the International Society for Technology in Arthroplasty, Palm Beach, Florida, USA, 2013.

[84] A. Nicolli, G. Bisinella, G. Padovani, A. Vitella, F. Chiara, and A. Trevisan, "Predictivity and fate of metal ion release from metal-on-metal total hip prostheses," Journal of Arthroplasty, vol. 29, pp. 1763-1767, 2014.

[85] R. F. Coleman, J. Herrington, and J. T. Scales, "Concentration of wear products in hair, blood, and urine after total hip replacement," J Bone Joint Surg [Am], vol. 1, pp. 527-529, 1973.

[86] S. Morapudi, "Serum metal ion levels in bilateral and unilateral metal on metal (MoM) stemmed hip arthroplasty: Is there a significant difference?," presented at the International Society for Technology in Arthroplasty, Palm Beach, Florida, USA, 2013.

[87] H. Watanabe, Y. Hachiya, H. Murata, K. Muramatsu, S. Taniguchi, M. Kondo, et al., "Risk factors for elevation of serum metal ion levels after metal-on-metal THA," presented at the International Society for Technology in Arthroplasty, Palm Beach, Florida, USA, 2013.

[88] A. C. Lewis, "Effect of synovival fluid, phosphate-buffered saline solution, and water on the dissolution and corrosion properties of CoCrMo alloys as used in orthopedic implants," Journal of Applied Biomaterials and Biomechanics Research Part A, vol. 73A, pp. 456-467, 2005.

[89] Wikipedia. (2014, October 14). Titanium [Online]. Available: http://en.wikipedia.org/wiki/Titanium

[90] P. Schaaff, "The role of fretting damage in total hip arthroplasty with modular design hip joints - evaluation of retrieval studies and experimental simulation methods," Journal of Applied Biomaterials and Biomechanics Research, vol. 2, pp. 121-135, 2004.

[91] J. J. Jacobs, J. L. Gilbert, and R. M. Urban, "Current concepts review - corrosion of metal orthopaedic implants," J Bone Joint Surg [Am], vol. 80A, pp. 268-282, 1998.

[92] J. Black, H. Sherk, J. Bonini, W. R. Rostoker, F. Schajowicz, and J. O. Galante, "Metallosis associated with a stable titanium-alloy femoral component in total hip replacement. A case report," J Bone Joint Surg [Am], vol. 72, pp. 126-130, 1990.

[93] B. F. Shahgaldi, F. W. Heatley, A. Dewar, and B. Corrin, "In vivo corrosion of cobalt-chromium and titanium wear particles," Journal of Bone and Joint Surgery [British], vol. 77B, pp. 962-966, 1995.

[94] U. K. Mudali, T. M. Sridhar, and B. Raj, "Corrosion of bio implants," J Bone Joint Surg [Am], vol. 28, pp. 601-637, 2003.

[95] M. Bryant, R. Farrar, R. Freeman, K. Brummitt, and A. Neville, "Fretting corrosion characteristics of fully cemented polished collarless tapered stems in a simulated biological environment," presented at the Orthopaedic Research Society, San Antonio, Texas, USA, 2013.

[96] H. G. Willert, L. G. Brobäck, G. H. Buchhorn, P. H. Jensen, G. Köster, I. Lang, et al., "Crevice corrosion of cemented titanium alloy stems in total hip replacements," Clinical Orthopaedics and Related Research, vol. 333, pp. 51-75, 1996.

[97] W. W. Tennese and J. R. Cahoon, ""Sensitization" still a problem in the intergranular corrosion of stainless steel surgical implants," Biomater. Med. Devices Artif. Organs, vol. 1, pp. 635-645, 1973.

[98] F. Silver and C. Doillon, Biocompatibility: Interactions of biological and implantable materials. New York, New York, United States of America: VCH Publishers, 1989.

[99] S. D. Cook, G. J. Gianoli, A. J. T. Clemow, and R. J. Haddad Jr., "Fretting corrosion in orthopaedic alloys," Artificial Cells, Nanomedicine, and Biotechnology, vol. 11, pp. 281-292, 1983.

[100] S. Virtanen, I. Milošev, E. Gomez-Barrena, R. Trebše, J. Salo, and Y. T. Konttinen, "Special modes of corrosion under physiological and simulated physiological conditions," Acta Biomaterialia, vol. 4, pp. 468-476, 2008.

[101] S. A. Leduc, MCAT: Physical Sciences Review. USA: Princeton Review, Inc., 2005.

[102] D. Voet and J. G. Voet, Biochemistry, 3rd ed. USA: John Wiley & Sons, Inc., 2004.

[103] U. P. Wyss, "MECH 7780: Critical issues of implantable biomechanical devices - Lecture," R. Dyrkacz, Ed., ed. Winnipeg, MB, Canada, 2011.

[104] Essortment. (2011, April 1). Acid alkaline balance in the human body [Online]. Available: http://www.essortment.com/acid-alkaline-balance-human-body-63202.html

[105] A. Oyane, H. M. Kim, T. Furya, T. Kokubo, T. Miyazaki, and T. Nakamura, "Preparation and assessment of revised simulated body fluids," Journal of Biomedical Materials Research, vol. 65A, pp. 188-195, 2003.

[106] M. B. Ellman and B. R. Levine, "Fracture of the modular femoral neck component in total hip arthroplasty," Journal of Arthroplasty, vol. 28, pp. 196.e1-e5, 2013.

[107] D. O. Molloy, S. Munir, C. M. Jack, M. B. Cross, W. K. Walter, and W. K. S. Walter, "Fretting and corrosion in modular-neck total hip arthroplasty femoral stems," Journal of Bone and Joint Surgery [American], vol. 96A, pp. 488-493, 2014.

[108] R. Pivec, R. M. Meneghini, W. J. Hozack, G. H. Westrich, and M. A. Mont, "Modular taper junction corrosion and failure: How to approach a recalled total hip arthroplasty implant," Journal of Arthroplasty, vol. 29, pp. 1-6, 2014.

[109] F. Witt, B. H. Bosker, N. E. Bishop, H. B. Ettema, C. C. P. M. Verheyen, and M. M. Morlock, "The relation between titanium taper corrosion and cobalt-chromium bearing wear in large-head metal-on-metal total hip prostheses: A retrieval study," Journal of Bone and Joint Surgery [American], vol. 96, p. [in press], 2014.

[110] Y. Yan, A. Neville, and D. Dowson, "Tribo-corrosion properties of cobalt-based medical implant alloys in simulated biological environments," Wear, vol. 263, pp. 1105-1111, 2007.

[111] A. I. Muñoz and S. Mischler, "Interactive Effects of Albumin and Phosphate Ions on the Corrosion of CoCrMo Implant Alloy," Journal of the Electrochemical Society, vol. 154, pp. C562-C570, 2007.

[112] C. V. Vidal and A. I. Muñoz, "Effect of thermal treatment and applied potential on the electrochemical behaviour of CoCrMo biomedical alloy,”" Electrochimica Acta, vol. 54, pp. 1798-1809, 2009.

[113] R. Pourzal, I. Catelas, R. Theissmann, C. Kaddick, and A. Fischer, "Characterization of wear particles generated from CoCrMo alloy under sliding wear conditions," Wear, vol. 271, pp. 1658-1666, 2011.

[114] T. M. Grupp, T. Weik, W. Bloemer, and H. P. Knaebel, "Modular titanium alloy neck adaptewr failures in hip replacement - failure mode analysis and influence of implant material," BMC Musculoskeletal Disorders, vol. 11, pp. 1-12, 2010.

[115] Y. Yan, A. Neville, and D. Dowson, "Biotribocorrosion of CoCrMo orthopaedic implant materials: assessing the formation and effect of the biofilm.," Tribology International, vol. 40, pp. 1492-1499, 2007.

[116] S. A. Mali, V. Swaminathan, and J. L. Gilbert, "Evaluation of mechanically-assisted corrosion response of orthopedic alloy couples," presented at the Orthopaedic Research Society, San Antonio, Texas, USA, 2013.

[117] J. P. Kretzer, E. Jakubowitz, M. Krachler, M. Thomsen, and C. Heisel, "Metal release and corrosion effects of modular neck total hip arthroplasty," Int. Orthop., vol. 33, pp. 1531-1536, 2009.

[118] S. D. Cook, R. L. Barrack, G. C. Baffes, A. J. T. Clemow, P. Serekian, N. Dong, et al., "Wear and corrosion of modular interfaces in total hip replacements," Clin. Orthop. Relat. Res., vol. 298, pp. 80-88, 1994.

[119] D. Williams and R. Roaf, Implants in surgery. London: Saunders, 1973.

[120] R. L. Williams, S. A. Brown, and K. Merritt, "Electrochemical studies on the influence of proteins on the corrosion of implant alloys," Biomaterials, vol. 9, pp. 181-186, 1988.

[121] I. M. A. Kocijan, "The influence of complexing agent and proteins on the corrosion of stainless steels and their metal components," J. Mater. Sci. Mater. Medicine, vol. 14, pp. 69-77, 2003.

[122] J. L. Gilbert and S. Sivan, "Cell-induced corrosion on Co-Cr-Mo acetabular liner taper," in Society for Biomaterials, Denver, Colorado, USA, 2014.

[123] J. L. Gilbert, S. Sivan, Y. Liu, S. B. Kocagoz, C. M. Arnholdt, and S. M. Kurtz, "Direct in vivo inflammatory cell-induced corrosion of CoCrMo alloy orthopedic implant surfaces," Journal of Biomedical Materials Research Part A, p. [in press], 2014.

[124] J. L. Gilbert, S. Sivan, Y. Liu, S. B. Kocagoz, C. M. Arnholdt, and S. M. Kurtz, "Evidence of direct cell induced corroison of CoCrMo implant systems," presented at the Society for Biomaterials, Denver, Colorado, USA, 2014.

[125] A. J. Dabbagh, C. W. Trenam, C. J. Morris, and D. R. Blake, "Iron in joint inflammation," Annals of Rheumatic Diseases, vol. 52, pp. 67-73, 1993.

[126] D. Cadosch, E. Chan, O. P. Gautschi, and L. Filgueira, "Metal is not inert: Role of metal ions released by biocorrosion in aseptic loosening," Journal of Biomedical Materials Research Part A, vol. 91A, pp. 1252-1262, 2009.

[127] D. Cadosch, O. P. Gautschi, E. Chan, H. P. Simmen, and L. Filgueira, "Titanium induced production of chemokines CCL17/TARC and CCL22/MDC in human osteoclasts and osteoblasts," Journal of Biomedical Materials Research Part A, vol. 92A, pp. 475-483, 2010.

[128] IUPAC. (2014, October 10). Fenton Reaction [Online]. Available: http://goldbook.iupac.org/FT06786.html

[129] ASTM, "Standard practice for fretting corrosion testing of modular implant interfaces: Hip femoral head-bore and cone taper interface," vol. F1875-98, ed. West Conshohocken, PA, USA: ASTM International, 2009.

[130] J. M. Brandt, L. K. Briere, J. Marr, S. J. MacDonald, R. B. Bourne, and J. B. Medley, "Biochemical comparisons of osteoarthritic human synovial fluid with calf sera used in knee simulator wear testing," Journal of Biomedical Materials Research Part A, vol. 94, pp. 961-971, 2010.

[131] H. A. McKellop, A. J. Hart, S. H. Park, H. Hothi, P. A. Campbell, and J. A. Skinner, "A lexicon for wear of metal-on-metal hip prostheses," Journal of Orthopaedic Research, vol. 32, pp. 1221-1233, 2014.

[132] J. J. Jacobs, R. M. Urban, J. L. Gilbert, A. K. Skipor, J. Black, M. Jasty, et al., "Local and distant products from modularity," Clin. Orthop. Relat. Res., vol. 319, pp. 94-105, 1995.

[133] W. F. Scully and S. M. Teeny, "Pseudotumor associated with metal-on-polyethylene total hip arthroplasty," Orthopedics, vol. 36, p. e666, 2013.

[134] H. J. Cooper, "The local effects of metal corrosion in total hip arthroplasty," Orthopedic Clinics of North America, vol. In press, pp. 1-10, 2013.

[135] J. Daniel, J. Holland, L. Quigley, S. Sprague, and M. Bhandari, "Pseudotumors associated with total hip arthroplasty," Journal of Bone and Joint Surgery [American], vol. 94A, pp. 86-93, 2012.

[136] J. T. Munro, B. A. Masri, C. P. Duncan, and D. S. Garbuz, "High complication rate after revision of large-head metal-on-metal total hip arthroplasty," Clinical Orthopaedics and Related Research, vol. 472, pp. 523-528, 2014.

[137] U. o. Illinois. (2012, May 3). What is wear? [Online]. Available: http://mechse.illinois.edu/research/microtribodynamics/tribology_intro/intro/wear.htm

[138] A. Kasko, "Biomaterials - Lecture," R. Dyrkacz, Ed., ed. Los Angeles, CA, USA, 2009.

[139] F. L. Group. (2011, May 4). Metallosis [Online]. Available: http://www.washingtoninjuryattorneyblog.com/medical_terms_glossary/

[140] B. J. Vundelinckx, L. A. Verhelst, and J. D. Scheper, "Taper corrosion in modular hip prostheses analysis of serum metal ions in patients," Journal of Arthroplasty, vol. 28, pp. 1218-1223, 2013.

[141] D. S. Garbuz, J. T. Munro, N. V. Greidanus, B. A. Masri, and C. P. Duncan, "High rate of complications following revision of large-head metal-on-metal total hip arthroplasty," presented at the Canadian Orthopaedic Association Winnipeg, Manitoba, Canada, 2013.

[142] C. Shahrdar, P. A. Campbell, and L. D. Dorr, "Painful metal-on-metal total hip arthroplasty," Journal of Arthroplasty, vol. 21, pp. 289-293, 2006.

[143] G. Grammatopoulos, H. Pandit, Y. K. Kwon, R. Gundle, P. McLardy-Smith, D. J. Beard, et al., "Hip resurfacings revised for inflammatory pseudotumour have a poor outcome," Journal of Bone and Joint Surgery [British], vol. 91B, pp. 1019-1024, 2009.

[144] D. R. Boardman, F. R. Middleton, and T. G. Kavanagh, "A benign psoas mass following metal-on-metal resurfacing of the hip," Journal of Bone and Joint Surgery [British], vol. 88B, pp. 402-404, 2006.

[145] R. B. Cook, B. J. R. F. Bolland, J. A. Wharton, S. Tilley, J. M. Latham, and R. J. K. Wood, "Pseudotumour formation due to tribocorrosion at the taper interface of large diameter metal on polymer modular total hip replacements," Journal of Arthroplasty, vol. 28, pp. 1430-1436, 2013.

[146] R. Chana, C. Esposito, P. A. Campbell, W. K. Walter, and W. L. Walter, "Mixing and matching causing taper wear: Corrosion associated with pseudotumour formation," Journal of Bone and Joint Surgery [British], vol. 94B, pp. 281-286, 2012.

[147] M. Huber, G. Reinisch, G. Trettenhahn, K. Zweymuller, and F. Lintner, "Presence of corrosion products and hypersensitivity-associated reactions in periprosthetic tissue after aseptic loosening of total hip replacements with metal bearing surfaces," Acta Biomaterialia, vol. 5, pp. 172-180, 2009.

[148] H. J. Cooper, C. J. Della-Valle, R. A. Berger, M. Tetreault, W. G. Paprosky, S. M. Sporer, et al., "Corrosion at the head-neck taper as a cause for adverse local tissue reactions after total hip arthroplasty," Journal of Bone and Joint Surgery [American], vol. 94A, pp. 1655-1661, 2012.

[149] D. S. Garbuz, "Metal-on-metal hip resurfacing versus large-diameter head metal-on-metal total hip arthroplasty: A randomized clinical trial," Clinical Orthopaedics and Related Research, vol. 468, pp. 318-325, 2010.

[150] D. J. Langton, S. S. Jameson, T. J. Joyce, J. N. Gandhi, R. Sidaginamale, M. P., et al., "Accelerating failure rate of the ASR total hip replacement," Journal of Bone and Joint Surgery [British], vol. 93, pp. 1011-1016, 2011.

[151] P. Schaaff, "The role of fretting damage in total hip arthroplasty with modular design hip joints - evaluation of retrieval studies and experimental simulation methods," J. Appl. Biomat. Biomech. Res., vol. 2, pp. 121-135, 2004.

[152] R. G. Bayer, Mechanical Wear Fundamentals and Testing, 2nd ed. New York, New York, United States of America: Marcel Dekker, Inc., 2004.

[153] Y. Mutoh, "Mechanisms of Fretting Fatigue," Japan Society of Mechanical Engineers International Journal, vol. 38, pp. 405-415, 1995.

[154] J. Cohen and B. Lindenbaum, "Fretting corrosion in orthopaedic implants," Clinical Orthopaedics and Related Research, vol. 61, pp. 167-175, 1968.

[155] P. Blanchard, C. Colombie, V. Pellerin, S. Fayeulle, and L. Vincent, "Material effects in fretting wear: application to iron, titanium, and aluminum alloys," Metallurgical Transactions A, vol. 22A, pp. 1535-1544, 1991.

[156] T. C. Doehring, H. E. Rubash, and D. E. Dore, "Micromotion measurements with hip center and modular neck length alterations," Clinical Orthopaedics and Related Research, vol. 362, pp. 230-239, 1999.

[157] J. R. Davey, D. O. O' Connor, D. W. Burke, and W. H. Harris, "Femoral component offset: Its effect on strain in bone-cement," Journal of Arthroplasty, vol. 8, pp. 23-26, 1993.

[158] D. Porter, R. M. Urban, J. J. Jacobs, J. Rodriguez, and H. J. Cooper, "Flexural rigidity of various trunnion designs in modular hip stems: A biomechanical and historical analysis," presented at the International Society for Technology in Arthroplasty, Palm Beach, FL, USA, 2013.

[159] R. J. Underwood, S. B. Kocagoz, R. Smith, R. S. Sayles, R. Siskey, S. M. Kurtz, et al., "A protocol to assess the wear of head/neck taper junctions in large head metal-on-metal (LHMoM) Hips," Metal-On-Metal Total Hip Replacement Devices, vol. 1560, pp. 209-234, 2013.

[160] J. M. Vincelli, E. M. Carlson, J. H. Currier, D. W. Van Citters, and J. P. Collier, "Methodology and validation of taper wear measurements in hip arthroplasty retrievals," presented at the Orthopaedic Research Society, San Antonio, Texas, USA, 2013.

[161] L. Duisabeau, P. Combrade, and B. Forest, "Environmental effect on fretting of metallic materials for orthopaedic implants," Wear, vol. 256, pp. 805-816, 2004.

[162] L. Duisabeau, P. Combrade, and B. Forest, "Environmental effect on fretting of metallic materials for orthopaedic implants," Wear, vol. 256, pp. 805-816, 2004.

[163] H. Fessler and D. C. Fricker, "Friction in femoral prosthesis and photoelastic model cone taper joints," Proceedings of the Institution of Mechanical Engineers, Part H: Journal of Engineering in Medicine, vol. 203, pp. 1-7, 1989.

[164] T. Zhang, N. M. Harrison, P. F. McDonnell, P. E. McHugh, and S. B. Leen, "Fretting wear-fatigue analysis for modular hip implant," presented at the 39th Leeds-Lyon Symposium on Tribology, Leeds, England, 2012.

[165] K. A. Abdullah, "Finite element modelling of the neck-stem interface of a modular hip implant for micro-motion study," presented at the Proceedings of the 19th IASTED International Conference, Quebec City, Quebec, Canada, 2008.

[166] W. H. Cater and J. H. Hicks, "The recent hsitory of corrosion in metal used for internal fixation," Lancet, vol. 268, pp. 871-873, 1956.

[167] M. Schramm, D. C. Wirtz, U. Holzwarth, and R. P. Pitto, "The morse taper junction in modular revision hip replacement - a biomechanical and retrieval analysis," Biomedizinische Technik, vol. 45, pp. 105-109, 2000.

[168] H. J. Cooper, R. M. Urban, R. L. Wixson, R. M. Meneghini, and J. J. Jacobs, "Adverse local tissue reaction arising from corrosion at the femoral neck-body junction in dual-taper stem with a cobalt-chromium modular neck," Journal of Bone and Joint Surgery [American], vol. 95A, pp. 865-872, 2013.

[169] L. C. Lucas, R. A. Buchanan, and J. E. Lemons, "Investigations on the galvanic corrosion of multialloy total hip prostheses," Journal of Biomedical Materials Research, vol. 15, pp. 731-747, 1981.

[170] G. B. Higgs, J. A. Hanzlik, D. W. MacDonald, W. M. Kane, J. S. Day, G. R. Klein, et al., "Method of characterizing fretting corrosion at the various taper connections of retrieved modular components from metal-on-metal total hip arthroplasty," Metal-On-Metal Total Hip Replacement Devices, vol. STP 1560, pp. 146-156, 2013.

[171] J. J. Jacobs, J. L. Gilbert, and R. M. Urban, "Current concepts review - corrosion of metal orthopaedic implants," Journal of Bone and Joint Surgery [American], vol. 80A, pp. 268-282, 1998.

[172] U. Vieweg, D. van Roost, H. K. Wolf, C. A. Schyma, and J. Schramm, "Corrosion on an internal spinal fixator system," Spine, vol. 24, pp. 946-951, 1999.

[173] S. A. V. Swanson, M. A. R. Freeman, and J. C. Heath, "Laboratory tests on total joint replacement prostheses," Journal of Bone and Joint Surgery [British], vol. 55B, pp. 759-773, 1973.

[174] O. Svensson, "Formation of a fulminant soft-tissue pseudotumor after uncemented hip arthroplasty: A case report," Journal of Bone and Joint Surgery [American], vol. 70A, pp. 1238-1242, 1988.

[175] J. U. Lindgren, B. H. Brismar, and A. C. Wikstrom, "Adverse reaction to metal release from a modular metal-on-polyethylene hip prosthesis," Journal of Bone and Joint Surgery [British], vol. 93, pp. 1427-1430, 2011.

[176] N. Goyal, H. Ho, K. B. Fricka, and C. A. Engh Jr., "Do you have to remove a corroded femoral stem?," Journal of Arthroplasty, vol. 29, pp. 139-142, 2014.

[177] J. R. Goldberg, J. L. Gilbert, J. J. Jacobs, T. W. Bauer, W. G. Paprosky, and S. Leurgans, "A multicenter retrieval study of the taper interfaces of modular hip prostheses," Clinical Orthopaedics and Related Research, vol. 401, pp. 149-161, 2002.

[178] H. Hothi, R. Berber, R. Whittaker, S. Cro, G. Blunn, J. A. Skinner, et al., "The inter-observer variability of the Goldberg method for corrosion and fretting of taper junctions of hip arthroplasties," presented at the International Society for Technology in Arthroplasty, Palm Beach, Florida, USA, 2013.

[179] R. J. Underwood, D. W. MacDonald, G. B. Higgs, J. S. Day, R. L. Siskey, and S. M. Kurtz, "Does visual inspection of the taper head / stem junctions in metal-on-metal hips accurtely characterize the corrosion and wear?," presented at the Orthopaedic Research Society, San Antonio, Texas, USA, 2013.

[180] S. Y. Jauch, G. Huber, E. Hoenig, M. Baxmann, T. M. Grupp, and M. M. Morlock, "Influence of material coupling and assembly condition on the magnitude of micromotion at the stem-neck interface of a modular hip endoprosthesis," Journal of Biomechanics, vol. 44, pp. 1747-1751, 2011.

[181] J. P. Collier, V. A. Surprenant, R. E. Jensen, and M. B. Mayor, "Corrosion at the interface of cobalt-alloy heads on titanium-alloy stems," Clinical Orthopaedics and Related Research, vol. 271, pp. 305-312, 1991.

[182] A. Panagiotidou, J. Meswania, J. Hua, S. K. Muirhead-Allwood, J. A. Skinner, A. J. Hart, et al., "Do surface topography and contact area effect fretting corrosion behavior of the modular taper interface in toal hip replacements?," presented at the International Society for Technology in Arthroplasty, Palm Beach, FL, USA, 2013.

[183] A. Panagiotidou, J. Meswania, J. Hua, S. K. Muirhead-Allwood, A. J. Hart, and G. Blunn, "Enhanced wear and corrosion in modular tapers in total hip replacement is associated with the contact area and surface topography," Journal of Orthopaedic Research, vol. 31, pp. 2032-2039, 2013.

[184] H. Meyer, T. Mueller, G. Goldau, K. Chamaon, M. Ruetschi, and C. H. Lohmann, "Corrosion at the cone/taper interface leads to failure of large-diameter metal-on-metal total hip arthroplasties," Clinical Orthopaedics and Related Research, vol. 470, pp. 3101-3108, 2012.

[185] S. J. Incavo, "CORR Insights: Adverse local tissue reaction associated with a modular hip hemiarthroplasty," Clinical Orthopaedics and Related Research, vol. 471, pp. 4087-4088, 2013.

[186] M. R. Whitehouse, M. Endo, and B. A. Masri, "Adverse local tissue reaction associated with a modular hip hemiarthroplasty," Clinical Orthopaedics and Related Research, vol. 471, pp. 4082-4086, 2013.

[187] V. Chandrasekaran, W. L. Sauer, A. M. Taylor, and D. W. Hoeppner, "Evaluation of the fretting corrosion behavior of the proximal pad taper of a modular hip design," Wear, vol. 231, pp. 54-64, 1999.

[188] C. Restrepo, D. Ross, S. Restrepo, S. Heller, N. Goyal, R. Moore, et al., "Adverse clinical outcomes in a primary modular neck/stem system," Journal of Arthroplasty, vol. 29, pp. 173-178, 2014.

[189] A. Weinstein, H. Amstutz, G. Pavon, and V. Francheschini, "Orthopedic implants - a clinical and metallurgical analysis," Journal of Biomedical Materials Research vol. 7, pp. 297-325, 1973.

[190] J. P. Collier, "Mechanisms of failure of modular prostheses," Clinical Orthopaedics and Related Research, vol. 285, pp. 129-139, 1992.

[191] S. D. Cook, "Wear and corrosion of modular interfaces in total hip replacements," Clinical Orthopaedics and Related Research, vol. 298, pp. 80-88, 1994.

[192] M. Manley and P. Serekian, "Wear debris: An environmental issue in total joint replacement," Clinical Orthopaedics and Related Research, vol. 298, pp. 137-146, 1994.

[193] J. P. Collier, "The tradeoffs associated with modular hip prostheses," Clinical Orthopaedics and Related Research, vol. 311, pp. 91-101, 1995.

[194] N. J. Hallab and J. J. Jacobs, "Orthopedic implant fretting corrosion," Corrosion Reviews, vol. 21, pp. 183-214, 2003.

[195] G. B. Higgs, J. A. Hanzlik, D. W. MacDonald, G. R. Klein, J. Parvizi, M. A. Mont, et al., "Does fretting and corrosion occur at modular interfaces other than the head-stem junction in metal-on-metal total hip arthroplasty devices?," presented at the Orthopaedic Research Society, San Antonio, Texas, USA, 2013.

[196] I. P. S. Gill, J. Webb, K. Sloan, and R. J. Beaver, "Corrosion at the neck-stem junction as a cause of metal ion release and pseudotumour formation," Journal of Bone and Joint Surgery [British], vol. 94/b, pp. 895-900, 2012.

[197] C. Silverton, J. J. Jacobs, J. Devitt, and J. Cooper, "Midterm results of a femoral stem with a modular neck design: Clinical outcomes and metal ion analysis," presented at the International Society for Technology in Arthroplasty, Palm Beach, Florida, USA, 2013.

[198] S. Murphy and D. Le, "Report of 3 cases of local tissue reaction in association with a CoCr modular neck on a conventional titanium alloy stem," presented at the International Society for Technology in Arthroplasty, Palm Beach, FL, USA, 2013.

[199] L. Barnes, C. Parks, and M. Bushmiaer, "Chromium and cobalt levels and associated MARS MRI findings in previously unreported design of chrome cobalt modular neck," presented at the International Society for Technology in Arthroplasty, Palm Beach, FL, USA, 2013.

[200] M. Meftah, P. C. Noble, and S. J. Incavo, "Unexpected high rates of corrosion related revisions: short-term results of the modular neck Rejuvenate stem," presented at the International Society for Technology in Arthroplasty, Palm Beach, FL, USA, 2013.

[201] M. Meftah, A. M. Haleem, M. B. Burn, K. M. Smith, and S. J. Incavo, "Early corrosion-related failure of the Rejuvenate modular total hip replacement," Journal of Bone and Joint Surgery [American], vol. 96A, pp. 481-487, 2014.

[202] J. P. Kretzer, J. Reinders, R. Sonntag, C. Merle, G. Omlor, M. Streit, et al., "Does modular neck total hip arthroplasty increases titanium ion levels?," presented at the International Society for Technology in Arthroplasty, Palm Beach, FL, USA, 2013.

[203] J. P. Kretzer, "Metal release and corrosion effects of modular neck total hip arthroplasty," International Orthopaedics, vol. 33, pp. 1531-1536, 2009.

[204] G. B. Higgs, J. A. Hanzlik, D. W. MacDonald, J. L. Gilbert, C. M. Rimnac, and S. M. Kurtz, "Is increased modularity associated with increased fretting and corrosion damage in metal-on-metal total hip arthroplasty devices?," Journal of Arthroplasty, vol. 28, pp. 2-6, 2013.

[205] G. Bergmann, F. Graichen, and A. Rohlman, "Hip joint loading during walking and running, measured in two patients," Journal of Biomechanics, vol. 26, pp. 969-990, 1993.

[206] K. Merritt and S. A. Brown, "Distribution of cobalt chromium wear and corrosion products and biologic reactions.," Clinical Orthopaedics and Related Research, vol. 329, pp. 233-243, 1996.

[207] W. C. McMaster and J. Patel, "Adverse local tissue response lesion of the knee associated with Morse taper corrosion," Journal of Arthroplasty, vol. 28, p. 375, 2013.

[208] C. M. Arnholdt, D. W. MacDonald, M. Tohfafarosh, J. L. Gilbert, C. M. Rimnac, S. M. Kurtz, et al., "Mechanically assisted taper corrosion in modular TKA," Journal of Arthroplasty, vol. 29, pp. 205-208, 2014.

[209] Wikipedia. (April 20). Tribology [Online] . Available: http://en.wikipedia.org/wiki/Tribology

[210] D. Li. (2013, April 20). Continuous Stribeck curve measurement using pin-on-disk tribometer [Online]. Available: http://www.nanovea.com/Application%20Notes/stribeckcurvetribology.pdf

[211] S. Shaffer. (2014, April 20). Generating a Stribeck curve in a reciprocating test [Online]. Available: https://www.bruker.com/fileadmin/user_upload/8-PDF-Docs/SurfaceAnalysis/TMT/ApplicationNotes/AN1004_RevA2_Generating_a_Stribeck_Curve_in_a_Reciprocating_Test-AppNote.pdf

[212] R. Budney. (2013, April 20). Good lubrication practices can reduce gearbox failures [Online]. Available: http://www.nawindpower.com/issues/NAW1309/FEAT_02_Good_Lubrication_Practices_Can_Reduce_Gearbox_Failures.html

[213] S. Mischler, S. Debaud, and D. Landolt, "Wear-accelerated corrosion of passive metals in tribocorrosion systems," Journal of the Electrochemical Society, vol. 145, pp. 750-758, 1998.

[214] Y. Yan, A. Neville, D. Dowson, and S. Williams, "Tribocorrosion in implants - assessing high carbon and low carbon Co-Cr-Mo alloys by in situ electrochemical measurements," Tribology International, vol. 39, pp. 1509-1517, 2006.

[215] ISO, "ISO 7206-10: Implants for surgery -- Partial and total hip-joint prostheses -- Part 10: Determination of resistance to static load of modular femoral heads," ed. Geneva, Switzerland: ISO, 2003, p. 10.

[216] T. Pandorf, R. Preuss, and R. Czak, "Impaction forces and proper seating of ceramic ball heads," presented at the Orthopaedic Research Society, New Orleans, LA, USA, 2010.

[217] R. Nassutt, I. Mollenhauer, K. Klingbeil, O. Hennig, and H. Grundei, "Relevance of the insertion force for the taper lock reliability of a hip stem and a ceramic femoral head," Biomedizinische Technik, vol. 51, pp. 103-109, 2006.

[218] M. L. Mroczkowski, J. S. Hertzler, S. M. Humphrey, T. Johnson, and C. R. Blanchard, "Effect of impact assembly on the fretting corrosion of modular hip tapers," Journal of Orthopaedic Research, vol. 24, pp. 271-279, 2006.

[219] A. Rehmer, N. E. Bishop, and M. M. Morlock, "Influence of assembly procedure and material combination on the strength of the taper connection at the head-neck junction of modular hip endoprostheses," Clinical Biomechanics, vol. 27, pp. 77-83, 2012.

[220] U. S. Schlegel, S. Rothstock, J. Siewe, K. H. Schiwy-Bochat, P. Eysel, and M. M. Morlock, "Does impaction matter in hip resurfacing? A cadaveric study.," Journal of Arthroplasty, vol. 26, pp. 296-302, 2011.

[221] T. Bitter, D. Janssen, B. W. Schreurs, I. Khan, and N. Verdonschot, "The effect of head impaction on contact stress and micromotions at the head-taper connection," presented at the International Society for Technology in Arthroplasty, Palm Beach, FL, USA, 2013.

[222] P. Wanjara and M. Jahazi, "Linear friction welding of Ti-6Al-4V: processing, microstructure, and mechanical-property inter-relationships," Metallurgical and Materials Transactions A, vol. 36, pp. 2149-2164, 2005.

[223] F. J. Kummer and R. M. Rose, "Corrosion of titanium/cobalt-chromium alloy couples," Journal of Bone and Joint Surgery [American], vol. 65A, pp. 1125-1126, 1983.

[224] H. A. McKellop, A. Sarmiento, W. Brien, and S. H. Park, "Interface corrosion of a modular head total hip prosthesis," Journal of Arthroplasty, vol. 7, pp. 291-294, 1992.

[225] J. M. Cuckler, "Fretting and corrosion in modular implants," Journal of Arthroplasty, vol. 8, p. 112, 1993.

[226] J. Parekh, H. Jones, N. Chan, and P. C. Noble, "Effect of angular mismatch tolerance on trunnion micro-motion in metal-on-metal THA designs," presented at the International Society for Technology in Arthroplasty, Palm Beach, FL, USA, 2013.

[227] N. Shareef and D. Levine, "Effect of manufacturing tolerances on the micromotion at the Morse taper interface in modular hip implants using the finite element technique," Biomaterials, vol. 17, pp. 623-630, 1996.

[228] D. E. Padgett, K. Stoner, N. Nassif, D. Nawabi, T. Wright, and M. Elpers, "The effect of taper geometry on large head MOM THA taper-trunnion damage," presented at the International Society for Technology in Arthroplasty, Palm Beach, FL, USA, 2013.

[229] S. M. Kurtz, "Taper corrosion update: What is the role of ceramic femoral ball heads?," CeraNews, vol. 1, pp. 3-6, 2013.

[230] N. J. Hallab, "Differences in the fretting corrosion of metal-metal and ceramic-metal modular junctions of total hip replacements," Journal of Orthopaedic Research, vol. 22, pp. 250-259, 2004.

[231] D. W. MacDonald, S. M. Kurtz, S. B. Kocagoz, J. A. Hanzlik, R. J. Underwood, J. L. Gilbert, et al., "Do ceramic femoral heads reduce taper fretting corrosion in hip arthroplasty? A retrieval study," presented at the International Society for Technology in Arthroplasty, Palm Beach, FL, USA, 2013.

[232] M. Flohr, K. L. Haeussler, R. Preuss, and R. M. Streicher, "Fretting, corrosion and connection strength of sleeved ceramic modular heads tested under in-vivo like conditions," presented at the International Society for Technology in Arthroplasty, Palm Beach, Florida, USA, 2013.

[233] R. Preuss, K. L. Haeussler, M. Flohr, and R. M. Streicher, "Fretting corrosion and trunnion wear - is it also a problem for sleeved ceramic heads?," Seminars in Arthroplasty, vol. 23, pp. 251-257, 2012.

[234] K. B. Fricka, H. Ho, W. J. Peace, and C. A. Engh Jr., "Metal-on-metal local tissue reaction is associated with corrosion of the head taper junction," Journal of Arthroplasty, vol. 27, pp. 26-31, 2012.

[235] J. J. Jacobs, R. M. Urban, N. J. Hallab, A. K. Skipor, A. Fischer, and M. A. Wimmer, "Metal-on-metal bearing surfaces," Journal of the American Academy of Orthopaedic Surgeons, vol. 17, pp. 69-76, 2009.

[236] M. A. Wimmer, A. Fischer, R. Buscher, R. Pourzal, C. Sprecher, R. Hauert, et al., "Wear mechanisms in metal-on-metal bearings: the importance of tribochemical reaction layers," Journal of Orthopaedic Research, vol. 28, pp. 436-443, 2010.

[237] U. Dorn, D. Neumann, and M. Frank, "Corrosion behavior of tantalum-coated cobalt-chromium modular necks compared to titanium modular necks in a simulator test," Journal of Arthroplasty, vol. 29, pp. 831-835, 2014.

[238] A. M. Maurer, S. A. Brown, J. H. Payer, K. Merritt, and J. S. Kawalec, "Reduction of fretting corrosion of Ti-6Al-4V by various surface treatments," Journal of Orthopaedic Research, vol. 11, pp. 865-873, 1993.

[239] A. Traynor, A. Kinbrum, J. Housden, and S. Collins, "Fretting and corrosion of tapered head-neck junctions of modular hip components," presented at the International Society for Technology in Arthroplasty, Palm Beach, FL, USA, 2013.

[240] P. C. Noble, A. K. Matthies, H. Jones, J. Gonzalez, and A. J. Hart, "The effects of cup compression on trunnion micromotion in metal-on-metal THA designs," presented at the Orthopaedic Research Society, San Antonio, Texas, USA, 2013.

[241] J. M. Latham, R. B. Cook, B. J. Bolland, and S. Yasen, "Big heads on stems: What have we learned?," presented at the International Society for Technology if Arthroplasaty, Palm Beach, Florida, USA, 2013.

[242] A. Panagiotidou, B. J. Bolland, J. Meswania, J. A. Skinner, F. Haddad, A. J. Hart, et al., "Effect of increased frictional torque on the fretting corrosion behaviour of the large diameter femoral head," presented at the International Society for Technology in Arthroplasty, Palm Beach, Florida, USA, 2013.

[243] R. M. R. Dyrkacz, J. M. Brandt, O. A. Ojo, T. R. Turgeon, and U. P. Wyss, "The influence of head size on corrosion and fretting behaviour at the head-neck interface of artificial hip joints," Journal of Arthroplasty, vol. 28, pp. 1036-1040, 2013.

[244] M. Lavigne, E. L. Belzile, A. Roy, F. Morin, T. Amzica, and P. Vendittoli, "Comparison of whole-blood metal ion levels in four types of metal-on-metal large-diameter femoral head total hip arthroplasty: The potential influence of the adapter sleeve," J. Bone Joint Surg. [Am], vol. 93, pp. 128-136, 2011.

[245] C. A. Engh, S. J. MacDonald, S. Sritulanondha, A. Thompson, D. Naudie, and C. A. Engh, "Metal ion levels after metal-on-metal total hip arthroplasty: A randomized trial," Clin. Orthop. Relat. Res., vol. 467, pp. 101-111, 2009.

[246] M. T. Clarke, P. T. H. Lee, A. Arora, and R. N. Villar, "Levels of metal ions after small-and large-diameter metal-on-metal hip arthroplasty," J Bone Joint Surg [Br], vol. 85B, pp. 913-917, 2003.

[247] C. P. Delaunay, "Metal-on-metal bearings in cementless primary total hip arthroplasty," J. Arthroplasty, vol. 19, pp. 35-40, 2004.

[248] P. A. Vendittoli, T. Amzica, A. G. Roy, D. Lusignan, J. Girard, and M. Lavigne, "Metal ion release with large-diameter metal-on-metal hip arthroplasty," J. Arthroplasty, vol. 26, pp. 282-288, 2011.

[249] D. S. Garbuz, M. Tanzer, N. V. Greidanus, B. A. Masri, and C. P. Duncan, "Metal-on-metal hip resurfacing versus large-diameter head metal-on-metal total hip arthroplasty: A randomized clinical trial," Clin. Orthop. Relat. Res., vol. 468, pp. 318-325, 2010.

[250] T. Visuri, H. Borg, P. Pulkkine, P. Paavolainen, and E. Pukkala, "A retrospective comparative study of mortality and causes of death among patients with metal-on-metal and metal-on-polyethylene total hip prostheses in primary osteoarthritis after a long-term follow-up," BMC Musculoskeletal Disorders, vol. 11, pp. 78-85, 2010.

[251] J. Girard, D. Bocquet, G. Autissier, N. Fouilleron, D. Fron, and H. Migaud, "Metal-on-metal hip arthroplasty in patients thirty years of age or younger," J Bone Joint Surg [Am], vol. 92A, pp. 2419-2426, 2010.

[252] O. Svensson, E. B. Mathiesen, F. P. Reinholt, and G. Blomgren, "Formation of a fulminant soft-tissue pseudotumor after uncemented hip arthroplasty: A case report," J Bone Joint Surg [Am], vol. 70A, pp. 1238-1242, 1988.

[253] P. A. Campbell, E. Ebramzadeh, S. Nelson, K. Takamura, K. D. Smet, and H. C. Amstutz, "Histological features of pseudotumor-like tissues from metal-on-metal hips," Clin. Orthop. Relat. Res., vol. 468, pp. 2321-2327, 2010.

[254] D. J. Langton, R. Sidaginamale, J. K. Lord, A. V. F. Nargol, and T. J. Joyce, "Taper junction failure in large-diameter metal-on-metal bearings," Bone & Joint Research, vol. 1, pp. 56-63, 2012.

[255] J. L. Fleiss, The design and analysis of clinical experiments. Toronto, Ontario, Canada: John Wiley & Sons, Inc., 1986.

[256] R. M. R. Dyrkacz, S. T. O'Brien, J. M. Brandt, J. B. Morrison, O. Ojo, T. R. Turgeon, et al., "Finite element analysis at the head-neck taper interface of modular hip prostheses," Tribology International, vol. Currently in press, 2015.

[257] J. P. Collier, "Corrosion between the components of modular femoral hip prostheses," Journal of Bone and Joint Surgery [British], vol. 74B, pp. 511-517, 1992.

[258] J. R. Lieberman, "An analysis of the head-neck taper interface in retrieved hip prostheses," Clinical Orthopaedics and Related Research, vol. 300, pp. 162-167, 1994.

[259] J. L. Gilbert, "In vivo corrosion of modular hip prosthesis components in mixed and similar metal combinations. The effect of crevice, stress, motion, and alloy coupling," Journal of Biomedical Materials Research, vol. 27, pp. 1533-1544, 1993.

[260] J. Moseley, S. Nambu, R. Obert, M. Roark, D. Linton, and S. Bible, "Accelerated fretting corrosion testing of modular necks for THA," presented at the Orthopaedic Research Society, San Antonio, Texas, USA, 2013.

[261] A. Hexter, G. Blunn, A. K. Matthies, J. Henckel, and A. J. Hart, "Head diameter is positively correlated with taper corrosion in retrieved large-diameter metal-on-metal modular hips," presented at the Orthopaedic Research Society, San Francisco, CA, USA, 2012.

[262] S. M. Kurtz, D. W. MacDonald, G. B. Higgs, J. L. Gilbert, G. R. Klein, M. A. Mont, et al., "Are 36+ mm diameter HXLPE bearings at risk of increased wear from modular taper corrosion with ceramic and CoCr heads?," presented at the International Society for Technology in Arthroplasty, Palm Beach, Florida, USA, 2013.

[263] N. A. Nassif, D. H. Nawabi, K. Stoner, M. Elpers, T. Wright, and D. E. Padgett, "Taper design affects failure of large-head metal-on-metal total hip replacements," Clinical Orthopaedics and Related Research, vol. 472, pp. 564-571, 2014.

[264] G. Triantafyllopoulos, M. Elpers, T. Wright, and D. E. Padgett, "Influence of head size and materials on fretting and corrosion of metal-on-polythylene total hip arthroplasty," presented at the Orthopaedic Research Society, New Orleans, LA, USA, 2014.

[265] J. R. Goldberg and J. L. Gilbert, "In vitro corrosion testing of modular hip tapers," Journal of Biomedical Materials Research. Part B: Applied Biomaterials, vol. 64B, pp. 78-93, 2002.

[266] D. Kluess, J. Wieding, S. Bierbaum, W. Mittelmeier, and R. Bader, "Femoral head diameter, neck and taper length influence the mechanical load and micromotion in the taper connection of total hip replacements," presented at the Orthopaedic Research Society, New Orleans, LA, USA, 2014.

[267] G. Bergmann, "Hip contact forces and gait patterns from routine activities," Journal of Biomechanics, vol. 34, pp. 859-871, 2001.

[268] D. A. Dennis, R. D. Komistek, E. J. Northcut, J. A. Ochoa, and A. Ritchie, ""In vivo" determination of hip joint separation and the forces generated due to impact loading conditions," Journal of Biomechanics, vol. 34, pp. 623-629, 2001.

[269] I. Aerospace Specification Materials. (2014, January 23). Titanium Ti-6Al-4V (Grade 5), Annealed [Online]. Available: http://asm.matweb.com/search/SpecificMaterial.asp?bassnum=MTP641

[270] J. M. Elkins, M. K. O'Brien, N. J. Stroud, D. R. Pedersen, J. J. Callaghan, and t. D. Brown, "Hard-on-hard total hip impingement causes extreme contact stress concentrations," Clinical Orthopaedics and Related Research, vol. 469, pp. 454-463, 2011.

[271] B. D. Ratner, Biomaterials science: An introduction to materials in medicine, 2nd ed. San Diego, California, United States of America: Elsevier Academic Press, 2004.

[272] P. A. Campbell, "Histological features of pseudotumor-like tissues from metal-on-metal hips," Clinical Orthopaedics and Related Research, vol. 468, pp. 2321-2327, 2010.

[273] R. M. R. Dyrkacz, S. T. O' Brien, J. M. Brandt, J. B. Morrison, O. A. Ojo, T. R. Turgeon, et al., "Head size and mixed alloys influence the micromotion along the head-neck taper interface of artificial hip joints," presented at the 2nd International Conference on Biotribology, Toronto, Ontario, Canada, 2014.

[274] R. M. R. Dyrkacz, U. P. Wyss, J. M. Brandt, O. Ojo, and T. R. Turgeon, "A comparison of the corrosion and fretting behaviour between large femoral heads and monopolar hip implants," presented at the International Society for Technology in Arthroplasty, Palm Beach, FL, USA, 2013.

[275] J. M. Elkins, J. J. Callaghan, and T. D. Brown, "Stability and trunnion wear potential in large-diameter metal-on-metal total hips: A finite element analysis," Clinical Orthopaedics and Related Research, vol. 472, pp. 529-542, 2014.

[276] Y. Y. Zou, Wang, Y. L., Zhang, T. L., "Finite element analysis of fretting at taper interface in modular hip implants," Chinese Journal of Clinical Anatomy, vol. 25, pp. 81-84, 2007.